Condition Monitoring of Pharmaceutical Powder Compression During Tabletting Using Acoustic Emission

A thesis submitted for the degree of Doctor of Philosophy in the Faculty of Technology

By

Salah Eissa

Brunel Centre for Manufacturing Metrology (BCMM)
Brunel University, Cleveland Road
Uxbridge, Middlesex UB8 3PH

March 2003

Acknowledgements

I owe a particular debt of gratitude to my supervisor Dr. Y H J Au for his valuable comments, assistance and support to guide my work to a satisfactory conclusion. I am indebted to him for his continued encouragement and for teaching me new ways of seeing the greater picture. Without his support and enthusiasm for research this project would have never been possible.

I am pleased to have had the opportunity to work with INTErSECT Faraday Partnership Flagship Project, "Acoustic Emission Traceable Sensing and Signature Diagnostics (AESAD)". I acknowledge the help and useful discussions from all my AESAD colleagues, especially Professor Barry E. Jones.

Special thanks are due to Dr. Dave Rudd (GlaxoSmithKline), Dr. Paul Frake (GlaxoSmithKline) and Dr. Peter Doyle (Unilever Research Port Sunlight).

My greatest debts are due to my father who had given me his love and support when he was alive. I would also like to express my deepest appreciation to my mother for her endless prayers and support. I am also extremely grateful to all of my brothers, sisters and my wife and other relatives for their continuous encouragement and support.

Dedication

To my beloved father (passed away), mother, brothers,
sisters, wife, my daughters Zahra & Fatimah
and those who waited so long…

Abstract

This research project aimed to develop a condition monitoring system for the final production quality of pharmaceutical tablets and detection capping and lamination during powder compression process using the acoustic emission (AE) method. Pharmaceutical tablet manufacturers obliged by regulatory bodies to test the tablet's physical properties such as hardness, dissolution and disintegration before the tablets are released to the market. Most of the existing methods and techniques for testing and monitoring these tablet's properties are performed at the tablet post-compression stage. Furthermore, these tests are destructive in nature.

Early experimental investigations revealed that the AE energy that is generated during powder compression is directly proportional to the peak force that is required to crush the tablet, i.e. crushing strength. Further laboratory and industrial experimental investigation have been conducted to study the relationship between the AE signals and the compression conditions. Traditional AE signal features such as energy, count, peak amplitude, average signal level, event duration and rise time were recorded. AE data analysis with the aid of advanced classification algorithm, fuzzy C-mean clustering showed that the AE energy is a very useful parameter in tablet condition monitoring. It was found that the AE energy that is generated during powder compression is sensitive to the process and is directly proportional to the compression speed, particle size, homogeneity of mixture and the amount of material present. Also this AE signal is dependent upon the type of material used as the tablet filler.

Acoustic emission has been shown to be a useful technique for characterising some of the complex physical changes which occur during tabletting. Capping and lamination are serious problems that are encountered during tabletting. A capped or laminated tablet is one which no longer retains its mechanical integrity and exhibit low strength characteristics. Capping and lamination can be caused by a number of factors such as excessive pressure, insufficient binder in the granules and poor material flowabilities. However, capping and lamination can also occur randomly and they are also dependent upon the material used in tabletting. It was possible to identify a capped or

laminated tablet by monitoring the AE energy level during continuous on-line monitoring of tabletting. Capped tablets indicated by low level of AE energy.

The proposed condition monitoring system aimed to set the AE energy threshold that could discriminate between capped and non-capped tablets. This was based upon statistical distributions of the AE energy values for both the capped and non-capped tablets. The system aims to minimise the rate of false alarms (indication of capping when in reality capping has not occurred) and the rate of missed detection (an indication of non capping, when in reality capping has occurred).

A novel approach that employs both the AE method and the receiver operating characteristic (ROC) curve was proposed for the on-line detection of capping and lamination during tabletting. The proposed system employs AE energy as the discriminating parameter to detect between capped and non-capped tablets. The ROC curve was constructed from the area under the two distributions of both capped and non-capped tablet. This curve shows a trade-off between the probabilities of true detection rate and false alarm rate for capped and non-capped tablet. A two-graph receiver operating characteristic (ROC) curve was presented as a modification of the original ROC curve to enable an operator to directly select the desired energy threshold for tablet monitoring. This plot shows the ROC co-ordinate as a function of the threshold value over the entire threshold (AE energy) range for all test outcomes.

An alternative way of deciding a threshold based on the slope of the ROC curve was also developed. The slope of the ROC curve represents the optimal operating point on the curve. It depends upon the penalties cost of capping and the prevalence of capping. Sets of guidelines have been outlined for decision making i.e. threshold setting. These guidelines take into account both the prevalence of capping in manufacturing and the cost associated with various outcomes of tablet formation.

The proposed condition monitoring system also relates AE monitoring to non-AE measurement as it enable an operator predicting tablet hardness and disintegration form the AE energy, a relationship which was established in this research.

Publications relating to this work

1. Eissa S, Au Y.H. J., (2000) Non-Invasive measurement of pharmaceutical processes. *Doctoral Research Conference*, Brunel University 16-17 September p 29-37.

2. Eissa S, Au Y.H.J., (2002), Condition monitoring of pharmaceutical processes, *COMADEM International*, Birmingham, 2-4 September, pp457-471.

3. Eissa S, Au Y. H. J., Terchi A, Jones B E, (2003) Powder compression monitoring using acoustic emission: Advanced fuzzy c-mean clustering method, Transactions of the Institute of Measurement & Control (accepted in 2002 and to be published).

4. Eissa S, Au Y.H.J., Terchi A, Jones B E., (2003) Powder compression monitoring with fuzzy clustering of acoustic emission signals, *International Conference on Mechatronics*, Loughborough University, UK 26&27 June (accepted).

5. Eissa S, Au Y. H.J, Jones B E, (2003) Receiver operating characteristic analysis for the selection of threshold values for detection of capping in powder compression, Ultrasonics International 2003, Granada, Spain on 30 June – 3 July 2003 (accepted).

Non-refereed papers

1. Eissa S & Doyle P (2001) Acoustic Measurement for monitoring chemical and pharmaceutical processes External Research Forum 8-9 November, Unilever, Port Sunlight, Bebington, Wirral, UK

2. Eissa S & Rudd D (2001) Pharmaceutical process monitoring using acoustic emission, Royal Society of Chemistry, London.

Contents

Chapter 4: Experimentation

Chapter 5: Results from the test rig

Chapter 6: AE monitoring of industrial tabletting

Chapter 7: In situ monitoring of capping and lamination during tabletting

PAGE NUMBERING AS ORIGINAL

List of Figures

Chapter 2

Chapter 3

Chapter 4

Chapter 5

Chapter 6

Chapter 7

Chapter 8

List of Tables

Chapter 7

Chapter 1

1.1 Tablet as dosage form

It is a remarkable fact that, in the new millennium, tablets still account for more than 80% of all dosage forms administered to man. The principal reasons for their continued popularity include their ease of manufacture, their convenience of dosing, and their stability compared with liquid and semi-solid presentations. One method of tablet manufacture is that of direct compression of the active ingredient with other appropriate excipients (filler) to form a tablet, normally for medium- to high-potency compounds where the drug content is less than 20% of the formulation. The advantages of direct compression are well known, the most important being fewer processing stages and the elimination of heat and moisture effects.

Tablets are solid dosage forms of medicinal substances usually prepared with the aid of suitable pharmaceutical excipients. Tablets may vary in size, shape, weight, hardness, thickness, and disintegration characteristics, depending upon the intended use of the tablet and their method of manufacture (Ansel *et al*, 1995).

The majority of tablets are used in the oral administration of drugs and many of these tablets are prepared with colorants and coatings of various types. Other tablets such as those intended to be administrated sublingually and vaginally may not contain the same excipients or possess the same types of features as tablets for oral administration.

Tablets are prepared primarily by compression. A limited number of tablets are prepared by moulding. Compressed tablets are manufactured with tablet machines capable of exerting great pressure on the powdered or granulated material through the use of various shapes of punches and dies. The tablet presses are heavy equipment of various capacities selected for use on the basis of the type of tablets to be manufactured and the production rate desired. Moulded tablets, on the other hand, are prepared by tablet machinery or manually by forcing dampened tablet material into a mould from which the formed tablet is then ejected and allowed to dry (Ansel *et al*, 1995).

Important parameters of the tablet constituents that may affect the characteristics of the final tablet are assessed before manufacture, and include density, flowability and purity of the compounds. Prior to the compression stage the homogenous granule or direct compression mixture can be assessed for particle size distribution and flow properties, thus giving an indication of the suitability of the pre-compression mixture for use in the tablet press.

The tablets produced are then assessed for uniformity of weight and content, consistency of diameter and thickness as well as hardness. Tablet hardness can be regarded as a factor that may affect the disintegration and dissolution characteristics. Hardness provides an indication of how resilient the dosage form will be to storage and transport conditions prior to its use.

1.2 Advantages of compressed tablet

The compressed tablet has a number of advantages over other forms of tablets; below is a list of these advantages:

1. It enables an accurate dosage of medicament to be administered simply.
2. It is easy both to transport in bulk and to be carried by the patient.
3. It is a uniform final product as regards weight and appearance and usually more stable than a liquid preparation.
4. The release rate of the drug from a tablet can be tailored to meet pharmacological requirements.
5. Tablets can be mass-produced easily and quickly and the resultant manufacturing cost is therefore very much lower when compared with other dosage forms (Aulton *et al*, 2000).

1.3 Problem definition

Chemical and pharmaceutical manufacturers still use some conventional methods of monitoring ongoing processes within their plants. These methods are no doubt very useful. However there are some problems still associated with these methods, for example the destructive nature, cost and reliability. Cost is a major problem when employing these methods particularly if anything goes wrong within the process. Official reports from the pharmaceutical industry in the UK indicated that approximately £10,000,000 of loss caused by failure of final product to fulfil the regulatory bodies' requirements. Monitoring still involves sampling and analytical tests in laboratories as well as various destructive testing methodologies. There is a danger of contamination when sampling takes place in an ongoing process. All these issues are very critical when manufacturers want to monitor chemical and pharmaceutical processes. At present there is unfortunately no on-line measurement system that can provide information about ongoing processes. Hence a non-invasive, reliable and cheap way of monitoring is vital for the manufacturer. The acoustic emission (AE) technique may be the answer.

With some modifications, conventional tablet processing methods and equipment can be used in the preparation of a fast-disintegrating dosage forms during tableting. Tablets made by conventional compression methods usually possess sufficient hardness to withstand the handling and rigours of transportation. Furthermore tablet is designed for a human treatment or diagnostics. Therefore, tablet hardness and dissolution characteristics are very important properties that the pharmaceutical manufacturers must establish. A fast disintegrating tablet with good crushing strength that could be manufactured with conventional processing equipment was the objective of the formulation development programmes.

Most of the techniques employed in testing the quality of the final tablets involve destructive testing. These tests such as measuring the crushing strength or the dissolution are still in use in the industry. For example, the crushing strength test technique requires that the tablet is placed in between the two metal anvils of a tablet test machine; this test enables the operator to record the peak force required to crush the tablet. Usually, samples of a batch are chosen and the test carried out to establish an important parameter called 'hardness'. Based on simple statistical analysis as well

as setting an acceptable level of tolerance the operator decides whether or not to release the batch for further processing e.g. coating. The need for non-destructive for testing tablets properties such as hardness and strength is vital. Therefore, this research aims to focuses on using acoustic emission as a method for condition monitoring of tabletting and detecting problems associated with this process such as capping and lamination which affect the tablets' final quality, including hardness.

1.4 Background

Many factors influence powder flow and compaction including physical and mechanical properties of the materials, such as environmental effects, as well as processing equipment design (Alderborn and Nystrom, 1996). This, in part, is the origin of the great difficulties encountered in pharmaceutical solid dosage form formulation and technological manipulation of powder. While physical properties such as size and shape clearly influence powder flow and compaction, systematic research on the effects of the mechanical properties of materials has only recently been evident and is a result of the rise in the use of instrumented tabletting presses and compaction simulators in pharmaceutical research. This has led to a preponderance of publications dealing with the analysis of energy and fundamental forces during powder compaction. Several authors have attempted to identify various stages during the compression of powders (Macleod, 1983; Jones *et al*, 1985). Currently, a consensus of opinion exists regarding the following defined stages: the initial rearrangement of particles or grains during pre-compression, particle solidification fragmentation of the particles, their plastic deformation and their elastic deformation. Although in some powders more than one phase occurs simultaneously in the powder compact depending upon the applied load or speed of compression, each phase contributing to the overall physico-mechanical characteristics of a material is subjected to a compression force.

Hardness is an important physical property of tablets in the field of pharmaceutical powder compaction. The hardness is of interest for elucidating the compression process, as well as for the quality control of tablet manufacture.

Hardness of a compact depends on the state of consolidation. Several equations have been proposed in attempts to describe the compressibility of powders (Kawakita and Ludde, 1970; Celik, 1992). Most of these formulas are based on transformations of

the classical stress/strain or force/displacement relationship, where either the compaction pressure or the volume is transformed. Early work by Hiestand *et al,* 1984, found that the logarithm of the hardness is a linear function of the relative density. Yet, it can be shown that in a broad density range exists more than one linear region in such a hardness plot. Thus, it seems to be a rather ambitious goal to obtain a single equation for the hardness that holds for the entire density range.

1.5 Benefit to the pharmaceutical industries

As has been mentioned earlier, tremendous loss is associated with tablet manufacturing when something goes wrong during batch production. Clearly if we can detect problems in manufacturing much earlier in the production process this will be very beneficial to the pharmaceutical industries.

Acoustic emission instrumentation and monitoring are relatively cheap in comparison with conventional destructive testing. This makes AE a favourable solution for on line process monitoring. On-line measurement and non-invasiveness are the characteristics of AE monitoring that no doubt have advantages over other techniques such as SPC or other statistical measurement.

1.6 Aims & Objectives of the research

From the literature survey conducted, it was evident that the most significant advances in tablet compaction research appear to have been made with the evolution of instrumentation used in powder compression e.g. presses. The methods used in tablet assessment together with the concurrent development in computer technology, have made possible accurate force and displacement measurements. This has enabled the researcher to characterise fully the complex physical changes occurring when materials consolidate. Force and displacement measurements are, however, only symptomatic of the process and much interpretation has to be applied to the generated data. Alternative approaches are required to directly characterise the material during compression and hence provide additional useful information about the process conditions. More than one approach was considered for this project. For example, the measurement of temperature, however, this was ruled out due to the fact that the mass of steel around the sample rapidly dissipates the heat generated by the tablet. The second approach is to use acoustic emission as a tool for characterising the

compression process. Preliminary experimentation showed that acoustic emission is very sensitive to the processes during tablet compression. Furthermore, the results obtained were very reproducible.

As this project focuses on tablet production, a wide range of investigation was conducted to examine the compression cycle of various pharmaceutical excipients and mixes of various tablet weights, particle sizes and compression speed.

1.6.1 Aim

The aim of this project is to develop a new methodology for monitoring powder compression during tabletting using acoustic emission as a non-destructive technique; and to characterise a number of pharmaceutical powders in terms of their acoustic emission behaviour. The ultimate aim is to develop a condition monitoring system for tablet quality and to detect capping and lamination in tablet manufacturing.

1.6.2 Objectives

In order to achieve the aims of this project the following objectives must be fulfilled:

1. To conduct a literature survey on previous attempts at tablet evaluation using non AE techniques.
2. To review the literature on acoustic emission theory, applications in the pharmaceuticals industry in general and powder compression in particular.
3. To monitor the acoustic emission signals that are generated from powder compression during tabletting.
4. To characterise the most common tablet excipients (fillers) in terms of their acoustic emission activity during compression.
5. To investigate the effect of compression conditions such as compression speed, particle size, tablet weight and type of material on the acoustic emission energy generated due to powder compression.
6. To propose a condition monitoring system that uses AE as on-line monitoring technique for industrial scale production of tablet processing.
7. To investigate the relationships between acoustic emission signals and tablet final properties such as hardness, dissolution and disintegration.
8. To propose a condition monitoring system for powder compression that can detect problems with tabletting such as capping and lamination.

1.7 Introduction to the Thesis

Chapter 2: describes the various attempts made by several researchers to solve problems in powder compression technology. This chapter includes an overview of some of the destructive methods used for testing the final tablet and assessing the powder before and after tablet production.

***Chapter 3*:** There are three sections in this chapter. The first section contains a review of the acoustic emission technique. It describes the basic principles of AE technology, instrumentation, wave propagation, type of AE signals and advantages of AE over other non-destructive testing techniques. The second section of this chapter describes the powder compression theory, compression cycle and various mechanisms occurring during tablet processing. The final section provides a review of the most significant AE applications in the pharmaceuticals industry and in powder technology.

***Chapter 4*:** This chapter describes in detail the design for the preliminary experimental investigation into AE in powder compression. It also provides brief descriptions of the instrumentation used in this project. The chapter also includes the details of experimentation and preparations for industrial testing at GlaxoSmithKline (GSK).

***Chapter 5*:** This chapter describes the results obtained from the experimental investigations made using the test rig at Brunel Centre for Manufacturing Metrology (BCMM). It provides an analysis of the effects of compression conditions such as speed, particle size and material weight on the AE signal generated during compression of a number of pharmaceutical powders.

***Chapter 6*:** This chapter describes the results obtained from monitoring powder compression using an industrial tablet press (Manesty F-press) at GSK. It reports the findings of AE monitoring for a common pharmaceutical powder during a typical compression cycle in the F-press. The chapter also provides a detailed analysis of the AE signal that is generated from various mechanisms during the compression cycle. The chapter also describes the implementation of the fuzzy C-mean clustering method which was used to discriminate between these mechanisms.

***Chapter 7*:** This chapter describes the proposed condition monitoring system for detecting capping in tabletting based on AE monitoring. A novel approach of condition monitoring that employs the receiver operating characteristic (ROC) was developed. Tablet prevalence and cost analysis which are related to the implementation of the proposed condition monitoring system are addressed in this chapter.

***Chapter 8*:** This chapter provides an a specification of the entire proposed condition monitoring system that can be implemented on-line for tablet quality and fault detection with reference to the key results in previous chapters. It describes the proposed condition monitoring system in terms of its sub-systems and provides guidelines for operation.

***Chapter 9*:** This chapter presents the conclusions, summarises the main findings of this research project and provides suggestions for further work that needs to be carried out in relation to this project.

References:

Ansel, H. C., Popovich, N.G., and Allen L.V (1995) Pharmaceutical dosage forms and drug delivery system. Sixth edition. Philadelphia; p 158-159, 182-184 & 200-202.

Aulton, M. E (2000) Pharmaceutics: the science of dosage form design. Edinburgh; Churchill Livingstone. 247-249, 304-305, 603-604, 654-655.

Jones T. M. (1983) Tablets, Tabloids ... and Tabloids. *Pharm. J*, Sept 17, 301-307.

Heistand H. E. N and Smith D. P (1984) Indices of Tabletting performance. *Powder Technology*, **38**, 145-159.

Alderborn G and Nystrom C (1996) Pharmaceutical Powder compaction technology. Marcell Dekker Inc., New York.

Macleod M.M and Marshall K. (1977) The determination of density distributions in ceramic compacts using autoradiography. *PowderTechnology*. **16**, 107-122.

Chapter 2 Assessment of Powder Compression

2.1 Introduction

This chapter provides a brief account of what has been done to solve problems which are related to hardness in tablet manufacturing. Various techniques and methods are discussed which dealt with powder compression and tabletting assessment. None of the techniques or methods involves acoustic emission work.

2.2 Physical properties of tablets

2.2.1 Stress distribution within compact

The finding by Shaxby and Evans (1923) that a loaded column of sand could be supported by cigarette paper led the authors to examine the variation of pressure within a column. They showed, experimentally, how lead shot and emery powder were supported by the sides of a column by measuring the pressure at the base of the column with successive increases in depth of powder. Their results indicated an exponential decay relationship of the pressure with increasing depth, showing that the pressure reached a limiting value. They also indicated that in a loaded column, the applied load would decay exponentially.

Train (1957) attempted to explain the complex stress distribution within compacts, see Figure 2.1. He aimed to evaluate the frictional effect of the column or die wall. Using gold chromium alloy (manganin) pressure gauges in a grid pattern in magnesium carbonate compacts, Train applied a range of forces with a hydraulic press. The pressure contours were found to be well correlated with the density distribution in the same compacts. To explain the distribution, Train first described the pressure built effect which is normally seen when applying pressure to an elastic solid and then proposed how this would be modified by the die wall. The work reported by Macleod and Marshall (1977) used autoradiography to measure the density of compressed ceramic materials. This work confirmed Train's finding. In addition, these authors went further to investigate the effects of the compact size, particle size and lubrication on the density distribution. Charlton and Newton (1981) proposed a similar method to examine the density distribution within compacts using gamma rays. Macleod and

Marshal (1977) found that the addition of a lubricant led to a more uniformly dense compact, an observation supported by the theoretical work of Hirai and Okada (1982). The density distributions in compacts observed by Train, Macleod and Marshall and Charlton and Newton were very similar, Figure 2.1. Interesting work done by Ridgway *et al* (1970), showed that Aspirin tablets were harder at the middle of the compact. They suggested that as Train had used a cylindrical compact this may be responsible and proposed a further type of distribution for a tablet which is thin in comparison with its diameter. They did not, however, directly link the outer hardness of the tablet with the inner density and may have observed the effect of work-hardening on the outer surface of the tablet. Aulton (1981), who also used a surface indentation technique, disputed the finding of Train for materials which are highly consolidated.

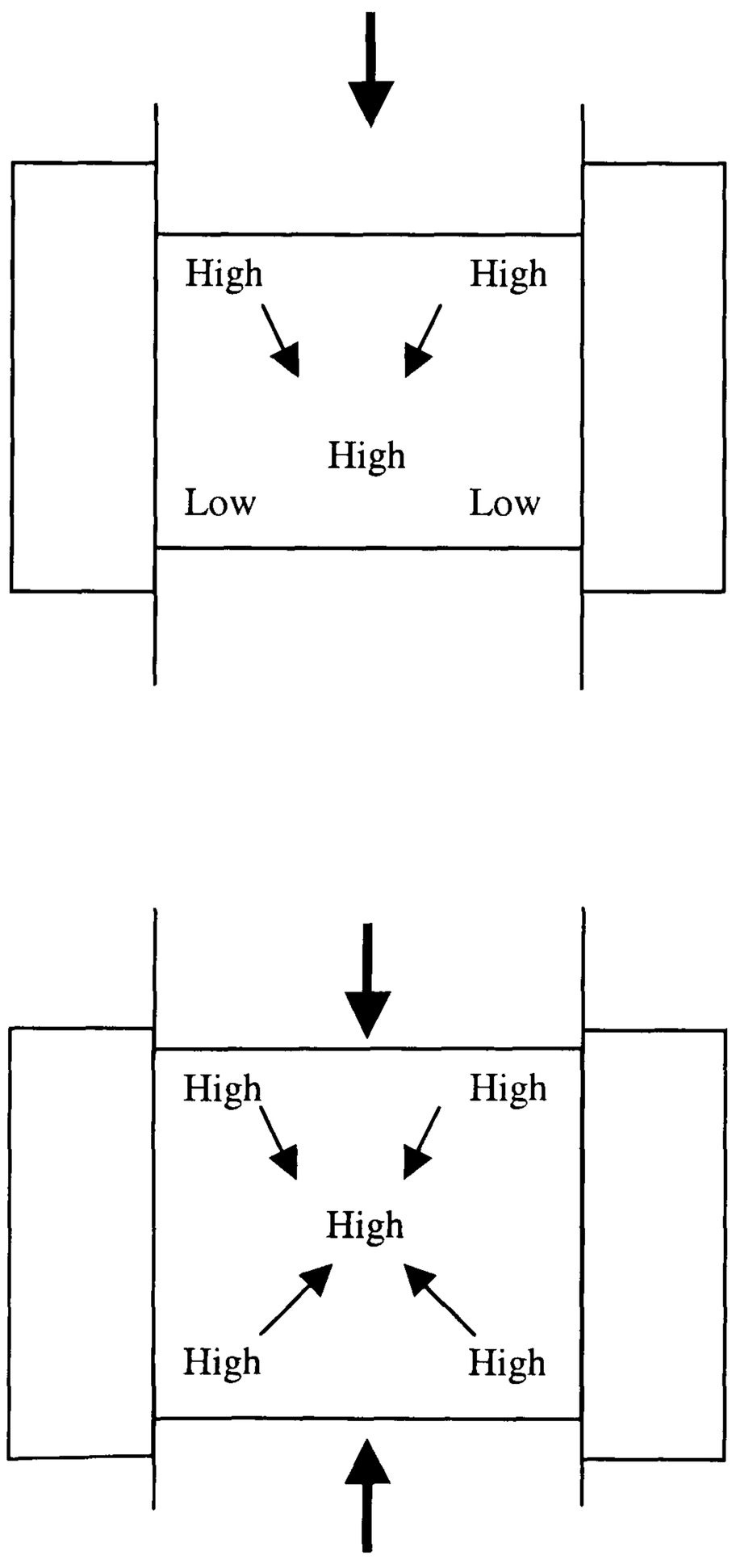

Single ended compaction
Train (1957)

Proposed double ended compaction
Ridgway *et al* (1970)

Figure 2.1. Stress distribution within a compact

2.2.2 Pressure cycle analysis

Carstenson and Toure (1980) described the pressure cycle as evolution of the Poisson ratio through the compression cycle. The Poisson ratio relates the radial expansion of cylinder to a compressive axial load. It is defined as the ratio of lateral strain, ε_1, to longitudinal stain ε_2.

$$\nu = \frac{\varepsilon_1}{\varepsilon_2} \qquad (2.1)$$

The relationship is commonly used when stressing solid materials to increase the sensitivity of the strain measurement systems. Carstenson and Toure (1980) recognised that the use of the Poisson ratio in porous powders was dubious; though they used the analogy of a solid material to show mathematically that the areas of the hysteresis loop of applied pressure versus die wall pressure were either a linear or quadratic function of the maximum applied pressure. This pressure depends on the type of material being compressed.

Windheuser *et al.* (1963) used a tabletting machine with instrumented upper punch and die wall to examine the applied pressure and die wall pressure for a range of materials. Although the die wall pressure during decompression was not measured, they proposed that materials, which permit good conversion of applied pressure to radial pressure, tended to form robust tablets. This finding was confirmed by Obirah (1978). They showed experimentally that a robust tablet has greater initial slopes and higher residual die wall pressures. However, Obirah did not, quantitatively, assess the tablets produced. Paracetamol, a material which is well known for its poor compressibility, exhibited the lowest initial slope.

2.2.3 Tensile strength and Hardness evaluation:

Tablet crushing strength is the most common method of assessing the physical properties of a tablet. This can be by measuring its crushing strength when a compression force is applied. This technique does not, however, take into account the size of the compact.

The tensile strength of a powder bed (such as a tablet or a powder compact) is a characteristic of the internal friction or cohesion of the particles. But unlike shear strength determinations, the powder bed fails in tension as a result of splitting, as opposed to shear which is caused by sliding (Aulton, 2000).

One method used to investigate powder compactability is by subjecting the compressed tablets to mechanical testing. The mechanical strength of tablets has been measured in a variety of ways, including diametral breaking strength, indentation hardness and friability measurement.

The most widely used test for characterising tablet properties is the diametral crushing test. The crushing strength of a tablet may be defined as the maximum force which, when applied diametrically to a tablet, results in a tablet fracture at right angle to the plane of the force applied. The tablet under test is placed against a fixed metal anvil and a moving anvil applies the force to the other side of the tablet until the tablet breaks, see Figure 2.2. As the crushing strength depends on the tablet dimensions, it is difficult to compare the strengths of tablets of different sizes. To overcome these problems, Fell and Newton (1970a) introduced the concept of tablet tensile strength (σ), defined as:

$$\sigma = \frac{2P}{\pi DT} \qquad (2.2)$$

where,

P is the applied load that causes tensile failure; D and T are the tablet diameter and thickness, respectively.

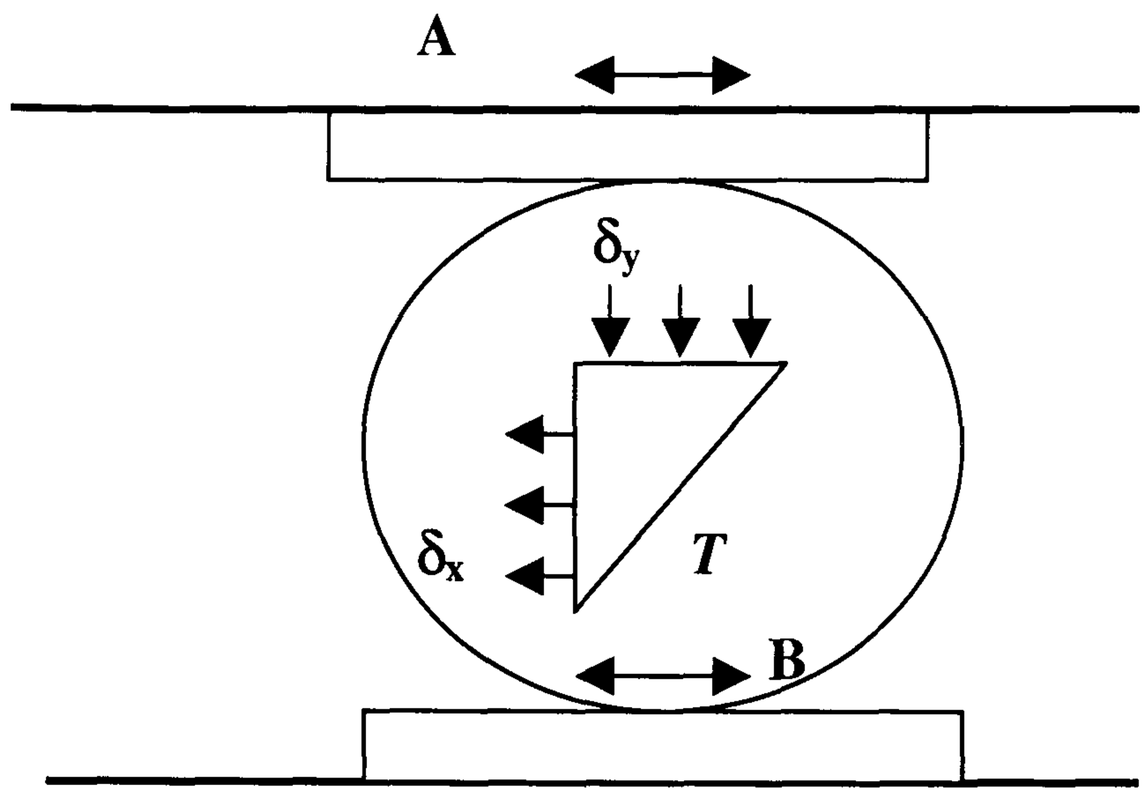

Figure 2.2 Tensile stress (δx), compressive stress (δy) and shear stress (*T*) on a tablet undergoing tensile testing. A and B are areas of contact between the tablet and metal anvils.

To ensure that the tablets fail in tension, they padded the jaws with various materials. Tensile failure was indicated by a single break normal to the jaws of the test. Ridgeway (1970). Hiestand and Peot (1974) observed the effect of crushing square tablet. They found that the size of the jaws to be critical indicating that if jaws larger than the tablets were used, the tablet was likely to fail in compression.

As a method of assessing the hardness of tablet, Rees and Rue (1977) proposed the concept of 'work of failure'. Their method involved not only measuring the applied crushing force but also the displacement of the jaws prior to failure using a displacement transducer. The work of failure is the integral of the crushing force/displacement profile.

Another method of assessing tablets has been to simulate test carried out by tablet machine operators, which involve breaking the tablet between the thumb and fingers, the so-called flexure test. Ritter and Sucker (1980) designed a system with two anvils fitted to a tablet 'hardness' tester, Figure 2.3. Gold and others (1980) used a similar method for measuring the flexure strength of capsule-shaped tablets.

The friabilator provides another measure of tablet toughness. Consisting of a rotating drum in which the tablets are lifted and dropped, it can usefully measure shocks that

tablets may incur during packaging and transport. The method is quantified by expressing the weight of eroded material as a percentage of the total weight of tablet. The friabilator is also used for determining the tendency of tablet to cap or laminate. As tablet compaction is a feature of time dependent process and because these processes are likely to continue, post compression, it is important that any comparison of the physical properties of tablets is made at similar time periods.

More recently, evaluation of the compact has been used to elucidate properties of the material, particularly the elastic modulus which can be evaluated using a rectangular compact (Bassam *et al*. 1988) or a cylindrical compact (Robert *et al*. 1989).

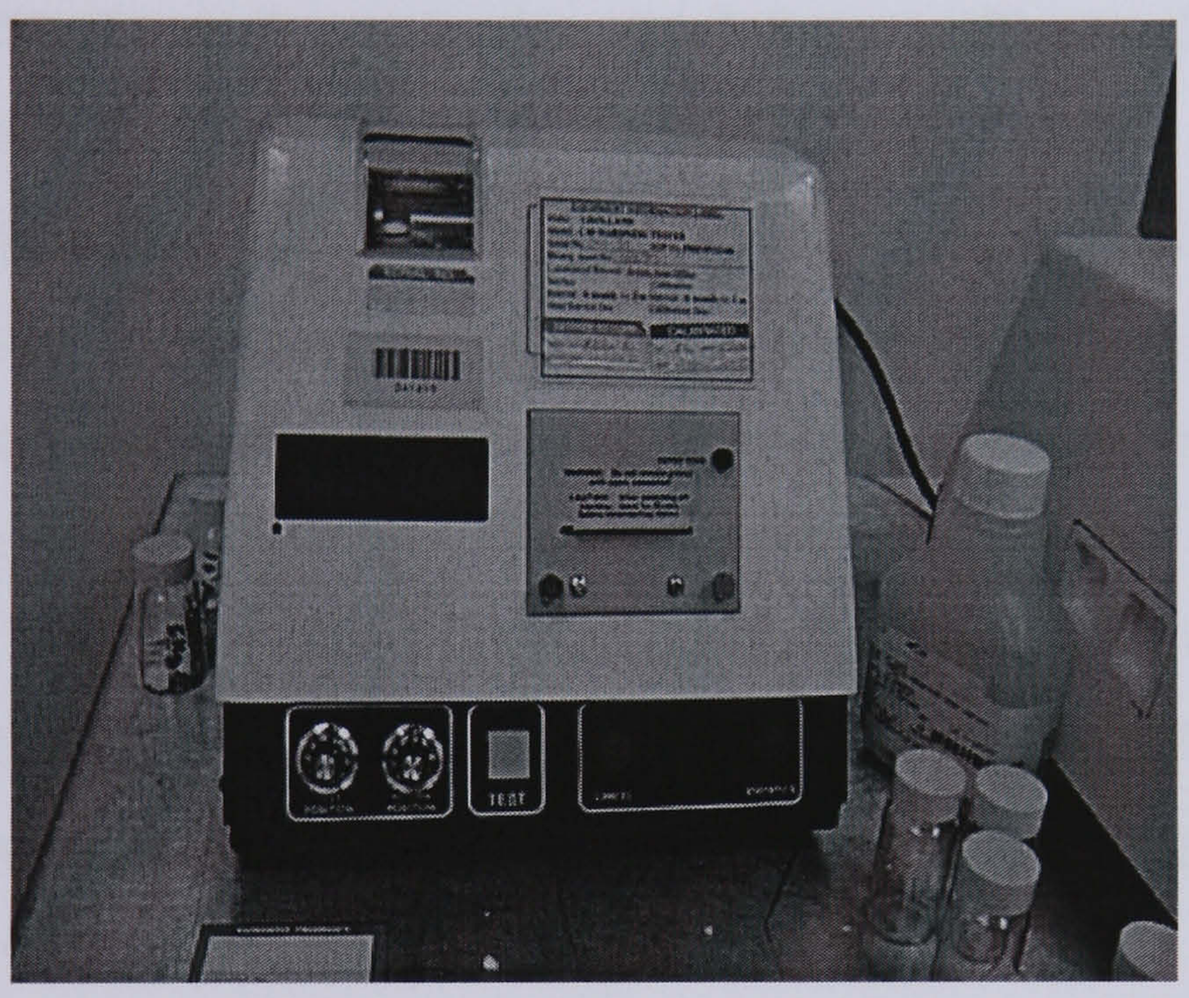

Figure 2.3 Tablet tester

2.2.4 Tablet disintegration

Commercially disintegration and dissolution apparatus is available. Most pharmacists do not have this equipment. However, a simple disintegration apparatus can be made. Start by supporting a 10 mesh screen about 50 mm (2 inches) above the bottom of a 1000 ml beaker. Fill the beaker with 1000 ml of water, add a stirring bar, and place the beaker on a magnetic stirring plate. Stir at a moderate speed. Drop the tablets onto the mesh screen and record the time needed for the tablets to disintegrate. A reasonable disintegration time is usually between 15 and 30 minutes, although the time will depend on the product, the stirring speed, etc.

2.2.5 Tablet dissolution

Disintegration time determination is a useful tool for production control, but disintegration of a tablet does not imply that the drug has dissolved. A tablet can disintegrate rapidly yet be biologically unavailable. The dissolution rate of the drug from the primary particles of the tablet is the important factor in drug absorption and for many formulations is the rate-limiting step. Therefore, a dissolution time is more indicative of the availability of a drug from a tablet than the disintegration time. Although this is an important parameter to measure, most pharmacies do not have the equipment needed to conduct these kinds of tests.

2.2.6 Mechanical properties related to stiffness: Determination of Young's Modulus

Tensile strength has been the most common property used to describe the strength of compacts, but tensile strength values alone are not sufficient to fully characterise a material's mechanical properties. The stress-strain behaviour of a material has been used to measure the toughness and stiffness of compacts.

Young's modulus, E, defined as the ratio of stresses, σ, to strain, ε, describes the stiffness of a material. Young's modulus of Avicel PH-101 has been determined using the four-point flexure test (Church and Kennerley, 1982). In such an arrangement the tensile stress σ and the associated strain ε are:

$$\sigma = \frac{3Wa}{2bd^2} \qquad (2.3)$$

$$\varepsilon = \frac{4\delta d}{k^2} \qquad (2.4)$$

where δ is the vertical displacement of the midpoint of the beam and k is the distance between the loading points on the upper surface of the beam, W is the applied load, a,b and d are the bending points. It was demonstrated that Young's modulus increases as the porosity decreases. Determination of Young's moduli for a range of pharmaceutical excipients demonstrated that there is no relationship between Young's modulus and the tensile strength of a material (Church and Kennerley, 1983).

2.2.7 Work of Failure

The diametral compression test has also been used to measure the 'toughness' of compacts, (Rees *et al.* 1977). In this case, the change in length of the loaded diameter was monitored throughout testing. Force values and the corresponding change in diameter were recorded. The product of these values, the area under a force-displacement curve, is called the work of failure, W_f,

$$W_f = \int P dx \qquad (2.5)$$

where dx is the rate of change of distance x and P is the applied load.

Tablets with a high work of failure were considered to deform plastically under compressive loading, thus requiring a relatively large platen displacement to produce failure while brittle materials require only a small displacement to produce failure. Since most specimens fail in tension during the diametral compression test, a further property, the normalised work of failure (NWF), was introduced to convert the applied load P to tensile stress:

$$NWF = \frac{2}{\pi D t} \int P dx \qquad (2.6)$$

where D is the diameter of tablet.

2.2.8 Indentation Hardness

While tensile strength describes the global strength of a specimen, indentation hardness test describes the "local" plasticity of a material deformation, and is usually measured by non-destructive indentation or scratch test.

The most widely used methods in determining hardness are static indentation methods. These involve the formation of a permanent indentation on the surface of the material to be examined, see Figure 2.4. Usually the diameter of the impression is first determined and, from it, the hardness is calculated by means of the following formula:

$$BHN(Q) = \frac{2W}{\pi D_i (D_i - \sqrt{D_i^2 - d_i^2})} \qquad (2.7)$$

where

W applied load

D_i diameter of the spherical indenter

d_i diameter of the indentation

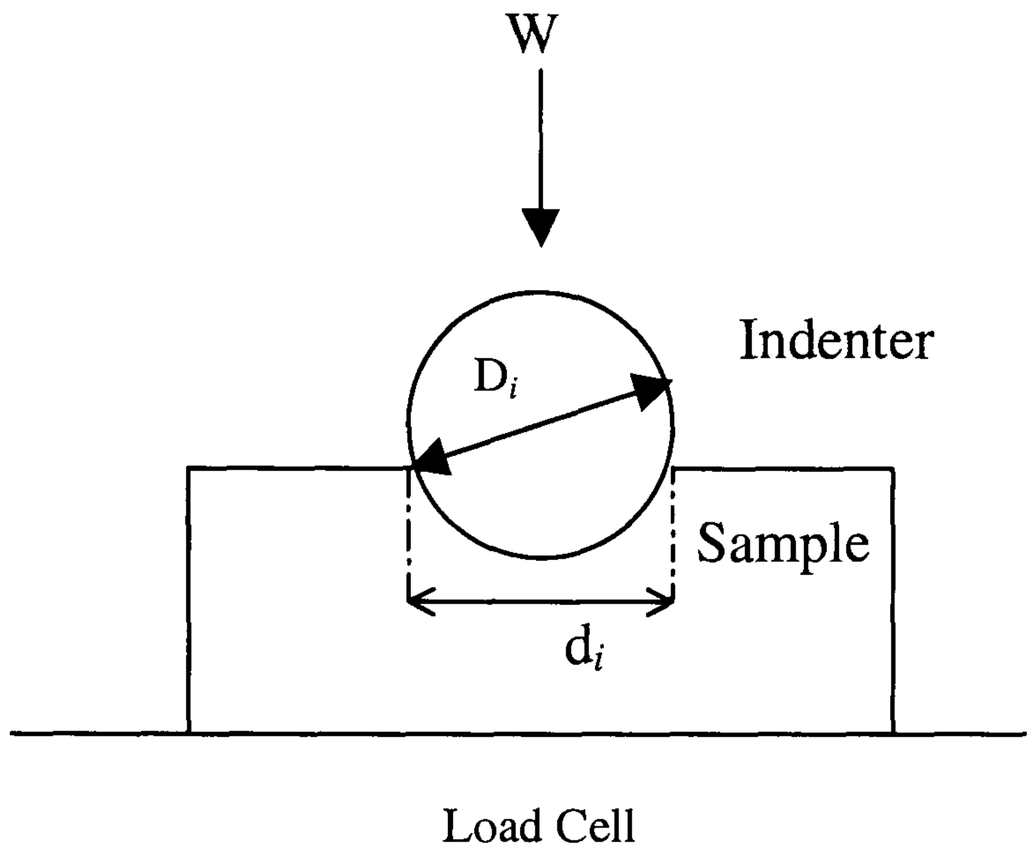

Figure 2.4 Indentation test

The Brinell hardness number (BHN) is not an intrinsic property for a material but depends on the load and the diameter of the indenter (Leuenberger and Rohera, 1986). The method has been used to determine the hardness at various points across the diameter of aspirin compacts (Ridgway *et al.* 1970) and direct compression excipients (Aulton *et al.* 1974). Studies on the surface hardness distribution over tablet faces with different face curvatures indicated that, as the degree of curvature increased, the hardness of the outer portions of the compact increased relative to the centre of the compacts (Aulton *et al.* 1973).

2.2.9 Powder flow properties

When examining the flow properties of a powder, it is useful to be able to quantify the type of behaviour and many different methods, either directly, using dynamic or kinetic methods, or indirectly, by measurements carried out on static beds (Aulton, 2000) have been described.

2.2.9.1 Indirect methods

1. Angle of repose

The angle of repose is a relatively simple technique for estimating the flowability of a powder. It can be easily determined experimentally by allowing a powder to flow through a funnel and fall freely onto a surface. The height and diameter of the resulting cone is measured and using the following equation, the angle of repose Φ, can be calculated by:

$$\tan \Phi = \frac{2H}{B} \qquad (2.8)$$

where

H is the height of the powder cone

B is the diameter of the powder cone

Powders with low angles of repose will flow freely and powders with high angles of repose will flow poorly. A number of factors, including shape and size, determine the flowability of powders. Spherical particles flow better than other particle shapes. Very fine particles do not flow as freely as large particles. In general, particles in the size range of 250-2000 μm flow freely. Particles in the size range 75-250 μm may flow freely, depending on their shape and other factors. With particle less than 100 μm in size, flow is a problem with most substances (Ansel, 1995).

Aulton *et al.* (2000) examined a large number of pharmaceutical powders and produced a qualitative measure of the flowability based upon their angle of repose. Table 2.1 shows the ranges of angle of the reposes and the corresponding class of flowability.

Table 2.1. Angle of repose as an indicator of powder flow properties

(Aulton, 2000)

Angle of repose (°)	**Type of flow**
< 25	Excellent
25-30	Good
30-40	Passable
>40	Very poor

2.2.9.2 Bulk density

Neumann (1967) and Carr (1965) developed a simple test to evaluate flowability of a powder by comparing the poured (fluff) density ($\rho_{B\ min}$) and tapped density ($\rho_{B\ max}$) of a powder and the rate at which it is packed. A useful empirical guide is given by the Carr's compressibility index. Here 'compressibility' is a misnomer since compression is not involved.

$$\text{Carr's Index} = \frac{\textit{Tapped density} - \textit{Poured density}}{\textit{Tapped density}} \times 100 \qquad (2.9)$$

This simple index can be determined on small quantities of powder and may be interpreted as shown in Table 2.2.

Table 2.2. Carr's index as an indication of powder flow properties

(Aulton, 2000)

Carr's Index (%)	**Type of flow**
5-15	Excellent
12-16	Good
18-21	Fair to passable
23-35	Poor
33-38	Very poor
>40	Extremely poor

2.2.9.3 Direct method: Flow rate

The simplest method of determining powder flowability directly is to measure the rate at which powder discharges from a hopper or a flow tube, Neumann (1967). A simple shutter is placed over the hopper outlet and the hopper is filled with powder. The shutter is then removed and the time taken for powder to discharge completely is recorded. By dividing the discharged powder mass by this time, the flow rate is obtained which can be used for quantitative comparison of different powders.

Hopper or discharge tube outlets should be selected to provide a good model for a particular flow application. For example, if a powder discharges well from a hopper into a tablet machine feed frame, but does not flow reproducibly into the tablet die, then it is likely that more useful information will be generated by selecting experimental conditions to model those occurring in flow from the feeder to the die rather than in flow from the hopper to the feeder.

2.2.10 Plastoelasticity (ER/PC) ratio

When a material is subjected to compression, the deformation process takes place in two phases: elastic and plastic deformation. After forming the final compact, the material springs back and recovers some volume, Parikh(1997). Elastic recovery (ER) can be expressed as:

$$ER = \left(\frac{H_o - H_t}{H_t}\right) \times 100 \qquad (2.10)$$

where

H_o = thickness of the tablet after the ejection from the die

H_t = thickness of the tablet at the end of the holding time

As can be seen in Figure 2.5.

Also plastic compression can be defined as

$$PC = \left(\frac{H_P - H_t}{H_t}\right) \times 100 \qquad (2.11)$$

where,

H_p = thickness of the tablet at the maximum force applied in the compression

The ratio ER/PC is called the plastoelasticity ratio.

In a previous investigation, Itiola and Pilpel (1986) showed that ER/PC values provide an inverse measure of the bond strength of the tablets.

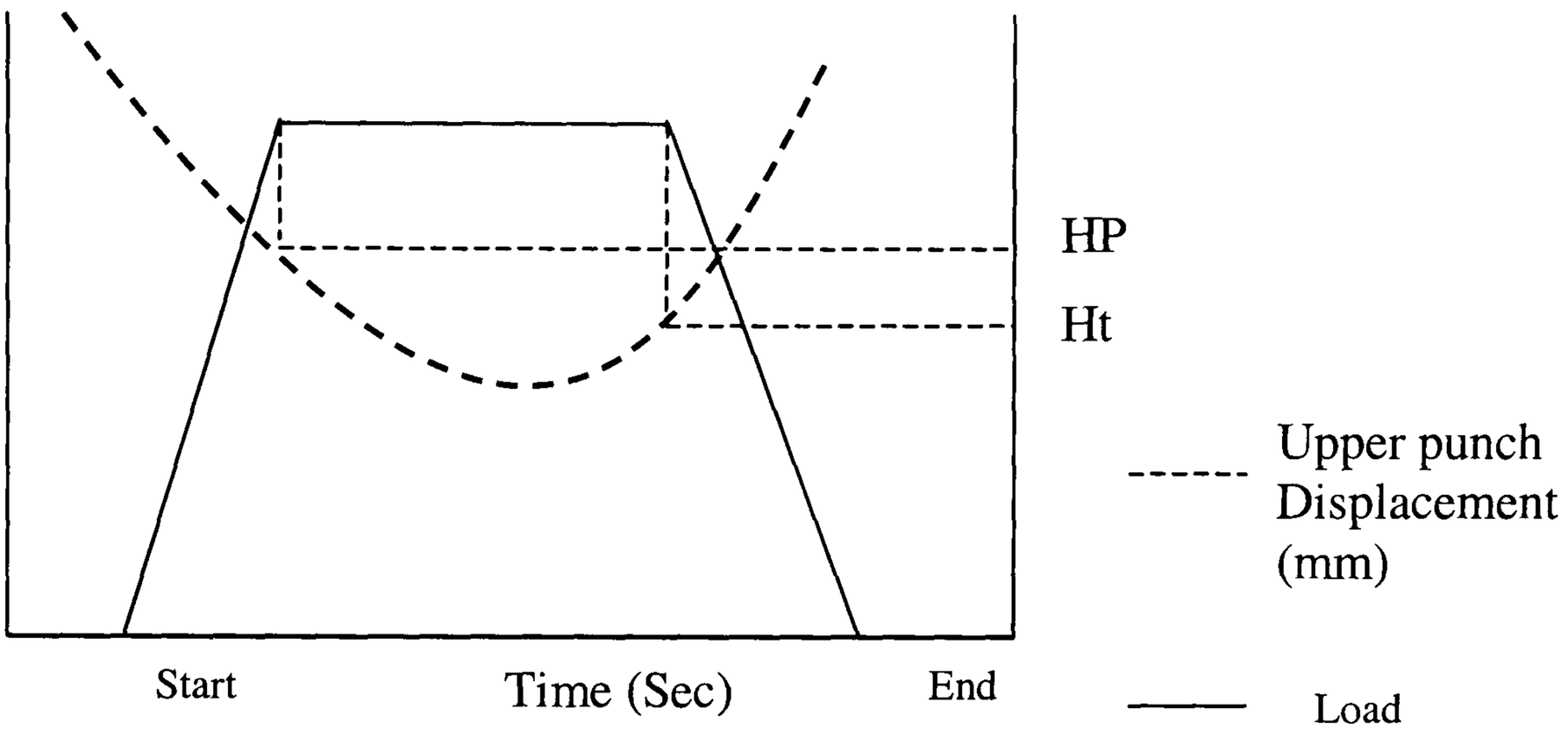

Figure 2.5 Schematic representation of load-time and displacement-time profiles.

2.2.11 Force-Volume relationships:

Kawakita and Ludde (1970) extensively reviewed a large number of compaction equations. Compaction equations are used to describe the density-pressure relationships of powder compaction. Since the first compaction equation (Walker, 1923), more than 2 different compaction equations have been proposed of which the most widely used equations are:

1. Balshin equation

$$\ln P = \frac{C_1}{D} + C_2 \qquad (2.12)$$

2. Heckel equation

$$\ln \frac{1}{1-D} = C_3 P + C_4 \qquad (2.13)$$

3. Kawakita equation

$$\frac{D}{D-D_o} = \frac{C_5}{P} + C_6 \tag{2.14}$$

In these equations,

P = applied pressure

D = relative density of compact

D_0 = relative density of loose powder at zero pressure

C_1 to C_6 = constants

Balshin's equation (Heckel, 1961a-b) is relatively insensitive to variations in pressure values at the high range of pressure. The equation describes the compaction of non-metallic powders better than metallic powders. Heckel's (1961-a, 1961a-b) and Kawakita's equations (1965, 1966, 1970) have been shown to be applicable to both metallic and non-metallic powder.

Ge (1991) developed a new compaction equation which gave improved accuracy when compared to the previous equations. The equation is given as:

$$\log\left[\ln\frac{(1-D_0)}{(1-D)}\right] = a\log P + b \tag{2.15}$$

where a and b are constants.

If 1/D is plotted against ln(P) for Balshin's equation, ln(1/(1-D)) against P for Heckel's equation, $D/(D-D_0)$ against 1/P for Kawakita's equation, and $\log[\ln\{(1-D_0)/(1-D)\}]$ against log(P) for Ge, each of the equations will give a straight line relationship.

2.2.11.1 Heckel plot

Heckel analysis (see appendix B3) assumed theat the compaction of powders is considered to be analogous to a first-order chemical reaction, the pores being the reactant and the densification of the bulk of the product, the "kinetics" of the process may be described by a proportionality between the change in density with pressure and the pore fraction. A schematic diagram of a Heckel plot based on the Heckel equation is shown in Figure 2.6. The initial curved region is due to densification as a result of particle slippage and rearrangement. The inner region at higher pressures is a result of deformation of particles. From B, the point where the Heckel plot intercepts the ln(1/(1-D)) axis, the density of powder at zero pressure, D_0 can be obtained. D_0 can be defined as the densification due to the filling or to initial powder packing.

From the intercept of the linear portion of the Heckel plot, A, the total densification of a powder bed due to die filling and particle slippage and rearrangement D_a may be obtained from the following equation:

$$A = \ln\frac{1}{1-D_0} + B \qquad (2.16)$$

where B describes the volume reduction purely due to particle rearrangement. The relative densities corresponding to the processes above are D_A, which includes both die filling and particle rearrangement, and D_B, which describe only the extent of particle rearrangement.

The relative densities can be related by the equation

$$D_A = D_0 + D_B \qquad (2.17)$$

and D_A may be calculated from

$$A = \ln\frac{1}{1-D_A} \qquad (2.18)$$

In his original work Heckel (1961) studied the densification of metal powder. The slope, *k*, of the Heckel plot was intended to give a measure of the plasticity of a compressed material. Consequently, greater slopes indicated a greater degree of plasticity of material. The slope was also related to the yield strength, *Y*, of the material by the equation:

$$k = \frac{1}{3}Y \qquad (2.19)$$

Hersey and Rees [1971] later defined the reciprocal of *k* to be the mean yield pressure, P_y, in order to study whether fragmentation of particles was the predominant compaction mechanism of powders.

The extent of particle slippage and rearrangement, D_B, is determined by subtracting D_0 from D_A . The values of D_0 , D_A and D_B may depend on the shape and size of the particles (Heckel, 1961-b; York, 1978), the rate of force application (Roberts and Rowe, 1987; Bateman, 1988) and moisture content (Nokhodchi, 1996).

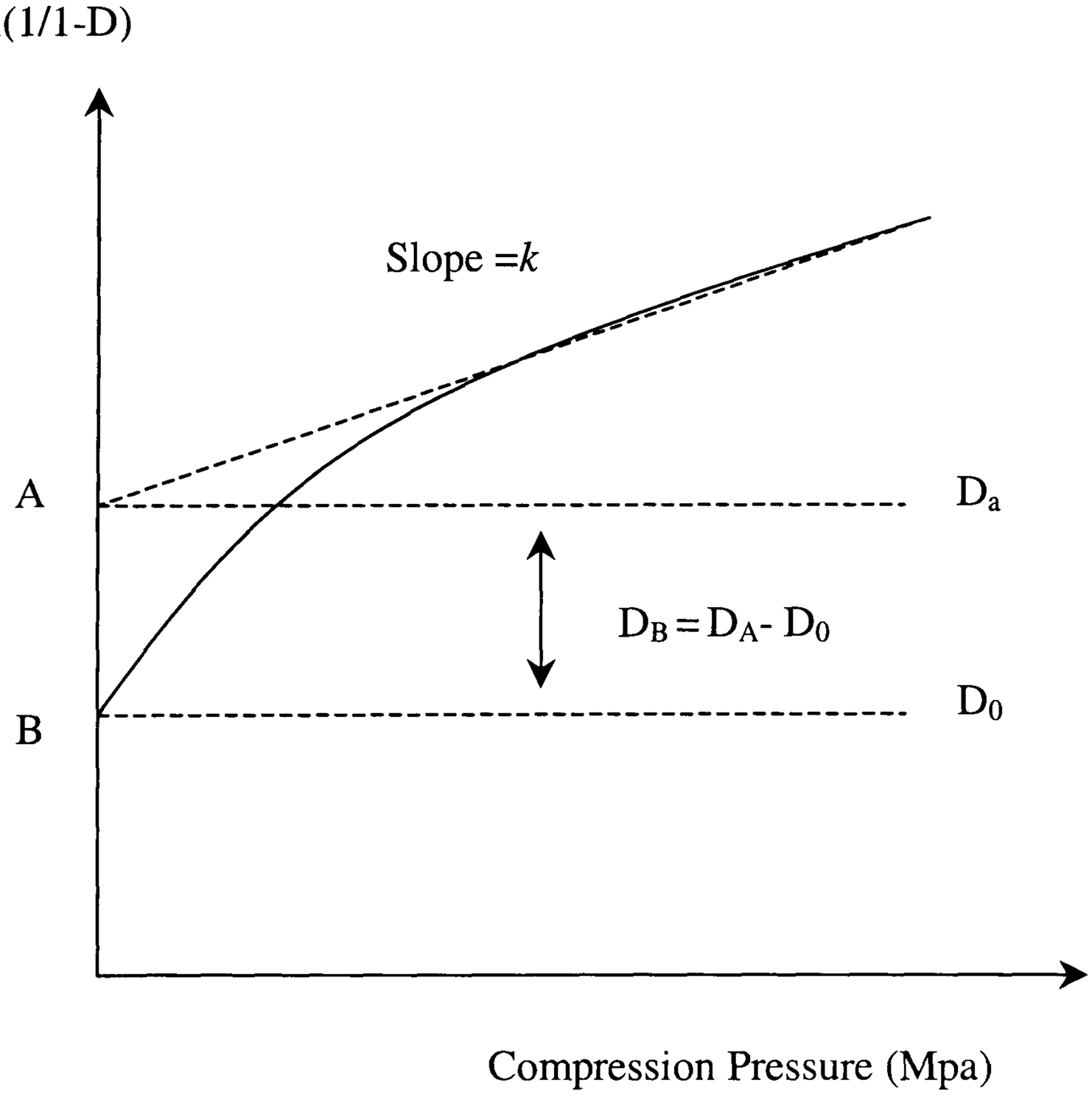

Figure 2.6 Schematic representation of Heckle plot.

The constant k is the slope of the straight line region of the Heckel plot and the reciprocal of the slope k is known as the mean yield pressure, which is related to the ability of a material to deform plastically under pressure (Hersey and Rees, 1970). Low values of mean yield pressure reveal the ability of material to deform plastically and high values are indicative of brittle materials (Humbert-Droz 1983).

2.3 Conclusion

This chapter provided an overview of several attempts which have been made to evaluate the final tablet quality and hardness. All these techniques are destructive, in the sense that the final tablet must be destroyed by one way or another in order to complete the evaluation task.

The choice of method used to determine the mechanical strength of pharmaceutical compact should relate to the required information. If the information is required for in-process control, it is preferable to provide a system which is reproducible and accurate with sufficient sensitivity to identify the differences between tablets. Several types of instruments are available. However, most simply crush the tablet and do not allow the assessment of the mode of failure of the tablet. The variable mode of failure could, however, allow such variations which are not directly related to the properties of the tablet. Simple crushing of tablets of complex shapes can be misleading. If well-controlled breaking with a consistently known mode of failure can be induced, the need for complex evaluation of poor-quality systems, as described by Bavitz et al. (1973), would be eliminated. There are instruments which can produce this consistent mode of failure and are adaptable for different shapes. When applied to the fundamental understanding of compaction mechanisms or characterisation of the mechanical properties of materials, then only tests which are fundamentally sound are acceptable. Even here there still remain some problems.

To perform tests, the powders have to be first compacted. The process of preparation is influenced by the mechanical properties of the material. Hence the final test procedure is an assessment of the mechanical properties of a specimen compounded by its method of formation. For example, the tensile strength of different quantities of

lactose at a range of formation pressures was found to depend on the sample weight (Newton *et al.* 1971). Subsequent characterisation of the tablet formation process by the area under the pressure/time curve rather than the maximum formation value provided a better comparison of tensile strength values for the different quantities of material (Newton and Rowley, 1972).

There does not appear, as yet, to be a single method of material characterisation which adequately describes the ability of material to form tablets. Hence a range of properties, as suggested by York (1992), would appear to be more appropriate.

Reference:

Ansel, H.C., Popovich, N.G., and Allen L.V (1995) Pharmaceutical dosage forms and drug delivery system. Sixth edition. Philadelphia; p 158-159, 182-184 & 200-202.

Aulton, M. E. (1981) Effect of compaction pressure and punch curvature on the indentation hardness profiles of some compressed tablet. *Pharm. Acta Helv.*, **56**, p 332-336.

Aulton, M.E (2000) Pharmaceutics: the science of dosage form design. Edinburgh; Churchill Livingstone. P 247-249, 304-305, 603-604, 654-655.

Bassam F, York P, Rowe R.C., and Roberts R.J (1989) Prediction of Young's Modulus of binary mixtures. *J. Pharm. Pharmacol.* **41**, (12) p29.

Bateman, S. D. (1988) the effect of compression speed on the properties of comacts. Ph.D thesis. School of pharmacy, Liverpool polytechnic, UK.

Carstensen J. T. and Toure P. (1980) Compression Cycles in tabletting . *Powder technology*, **26**, 199-204.

Charlton B. and Newton J. M. (1984) Theoretical estimation of punch velocities and displacement in single punch and rotary tablet machines. *J. Pharm. Pharmacol.* **36**, 645-651.

Fell, J.T and Newton, J.M (1970a). *Journal of pharmacy and pharmacology*, **22**, 247.

Fell, J.T and Newton, J.M (1970b). Determination of tablet strength by the diametral compression test. *Journal of pharmaceutical Science*. **59**,688-691.

Gold G., Duvall R. N. and Palermon B. T. (1980) New instrumentation for determining flexure breaking stress of capsule-shaped tablets. *J. Pharm. Sci.* **69** (4), 384-386.

Hersey, J.A and Rees, J.E (1970). 2nd particle size analysis conference, *Society for Analytical chemistry*, Bradford. P 33-41. Proceedings S.A.C.

Hirai Y., and Okada T (1982) Caculated stress and strain condition of lubricating KCl powder during die compression. *Chem. Pharm. Bull*, **30**, 202-207.

Humbert-Droz, P. (1982) Analyse des caracteristiques de compression des substances medicamenteuses en relation avec le phenomene de dissolution. Doctorat es sciences, Faculte des Sciences, University of Geneva, Swithzerland.

Itiola, O. A and Pilpel, N. (1986) *International Journal of Pharmacy*. **31**, 99-105.

Kawakita, K and Ludde, K. H (1970). Some considerations on powder compression equations. *Powder Technology*, **4**, 61-68.

Macleod M.M and Marshall K. (1977) The determination of density distributions in ceramic compact using autoradiography. *Powder technology*. **16**, 107-122.

Neumann, B. S (1967) Advance Pharmaceutical Science, 2, 181-220. Academic Press, London.

Nokhodchi, A. (1996) The compaction properties of hydroxy-propyl methylcellulose and Ibuprofen. Ph.D thesis, School of pharmacy and chemistry, Liverpool John Moores University, UK.

Obirah B. A. (1978) Possible prediction of compression characteristics from cycle plots. *Int. J. Pharm.* **1**, 249-255.

Parikh, D. M. ed. (1997): Handbood of Pharmaceuitcal Granulation Technilogy. New York: Marcel Dekker, Inc. p 100-235.

Rees J. E. and Rue P.J. (1977) Work required to cause failure of tablets in diametral compression. Expo.Congr. *Int. Technol. Pharm.* 1st , **5**, 85-97.

Ridgway K (1970) Testing tablet by diametral crushing. Pharm. J. Dec. 26th , 709-712.

Ridgway K., Aulton M. E. and Rosser P. H (1970). The surface hardness of tablets. *J. Pharm. Pharmacol*, **22**, Suppl. 70s-78s.

Ritter A. and Sucker H. B. (1980) (1) Studies of variables that effect tablet capping. *Pharm. Tech*. March 57-65 and 128.

Roberts R. J., Rowe R. C. and York P. (1989) A dynamic mechanical method for the determination of the Young's modulus of powdered drugs and excipients, *Journal of pharmacy and pharmacology*, **41** (12) p 30.

Roberts R.J and Rowe, R. C (1987) *International journal of Pharmaceutics*, **36**, 205-209.

Shaxby J. H. and Evans J. C. (1923) The variation of pressure with depth in columns of powder. *Trans. Farad. Soc.* **19**, 60-72.

Train D. (1957) Transmission of Forces through a powder mass during the process of pelleting. *Trans. Instin. Chem. Engres.* **35**, 258-266.

Windheuser J.J, Misra J., Eriksen S. P. and Higuchi T (1963) Development of die-wall pressure during compression of materials. *J. Pharm. Sci.* **52**, 767-772.

Chapter 3

Literature review

3.1 Acoustic emission

3.1.1 Definition of AE

Acoustic emissions are transient elastic waves generated by the rapid release of energy from localised sources within a material, (McIntire, 1987). These elastic waves can be detected by microphones or transducers attached to the surface of the specimen. When a material undergoes deformation it releases elastic energy as AE. Transient elastic waves propagate through the material as a result of this rapid energy release. An array of resonant piezoelectric sensors, mounted on the surface of the material is used to detect these waves. When a wave 'hits' the sensor this causes the output signal from the sensor to rise above a threshold level. Various attributes of the signal are measured: number of times the signal rises above the threshold, time between the first and last crossing of the signal above the threshold and the signal strength.

When a solid is subjected to stress at a sufficient level, sound is generated in the material and emitted in discrete pulses. This is called acoustic emission as it has been mentioned earlier in this chapter or stress wave emission (SWE) (Scruby, 1985; Halmshaw, 1987; Raj and Jha, 1994). The emission originates, basically, when a body suddenly deforms locally and releases local stresses. A burst of elastic energy is then emitted. Such emission can come from several phenomena, e.g. from grain boundaries sliding over one another during stressing, plastic deformation, inclusion cracking, crack initiation and crack growth, etc. External factors such as mechanical impact, friction, machinery vibration, and welding operations, can also produce acoustic emission (Halmshw, 1987; Raj and Jha, 1994).

The application of AE methods can be in several ways (Lenain, 1981): (1) as an investigative technique to assist in understanding the behaviour of materials, e.g. rupture, yielding, fatigue, corrosion, creep, rock mechanics, (2) as an NDT technique during manufacturing processes, e.g. phase transformation, detection of

defects (pores quenching cracks, inclusion, etc.), (3) monitoring structures, e.g. leak detection, periodic testing (pressure vessels, pipelines, bridges, etc.) and (4) for special application, e.g. in petrochemical (storage tanks, reactor vessels, offshore platforms, drill pipe, etc.), in aircraft and aerospace (fatigue cracks, corrosion, etc.).

3.1.2 AE as NDT technique

Acoustic emission is a powerful technique for non-destructive testing (NDT) and material evaluation. AE is a passive technique. The growing defect generates signal that travels to the detecting sensors. The main benefits of AE compared to other NDT methods are that AE is a real time method and it is less intrusive. The discontinuities of defects can be detected by AE at an early stage of formation and growth. AE techniques can be used as a warning system before the tested material is severely damaged. AE requires access only at sensors while most other NDT techniques require access to entire regions inspected.

Much of the early work concentrated on metals, but more recent work has been of wider scope, covering composites (Arrington, 1987), plastics, ceramics (Schuldies, 1973; Sklarczyk, 1992), rock (Boyce, 1981; Atkinson and Rawlings, 1981), refractories (Konsztowcz, 1990), and concrete (Arrington and Evans, 1977). Only recently, the technique has been applied to a number of pharmaceutical applications (Belchamber *et al.* 1986, Hakanen and Ensio 1993, Salonene *et al.*1997, Whitaker et al 2000).

The principle of the AE technique as an NDT method is shown in the block diagram of Figure 3.3. Acoustic emissions are detected by a transducer which is fixed on the surface of the specimen which in turn generates electrical signals. The signals, after being amplified and filtered, are usually converted into digital data, but can equally be displayed on a digital oscilloscope.

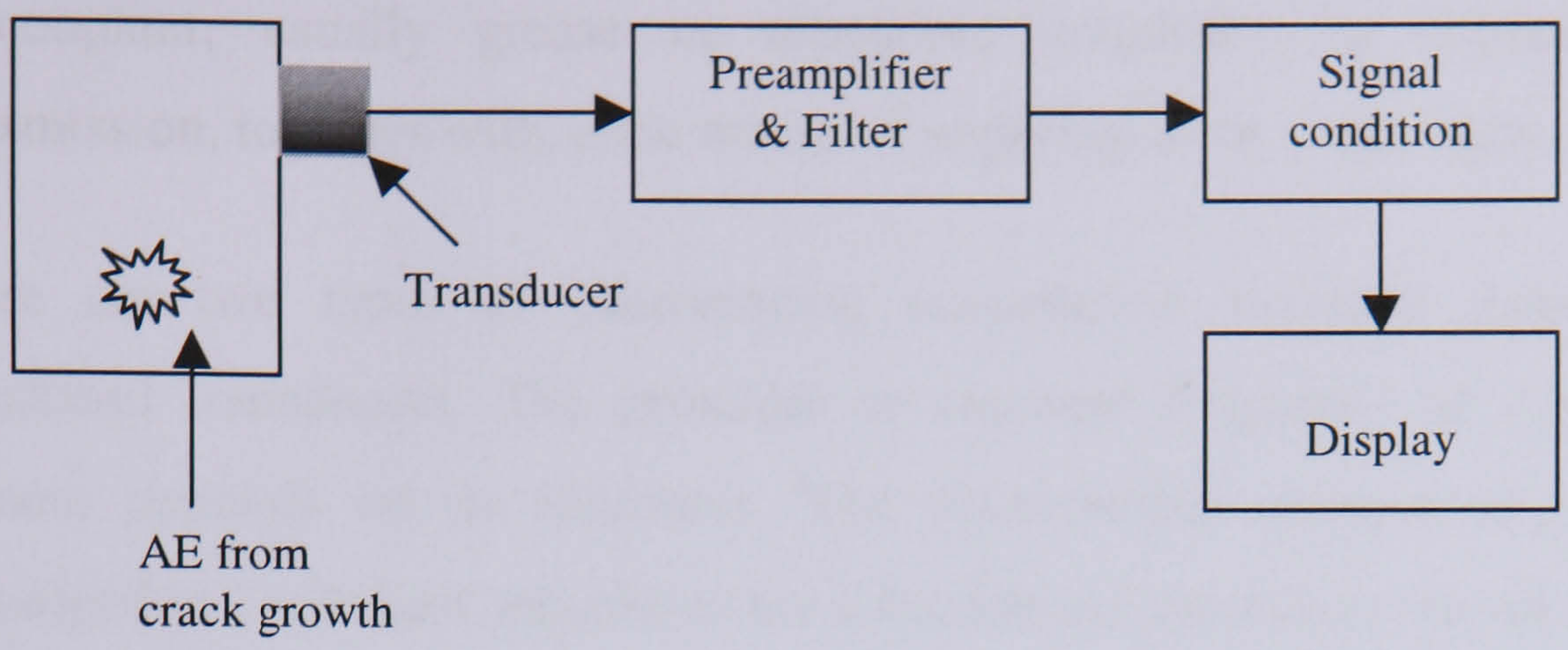

Figure 3.1: Block diagram of basic acoustic emission equipment

There are, of course, numerous NDE techniques, such as radiography, acoustic (ultrasonic, acoustic emission, acoustic ultrasonic), optic, dye-penetrant. However, all are not suitable for brittle materials or pharmaceutical powder. The acoustic emission technique is applicable to brittle materials (e.g. ceramic, lactose) because the high frequency of acoustic waves can penetrate deeply within material and these techniques tend to monitor the bulk condition rather than detect and size individual defects.

Acoustic waves are sensitive not only to defects but also to certain material properties, such as homogeneity, grain size, texture, elastic modulus, plasticity and hardness. Service conditions such as stress and temperature affect these properties and hence the acoustic waves. If there were one-to-one relationships, first between the measured parameters, such as the AE energy, and the material properties, and second between the material properties and the mechanical properties, then the application of AE would be straightforward (Scruby and Colbrook, 1992).In practice, the relationships are complex, each NDT parameter and each desired material property being in, is dependent on of a range of micro structural features and material properties. There are thus many challenges not only in the technology, but also in the basic understanding and data interpretation before some of these properties can be monitored reliably.

To detect AE events, a piezoelectric transducer (Figure 3.2) is required to convert the very small surface displacement to a voltage variation. Sensitive sensors can detect displacements as small as 10^{-14} metres. The most common types of transducers are piezoelectric which are sensitive, easy to apply and cost effective.

A couplant, usually grease or ultrasonic couplants, is needed for good transmission, together with some means of applying force to maintain contact.

There are two types of piezoelectric transducers: resonant transducers and broadband transducers. The principal or resonant frequency of a piezoelectric element depends on its thickness. The piezoelectric element is unbacked or undamped in a resonant transducer but a broadband transducer has an element that is backed with an attenuating medium. Most AE resonant transducers operate in the frequency range of 100 kHz to 1 MHz. Resonant sensors are more sensitive than broadband types because of the additional gain provided by mechanical resonance. Broadband sensors are used when the object of interest is the frequency spectrum of AE but they are less sensitive than resonant transducers. Because they rely on mechanical resonance, resonant sensors can be used to detect a preferential frequency range which has been shown from previous experience to give a good indication of the AE changes. Alternatively, a broad-band sensor can be used and the required frequency range is selected by appropriate filters.

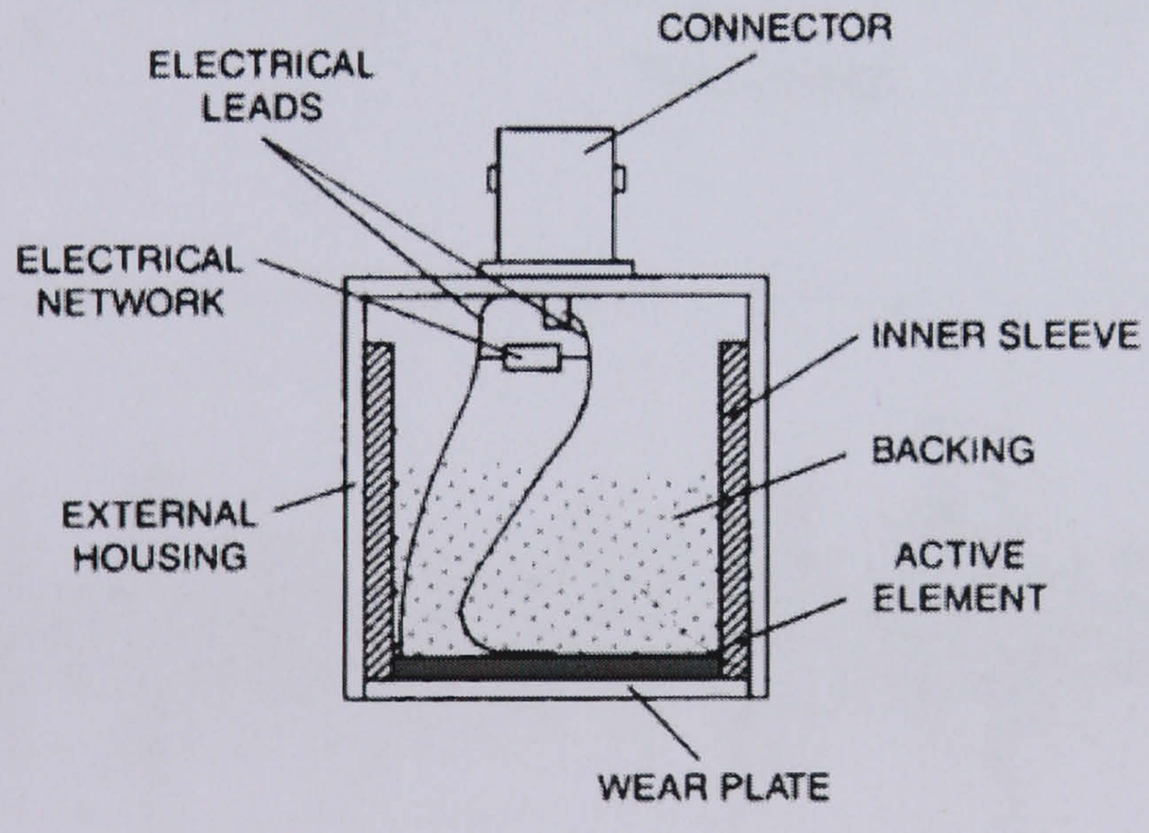

Figure 3.2 Construction of piezoelectric transducer.

The AE signal has been classified into two different types; namely (a) continuous type, and (b) burst type. The difference between these two types (Figure 3.3) is in the average repetition rate. Above a certain values of average repetition rate the length of the bursts exceeds the time interval between them leading to the inability of the instrumentation to resolve two successive burst emissions. This result in the superposition of bursts giving the appearance of the so-called continuous signal. It is important to note that the amplitude (electrical voltage) of continuous signal is usually lower than that of burst signal.

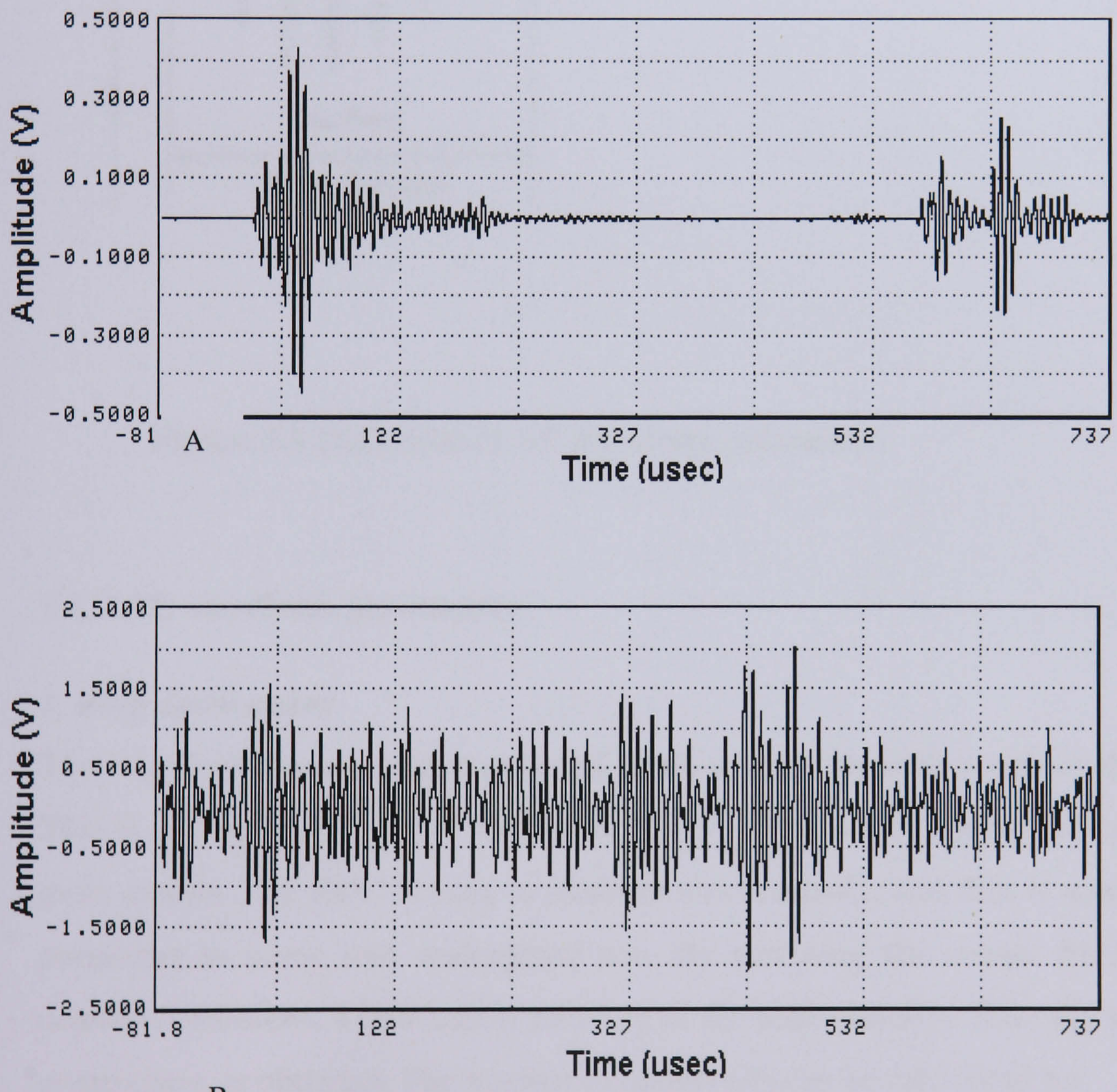

Figure 3.3 Two types of AE signals, (A). Burst and (B). Continuous

An AE burst, shown in Figure 3.4, can be described by the following parameters: event, ring down count, event energy, signal amplitude, duration and rise time.

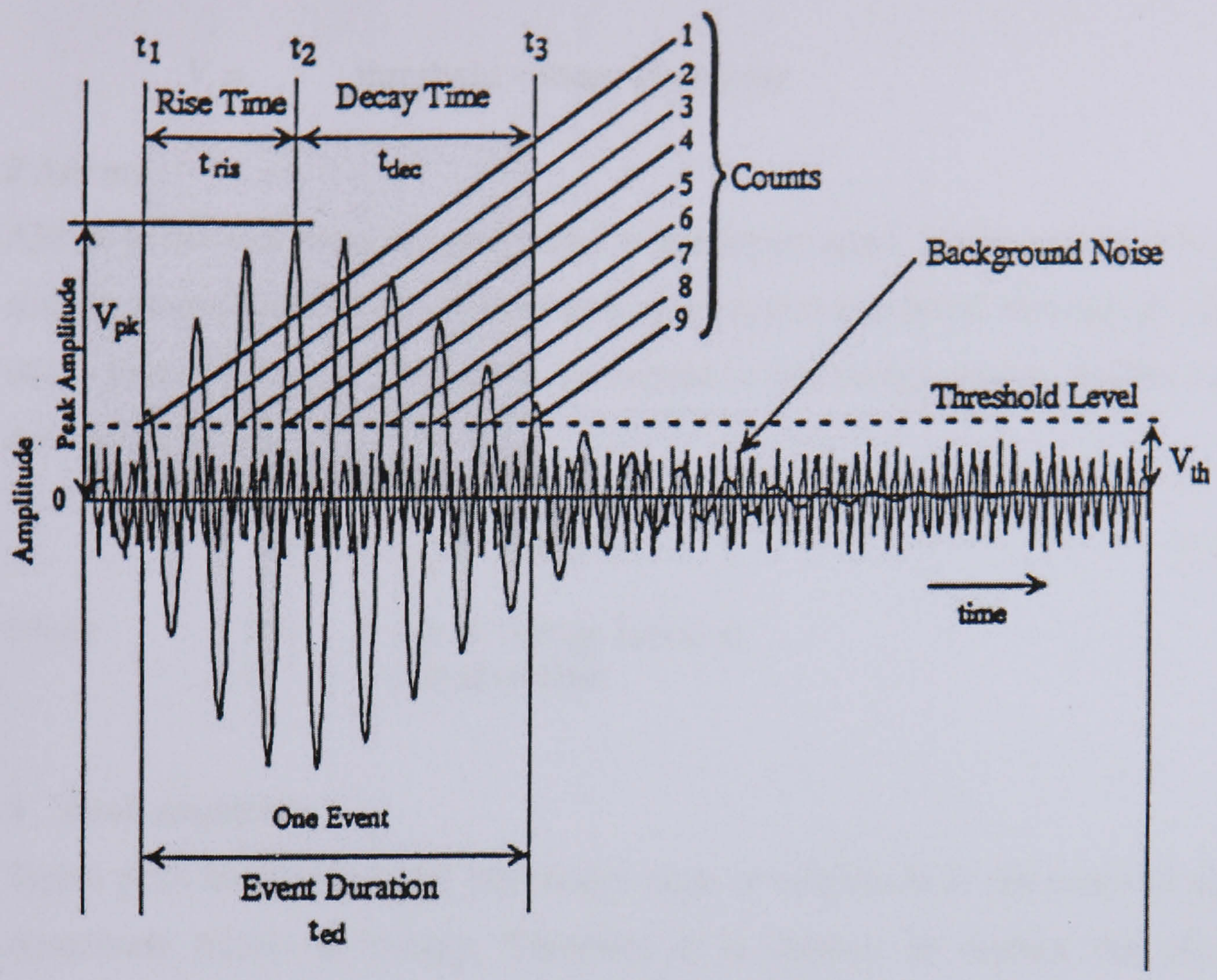

Figure 3.4 Definition of AE waveform parameters.

3.1.3 AE waveform parameters

1. Ring down count

The ring down count is the number of times a signal exceeds a pre-set threshold. This is a simple measure of the signal "size", since larger signals typically give more counts. The RDC is easy to measure electronically, and thus it was the first parameter to come into widespread use. By summing the counts from all the detected emissions, a convenient measure of the total emission from the specimen or structure, is obtained. The number of counts (N) can be calculated by:

$$N = \frac{\omega}{2\pi B} \ln \frac{V_0}{V_t} \tag{3.1}$$

where ω = angular frequency
B = decay constant(greater than 0)
V_0 = initial signal amplitude

V_t = threshold voltage of counter

2 AErms

AErms is the root mean squared value of the input signal. Since acoustic emission activity is attributed to the rapid release of energy in a material, the energy content of the acoustic emission signal can be related to the energy release. AErms can be defined as

$$V_{rms} = (\frac{1}{T}\int_0^T V^2(t)dt)^{\frac{1}{2}} \qquad (3.2)$$

where $V(t)$ = signal voltage function
T = period of time

3 Peak amplitude

Signal peak amplitude is the maximum value of amplitude of the received signal. Amplitude relates to energy. Therefore it is simpler to discern the physical meaning from this kind of signal processing. This is an important parameter because it governs the detectability of the event (detection depends on the amplitude exceeding the pre-set threshold). Like counts, amplitude is a useful measure of the signal size; and it is the appropriate variable to use for attenuation measurements.

4 Event duration

Duration is the time between the point at which the event first exceeds the threshold and the point at which the event goes below the threshold. This parameter is closely related to the ring down count, but it is used more for discrimination than for the measurement of emission quantities. For example, long duration events (several milliseconds) in composites are a valuable indicator of delamination. Signals from electromagnetic interference typically have very short duration, so the duration parameter can be used to filter them out.

5 *Rise time*

The rise time is the time between the point at which the event first exceeds the threshold and the point at which the amplitude reaches its peak value. This parameter is useful for source discrimination and signal filtering. It can be used to

filter out signals from electromagnetic interference, which usually have very short rise times.

6 Average signal level (ASL)

The average signal level is a measure of the continuously varying and "averaged" amplitude of the AE signal. This measurement is similar to that of RMS in that it is an average reading. The main difference is that the RMS is following the root mean square and is measured in volts, whereas the ASL is following the amplitude variation and is measured in dB, (MISTRAS 2000 manual).

3.1.4 AE wave propagation

The AE waveform detected by a sensor is much more complex compared to the AE at the source. It is shaped by the propagation effects between the source and the sensor. The important factors of wave propagation for AE are wave modes and wave velocity, wave reflection and mode conversion, and attenuation.

3.1.4.1 Wave modes and wave velocity

There are 4 types of wave modes; compression (longitudinal), shear, surface (Rayleigh) and plate (Lamb). In an infinite medium, the longitudinal wave and the shear wave are the only two wave types that can exist. The Rayleigh wave exists in a semi-infinite medium and the Lamb wave mode in a finite plate. Each wave mode travels at the different speed depending on the material; and, for Lamb waves, the speed depends also on the thickness of material as well. The velocity varies with frequency, a phenomenon known as velocity dispersion. The compression wave is the fastest. Shear and surface waves travel approximately 60% and 50%, respectively, slower than the compression wave (Course Handbook for SNT-TC-1A (1991).

3.1.4.2 Wave reflection and mode conversion

When a wave strikes an interface or boundary between two materials, the energy is partly reflected and party transmitted. The partition of energy between the transmitted and the reflected waves depends on the angle of incidence and on a material property known as the acoustic impedance.

Mode conversion is the conversion of one wave mode into another. Mode conversion can occur only at an interface between two media.

3.1.4.3 Attenuation

Attenuation is the loss of amplitude with distance as the wave travels through a structure. The major causes of attenuation are:

(1) Geometric spreading of the waves by simple geometry and by loss in adjacent media. The amplitude falls off inversely with the distance in three-dimensional media such as concrete blocks, and inversely with the square root of distance in two-dimensional media such as pressure vessel shells (LOCAN 320 User's Manual ,1990). The geometric speeding is particularly dominant close to the source.

(2) Absorption or damping in the propagation media. The amplitude falls off exponentially with distance. Attention depends on material and on the operating frequency. The higher the frequency the higher the attenuation.

3.2 AE applications in fine chemical and pharmaceutical industries

3.2.1 Crystallisation

Crystallisation is a separation and a purification process used in the production of a wide range of materials ranging from bulk commodity chemicals to speciality chemicals and pharmaceuticals. Crystallisation occurs in three phases: solution, nucleation and crystal growth. Hence, crystallisation can be defined as a phase change in which a crystalline product is obtained from a solution. Nucleation is the start of the crystallisation process and involves the birth of a new crystal, (Myerson, 1993). Frequently, it is useful to be able to detect the onset of nucleation in operating industrial processes.

Ahmed (1997) studied the use of acoustic emission in a liquid nitrogen cooled crystalliser. He applied the AE technique for monitoring sugar crystallisation. An aqueous solution of white, refined cane-sugar was employed in one set of experiments. The solution concentration was 625g sugar/litre water in 4.5 litres vessel. The solution was mixed using an agitator rotating at 600 rpm. A wide band piezoelectric AE transducer was employed, together with a preamplifier containing a built-in bandpass filter (100-1200 kHz). The AE transducer was connected to the stirred liquid via a waveguide. Control of the rate of heating was performed by a variable transformer and of the cooling rate by a regulating valve coupled to the vacuum pump. The solution was stirred for about 30 minutes to dissolve the sugar completely at room temperature. The data acquisition was started when the temperature had fallen to 0°C and the average RMS amplitude level of the AE signal was estimated in real time. It was noticed that the level of RMS has increased as the crystallisation initiated. This rise continued during the crystallisation phase at temperatures between –2 to –5°C. When the operator changed the temperature above 0°C, it was noticed that the RMS level had fallen to a value below what it was during the crystallisation phase.

Bouchard *et al.* (1994) used a wave-guide coupled to a piezoelectric transducer to non-invasively monitor a batch crystallisation process. A steel rod wave-guide was inserted into the reaction vessel. Both temperature and pressure were monitored via probes inserted inside the vessel. Several acoustic descriptors such

as the peak amplitude, the rise time, the ring down count were recorded. The effect of the particle size upon the AE signal was simulated by using glass ballotini of known sizes. It was found that the pulse count rates and the ring down count increased with increasing amounts of material and particle size.

3.2.2 Hydration

Many researchers (Belchamber, 1986; Eissa and Au, 2000) have investigated the acoustic monitoring of hydration of silica gel (Figures 3.5 and 3.6). As silica gel hydrates, gas caused the granules to fracture and to produce sound. Belchamber *et al.* (1986) used the AE signals from silica gel hydration to give quantitative information concerning the amount of material present, the average particle size, and the percentage of water content of the partially hydrated silica gel.

For every measurement, five acoustic emission parameters, also called descriptors, were calculated. These parameters were used as signal descriptors in the pattern recognition analysis. Principal component analysis (PCA) was used for multivariate data manipulation. The projection of principal component of five-dimensional acoustic emission data suggested the existence of four sources, which gave rise to acoustic signals. It was believed that 2 classes belong to low-energy emissions caused by the gas bubbles release. The remaining classes corresponded to high energy emission caused by the fracture of the silica gel granules themselves. Eissa and Au (2000) investigated the same phenomenon of gel hydration. Similar results were reported. Eissa and Au (2000), also distinguished between two sets of data representing gel hydration. The first set was a pure hydration process, the second set was hydration with stirring using a three bladed impeller. It was possible to distinguish between the two sets using the PCA approach. The two clusters from both sets differ from each other in shape and size.

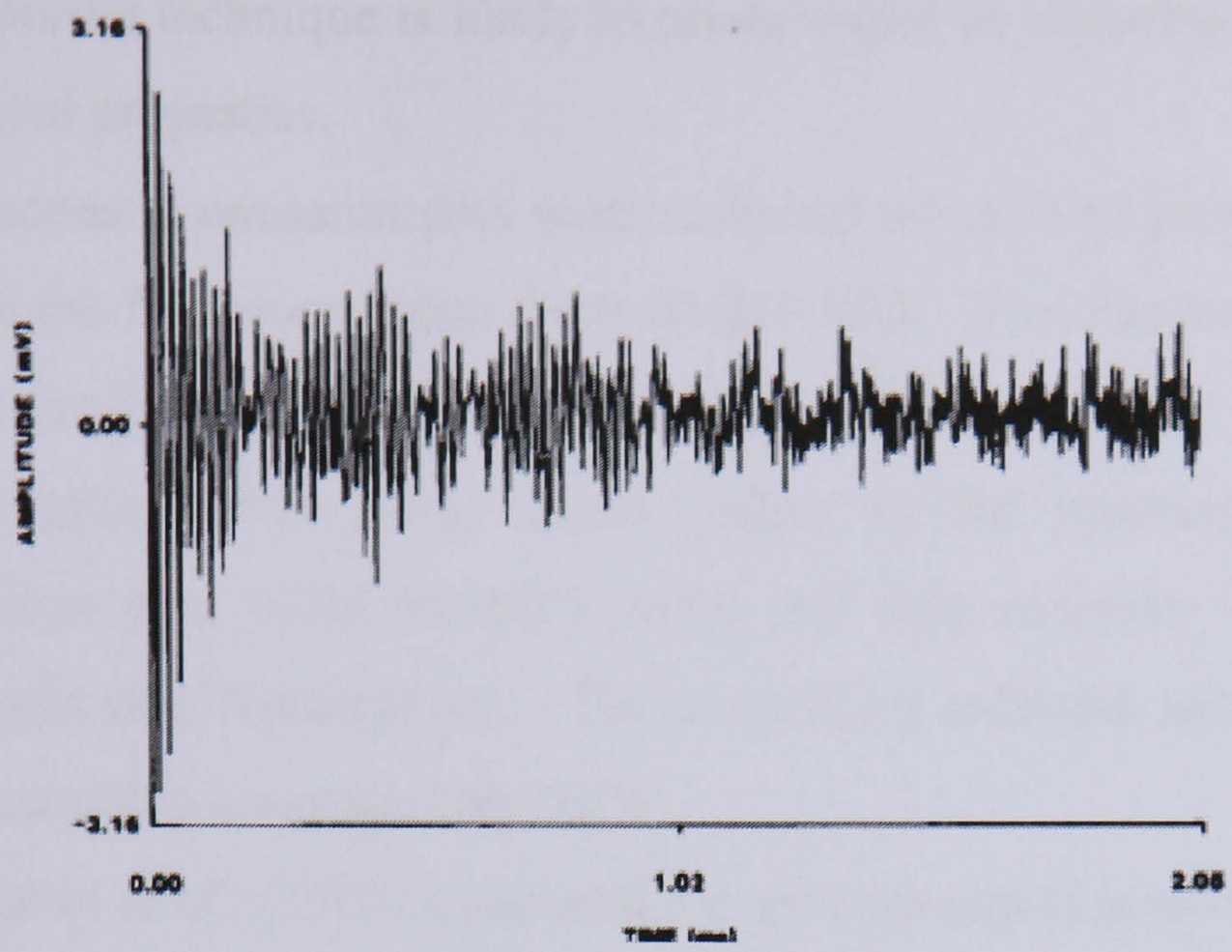

Figure 3.5 Typical acoustic emission produced by gas evolution.

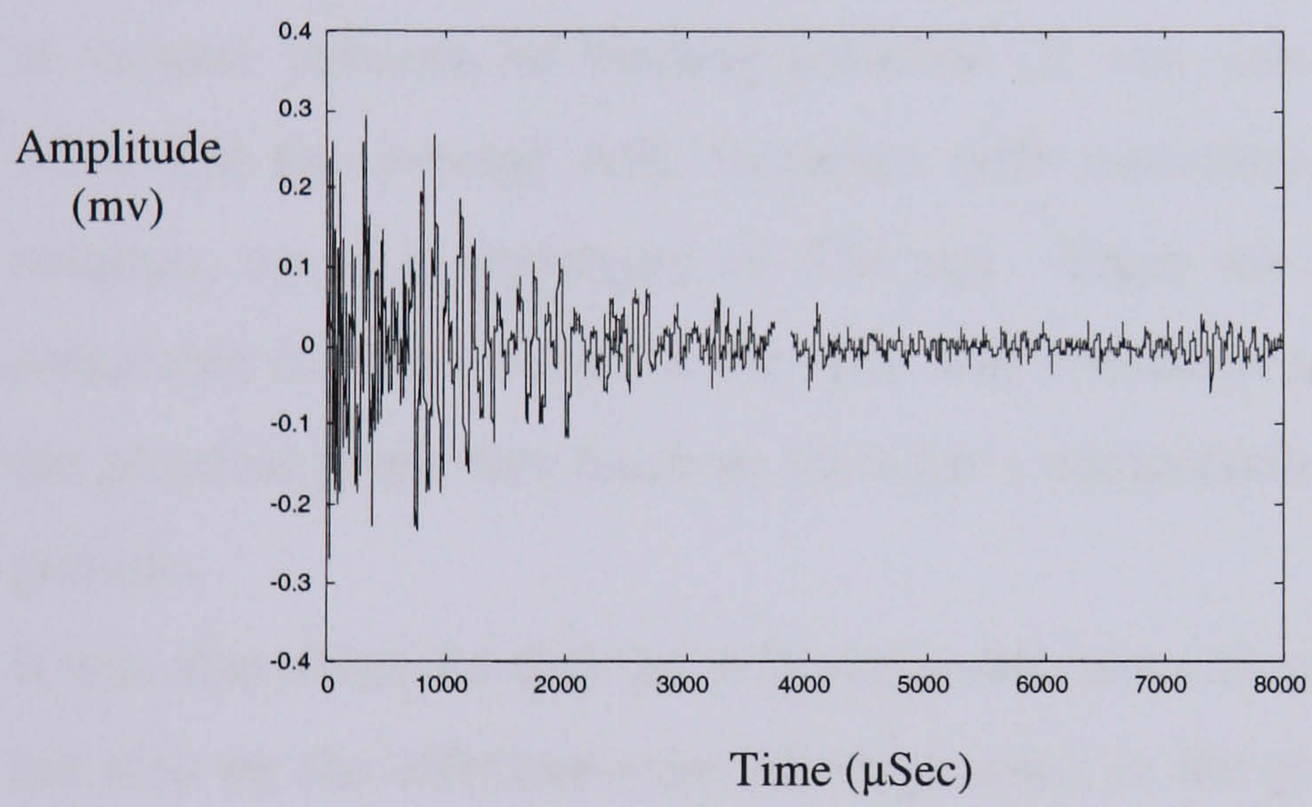

Figure 3.6 Typical acoustic emission signal produced by a silica gel granule fracturing

3.2.3 Granulation

The application of acoustic emission to the on-line determination of the particle size, flow and compression properties of a model high shear granulation process was reported by Whitaker *et al.*(2000). The underlying idea is that the particle size changes that occur during granulation affect the powder flow and compression properties. As the particle size and granule density (both of which influence the compression properties) affect the acoustic emission signal, this

monitoring technique is likely to prove useful in assessing changes in the relevant physical properties.

The acoustic emission data were collected using three piezoelectric transducers to cover the frequency range from 20-350 kHz. The transducers, maintained at the same positions throughout experiments, were coupled to the outside of the high shear mixer bowl using silicon sealant as the coupling agent. The acoustic emission data were recorded using AE data recorder Osprey[1] AE-8 (Process Analysis and Automation). The controlling software was written in a graphical programming language LabVIEW.

Whitaker *et al.* (2002) examined the average signal level (ASL). This AE feature is a measure of the AE signal amplitude variation. The time domain signals were converted by FFT into the frequency domain for all the granulation batches.

Figure 3.7 shows the relative average signal level difference for all the transducers at various volumes of binding solution. (It was noticed from the experimental work that the average ASL increases with increasing amounts of added binder solution, up to a maximum of 550 ml). From the experimental work, it was noticeable that the change in the ASL was consistent with the observed change in the physical properties (such as the Carr's compressibility index) of the resulting granule.

It was also observed that the ASL depended, not only on the extent of granulation, but also on the effective mass of the product in the granulation bowl. Hence, the ASL can be used to measure the extent of granulation of a material.

Although the authors recorded the raw AE signal, very little have been mentioned about data processing. The authors investigated only one AE parameter which is the ASL. Other AE features may lead to more useful information.

Tsujimoto *et al.*(2000) monitored particle behaviour in a fluidised bed granulator. It was believed that when the solid particles move in a confined space, they collide with each other. This causes intense friction in the equipment during the operation. The sounds generated during this process are indicative of the particle motion and are believed to be related to the particle behaviour in the operating

[1] Osprey is trademark of Process Analysis and Automation

system. The following AE sources occur in the fluidised bed granulator: (1) Inter-particle or particle-chamber friction (friction sound), (2) particle-particle or particle-collisions (impact sound), and (3) air turbulence in particle beds (aerodynamic sound). Tsujimoto (2000) studied the effects of the fluidising gas velocity and particle size on the mean AE amplitude. He found that beyond the minimum fluidising gas velocity U_{mf}, the motion of bed particles is proportional to the fluidising gas velocity U_s. The mean AE amplitude was the mean amplitude value of the AE waves for 5 s calculated using the AE amplitude distribution. There was a noticeable increase in the AE amplitude as fluidised particles grew in size while the dimensionless gas velocity (U_s/U_{mf}) remained the same. This is due to the fact that when the particle size increased, the force of their collisions with the chamber wall and the force of their friction also increased. A previous study by Hidaka *et al.* (1999) suggested a relationship between the sound pressure of flow sound, the particle flow rate and the particle size, supported the findings by Tsujimoto *et al*, (2000). However the assumption that the increase in the frequency and the strength of particle-particle and or particle-chamber wall friction and collisions due to the movement of bed particles was not justified.

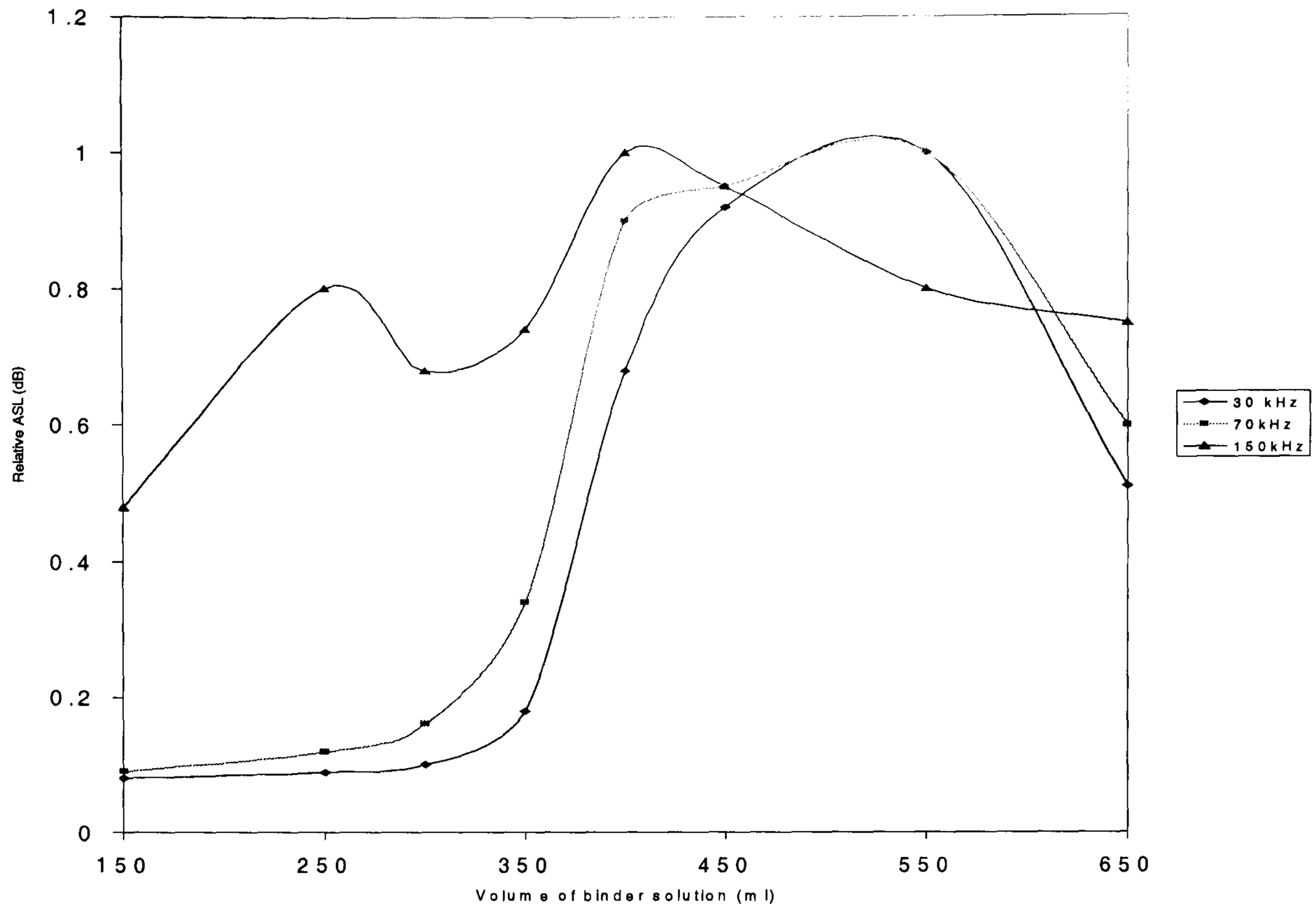

Figure 3.7 Relative average signal level (ASL) difference for the 30-, 70- and 150-kHz sensors for various volumes of binder solution.

3.2.4 Leak detection

Acoustic leak monitoring systems have been successfully applied to detect and localise leaks in simple geometrical structures such as pipelines in production plant, pressure vessels with a smooth surface and in more complicated situations such as a small number of connection branches. Investigation of the mechanical integrity by acoustic leak monitoring is of particular importance for the safety of pressurised water reactors. To achieve this aim, an advanced leak monitoring system should be capable of promptly detecting a leakage, determining its location, and possibly relating the AE signal to the leak rate.

Hessel *et al* (1999) used a neural network approach in combination with acoustic methods to identify leakage within pressure vessels. Experimental work was carried out on a VVER vessel because numerous leaks were known to have occurred especially in the standpipe region of the pressure vessel head. The leaks were simulated by sound sources, driven by a compressed air jet: a piezoelectric transmitter or a thin metal-blade was excited by a jet of compressed air. An array of twelve acoustic emission transducers were mounted at the standpipes measuring the leak-induced structure-borne sound in the frequency range from 50 to 500 kHz. RMS values of the structure borne sound were appropriate feature for data analysis.

3.2.5 Agitated vessels

The sound (audible and non-audible) of gas bubbles as they are formed in a liquid has been widely researched in oceanography to identify the sources of the ambient sound in the sea and to separate it from the sound of marine traffic. Acoustic bubble is reviewed in Leighton (1994). Minnaert (1933) was the first to use a simple energy balance calculation and relate the frequency of the sound f, produced by a bubble of radius r when formed at a nozzle, to the bubble's size:

$$f = \frac{1}{2\pi r}\sqrt{\frac{3\gamma P}{p_l}} \qquad (3.3)$$

where γ, p_l and P are the ratio of specific heats of gas, density of liquid and the pressure in liquid respectively.

Equation.3.3 indicates a simple inverse proportionality between the frequency of AE from a bubble and its diameter (assuming a spherical bubble). This relationship has since been investigated and demonstrated by many authers (e.g. Strasberg, (1956); Leighton, Fagan, & Field, (1991)). Volumetric bubble oscillation is caused by shock excitation, generally due to its formation, where the bubble's volume moves from its equilibrium. When bubble oscillates it produces an acoustic pressure pulse, and eventually returns to its equilibrium bubble size. For small-amplitude oscillations, the resulting sound pressure pulse is an exponentially damped sine wave.

The magnitude of the measured sound pulse caused by the bubble oscillation depends on the distance and the attenuation between the bubble source and the sensor.

Estimation of the bubble size distribution in gas-liquid dispersions from the sound spectrum was investigated by Pandit, Varley, Thorpe, and Davidson (1992) in pipe flow and pressure vessels. The magnitude of an individual pressure pulse was estimated in terms of the displacement of the bubble radius.

The sound spectra within large-scale agitated gas liquid dispersions have been investigated by Hsi *et al.*(1985), Usry *et al.* (1987), Sutter *et al.* (1987) and De More *et al.* (1988). In these studies the same equipment was used: a 900 mm diameter vessel; a 305 mm diameter, 6 bladed turbine and a ladder-type sparger with 3.2 mm diameter orifices. Bruel and Kjaer (Model 8103) hydrophones were used to measure the sound and spectrum analyser to analyse the signals. Hsi *et al.* (1985) began the studies by investigating the sound spectra caused by the gas dispersion at various positions within the agitated vessel. From the sound pressure spectra produced at the sparger ring, they concluded that it was possible to distinguish between gas sparging controlled by the sparge ring itself and the natural volume pulsation frequency of the bubbles and gas sparging controlled by impeller flow. It was also concluded that a coupling phenomenon exists between the impeller and the sparger ring when, under certain conditions, the sparger ring

resonates at 10 times the blade passing frequency. De More *et al.* (1988) investigated the relationship between their cavity sound resonance measured by a hydrophone fixed to the impeller and mass transfer. The maximum cavity peak resonance was believed to correspond to the maximum production of the interfacial area for electrolytic systems. Also choked flow conditions for disc style impeller were also identifiable from the sound spectra.

Although, bubbles, visually observed in the mixing vessel, were of the order of size to be causing the high frequency sound, this was not confirmed quantitatively.

Boyd and Varley (1997, 1998) investigated the relationship between the bubble size and the acoustic emission spectrum in agitated vessels (see Figure 3.8). They identified the bubble sound pulses in pressure-time samples measured close to the impeller superimposed on the hydrodynamic pressure fluctuations. They also showed that it was possible to estimate the bubble size distribution formed at the impeller region.

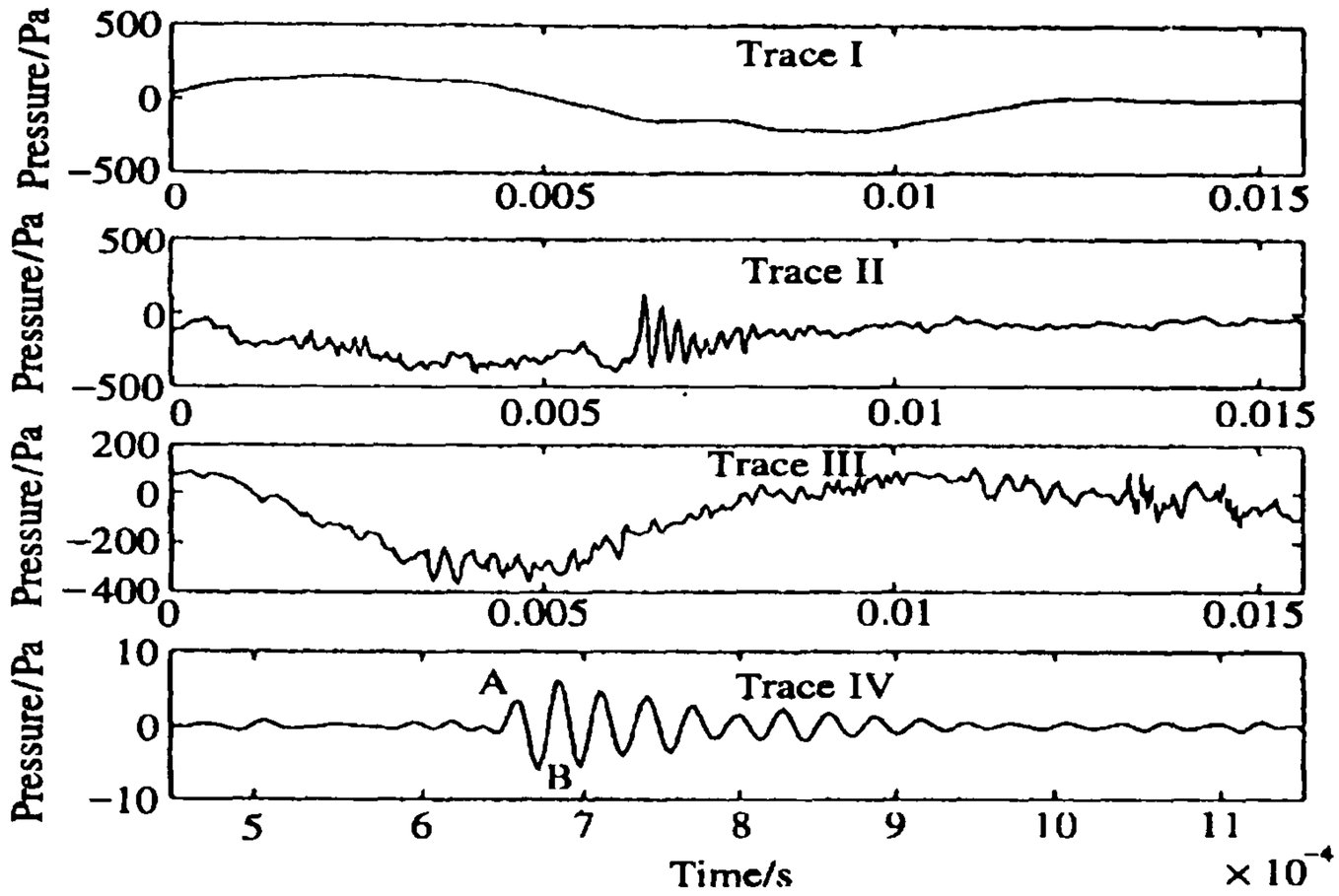

Figure 3.8 Examples of acoustic emissions and spectra from gas mixing in agitated vessels (from Boyd and Varley (1998))

Turbulence noise occurred at a lower frequency range than the sound from the bubbles; thus enabling the identification of bubble sound in the spectra. Tank resonance was believed to exist but its effect on the spectra was not quantified.

Manasseh *et al.* (2000) also estimated bubble size from sound measurements inside an agitated vessel. Bubbles size distributions were not calculated from the generated spectra but the average bubble size was estimated from the average frequency in the spectrum. Assuming that bubbles within a critical radius of the hydrophone were detected and only one bubble existed in that region and during the measurement period, the void fraction was also estimated. The void fraction estimation results were in a good qualitative agreement with the conductivity measurements. However, Manasseh *et al.* (2000) emphasised that these void fraction measurements could only be regarded as qualitative because the assumptions that underpins the estimations may not be completely valid.

3.2.6 Gas evolution processes

Different gas evolution processes have been the subjects of study using the acoustic emission technique. Cao *et al* (1998) monitored different processes which included different metals in diluted inorganic acids for evolving hydrogen gases and different carbonate/bicarbonate solutions droppings into diluted inorganic acids for evolving carbon dioxide gases. They also studied bubbling nitrogen into the above-mentioned saline solutions of corresponding reaction products and the above-mentioned saline solutions without background gas evolution. The reaction was carried out in a glass cell consisting of an ordinary 10ml laboratory beaker. The AE signals were detected by a broadband piezoelectric transducer, which was attached to the bottom of the cell. The A.C output from the amplifier was sampled by a 100 MHz digital oscilloscope. In each experiment, the trigger mode was set to AUTO, which caused the oscilloscope to self-trigger repeatedly and so was useful for acquisition of continuous waveforms. The AE signal was recorded for typical examples of three gas evolution systems and one background noise system. All individual AE signals from four systems were acquired over a 2.0 ms time span. The background signal is nearly a horizontal line with rather low amplitude, the other three signals are of different densities of oscillating peaks, indicating that they contain different frequency components. The analysis for an individual signal was carried out by the FFT and the characteristics of the resulting frequency components of the signal were

displayed as a power spectrum. Figure 3.9 shows typical power spectra of the four above mentioned time domain signals.

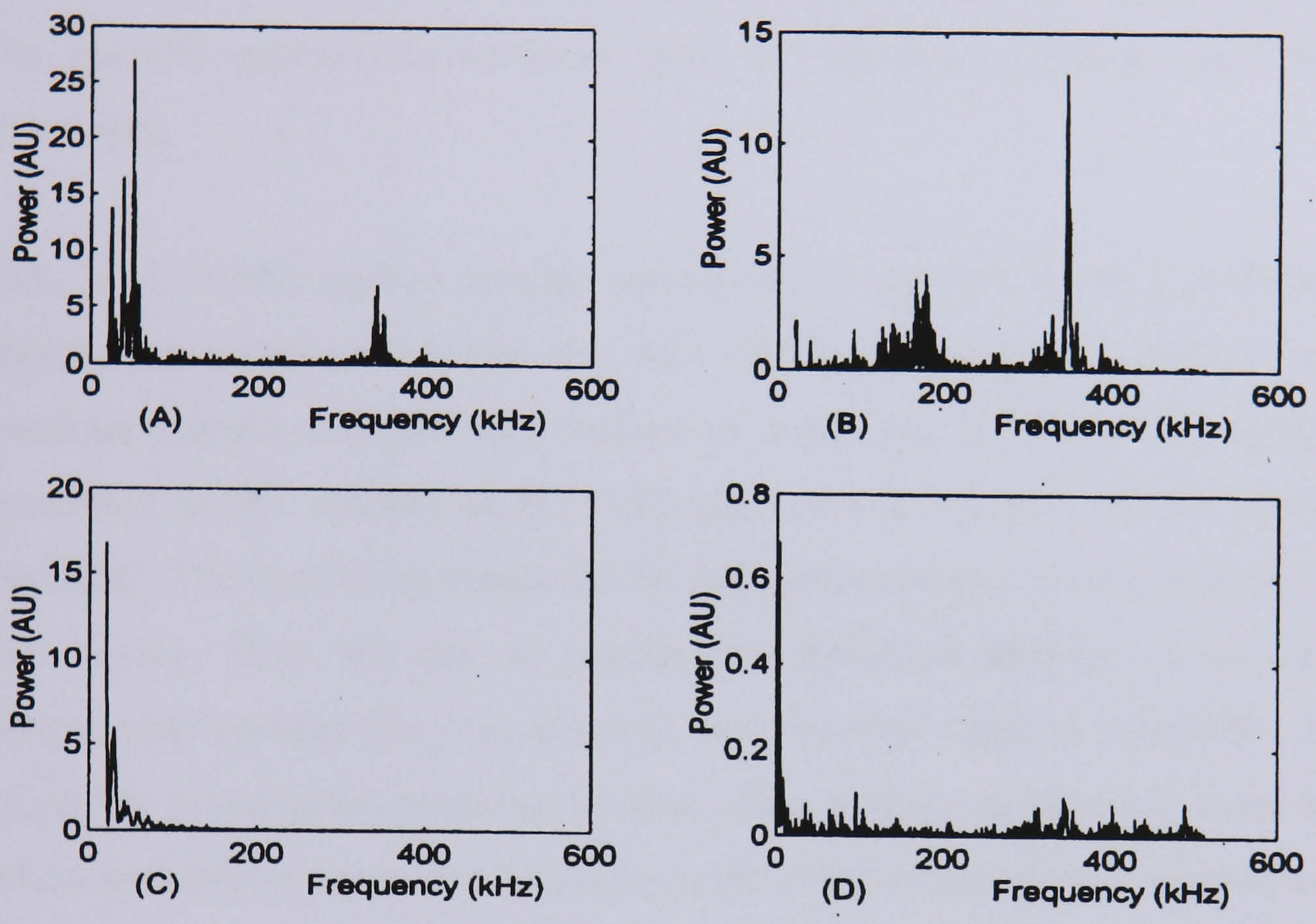

Figure 3.9 Typical individual AE signals produced by four reactions processes in four systems. (A) Example of metal-acid reaction process, (B) Example of carbonate/bicarbonate-acid reaction process, (C). Example of bubbling N_2 into salt solution, (D) Example of salt solution-background noise. (Cao *et al*. 1998).

3.2.7 Pipeline flow

Pipelines are ubiquitous in various industrial processes. The operating conditions prevailing in a pipeline flow may vary widely for different applications. The line pressure, for instance, can be as low as just a few bars in water transportation, to as high as 1000 bar in a slurry conveying operation. Fluid characteristics also

range from clean water to highly abrasive cement slurries, viscous gel suspension, or erosive and dangerous chemicals.

Different techniques are applied for monitoring flow and related process parameters. This includes radioactive probe, optical techniques and ultrasound transmission measurements. These methods unfortunately can be cumbersome to use. The measurement accuracy may also be seriously affected by the changes in the specific process environment such as viscosity, pressure, and solution chemistry.

Hou *et al.* (1999) applied acoustic monitoring to the flow inside a pipeline. The monitoring technique exploits the fact that when particulate slurries or solid particles interact with the inner surface of a pipeline, sound waves impulses are generated in the vicinity of the collision, causing the bulk of the pipeline to oscillate. The oscillation signal can be collected through a clamp-on piezoelectric AE sensor. With the aid of appropriate statistical analysis techniques, the relationship between the flow property and recorded signal is estimated. Hou *et al.*(1999) investigated pumping of fine silica particle suspensions running in a 44.5mm diameter pipe. The frequency spectral behaviour of the collected acoustic emission signal is correlated with the process parameters of the system.

3.2.8 Chemical reactions

Most of pharmaceutical processes, particularly those with phase transformation, are acoustically active. AE monitoring has also been investigated as a means of obtaining information about specific chemical reactions. Van Ooijen, van Tooren, and Reedijk (1978) noted a loud crackling sound when $ZnCl_2$ was added to pyrazine in water (addition of pyrazine to water results in the formation of a precipitate). The crackling sound was heard again when the mixture was shaken hours later. Increases in temperature and AE were observed to occur at the same time. The intensity of the sound appeared to be proportional to the concentrations of both the reactants used. The sound produced by the crackling was analysed in terms of frequency. It was observed that the most intense part of the emissions

occurred at approximately 100 kHz; a frequency which is outside the range of human hearing.

Betteridge, Joshlin and Lilley (1981) expanded the study of AE caused by chemical reactions, investigating 43 reactions. Table 3.1 shows examples of some of the reactions and description of their AE investigated by Betteridle *et al.* (1981). The reactions occurred in a glass beaker with a piezoelectric transducer placed on the underside of the beaker. The signal from the transducer was band passed filtered to remove frequencies outside the range of 100-300 kHz.

Table 3.1 Summary of chemical reactions investigated for acoustic emission

Study	**Reaction**	**Description of the resulting AE**
Betteridge *et al* (1981)	Addition of sodium carbonate to copper sulphate solution	Initially large spike in AE power, decaying exponentially
Betteridge *et al* (1981)	Addition of concentrated sulphuric acid to water or NaOH	Large spike in AE on addition of acid and rise in temperature. Spikes in AE continue with reaction. Intensity of AE decrease with increasing H_2O volume.
Betteridge *et al* (1981)	Oscillating reaction between iodate, peroxide and malonic acid	AE oscillated with the oscillating reaction
Sawada *et al.* (1985a)	Addition of sodium carbonate to calcium chloride	Phase separation, precipitation and gel formation were identified from AE
Sawada *et al.* (1985b)	Dissolution and precipitation of sodium thiosulphate	AE from phase transitions are more intense for contraction volume changes than for volume expansions
Belchamber *et al.* (1986)	Hydration of silica gel	Gas evolution fractured the granules causing the AE
Wentzell and Wade (1980)	Hydration of silica gel and quicklime Aqueous dissolution of NaOH and Na_2CO_3	Granule fracture causes AE Effervescence AE occurred in the 50-100 kHz band range
Cao et al. (1998)	Metal-acid reactions Carbonate/bicarbonate-acid reactions	Significant AE in the 320-360 kHz region of power spectrum Bubble effervescence occurred below 150 kHz
Crowther *et al.* (1991)	Electrolysis cell	AE occurred up to 800 kHz. Increasing the applied voltage resulted in greater intensity of AE. Frequency mean and median, RMS and kurtosis all correlated well with the applied voltage

3.2.9 Equipment monitoring

The development of methods for monitoring equipment performance is important for the safe and reliable operation of a process plant. Parkinson (1991) introduces the term 'holistic maintenance' to describe situations in which predictive and preventive maintenance are used together to reduce maintenance costs and increase production performance. Acoustic measurement has been employed in industry as a non-invasive tool to monitor equipment performance so that potential problems can be predicted and treated before they become serious.

3.2.10 Structural integrity

Pollock, Vahaviolos and Lew (1991) review several examples where companies such as Monsanto, Dupont, Union Carbide and Exxon have used AE as an indicator of structural integrity in the chemical industry. AE testing is described as an economic method for 'screening' which is then complemented by further test methods such as visual inspection (Fowler, 1992).

Drouillard (1988) charts the history of the development of AE monitoring for testing structural integrity. Acoustic emission monitoring of structural integrity, equipment parts and leak detection are now an established non-destructive testing method with international codes and standards, (Physical Acoustic Corporation).

3.3 Review on Acoustic emission application during pharmaceutical materials compression

The technique of acoustic emission has recently become a popular non-destructive test method in ceramics and powder metallurgy. The use of the technique in pharmaceutical industry in general has been reviewed in Section 3.2; this section focuses on the application of acoustic emission in pharmaceutical powder compaction during tabletting.

When powder is compressed, friction together with possible powder particle fractures give rise to acoustic emission. Thus acoustic emission signals are influenced by the materials size and compression conditions.

Rue *et al.* (1979) monitored the acoustic emissions of compressed and ejected tablets of a sodium chloride powder through a band-pass filter of 70-500 kHz, via a thin layer of an acoustic coupling agent on one face of the tablet. They found that the AE activity of the tablets decreased exponentially during one hour after compression while the strength of the tablets increased exponentially. They suggested that the mechanism of strength increase is related to the deformation process, which produced the acoustic emission.

After the first acoustic emission measurements with pharmaceutical powders using the roller compactor (Hakanen *et al.*, 1993, Salonen *et al.*, 1997), hopes of developing a novel method for monitoring powder compaction process have risen. In both publications, the authors reported a noticeable AE signal from compressing various powder used for tabletting. Salonen, *et al* (1997) conducted a study on acoustic emission from microcrystalline cellulose (MC) and maize starches (MS). AE signals were detected during roller compaction using microphone filter. The noise from the compactor was found to appear mainly below 15 kHz.

The acoustic emission intensity of MC was observed to increase as a function of the applied compression force up to 45 kN, while the acoustic emission intensity-force curve of MS had a maximum at 50 kN. The authors reported that the AE signal from compaction powder consists of short acoustic pulses with varying intensities.

Wong *et al.* (1991) monitored the acoustic activity during the deformation of single crystals of α-lactose monohydrate and anhydrous α-lactose in a crushing strength rig. Well-formed single crystals of α-lactose monohydrate and anhydrous α-lactose of length range 2.5-4.5 mm were individually mounted on the crystal holders using cyanoacrylate adhesive. The arrangement of the compression test allowed direct crushing of the crystal onto the acoustic transducer with simultaneous monitoring of the acoustic activity and the force-displacement profile. They have observed differences in the acoustic activity as indicated by the ASL profile between the two types of α-lactose. Only qualitative analysis was carried out on the ASL profile and no attempt was made to quantify the differences between the AE activities for both signals. However analysis and comparison of the ASL and force-displacement profiles revealed that the major force matched the large distinctive peaks on the ASL profile peaks on the force-displacement curves. Their study showed in particular that fractures, which were otherwise not detected either by monitoring the force-displacement curves or visual observation, could be picked up by monitoring the acoustic activity emitted during the deformation process. The study concluded that α-lactose monohydrate crystals which fracture by spalling cracks is more acoustically active than anhydrous α-lactose crystal which fragment by crumbling without any progressive fracture.

Acoustic emission was detected by Hakanen *et al.* (1993) for three different pharmaceutical materials using a roller compactor. The AE signal were recorded on magnetic tape with a microphone and transformed to frequency spectra by using FFT-analysis. Audible frequencies of the range 50Hz-12kHz were detected. It was possible to separate the sound produced by the roller compactor from the emission generated by pharmaceutical material, although the author did not mentioned the range of the mechanical noise frequency. The author identified certain peaks in the frequency domain signal. However, due to the problem of some peak overlapping, no attempt has been made to quantify the signals. The author also did not undertake time domain analysis of the signal. The frequency components of each spectrum were divided into three bands and many frequency peaks were observed.

Hakanen *et al.* (1993) suggested that friction together with possible powder particle fractures generated acoustic emission when the powder is subjected to a compression force. The range of the force used varied between 5-6 kN for three different materials namely microcrystalline cellulose, maize starch and lactose monohydrate. The author reported that the acoustic energy generated from a powder during both compression and post-compression appears at a large part of higher frequencies, however, no attempt has been given to investigate the high frequency components of the AE signal during tabletting process.

Hakanen *et al.* (1995) also, studied the acoustic emission generated from the compression of microcrystalline cellulose powder using roller compaction. In this work, they investigated the capping phenomenon during tabletting. The capping was indicated by an enhancement of acoustic emission in the region of about 17-23 kHz. The differences between this study and his previous work was that according to Hakanen *et al.* (1995), the post-compression peak appeared independently of material every time when the compression load was removed. In his latest work Hakanen *et al* attempted to find some correlation between the acoustic emission signal and the capping phenomenon. The author agreed, as most authors did, that the plastic deformation of crystalline materials such as metals gives rise to acoustic emission energy.

Both crystalline (and brittle) materials like lactose, and relatively amorphous (and ductile) materials like maize starch and microcrystalline cellulose were investigated by Hakanen. The observed capping phenomenon of microcrystalline cellulose was not clearly indicated in the early publication and hence further studies was conducted by Hakanen using a microphone with a flat frequency response up to 20 kHz.

In most of the previous publication, it was suggested that the two main sources of acoustic emission are (i) non-stationary dislocation motion and (ii) dislocation annihilation process mainly related to the operation of a Frank-Read source during plastic deformation of crystals (Pawelek ,1988).

3.4 Theory and practice of powder compaction

3.4.1 Introduction and history of tabletting

William Brockedon was granted the patent for the compaction of dry powder in 1843. His method was to compress powders within a die, using two punches and a hammer to apply the force of compaction. The press machine was developed from his idea with a semi automatic stage to the one known as the single punch or eccentric tablet press.

J.F. Buckley first patented the rotary tablet machine in 1908. Both the rotary and the single punch machine changed little up to the 1960's. The only development is the speed at which the machine operates. New tablet presses have the capability of producing 240 tablets per minute. More recently, the influence of microelectronics and computer technology has led to the development of a new generation of tablet presses, capable of controlling the physical properties of the compact (Korstch 1980).

The rate of progress observed in tablet machines and their operating speeds was not, however, complemented by an understanding of the compaction process in the pharmaceutical industry. The research performed in other disciplines, namely metallurgy and ceramics, was responsible for much of the knowledge of the compaction process, Shaxby and Evans (1923) and Heckel (1961 (a,b)), Cooper and Eaton (1962). It was not until the pioneering work of Train (1956) in the mid fifties, who examined the stress distribution within compacts, that pharmaceutical research started looking at the fundamentals of tablet compression. More recently pharmaceutical research has investigated why some materials are capable of forming a coherent compact while others exhibit the well-known problems of powder compaction such as *capping* and *lamination* problems often seen at high tabletting speeds.

Researchers have been restricted to applying similar rates of compression to those used in industry and have not been able to examine 'scale-up' or 'speed-up' effects on tabletting formulations due to the high cost of tabletting machinery and the large quantities of compaction material required.

With the development of compaction simulators which is capable of operating at high compaction rate, it has become possible to gain a better understanding of the high speed compression of powder in a die with two hardened steel punches, Mann *et al.* (1981), Hunter *et a*l (1976) and Bateman *et al.* (1989). The quality of the tablet produced depends not only on the force applied, but also on the speed of compression, David and Augsburger (1977), Huttenrauch (1978) and Ridgway *et al.* (1972).

3.4.2 Compression and Compaction of Powder

Powder compaction refers to compression of powder to form a product that can be crushed into granules of a desired shape and size. Powder compaction is an important part of dry granulation and final product delivery in pharmaceutical technology.

Direct compression of organic powder is performed on the basis that the van der Waals forces are able to cause binding between powder particles whose distances are smaller than 0.001 nm. In addition, the vicinity and the large number of the connection points are the two presumptions of improved organic powder binding.

The following terms are used so frequently in this thesis that here their definitions are given below:

Compaction

The transformation of a powder into a coherent specimen of a defined shape by powder compression

Compression

The reduction in volume of a powder bed due to the application of a stress, eg loading or vibration.

Consolidation

Mostly used synonymously with compaction. The term has also been used to describe compression of powders (Alderborn *et al*, 1996).

3.4.3 Method of tablet preparation

The three basic methods for preparation of compressed tablets are wet granulation, dry granulation and direct compression. In addition to these methods, recent technology has permitted the production of tablet granulation by a fluid-bed process.

3.4.3.1 Wet granulation

Wet granulation is a widely employed method for the production of compressed tablets. The steps required in the preparation of tablets are:

1. Weighing and blending the ingredients.
2. Preparing the wet granulation.
3. Screening the damp mass into pellets or granules
4. Drying.
5. Dry screening.
6. Lubrication and blending.
7. Tableting by compression.

3.4.3.2 Dry granulation

In this method, the granulation is formed not by moistening or adding a binding agent to the powdered drug mixture but by compacting large masses of the mixture and subsequently crushing and sizing these pieces into smaller granules. For this method, either the active ingredient or the diluent must have cohesive properties in order for large masses to be formed. This method is particularly suitable for materials that cannot be prepared by the wet granulation method due to their degradation by moisture or to the elevated temperatures required for drying (Ansel *et al.*, 1995)

3.4.3.3 Direct compression

Direct compression is viewed as the technique of choice for the manufacture of tablets containing thermoliable and moisture-sensitive drugs. As a powder is compressed within a die, the various stages of the compaction process can be outlined as follows:

1. Rearrangement- where particles move within the die cavity to occupy void spaces that exist between the particles;
2. Deformation- when particles can no longer rearrange themselves, the material will start to deform elastically;
3. Compaction- when the elastic limit of the material is exceeded, the material will deform either plastically or destructively (through fragmentation or brittle fracture). Either mechanism can occur and depends upon the material characteristics, the compaction speed, compaction pressure and particle size. Plastic deformation will aid bonding because it increases the area between particles and fragmentation produces newer surfaces, which also favours stronger bonding.
4. Relaxation- once a compressional force has been withdrawn from a compressed mass (during punch withdrawal and ejection from the die cavity) the compact will undergo relaxation; if these elastic forces exceed the tensile strength of the tablet, then tablet integrity will fail.

When a pressure is applied to compress pharmaceutical powder, the particles start to rearrange within the die vicinity. As the pressure increases the particles go into elastic and plastic deformation. When the applied pressure is further increased, the smaller particles formed could again undergo deformation. Thus, a single particle may pass through one or several of these processes several times during a compression cycle. As a consequence of the compression of the powder, particle surfaces are brought into close proximity to each other and the porosity level assumed reaches its lowest value, and inter-particulate attraction or bonds will be formed.

All materials possess both elastic and a plastic component. Examples of materials consolidating mainly by plastic deformation are sodium chloride, starch, and microcrystalline cellulose. Essentially fragmenting materials are, for example, crystalline lactose, sucrose, and emcompress.

3.4.4 Advantages and disadvantages of direct compression

Advantages

- Requires fewer operations compared with wet granulation (shorter processing time and lower energy consumption).
- Fewer stability issues for actives that are sensitive to heat or moisture.
- For certain compounds, faster dissolution rates may be generated from tablets prepared by direct compression compared with wet granulation; an example is norfloxacin.
- Fewer excipients may be needed in a direct compression formula.

Disadvantages

- Issues with segregation-these can be reduced by matching the particle size and density of the active drug substance with excipients.
- In general, the drug content is limited to approximately 30% or approximately 50 mg.
- May not be applicable for materials possessing a low bulk density because after compression the tablets produced may be too thin.
- Not suited for poorly flowing drug compounds.

3.4.5 Particle –bonding process

The processes of compression and compaction rely on interparticulate bond formation. Granule bond formation occurs in the following ordered stages:

A. Particle rearrangement

Particle rearrangement occurs initially as powder movement begins to fill void spaces. As a result, air begins to leave interstitial spaces of the powder blend and particles begin to move closer together, thereby increasing the powder blend density. The important factors in this process are particle shapes and sizes. For example, spherical particles will move less than other-shaped particles because of their closer initial packing.

B. Particle deformation

Particle deformation, described as plastic deformation, occurs as compressional forces are increased. This deformation increases the points of contact between particles where bonding occurs. After the applied force or stress is released from the compact, the granules attempt to return to their original form and the deformation said to be elastic. Conversely, a deformation that does not totally recover after the stress is released is a plastic deformation. Both types of deformation can occur simultaneously in some materials.

C. Particle fragmentation

Particle fragmentations take place at higher compressional force levels than that required for the former stages of bonding formation. Here, particle fracturing creates multiple new surface sites, additional contact points and hence potential bonding sites.

D. Particle bonding

Particle bonding is caused by plastic deformation and fragmentation. In general, particle bonding occurs at the molecular level due to Van der Waals forces (Parikh, 1997).

3.4.6 Compression mechanism

The bulk volume of a powder mass, which is subjected to the mechanical forces of the compressional machine, reduces as a result of one or more of the following effects. The main mechanism of initial volume reduction is the onset of loading which is usually accompanied by closer re-packing of the powder particle. As the load increases, the rearrangement process becomes more difficult, and further compression involves some type of particle deformation. For instance, with several pharmaceutical materials, such as acetyl salicylic acid and microcrystalline cellulose, elastic deformation is the dominant mechanism of compression in such materials. This deformation is to a large extent spontaneously reversible on removal of the applied force. However, in other materials, there is a limit to their elastic behaviour. Loads that exceed would result in a plastic deformation which is not immediately reversible on removal of the applied force. This mechanism

predominates in materials that has a shear strength less than the tensile or breaking strength.

Conversely, brittle fracture occurs with hard and brittle particles in which the shear strength is greater than the tensile or breaking strength. For example, sucrose particles in which, when preferentially fractured, the smaller fragments help to fill up any adjacent air space. The ability of a material to deform in a particular way depends on its lattice structure; in particular whether weakly bonded lattices are inherently present. Some deformation processes, such as creep, are time-dependent and occur at various rates during the compaction sequence. This means that the rate at which the load is applied and removed may be a critical factor in materials for which dependence on time is significant. For example, if a plastically deforming solid is loaded too rapidly, the solid may exhibit brittle fracture resulting in structurally flawed tablets. However, relatively slower machine speeds and compression rolls of a large diameter can help with difficult tablet formulations (Lachman *et al*, 1986).

3.4.7 Compression cycle

3.4.7.1 Pre-compression

Modern rotary machines have a pre-compression (Figure 3.10) facility, to aid compaction. Vezin *et al.* (1983) studied the effects of pre-compression on different materials and suggested that it might be assisted by enabling time dependant plastic flow, relieving elastic stress, or reducing entrapped air. They also indicated that the pre-compression dwell time was not important and that its benefit was material dependent. During this phase of the compression cycle, material undergoes fast rearrangement, high friction, and collisions between each other and slippage inside the die vicinity. Hunter *et al.* (1976) used a compaction simulator to predict the effect of pre-compression on high-speed rotary machines.

3.4.7.2 Compression

Compression according to most researchers is the reduction of powder volume to form the final compact. Particle deformation and fragmentation usually occurs during this phase of compression cycle. Due to fast powder compression using a modern press it is very difficult to understand the mechanism of compression. However, enormous friction and particle slippage inside the die occur at a very short time.

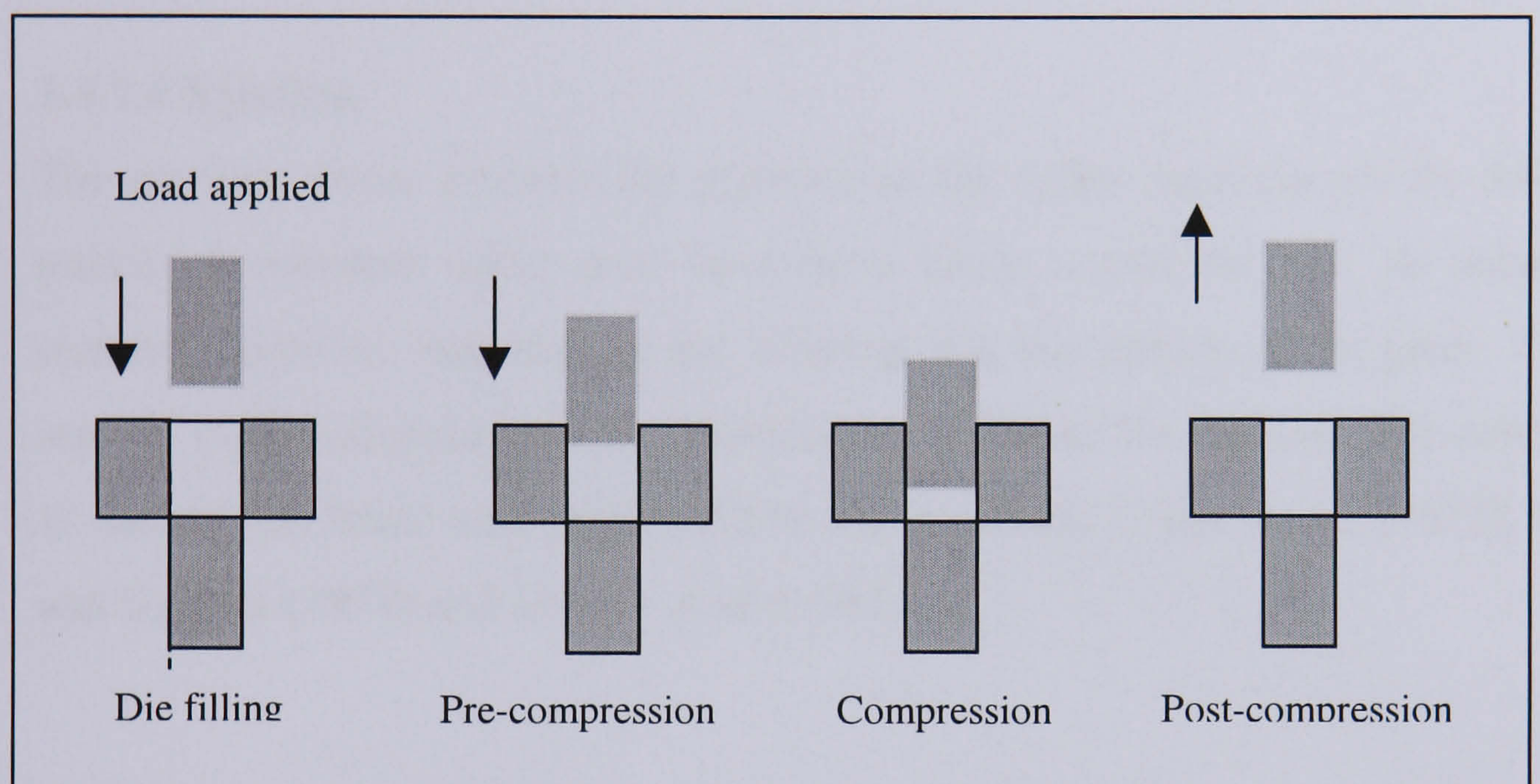

Figure 3.10 The stages of compression

3.4.7.3 Decompression

The usefulness of decompression in a typical compression cycle was not realised until researchers began to investigate the reasons for compression problems such as capping and lamination. Shlanta and Milosovitch (1964) used a Carver hydraulic press to determine the post-compressional behaviour of different materials, suggesting that superior tablets were obtained from materials which exhibited medium relaxation. David and Augsburger (1977) further investigated this phenomenon and developed viscoelastic relationships and plotted these for a range of directly compressible tablet fillers. Rippie and Danielson (1981) also studied viscoleastic relationships and split the decompression phase into two distinct steps:

(1) unloading: where the pressure on the material is reduced but the punch is still in contact with the compact.

(2) post compression: where the punch is removed and the compact is residing stationary within the die cavity.

Ritter and Sucker (1980) showed that an increasing decompression rate is deleterious to the final physical properties of tablet and emphasised the importance of the decompression rate in Phenazone with reference to capping.

3.4.7.4 Ejection

The ejection phase involves the removal of the tablet from the die by the lower punch. A coherent tablet may have been made within the die; its subsequent removal however, may disrupt the bonding that has already taken place. For this reason, most materials require a lubricant to facilitate the ejection. The lubrication of tablets has been well researched in the literature. Conte *et al.* (1972), Holzer and Sjogren (1978) and Moody *et al.* (1981).

3.4.8 Problems in tabletting

Capping and lamination have been problems as long as tablets have been compressed. The term capping generally refers to the lid of biconvex tablet being separated from the cylindrical portion, (Figure 3.11). Capping may occur at one end of a compact or both. Lamination generally refers to the layered splitting of a compact normal to the punch face. Lamination may cause capping and the term may sometimes be used to describe capping.

Wood in 1906 described eight cases of capping:

1. imperfect upper punch, particularly unpolished.
2. imperfect or worn die.
3. imperfect alignment of punches and dies.
4. too much pressure.
5. damp granulation.
6. too much fine powder.
7. too soft granulation.
8. wrongly proportioned excipients.

Little and Mitchell in 1951 listed five similar causes:

1. insufficient binder in the granules.
2. excess of fine powder.
3. worn top punch or die.
4. excessive pressure.
5. damp granulation.

It is interesting to note that in neither references was compression speed considered to be a cause of the capping phenomenon. Entrapped air was also suspected of being a cause of capping in tablets. However, Ritter and Sucker (1980) dismissed the influence of air by observing capping in tablets compressed in air.

The size and shape of compacts may also influence capping. Tablet compressed on deep concave punches are generally more likely to cap than others pressed using normal concave or flat punches. With deep concave punches, the domed portion to the tablets provides an ideal failure plane and the punch is also more likely to entrap air. Seitz and Flessland (1965) observed that capping was more prevalent on larger diameter tablets than smaller diameter tablets when they compressed a sugar based material to a common density and thickness.

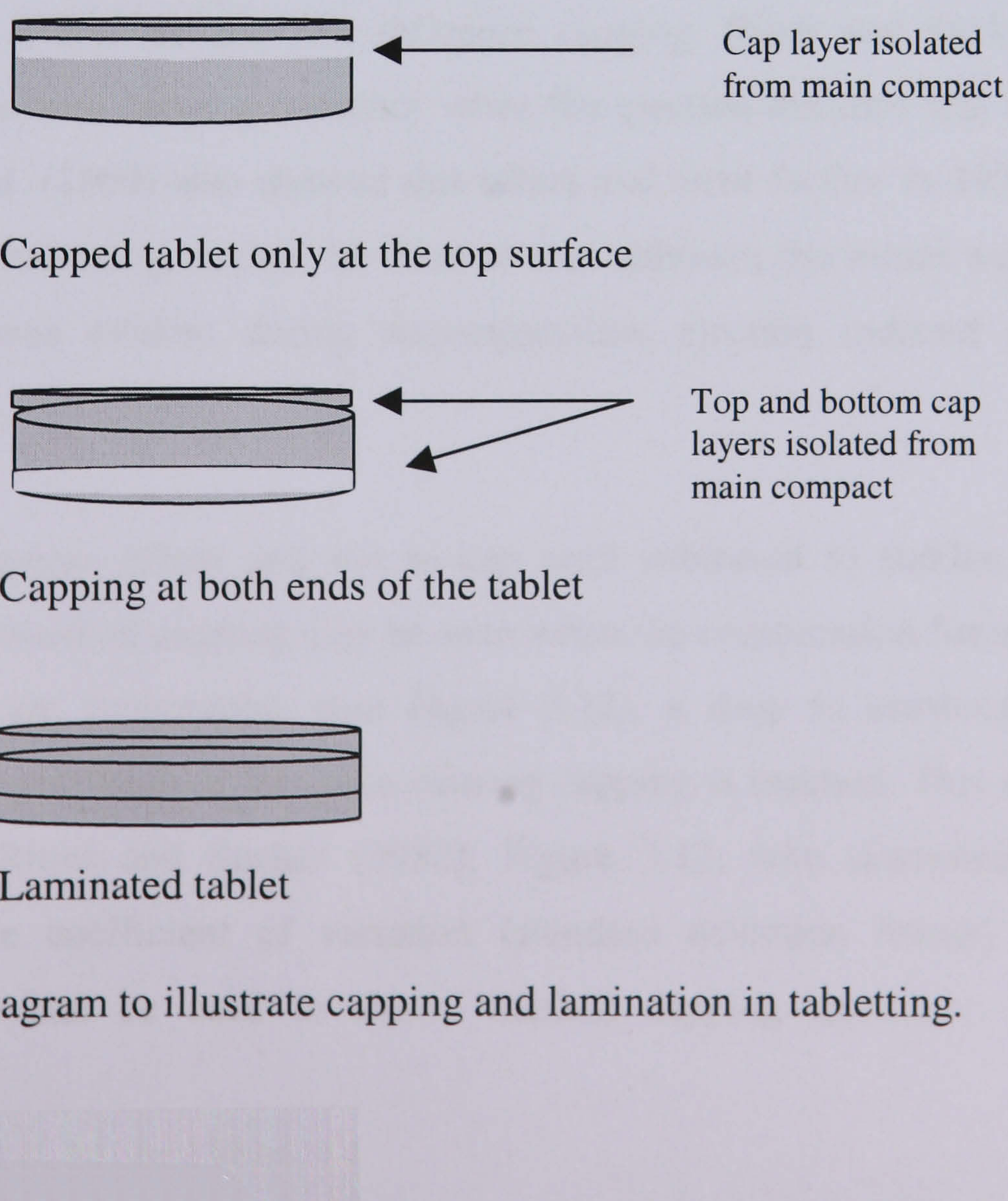

Figure 3.11 Diagram to illustrate capping and lamination in tabletting.

Nystrom (1977 and 1978) and Jarosz and Parrot (1982) measured the radial and axial tensile strengths of tablets as a method of predicting capping tendency. Although successful in predicting capping in tablets with low axial tensile strengths, the method involved the use of adhesive and was time consuming.

Ritter and Sucker (1980) conducted an extensive study in capping and examined a number of variables including compression force, tabletting speed, moisture content and punch penetration depth. They concluded that although other factors may influence capping, only when elastic recovery exceeds the inter-particle bonding forces is capping likely to occur. This was supported by Jones (1983) who hypothesised that short dwell times will induce strains within compacts, which, if not accommodated by elastic or plastic deformation of the bonds made during compression, would initiate micro-fractures and crack. This would indicate that at the particle level plastic flow requires time to allow adequate bonding. When using this model to study the compact as a whole, however, pressure distributions within the compacts make it difficult to predict the conditions which will cause capping.

The problem in discriminating between capped and uncapped tablets is made more complex as the occurrence of capping appears to depend on both material and time. Stresses within the die also influence capping. Ritter and Sucker (1980) showed an increased capping tendency when the ejection distance was increased. Funakoshi *et al.* (1969) also showed this effect and went further in 1975 using a 'drilling load measuring device' he showed that although the initial weakness in the compact was evident during decompression, ejection induced additional strains.

Tablets may appear robust and not to cap until subjected to sudden shock or breakage. The onset of capping may be seen when the compression force/crushing force profiles are constructed, (see Figure 3.12), a drop in crushing force is observed when the value of the force causing capping is reached. This effect was described by Ritter and Sucker (1980), Figure 3.12, who described how an increase in the coefficient of variation (standard deviation /mean) of tablet crushing force can be used to show 'masked capping tendency'. Although

researchers dispute when capping occurs, the evidence that the process may be time dependent suggest that individual tablets compressed from the same material may be capped at any time. Materials in general show varied capping tendencies; paracetamol, as an example of brittle material, usually caps and laminates. The use of binders in tablet formulations can assist in overcoming the forces which disrupt the bonds made during compression.

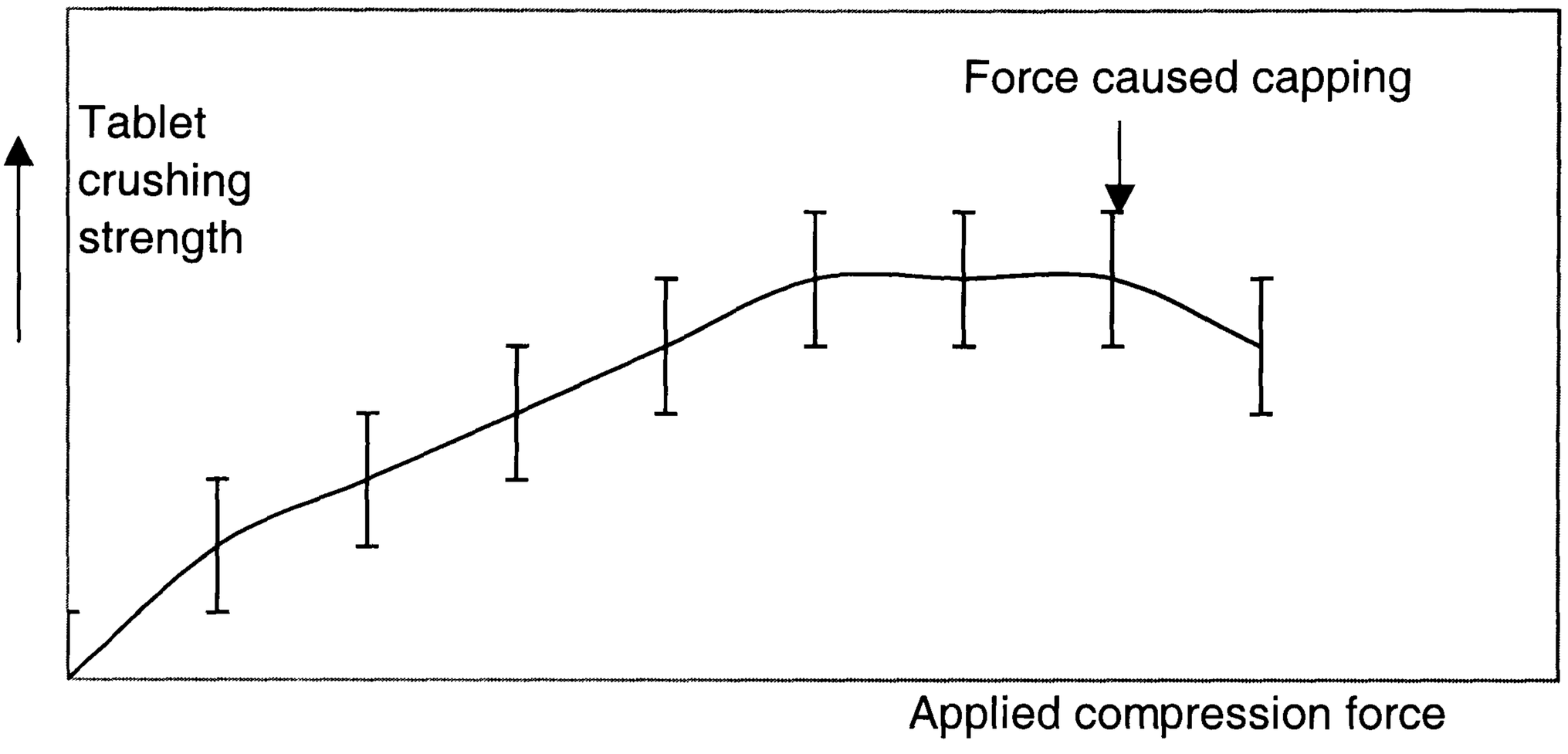

Figure 3.12 Hidden capping tendency with error bars (Ritter and Sucker, 1980).

3.5 Summary

This chapter comprises three sections. In Section one, introduction of acoustic emission theory and background was presented. Description of AE parameters and measurement systems were introduced. Section two reviewed previous applications of acoustic emission for monitoring various chemical and pharmaceutical processes. Some processes produce emissions that can be heard. Many more emit sound of much higher frequencies in the region of 100 kHz to 1 MHz. It was shown through this review that AE could provide useful information about the process being monitored. Details of previous AE applications in powder compression were also presented.

Section three discussed the basic theory of powder compression. It also contains a brief explanation of the various mechanisms that govern the compaction process.

In the following chapter, details of experimental design, instrumentation and material used in this project are presented.

Reference:

Ahmed, N & Payne, P. A. (1994) A liquid nitrogen cooled crystalliser for process monitoring using acoustic emission techniques. *Measurement +Control*, **30**, 146-148.

Bateman S. D, Rubinstein M.H. and Thacker H.S. (1989), Properties of Paracetamol Tablets Produced using High Pre-compression Pressure, J. *Pharm. Pharmacol*. **41**. 12-32

Belchamber, R. M., Betteridge, D., Collins, M. P., Lilley, T., Marczewski, C. Z., & Wade, A.P. (1986). Quantitative study of acoustic emission from a model chemical process. *Analytical Chemistry*, **58**, 1873-1877.

Cao, Z., Wang, B. G., Wang, K.-M., Lin, H.-G., & Yu, R.-Q. (1998). Chemical acoustic emissions from gas evolution processes recorded by a piezoelectric transduce. *Sensors and Actuators* B, **50**, 27-37.

Conte U. Columb P., Caramella C. And La Manna A. (1972), The effect of Magnesium Stearate and Polytetrafluoroethylene ona Lubricant in Direct Compression of Acetylsalicylic Acid. Farmaco Ed. Pract. **27**, 440-452.

Cooper Jr. A.R. and Eaton L.E (1951) Compaction behaviour of several ceramic powders. J.Am. Cer. Soc., 45, 97-101.

Danielson D. W., Morehead W. T. And Rippie E. G. (1983) Unloading and postcompression Viscoelastic Stress versus Behaviour of Pharmaceutical Solids. J. Pharm. Sci. **72**, 4. 342-345

David S. T. And Augsburger L.L. (1977), Plastic Flow During Compression of Directly Compressible fillers and its Effects on Tablet Strength. *J. Pharm. Sci*. **66**. 155-159.

Drahos, J., Zahradnik, J., Puncochar, M., Fialova, M., & Bradka, F. (1991). Effect of operating conditions on the characteristics of pressure fluctuations in a bubble column. *Chemical Engineering Processes*, **26**, 147-164.

Drahos,J., & Cermak,J. (1989) Diagnostics of gas-liquid flow patterns in chemical engineering systems. *Chemical Engineering and Processes*, 22, 45-52.

Drouillard, T. F.(1988). Introduction to acoustic emission. *Material Evaluation* , **46**, 175-180.

Eissa S, Au Y.H. J., (2000) Non-Invasive measurement of pharmaceutical processes. *Doctoral Research Conference*, Brunel University 16-17 September p 29-37.

Fowler, T. J (1992). Chemical industry applications of acoustic emission. *Material evaluation*, 875-882.

Funakoshi Y. (1975), Some observation on the capping properties detected in the tablet making compaction process, *Zairoyo* **24** 673-676.

Funakoshi Y., Kajuira T. And Asogowa T. (1969) Ruling factors of capping in the compressing process and the method of preventing capping, *Zairyo* **18** 547-553.

Gennaro M. C and Bertolo P.L, J. Chromatography., 472 (1989) 433.

Gurel O and Gurel D, Topics in current chemistry, Springer Verlag, Berlin, vol. 118 (1984).

Hakanen A, Laine E, Jalonen H, Linsaari K and Jokinen J, (1993). Acoustic emission during powder compaction and its frequency spectral analysis. *Drug Development and Industrial Pharmacy*, **19** (19), 2539-2560.

Hakanen A, Laine E. (1995) Acoustic characterisation of a microcrystalline cellulose powder during and after its compression. *Drug Development and Industrial Pharmacy*, **21**(13), 1573-1582.

Handbook of Pharmaceutical Excipients, (1994) second Edition (Wade, A. And Weller, P.J., eds), The pharmaceutical Press, London UK.

Heckel R. W. (1961a). Density-Pressure Relationship in Powder Compaction. *Trans. Met. Soc.* A.I.M.E **221**, 671-675.

Heckel R. W. (1961b). An anlysis of powder compaction phenomena. Trans. Metall. Soc. AIME **221**, 1001-1008.

Hersey J. A and Rees J. *Nature* PS. 230: 96 (1971).

Hessel G, Schmitt W, Van der Vorst K and Weiss F. P (1999), A neural network approach for acoustic leak monitoring in the VVER-440 pressure vessel head. *Progress in Nuclear Energy*, **34**, No3, 173-183.

Holzer A. W and Sjogren. (1979(1)). Evaluation of Sodium Stearyl Fumarate as a *Tablet Lubricant. Int. J. Pharm.* **2**, 145-153.

Holzer A. W and Sjogren.(1979(2)) Instrumentation and Calibration of a Single Punch Press for Measuring the Radial Force During Tabletting. *Int. J. Pharm.* **3**, 221-230.

Hsi, R., Tay, M., Bukur, D., Tatterson, G.B., & Morrison, G. (1985). Sound spectra of gas dispersion in an agitated tank. *Chemical Engineering Journal*, **31**, 153-161.

Huckle P. D and Summers M.P. (1984), The Effect of Strain Gauge Size and Configuration of Radial Stress Measurement During Tabletting. *J. Pharm. Pharmacol.* **36**. 6p.

Hunaida, O., & Chu, W. T. (1999). Acoustical characteristics of leak signals in plastic water distribution pipes. *Applied Acoustics*, **58**, 235-254.

Hunter B.M. Fisher D. G, Pratt, R. M and Rowe R. C (1976), A high Speed compression simulator. *J. Pharm. Pharmacol.* **28**, 65.

Huttenrauch R. (1978) The Mechanism of Tablet Forming, A new Conception. *Acta.Pharm. Technol. Suppl.* **6**, 114-120.

Jarosz P. J and Parrot E. L. (1982) Factors influencing axial and radial tensile strengths of tablets.

Jones T. M. (1983) Tablets, Tabloids ... and Tabloids. *Pharm. J*, Sept 17 301-307.

Katdare, A.V and Bavitz, J.F (1987) A study of the compatibility characteristics of a direct compression and a wet granulated formulation of norfloxacin. *Drug Dev. Ind. Pharm.* **13**, 1047-1061.

Khan, K.A et al. (1981) the effect of moisture content of microcrystalline cellulose on the compressional properties of some formulations. Drug. Dev. Ind. Pharm., 7, 525-514.

Korsch W. (1980). Automatic Tablet Production. *Drugs Made Germ.* **23**, 173-177.

Leach, M. F., Rubin, G. A., & Williams, J. C. (1977) Particle size determination from acoustic emissions. *Powder Technology*, **16**, 153-158.

Leach, M. F., Rubin, G. A., & Williams, J. C. (1978) Particle size distribution characterisation from acoustic emissions. *Powder Technology*, **19**, 157-167.

Little A. and Mitchell K. A. (1951) Tablet Making. Northern Publishing Co.

Little M. J and Wentzell P. D (1995), *Analytica Chimica Acta* **309** 283-292.

Little, M. J. & Wentzell, P. D (1995). Evaluation of acoustic emission as a means for carbonate determination. *Analytica Chimica Acta* **309**, 283-292.

Mann S. C, Bowen D. B., Hunter B. M., Robert R. Rowe R. C and Tracey R. H. (1981). The Influence of Punch Tolerance on Capping. *J. Pharm. Pharmacol. Suppl.* 25p.

Marshall K. 'Powder Advisory Centre Some observation on the Elucidation and control of the die compaction process' *Proceedings Int. Conference on Compaction and Consolidation of Particulate Materials* 173-181 (1972).

McIntire P. (1987), "Nondestructive Testing Handbook Second Edition" Volume 5 Acoustic Emission Testing, *American Society for Nondestructive Testing*.

Mikiel, W., Ranachowski J., Rejmund F., Rzeszotarska J., Information contents of the acoustic emission exemplified by the selected physico-chemical processes, *Archieves of Acoustics*, **15**, 1-2, 185-192 (1990).

Myerson, A.S. (1993) Handbook of industrial Crystallisation, Stoneham, MA: Butterworth-Heinemann.

Nystrom C., Alex W and Malmqvist K. (1977) New Approach to tensile strength measurement of tablets. *Acta. Pharm. Suec.* **14** 317-320.

Nystrom C., Malmqvist K., Mazier J., Alex W., and Holzer A. W. (1978) Measurement of axial and radial tensile strength of tablet and their relation to capping.

Pawelek A, (1988) Possibility of a soliton description of acoustic emission during plastic deformation of crystals, *J. Applied Physics*, **63**, 5320

Reier G. E. And Shangraw R. F. Microcrystalline Cellulose in Tabletting, *J. Pharm. Sci.* **55** 510-514.

Riano M. D. G , Garcia-Vargas M, and Leyva J. A. M. Analyst, 115 (1990) 973

Ritter A and Sucker H. B, (1980) Studies of Variables that effect Tablet Capping, *Pharm. Tech.* March 57-65 and 128.

Rue P.J, Barkworth P.M, Ridgway-Watt P, Rough P, Sharland D, Seager H and Fisher H, (1979). Analysis of tablet fracture during tabletting by acoustic emission techniques. *Int. J. Phar. Tech &Prod.* Mfr., **1**(1) 2-5.

Sawada, T., Gohshi, Y., Chikako, A., & Furuya, K. (1985a). Acoustic emission arising from the gelation of sodium carbonate and calcium chloride. *Analytical Chemistry*, **57**, 366-367.

Sawada, T., Gohshi, Y., Chikako, A., & Furuya, K. (1985b). Acoustic emission from phase transition of some chemicals. Analytical Chemistry, 57, 1743-7145.

Seitz J A and Flessland G. M (1965), Evaluation of the physical Properties of Compressed Tablet 1: Tablet Hardness and Friability, J. Pharm. Sci. (54) 9 1353-1357.

Tabor D , "The hardness of Metal ", Oxford University Press, London 1951.

Takano S., Kondoh Y and Ohtsuka H. Analytical Chemistry., 57 (1985) 1523.

Train, D, (1956) An investigation into the compaction of powders. J. Pharm. Pharmacol. 8, 745-761.

Tsujimoto, H., Yokoyama, T., Huang, C. C., & Sekiguchi I (2000)., Monitoring particle fluidization in a fluidized bed granulator with an acoustic emission sensor. *Powder Technology*, **113**, 88-96.

Vahaviolos, S. J., Pollock, A., & Lew, N. (1991). Pinpoint structural defects with acoustic emissions. *Chemical Engineering Progress*, **87**(1), 60-67.

Wentzell P. D., Lee, O., & Wade, A. P (1991) Comparison of pattern recognition descriptors for chemical acoustic emission analysis. *Analytical chemistry* **5**, 389-403.

Whiaker, M., Baker G., Westrup J., Goulding P., Rudd., Belchamber R., Collins M.,(2000) Application of acoustic emission to the monitoring and end point determination of a high shear granulation process. *International Journal of Pharmaceutics*. **205**, 79-91.

Wong, D. Y, Waring M, Wright P and Aulton M, (1991). Acoustic emission during the deformation of α-lactose monohydrate and anhydrous α-lactose monocrystals. *J. Pharm. Pharmacology*, **43**, 659-661.

Chapter 4 Experimentations

4.1 Introduction

This chapter describes in detail the experimental design and set up conducted for the acoustic emission monitoring of powder compression. The preliminary test and design are described. Details of industrial tests are also presented using an industrial tablet press. In addition, the acoustic emission interfacing for monitoring is considered. Careful consideration is given to the choice of pharmaceutical powders used in the experimentation. This chapter also describes the tablet hardness evaluation test using a tablet hardness tester and dissolution bath. Finally, the AE signals generated from powder compression using the industrial press were evaluated to discriminate between the events generated from pure compression from those that emanate from other sources within the process.

4.2 Design of test rig for AE powder compression test

4.2.1 Test rig

A compression test rig was designed for the preliminary investigations. The purpose of designing this test rig is to carry out a number of experimental investigations using the AE technique. These investigations include study of the effect of compression speed, material weight, material type and particle size on the AE produced from the compression process. Figures 4.1-4.3 shows the engineering drawings with full dimensions. All the parts were assembled to produce the final test rig as shown in Figure 4.4.

4.2.2 Compression machines and calibration

Tablet compression tests were conducted on two universal tensile testing machines (Instron Ltd, High Wycombe, model 1011 (5 kN load frame) and model 8502 (100 kN load frame)). See Figures 4.5 and 4.6.

Both load cells were certificated to class A and compression energies were calculated from the integrator fitted to the testing machines. The integrator was calibrated at the start of each compression set of experiment. The calibration was done using the internal calibration system fitted to the load cell. Initial study showed that the calibration remained stable through the day. Where the net compression energy was calculated this was found by subtracting the energy required to compress the punches

and load frame without powder between the punches from the total energy found for tablet compression; both compressions being made to the same applied load.

4.2.3 Acoustic emission interfacing

Acoustic emission was detected using a broadband piezoelectric transducer (WD AE48); the transducer was connected to a 40-dB preamplifier with a built in filter (20Hz – 1.2MHz). The output from the preamplifier was fed into a 4-channel acoustic emission instrument MISTRAS 2000 (Physical Acoustic Ltd, UK). This instrument can extract and record in real time the AE descriptors: ring down count (RDC), event duration (ED), peak amplitude (PA), rise time (RT), energy (ENG) and average signal level (ASL). The binary data files obtained from the MISTRAS 2000 were converted to ASCII files so that the data could be analysed by Excel 7 and Axum 6. Conversion of binary data to ASCII was performed using a built-in program in the MISTRAS system.

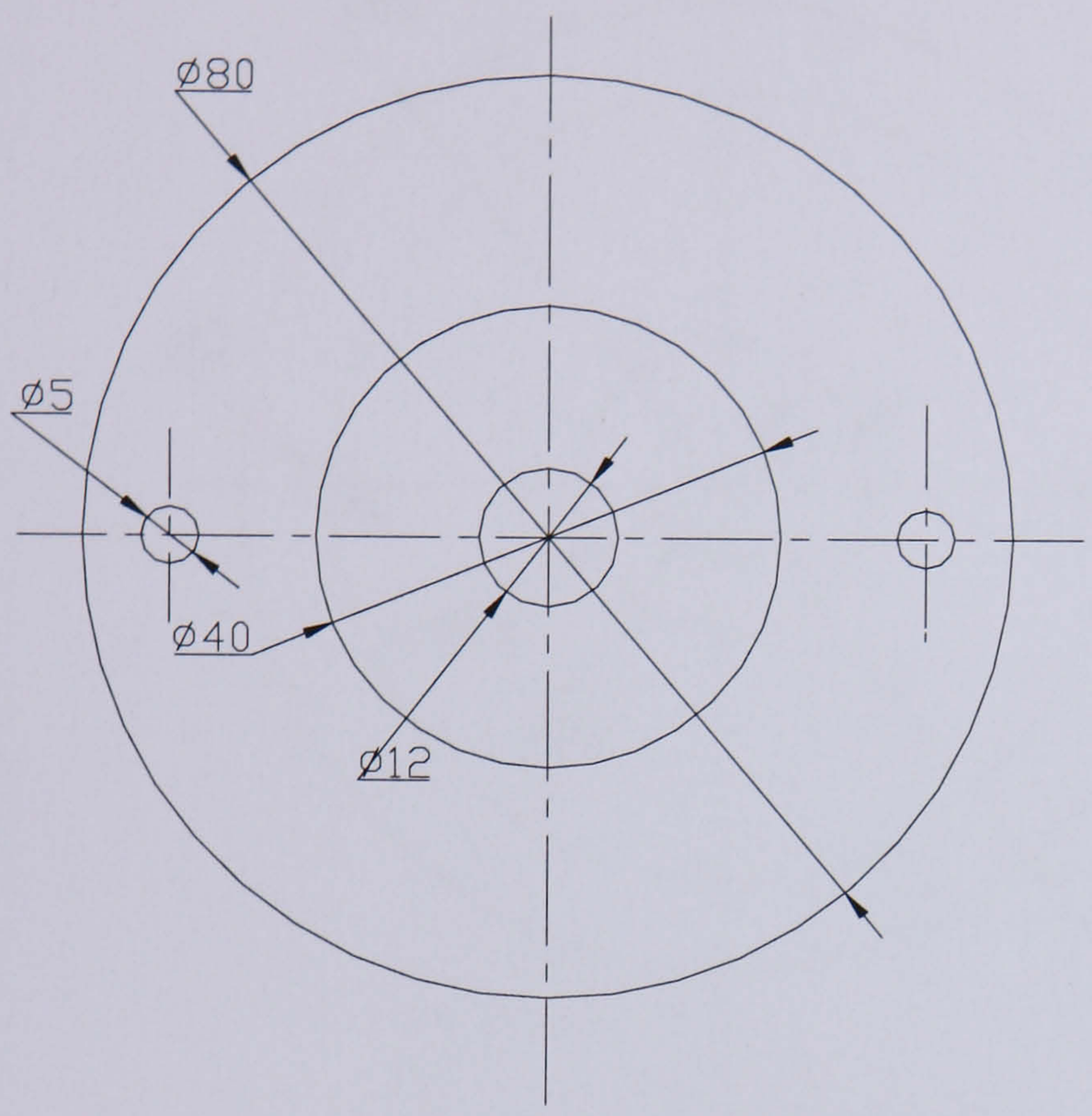

PLAN VIEW

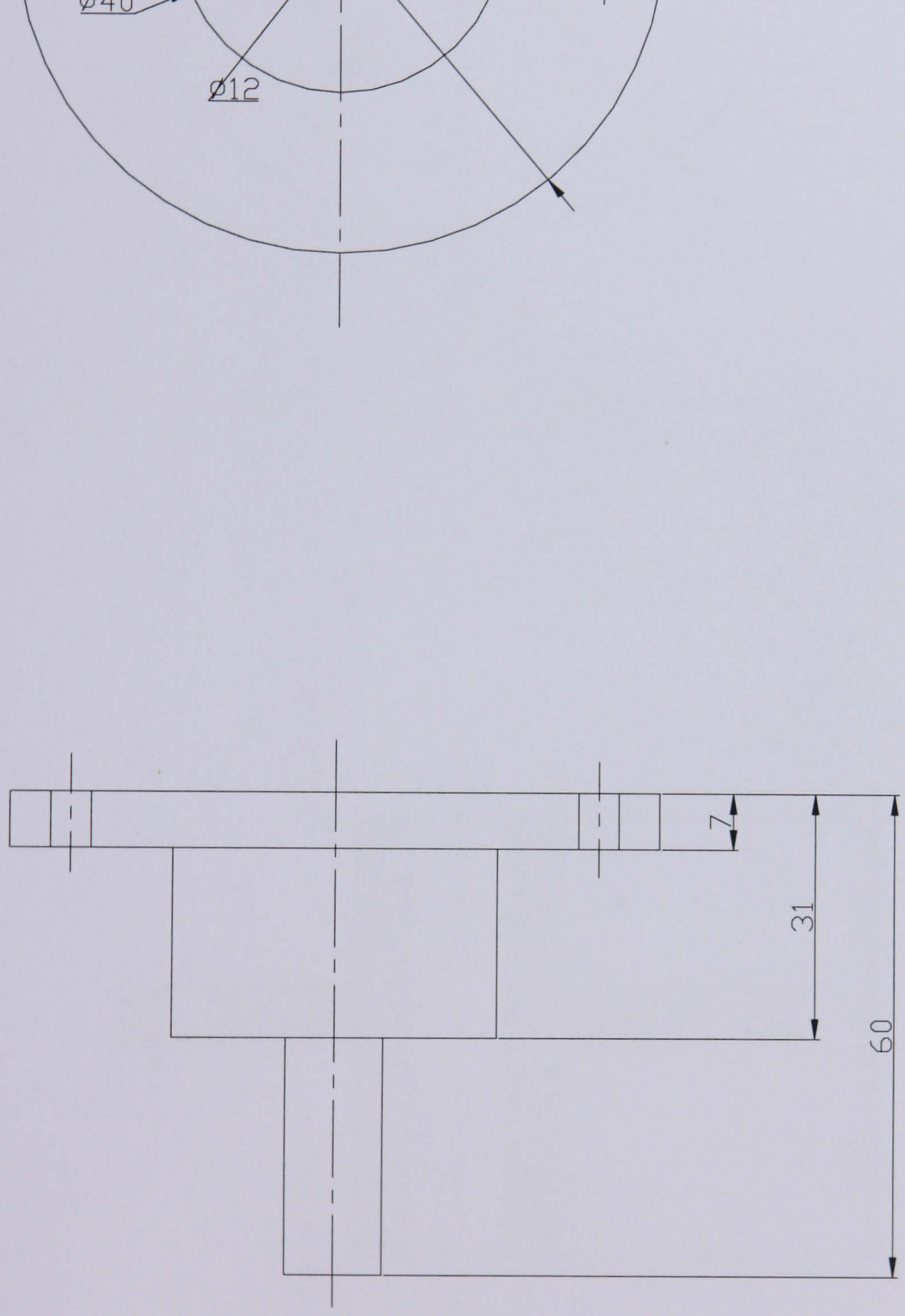

ELEVATION VIEW

Figure 4.1 Diagram showing the upper punch design of the test rig, (dimensions in millimetres) made of steel.

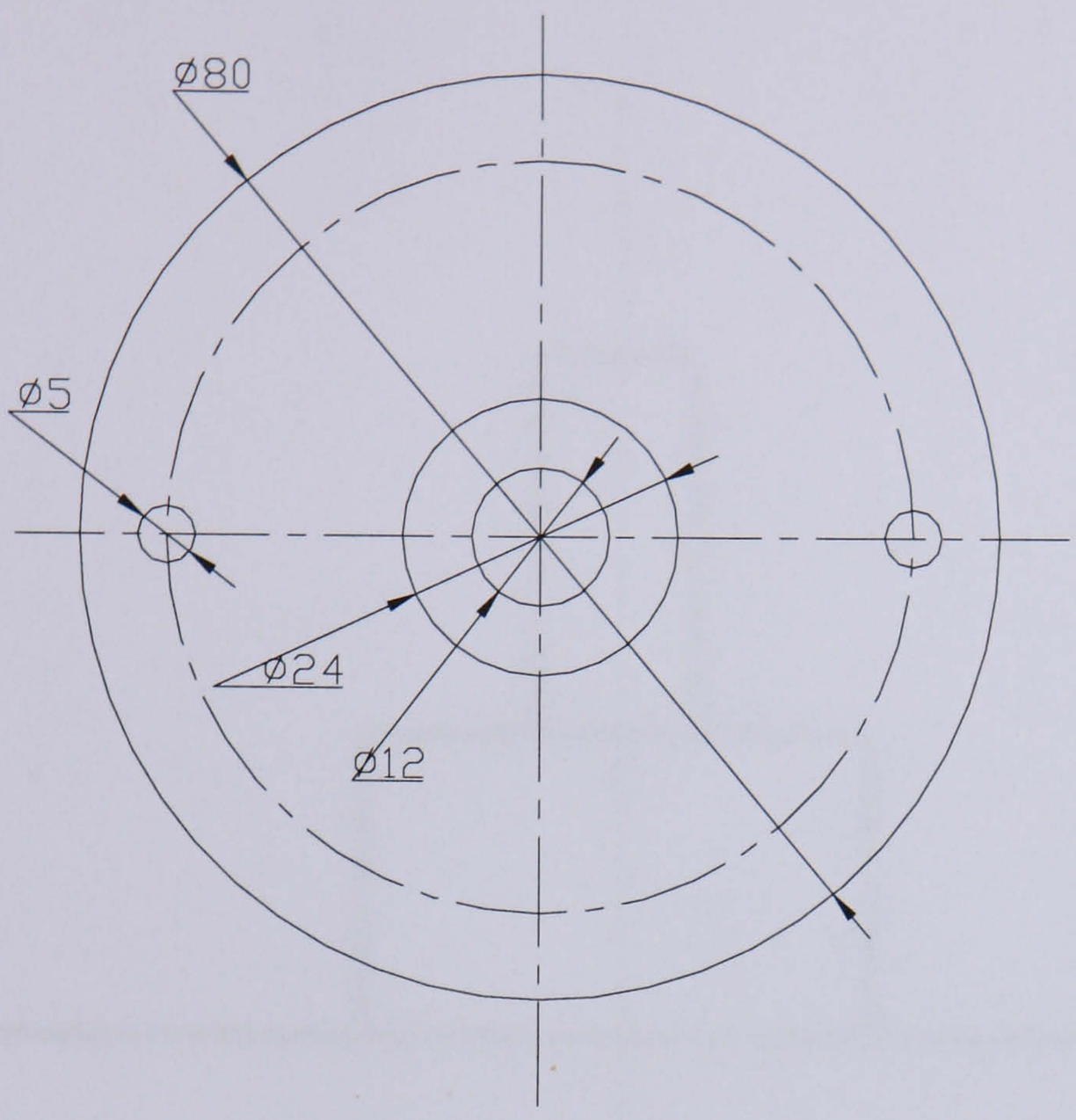

Figure 4.2 Diagram showing the die design of the test rig, (dimensions in millimetres).

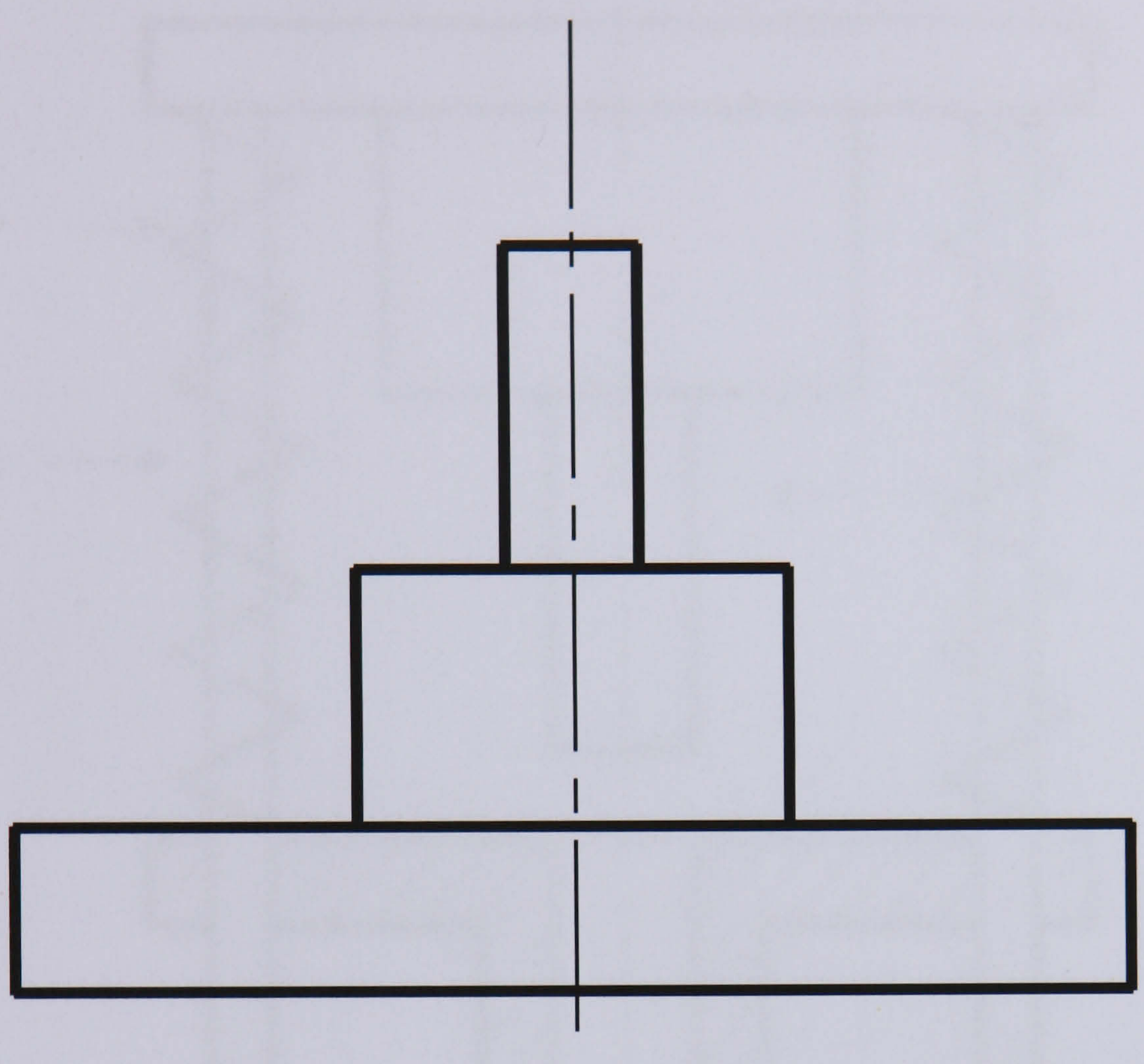

Figure 4.3 Diagram showing the lower punch design of the test rig

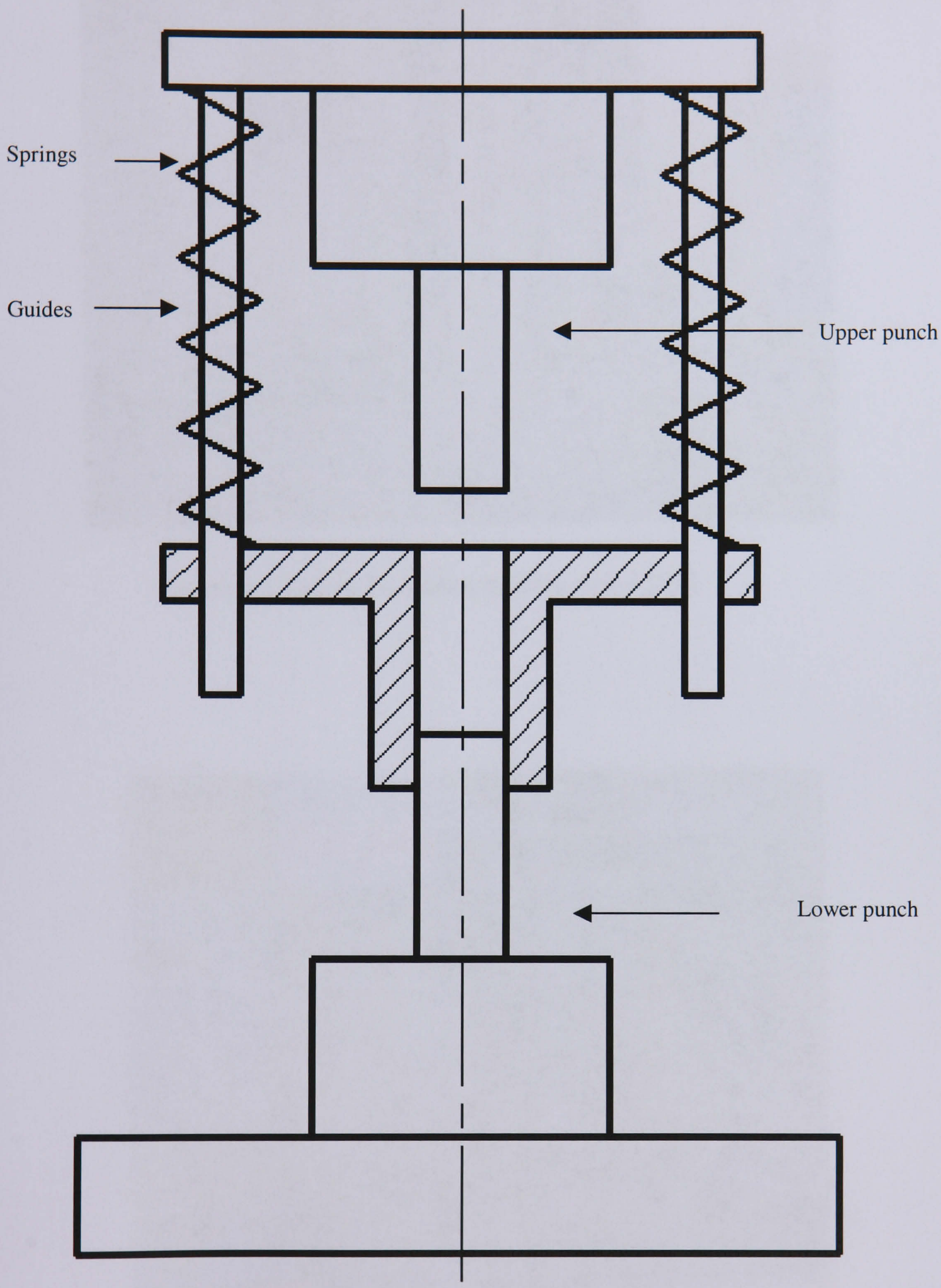

Figure 4.4 Schematic diagram of the final assembly of the test rig

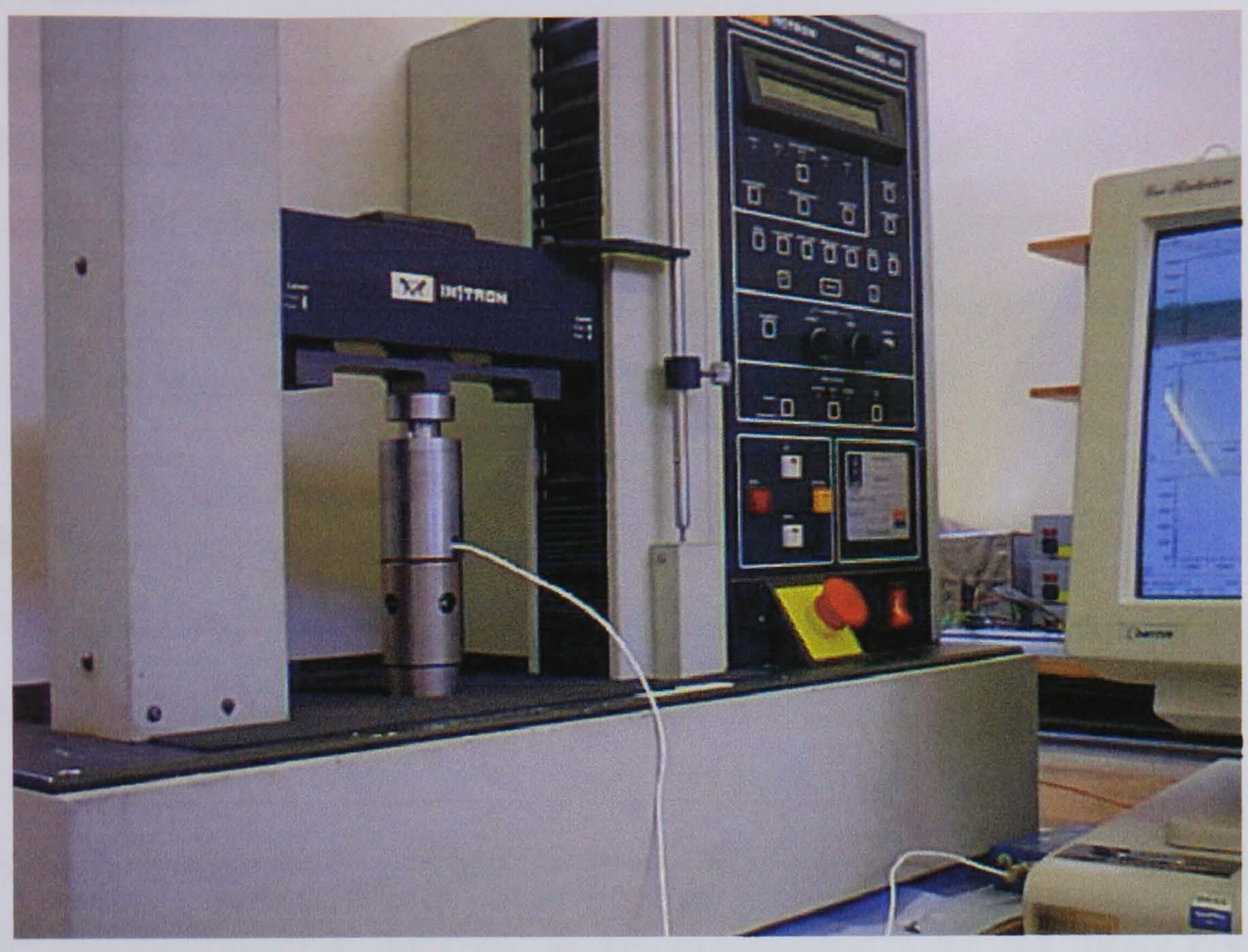

Figure 4.5 Test rig on Instron machine model 1011.

Figure 4.6 Instron machine, model 8502.

4.2.4 Material

The materials used in the investigations were selected such that different compression mechanisms could be examined. These materials have either plastic or brittle characteristics. Lactose, paracetamol, microcrystalline cellulose and sodium chloride were selected initially as examples representing the above mechanisms. All these materials were used as received because they can be directly compressed.

4.2.4.1 Microcrystalline cellulose (Avicel)

Microcrystalline cellulose is purified, which is prepared by treating α-cellulose with mineral acids, producing bundles of needle-like microcrystals. In terms of appearance, this excipient is a white, crystalline powder composed of agglomerated porous particles (Handbook of Pharmaceutical Excipients). Many formulation scientists ranked microcrystalline cellulose as the most useful filler for direct compression. Its popularity can be ascribed to its excellent compactibility at low pressures, high dilution potential and superior disintegration properties. However, using paracetamol and potassium phenethicillin as a model compound, Wade & Willer (1994) found that the compactibility of microcrystalline cellulose decreases with reduction in its moisture content.

Microcrystalline cellulose occurs as a white-coloured, odourless, tasteless, crystalline powder composed of porous particles. It is commercially available in different particle size grades, which have different properties and applications.

Table 4.1 list typical properties of microcrystalline cellulose and other materials used in the current studies.

4.2.4.2Lactose (Zeparox)

White to off-white crystalline particles or powder, lactose is colourless and slightly sweet-tasting; α-lactose is approximately 15% sweet as sucrose, while β-lactose is sweeter than the α-form.

The moisture measurement sensing requirement is often the need to detect levels of moisture in a particular material without being able to contact it to permit control of a drying process. Measuring moisture content allows control of the drying process such that drying is carried out until a specific level of moisture content is achieved rather

than for a fixed time period. In industry, moisture content of a material can effect it's ability to successfully be processed by some subsequent task. Fine drying control may be required to maintain quality of production as well as control the costs involved.

Capacitive sensing is very suitable for economic moisture measurement, water has a high dielectric value and is consequently easily detectable with capacitive techniques having as it does a significant effect on electric fields.

Table 4.1 Typical properties of the materials used.

Properties	**Materials**				
	Avicel	Lactose	Paracetamol	NaCl	Isomalt
Density (g/cm^3)	1.618	1.54	1.29	1.91	1.7
Compressibility %	8.9	7.4	7.5	11.6	8.6
Particle size (μm)	20-100	50-75	100-150	100-150	50-150
Moisture content (w/w)	<5%	4.5-5.5	4	3	3-4

4.2.5 Determination of crushing strength

The resulting compact was removed from the cell by disassembling the die set and the thickness of the compact was accurately determined with the aid of a micrometer. The compact was then subjected to axial compression at a rate of 0.5 mm/min until rupture occurred. This was done on the tablet hardness tester (Schleuniger model 4M, Switzerland, see Appendix A3).

Tablet hardness tester

Basically the strength measurement is performed on the counterweight principle. The power jaw (left) Figure 4.7, which is driven by a speed regulated motor, presses the tablet with constant and controlled load against the measuring jaw (right). The pressure force on the tablet is proportional with the time during which the counterweight is lifted. An angle transmitter going through an A-D transformer to the computer measures the turning angle of the counterweight axis. When the tablet is crushed the counterweight drops back slightly and this is registered by the

microcomputer. The test result is calculated by the microcomputer from the highest angle attained by the counterweight axis and then shown on the digital display.
The motor returns the power jaw to a memorised position for the tablet diameter being measured. At the moment of crushing the computer engages the counterweight brake system allowing the counterweight to fall back down gently.

Calibration of the tablet tester

The calibration of the tablet tester is done by exerting a known, constant force on the right measuring jaw in an exact axial direction and adjusting the digital display reading by means of turning the potentiometer to coincide with the force exerted.

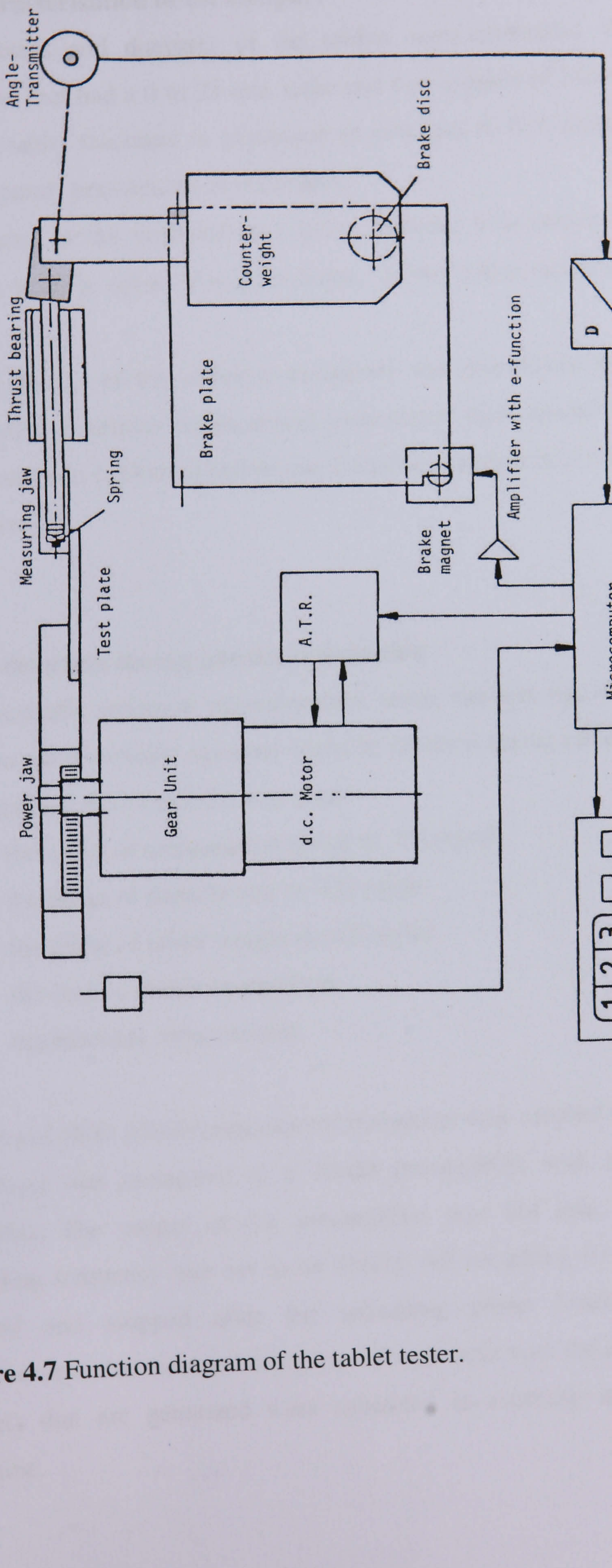

Figure 4.7 Function diagram of the tablet tester.

4.2.6 Characterisation of the compact

The thickness and diameter of the tablets were measured with a screw gauge micrometer that had a 0 to 25 mm scale and was capable of differentiating up to 0.01 mm. The tablet thickness is expressed as averages of five measurements made at 5 different points between the two surfaces.

The volume of the compact at a given pressure was calculated according to the equation: $V=\pi r^2 h$, where V is the volume, r is the radius, and h is the thickness of the compact.

The true density of the cellulose excipients was determined using a Quantachrome Model MPY-2 helium displacement pycnometer (Quantachrome Corporation). The pycnometer was calibrated before use. Detailed description of this test can be found in Appendix A1.

4.3 AE detection during powder compaction

Initial acoustic emission measurements, using the test rig, on powder compaction aimed to see if acoustic emission could be detected during tablet compression. Further investigations were carried out to study:

1. the effect of compression speed on AE signal.
2. the effect of particle size on AE signal.
3. the effect of tablet weight on AE signal.
4. the batch to batch comparison.
5. the hardness measurement.

Wide band (WD AE48) piezoelectric transducer was coupled to die. The output of the transducer was connected to a 40-dB preamplifier with a built in filter (20Hz-1.2MHz). The output of the preamplifier was fed into the MISTRAS system. Sampling frequency was set to be 4MHz. AE recording started as soon as the load applied and stopped after the unloading phase finished. Force-displacement measurement also recorded using the software built with the Instron machine.

Tablets that are generated were subjected to crushing strength using tablet test machine.

4.4 Experimentation at GSK

4.4.1 Tablet press

The Manesty F3, Figure 4.8 and Figure 4.9, is a single-stroke, power-driven tablet machine capable of producing tablets up to 22mm (7/8 inches) in diameter with a maximum output, using single-tip punches, of 85 tablets per minute (5,100 per hour). The machine is of robust design and is built to the customary high Manesty standards. The drive is from a 2 hp motor fitted with a timing pulley and toothed belt drive to the ball bearing mounted worm shaft which has a nickel-steel, case-hardened and accurately-ground worm. This worm drives the Holfos bronze worm wheel mounted directly on the main shaft running in a bronze main bearing and ball-bearing races. The main shaft carries the ejection and the feed shoe-operating cam and the adjustable eccentric strap, which operates the crosshead where the upper punch is mounted. Tablet weight is adjusted by means of the lower plunger nuts mounted below the die-table. Provision is made for lubrication of all vulnerable points with an oil-gun, and the worm and wheel are contained in an enclosed oil bath.

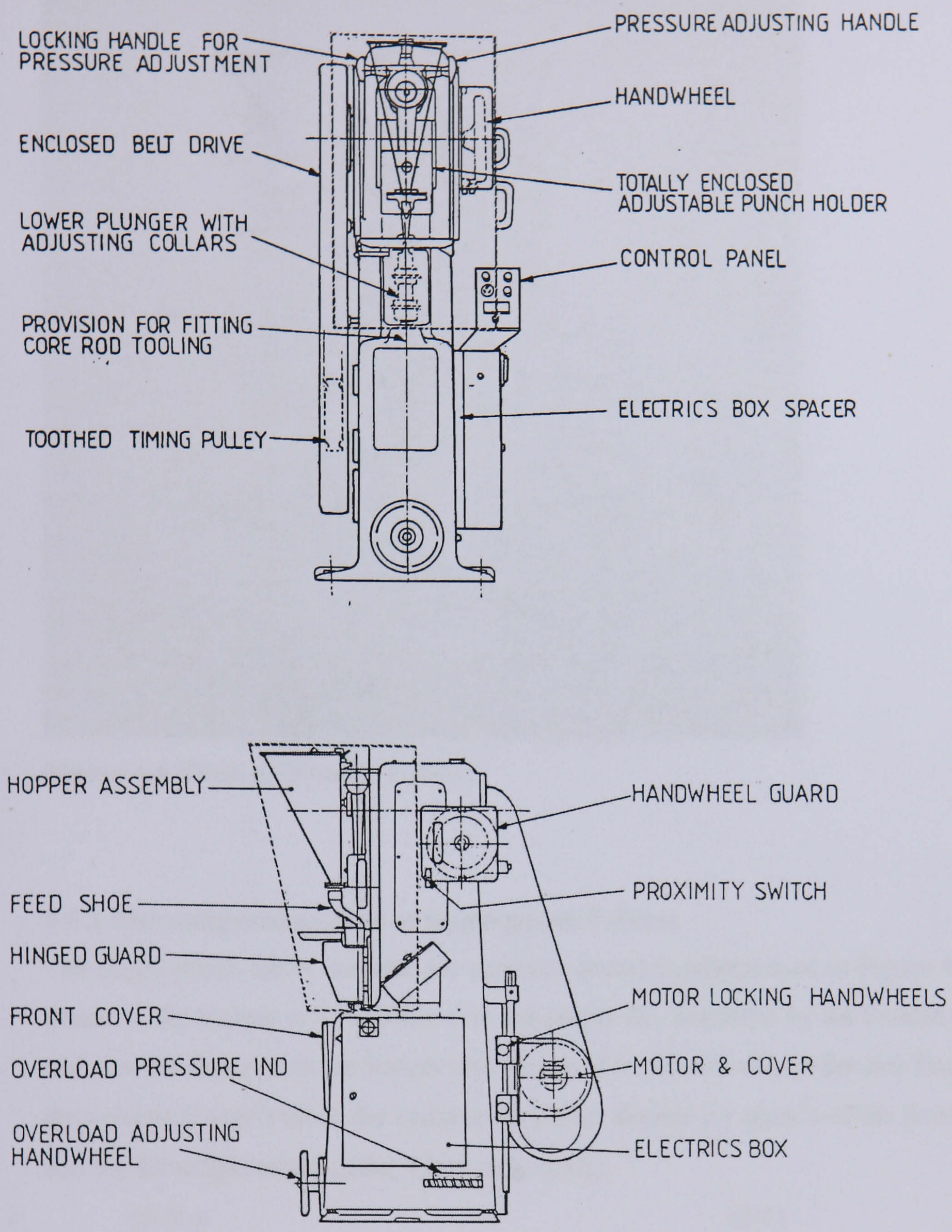

Figure 4.8 Manesty F-press feature and control.

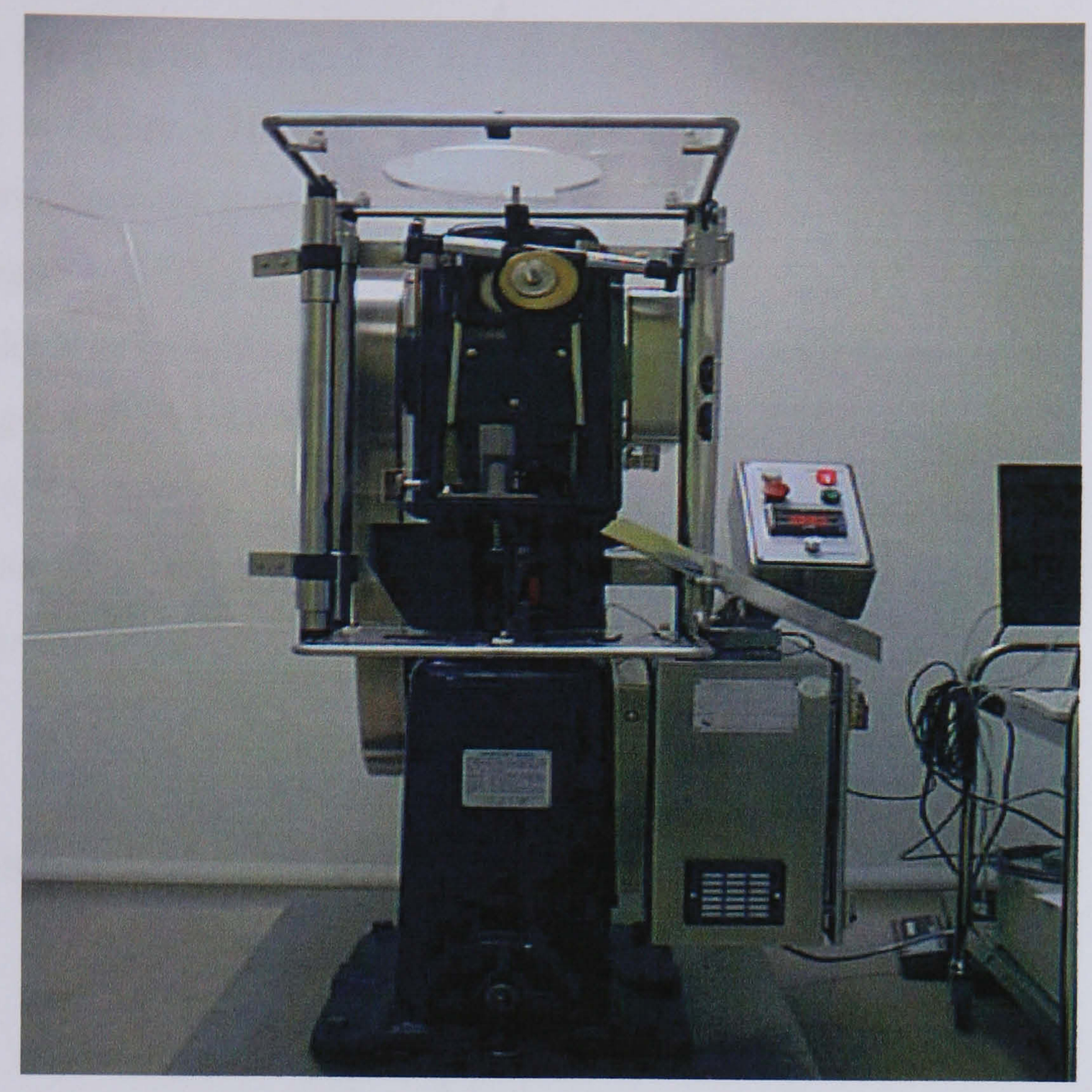

Figure 4.9 Photo of Manesty F-press.

4.4.2 The compression cycle of single-punch F-Press

The single-punch tablet machine (or eccentric press) is schematised in Figure 4.10. In frame A, the hopper is in position over the empty die, bordered by the bottom punch, and powder flows from the hopper into the die. The amount of powder that flows in is the volume V (cm^3) times the cascaded apparent density ρ (g/cm^3) of the powder, so that the fill weight of the tablet, U (g), is given by:

$$U=V\rho \qquad (4.1)$$

If the fraction of the powder consisting of drug is F, then the dose D (g), is given by:

$$D=F\,V\,\rho \qquad (4.2)$$

It is obvious that the accuracy and precision of the dose are a function of the accuracy and precision of the fill weight U, and the precision and accuracy of the fraction F. *Content uniformity*, hence, is a function of both these factors. It is also obvious that

the fill may be adjusted by the position of the lower punch in the first phase (frame A). In Figure 4.7B, the hopper has swung away, and the top punch comes down and compresses the powder into a tablet. The dimensions of the tablet are a function of the longest path this punch takes, and this can be adjusted, so that the thickness of the tablet may be adjusted in this way. This also adjusts the *hardness* of the tablet. Hence, in general, in tablets made on a single-punch machine, there is a functional relation between the thickness and the hardness. Single-punch machines produce, at top speed, about 85 tablets per minute. If the number of tablets per second is denoted N, then the amount of powder flowing into the die per second is:

$$W=NU \tag{4.3}$$

W (g/s) is the required flow rate for the powder.

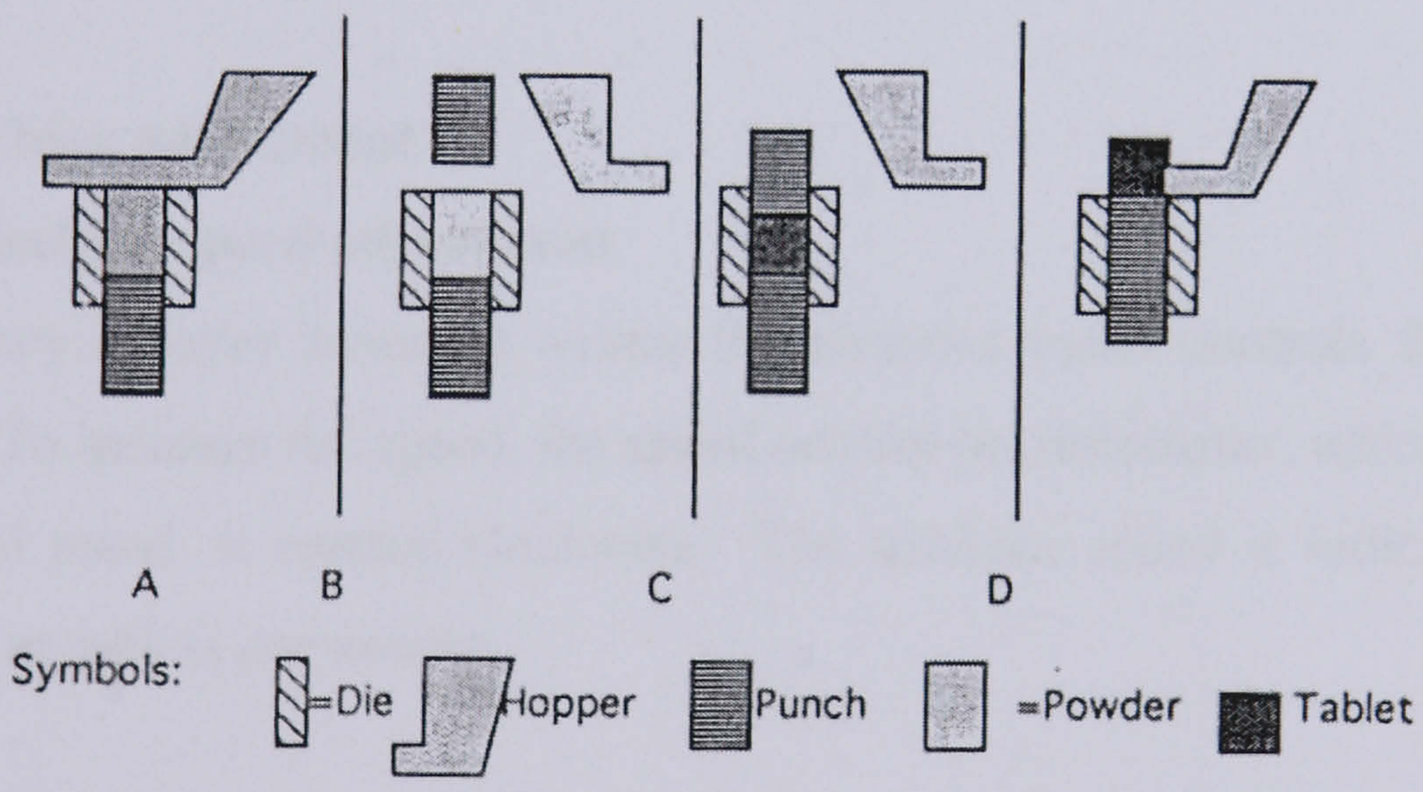

Figure 4.10 Principle of operation of single-punch tablet press.

4.4.3 Punch and die

Normal concave punches were used in the experiments. The punch diameter D was 10 mm, the radius R of the normal concave was 112.7 mm (½ inch) and the depth d was 1.09 mm (0.0431 inch). Figure 4.11 shows a sketch of punch dimensions. The maximum allowable load on punch tips is 6.5 tons

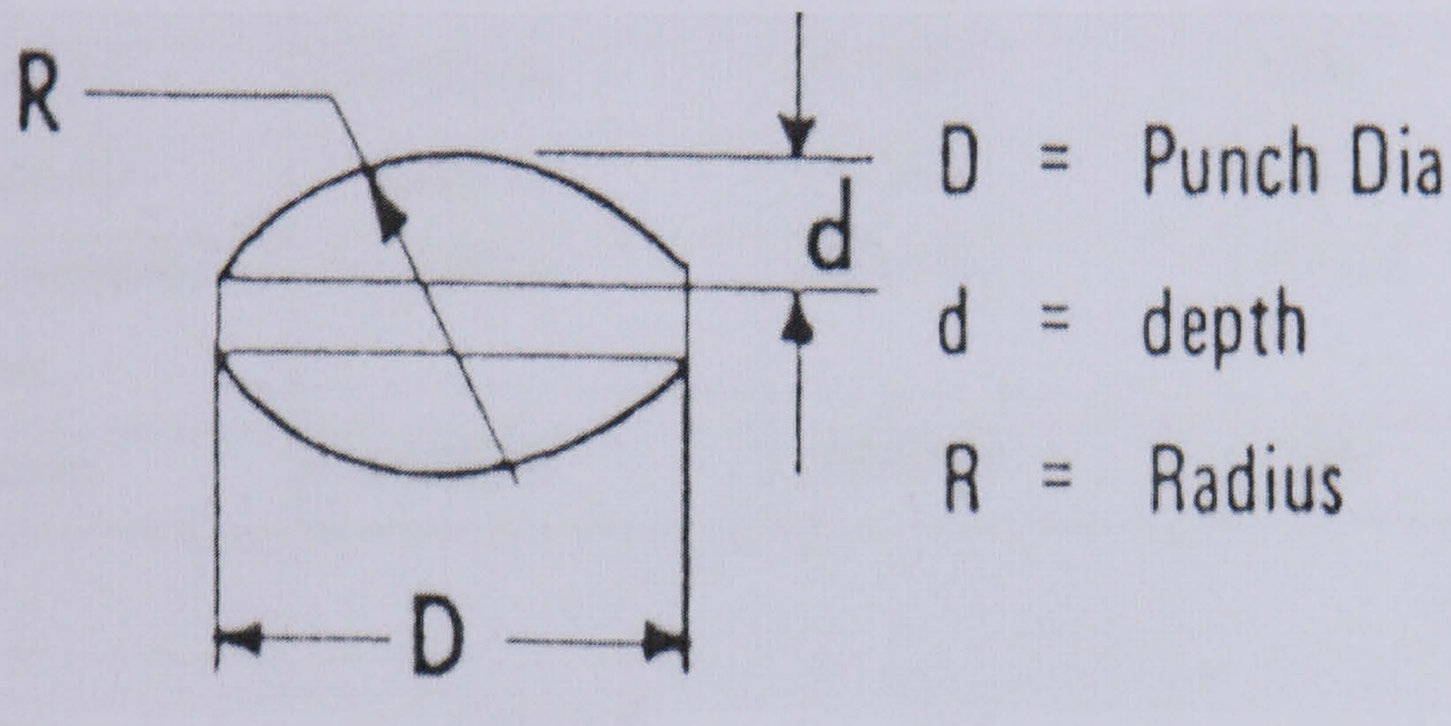

Figure 4.11: Punch dimensions

4.4.4 Machine adjustment

4.4.4.1 Machine speed adjustment

A frequency inverter mounted within the electrics panel controls the speed of the machine. To increase the speed, the speed control potentiometer, which is mounted on the control panel, is rotated clockwise. The machine speed is indicated by a meter presented as tablets per minute.

4.4.4.2 Weight adjustment

The weight of the tablet is determined by the depth of fill and hence by the position at which the lower regulating collars is set, Figure 4.8. Adjustment can be made to obtain any depth of fill from zero to maximum by rotating the collar.

4.4.5 Materials

The materials used in the studies were chosen so that different compression mechanisms could be examined. Initially, lactose and Aspartame were selected as have similar physical properties to common classical active ingredients available in many forms of tablets. As the studies progressed additional materials were examined

all of which could be classified as brittle materials. The materials studied, type and source are shown in Table 4.1. All the materials were used as received apart from those in the binary mixture study.

Table 4.2 Materials used in GSK studies

Material	Type	Batch NO	Source
Lactose	B.P	W04726	GSK
Povidone 30	Crystalline	BU7062	GSK
Povidone 90	Crystalline	21-6939	GSK
Microcrystalline cellulose	Crystalline	2970024	B.D.H
Aspartame	Crystalline	E006090	GSK

4.4.6 Tablet preparation

Tablets were compressed on Manesty F3 tablet press described in section 4.4.1. Compression speed was adjusted as described 4.4.4.1. Two loading condition were selected such that tablets produced can be crushed by either 5 or 10 kg using the tablet tester. The crushing strength was recorded as an indication of the load applied.

4.4.7 Acoustic interfacing

Initial experiments with acoustic emission held in BCMM laboratory at Brunel University entailed holding an acoustic emission transducer underneath the die to ensure an intimate contact by use of an acoustic couplant. However, during the experimental work at GSK, it was decided to fit the AE transducer on the upper punch Figure 4.12. This is because the complex press structure makes it very difficult to attach the transducer to the lower punch.

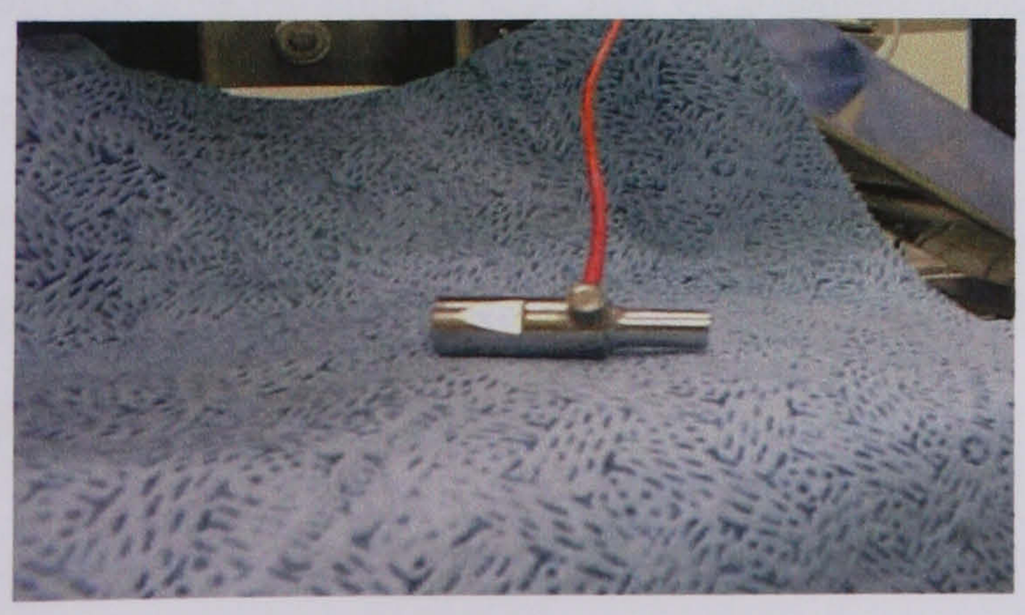

Figure 4.12 AE transducer fitted on the upper punch.

4.4.8 Measurement chain

Initial studies to establish if acoustic emission signals could be detected during compression were carried out using the miniature transducer, Model nano 30 from Physical Acoustic Corporation, PAC. The transducer was attached to the upper punch using an acoustic coupling gel to facilitate signal transmission. The output of the transducer was connected to a 40 dB preamplifier, model 214/6 (28Volts DC, Filter 100-1200 kHz, from PAC).

4.4.9 Signal conditioning (MISTRAS)

The signal then was conditioned using the acoustic emission data recording and acquisition system, MISTRAS 2000 (Physical Acoustics Corporation). The system is set to record the traditional acoustic emission features such as the ring down count (RDC), peak amplitude, absolute energy, RMS, rise time and average signal level (ASL). Data were sampled at 10MHz. Acoustic emission measurements start as press turned on. The MISTRAS system is capable of analysing acoustic information up to four inputs and from these inputs locating the source of emissions. In these studies the instrument was used in the single channel mode to provide acoustic information from one single transducer. The MISTRAS software allows setting various parameters for signal conditioning purposes.

In order to take into account the effect of various noises associated with the press, the data recorded from the compression test were processed against the cycle time (1.2s). it was noted that the AE level that is generated from mechanical noise and other noise in the process are of low energy. It was also possible to identify certain AE event at different punch displacement. For example, there are repeated events at the moment where the punch enters the die, in contact with the powder and when its depart from the die. Using classification technique, fuzzy C-mean clustering, it was possible to isolate these events and hence process those which are associated with only pure compression without any noise. The fuzzy C-mean analysis will be discussed in chapter 6.

4.4.10 Computer software

The large amount of data generated from acoustic emission experiments particularly from the MISTRAS system necessitated the development of software for experimental analysis. Most of the software was developed using MATLAB and its signal processing toolbox. Other analyses have been done using other software packages including MATHCAD and AXUM6.

4.4.11 Non acoustic measurement

Crushing strength was determined using the tablet hardness tester (Holland C50), Figure 4.13. Dissolution studies were conducted using a dissolution bath (CALEVA), Figure 4.14 at the GSK site.

Figure 4.13 Tablet Hardness (Holland C50).

Figure 4.14 CALAVA dissolution bath.

4.5 Conclusion

This chapter provided detailed description of the experimental design and method. A test rig was designed to perform acoustic emission studies on powder compression using the Instron universal tensile machine. Acoustic and non-acoustic measurements were also outlined. This chapter also described the method and equipment used for industrial studies on AE monitoring of powder compression.

The following chapter will present the results from acoustic emission investigation on powder compression performed on the test rig.

References

Wade, A. & Weller, P. J. (1994): Handbook of Pharmaceutical Excipients. 2nd ed. Ajoint publication of London; The pharmaceutical Press& Washington; American Pharmaceutical Association. P5 6-56-59, 84-86, 252-259 & 392-398.

Chapter 5 Results from test rig

5.1 Introduction

This chapter describes the experimental investigations conducted on a number of pharmaceutical materials using the designed test rig. It provides detailed analysis of acoustic emission measurement during powder compression. Initially it describes the acoustic emission characteristics during a compression cycle, followed by AE monitoring of compression of various powder materials. The chapter also includes detailed investigations of the effect of material type, compression speed and particle size and tablet weight on the AE signal produced from powder compression using the test rig designed and described in Chapter 4.

5.2 Acoustic emission from powder compaction

Preliminary studies were carried out to see if acoustic emission could be detected during pharmaceutical powder compressing for a tabletting process using a wide-band piezolectric transducer and the MISTRAS system. Initial observation suggested that different materials gave different acoustic emission response. Although the compression process is a pure mechanical process, the materials type has a big influence on the AE signal measured by the transducer. For example microcrystalline cellulose (Avecil 101) was found to be a more extensive emitter than the lactose or calcium carbonate. It was also noticed that most of the acoustic emission appeared at low compression loads for most materials except microcrystalline cellulose. Materials that have low flowability showed low acoustic emission. This was expected because the main causes of AE signals are the particle-particle collision and deformation. Therefore, for a material of poor flowability such as Isomalt or Aspartame very low emission is generated.

It was also hypothesised that emissions would be greater with increasing compression loads and speed and particle size. This investigation will be discussed in detail in later sections.

The preliminary experimentation though inconclusive to enable pharmaceutical powder characterisation, clearly showed that emissions were less reproductive for smaller particle sizes of the same materials.

5.3 Acoustic emission analysis of powder compression cycle

A detailed acoustic emission analysis of the compression cycle was undertaken using the MISTRAS 2000 system to capture the acoustic emission signal's traditional features such as peak amplitude (PA), ring down count (RDC), event duration (ED), AE energy, average signal level (ASL) and rise time (RT). Using a 10 mm diameter flat faced punch and die set, pharmaceteutical powders were compressed to an applied load of 10 kN with a powder mass of 300 mg and compression speed of 10 mm/min. It was an obvious finding that materials, which gave rise to acoustic emission during compression, were shown to have three distinct stages during the compression of powder material. These stages were clearly observed from both the ASL and peak amplitude profiles as shown in Figures 5.1 and 5.2 respectively. The maximum applied load of 10 kN was reached at approximetly 8.5 seconds. The force time profile was used to draw up the boundaries indicated in Figures 5.1 and 5.2 to separate the three stages of the compression cycle of the test rig.

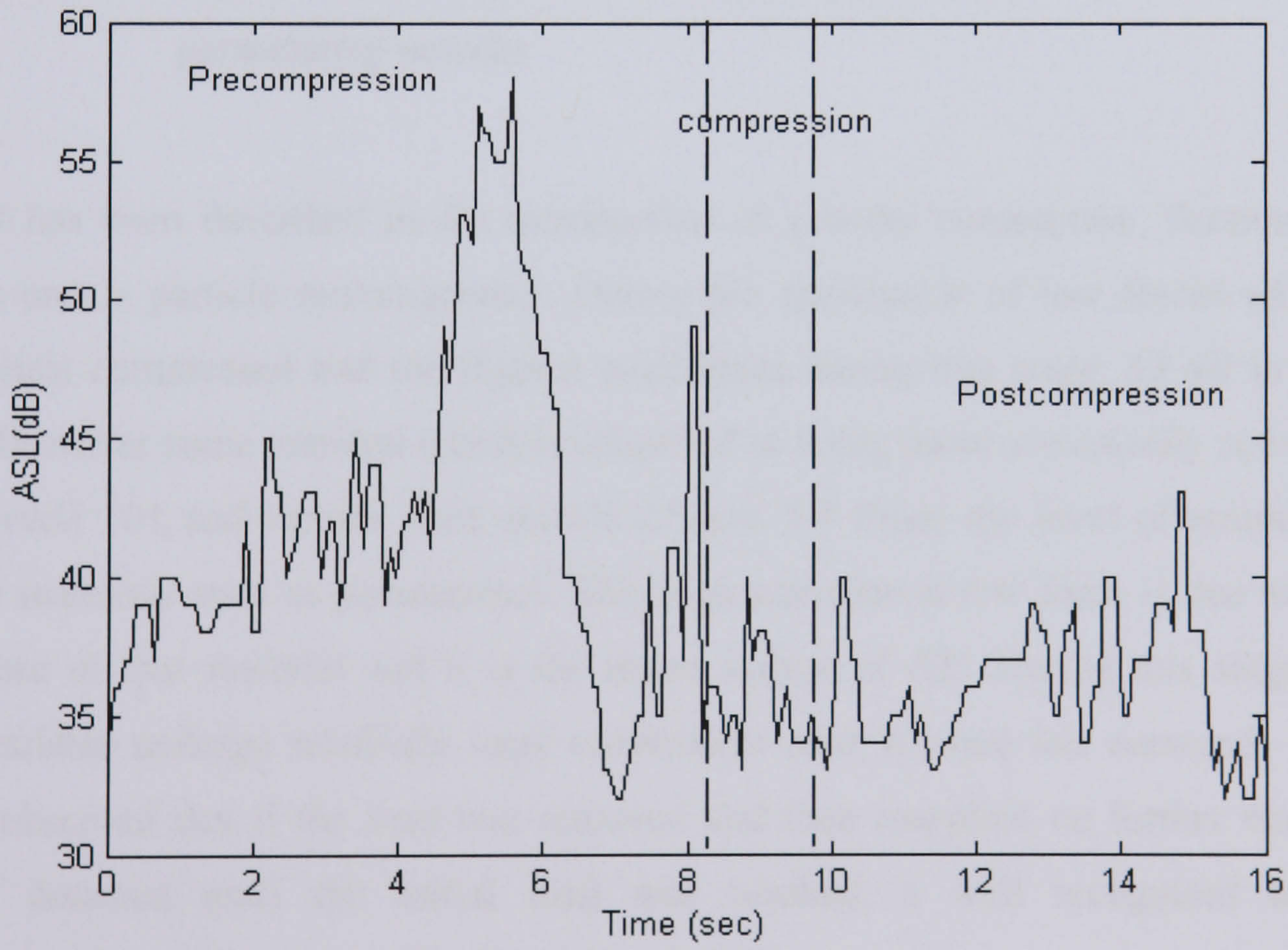

Figure 5.1 Acoustic emission profile as expressed by ASL for compression phase of paracetamol powder.

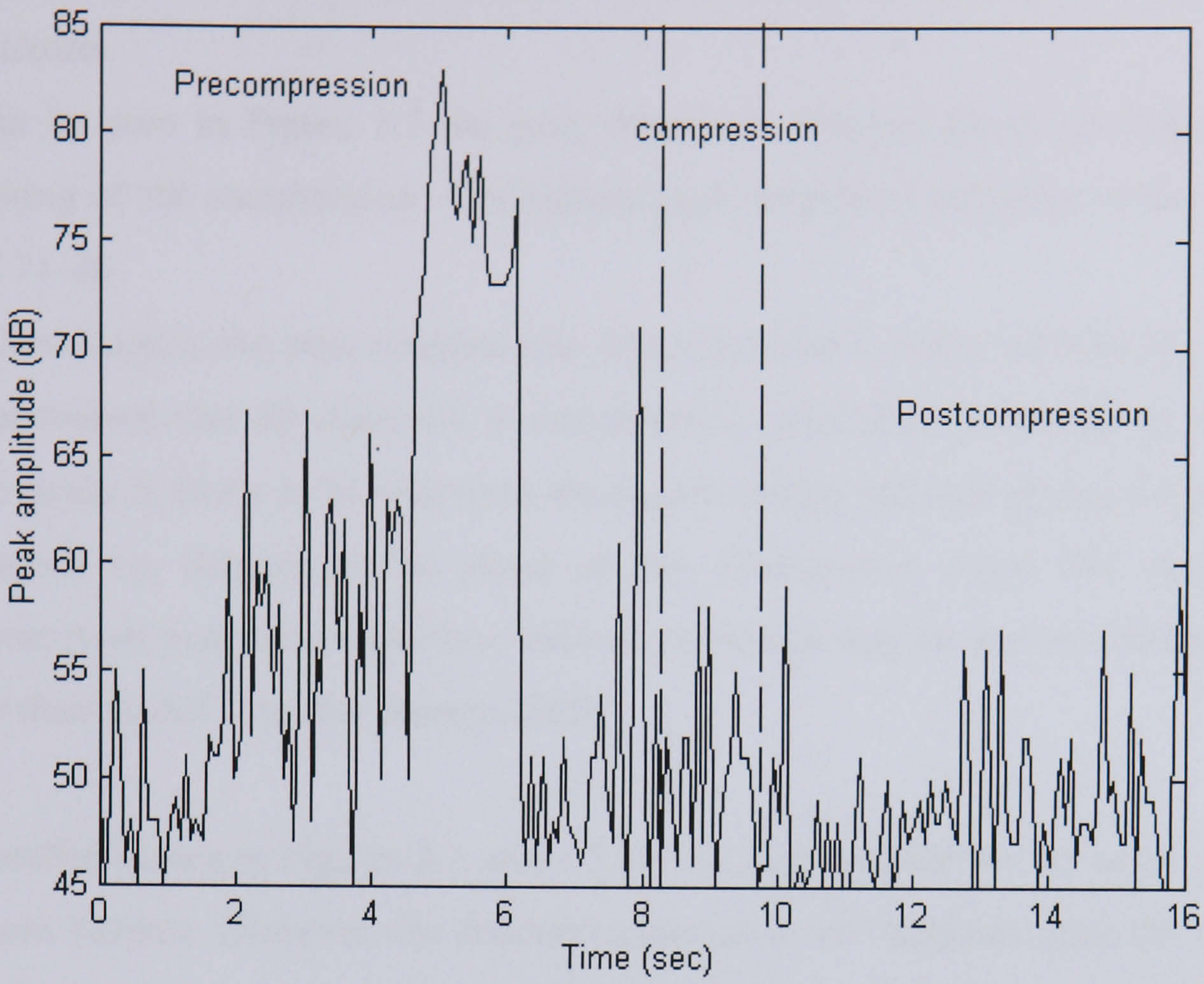

Figure 5.2. Acoustic emission peak amplitude for compression of paracetamol powder

As it has been described in the introduction of powder compaction, Section 3.4.7, stage one is particle rearrangement. During the application of low forces all of the materials compressed had the highest amplitudes during this stage, 83 dB in Figure 5.2. However some material which is classified as being more acoustically active such as Avecil 101 and lactose were shown to have 3-5 times the level of emissions of other materials such as paracetamol. This high emission at low force is due to brittle fracture of that material and it is the major source of AE. During this stage small particulates undergo relatively large movements after fracture has occurred. It was also observed that if the load was removed and then reapplied no further emissions were detected until the initial load was reached, a well recognised acoustic phenomenon originally described by Kaiser (1950).

The second stage of compression phase is sometimes referred to as consolidation. It was noticed that most materials exhibit relatively quiet acoustic emission in

comparison to the first stage. Emission was however detected for both paracetamol and lactose.

As can be seen in Figure 5.2 the peak amplitude dropped after 6 seconds from the beginning of the compression. The highest peak amplitude recorded in this stage was about 71 dB.

The third stage is the post compression where the load is removed from the materials. It was evident that all materials demonstrated a noticeable peaks during this phase. These peaks is likely to be related to the elastic energy released during the removal of the punch i.e. decompression phase of the compression cycle. See Appendix B. however most material exhibit low level of AE which may be due to mechanical noise rather than an AE from the process itself.

The profile shown in Figures 5.1 and 5.2 is very reproducible for the same material of different batches. However, for different material, it will depends upon the type of the material used and the types of deformations that may present during powder compression.

The large variation in the signal rise time, Figure 5.3, suggests that the emission during the entire compression cycle emanates from different mechanisms. For instance during the pre-compression phase, it is the particles rearrangement and slippage inside the die that cause the rising AE signal whereas in post compression it is most probably the relief of internal stresses rather than brittle fracture. The steady increase in rise time during the pre-compression phase as seen in the bottom of Figure 5.3, probably reflects the contribution of particle/die wall interaction as the material slip inside the die. This is justified on the basis that longer rise times are indicative of frictional events (Cole, 1986).

Figure 5.4 shows the acoustic emission count during compression of paracetamol powder at the compression speed of 10 mm/min. At the start of the compression, a high AE count was noticed particularly during the first 3 seconds of the compression, then dropped slightly till the just before the maximum load reached at time 11 seconds. The number of count appeared to be less during the consolidation, however as the punch was removed from the powder compact (during post compression) a high AE count was also noticed due to the relaxation effect.

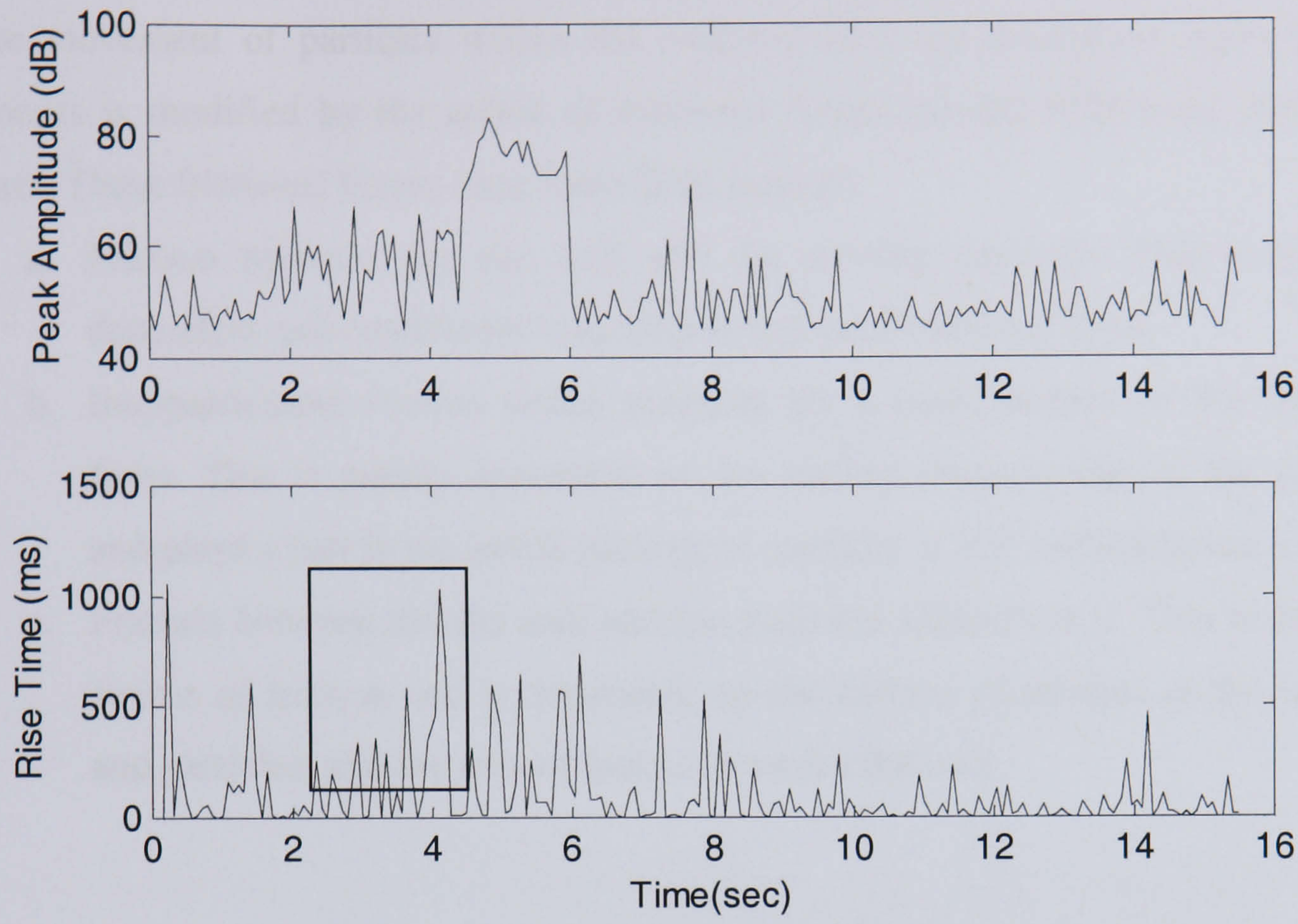

Figure 5.3 AE parameters versus time for paracetamol compression.

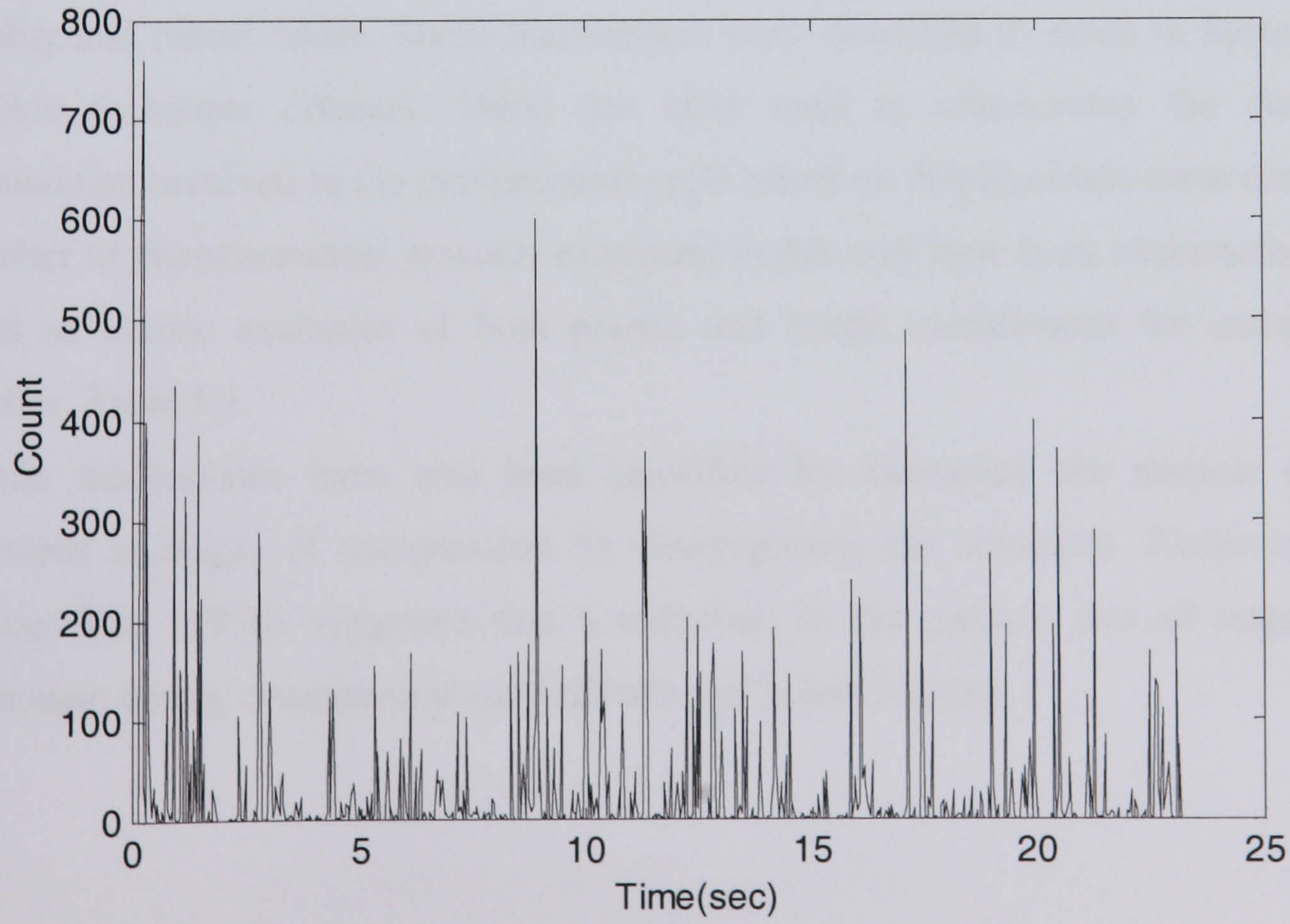

Figure 5.4 AE Count from compression Paracetamol.

5.4 Pressure Transmission through compact of particulate solids

The movement of particles within the confines of a die during the consolidation process is modified by the action of frictional forces on and within the particulate mass. These frictional forces arise from three sources:

a. Friction between the die wall and the moving punches. This is machine dependent and contributes very little to the total frictional force.
b. Interparticulate friction which accounts for a small portion of the frictional force. This is mainly dependent on the surface characteristic of the particles and plays a part in the initial packing of particles at low consolidation loads.
c. Friction between the die wall and the particles adjacent to it. This is the main source of friction and is dependent on the surface conditions of the die wall and particles, and the area of contact between the two.

5.5 Effect of material type and characteristics

This section briefly describes the observations from the outcome of the experimental investigations of acoustic emission during tablet formation for various materials.

Previous powder compaction research investigations established that the type of deformation mechanism inherent in the materials affects the production of a good quality and robust tablet. These mechanisms were described in detail in Section 3.4. Heckle technique (Heckel, 1961) has been used to characterise the dominant mechanism involved in the compression cycle based on displacement-force curves. A number of pharmaceutical powders examined in this way have been characterised and used as classic examples of both plastic and brittle mechanisms for compaction studies, Table 5.1.

Brittle mechanisms have also been identified by measuring the particle size of fractions at stages of compression by disintegrating the compacts. Armstrong and Haines-Nutt (1970) suggested that a reduction in the particle size of magnesium carbonate during compression was indicative of brittle fracture.

Table 5.1 Dominant deformation mechanisms for different materials classified using the Heckel Technique

Plastic deformation	Brittle Fracture
Sodium chloride – Roberts and Rowe (1985) Microcrystalline cellulose – McKenna and McCafferty (1982)	Lactose – Hersey Cole and Rees (1972) Paracetamol –Humbert-Droz *et al* (1983), Yu *et al* (1989) Potassium Citrate – Hersey Cole and Rees (1972). Calcium Carbonate – Roberts and Rowe (1985)

Just as the Heckel technique was developed from the discipline of metallurgy, metals are also seen to undergo plastic flow and brittle fracture during deformation. The mechanisms in metals have been characterised by acoustic emission in particular for finding defects in pressure vessels where sub-critical plastic zone growth may be detected at the start of a brittle fracture, (Harris and Dunegan, 1974). Brown (1979) in reviewing AE as a quantitative technique suggested that although brittle fracture can be accompanied by acoustic emission it involves minimal dissipative processes and proposed that AE from brittle sources is a different phenomenon from ductile materials. Swindlehurst in 1974 classified two types of signal: continuous low-level signals associated with plastic deformation and burst acoustic emission of higher amplitudes more likely to emanate from brittle sources. Swindlehurst went further, however, to warn that the distinction is one of degree and is not absolute.

The work by Brown (1979) also suggested that the differences observed in AE signals generated from metals under stress might also be applied to non-metallic materials in order to classify their compression mechanisms. Evaluation was carried out by selecting materials which had previously been characterised as having the classical deformation mechanism.

A number of materials were selected for acoustic emission studies. These materials had previously been characterised as having the classical deformation mechanism.

Acoustic emission analysis was undertaken using both MISTRAS 2000 system and LabVIEW recording facilities.

5.5.1 Lactose

The lactose powder used in this experiment is classified as brittle material, Table 5.1, and was shown to be acoustically active at low compression forces 2-5 kN and 10 mm/min compression speed. High peak amplitudes were recorded during both pre-compression and post compression. It was also noticed that the AE energy increased exponentially during the pre-compression phase, Figure 5.5. A similar trend was found with the number of ring down count, as can be seen in Figure 5.6. Lactose was shown to have good flowability characteristics and hence it was expected to be acoustically active during the rearrangement phase as more particles-particles frictions occurred.

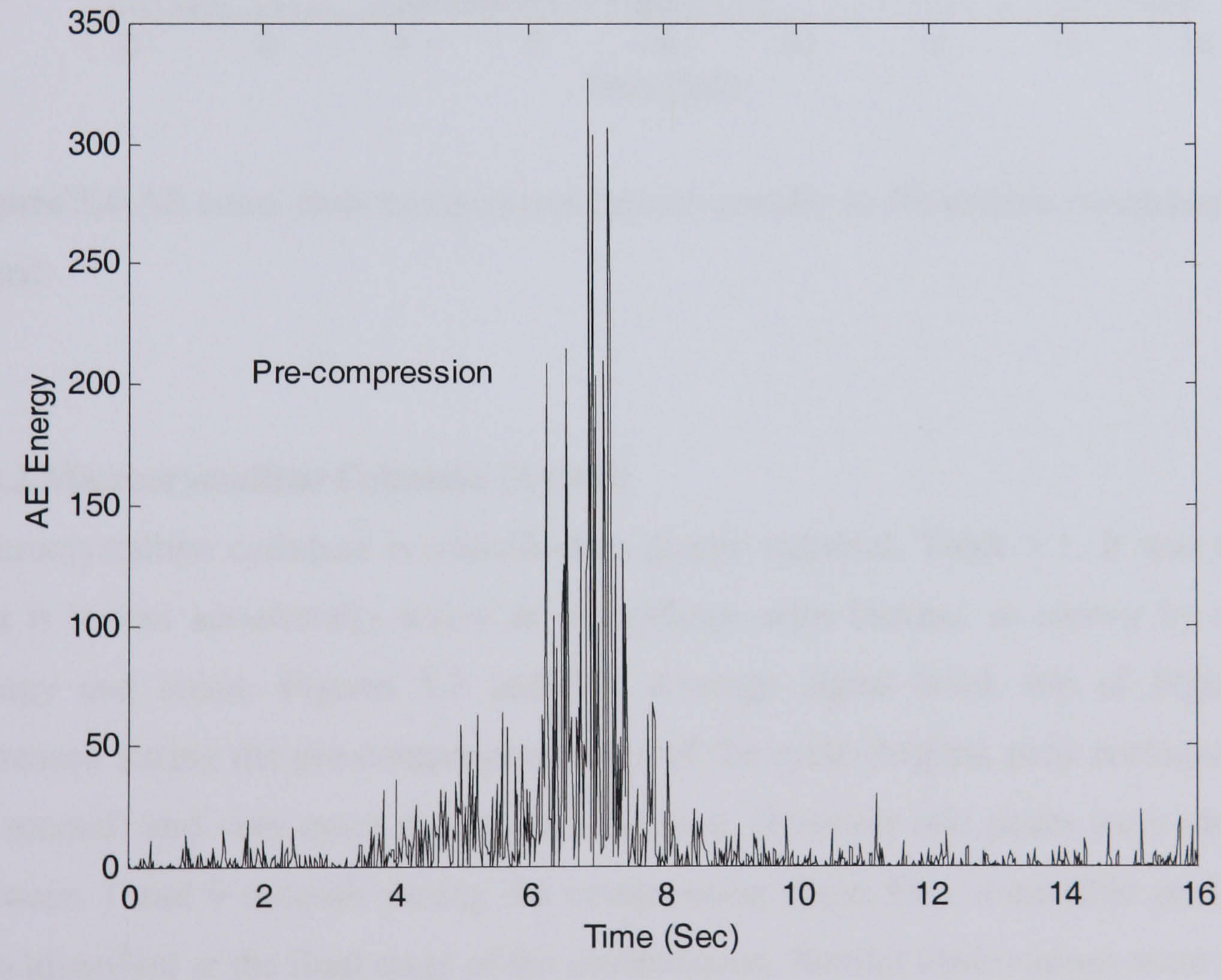

Figure 5.5 AE energy from compression lactose powder at 10mm/min compression speed

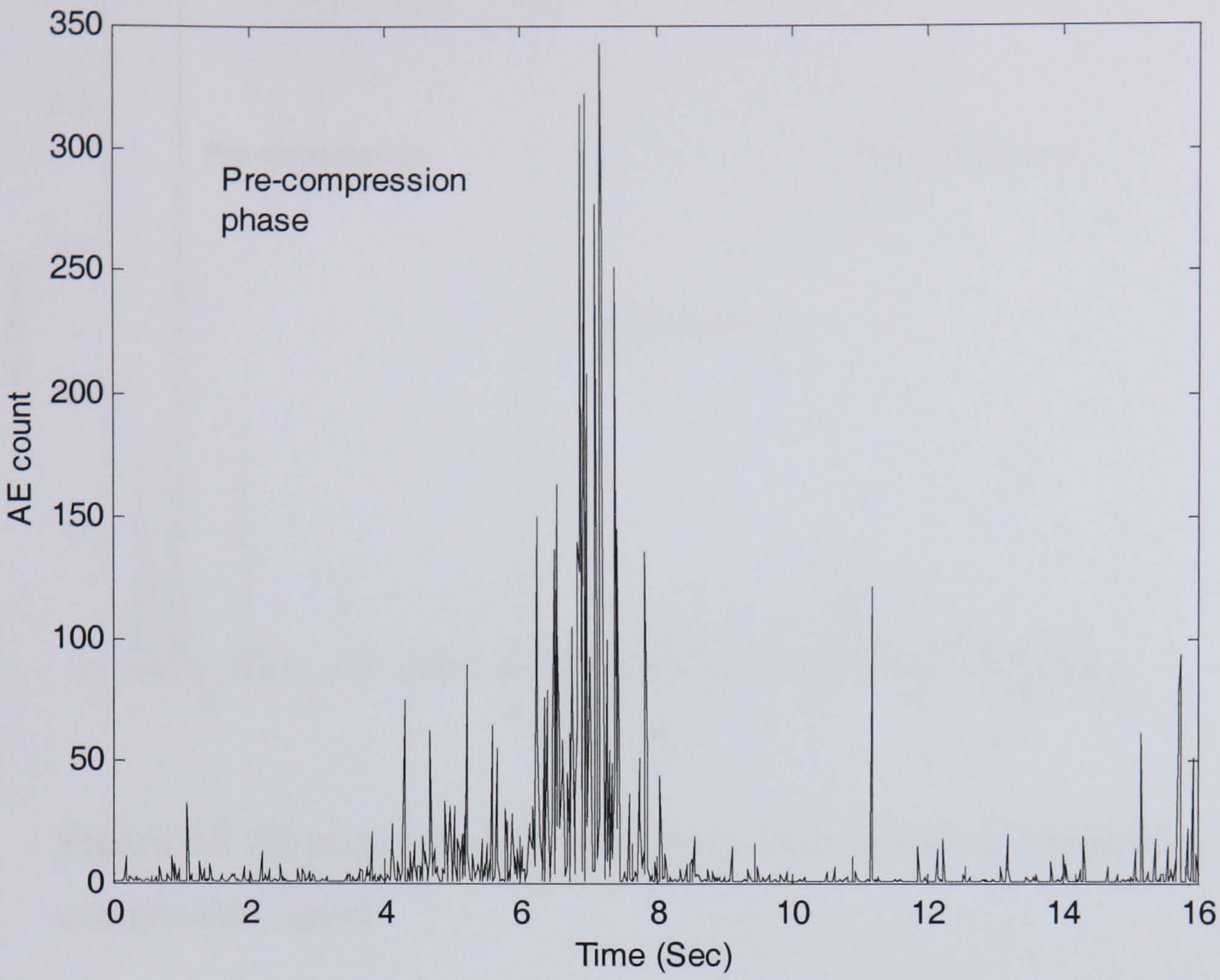

Figure 5.6 AE count from compression lactose powder at 10mm/min compression speed

5.5.2 Microcrystalline Cellulose (Avicel)

Microcrystalline cellulose is classified as plastic material, Table 5.1. It was noticed that it is less acoustically active in comparison with lactose, as shown by the AE energy and count, Figures 5.7 and 5.8. Average signal level, top of Figure 5.9, increased during the pre-compression stage of the cycle (highest peak recorded at the 4th second) and very quiet during consolidation. However two peaks were identified between 7 and 9 seconds during the compression cycle. Few noticeable peaks were also identified at the final stage of the compression. Similar observations were noticed during the peak amplitude profile, bottom of Figure 5.9, of the AE signal generated.

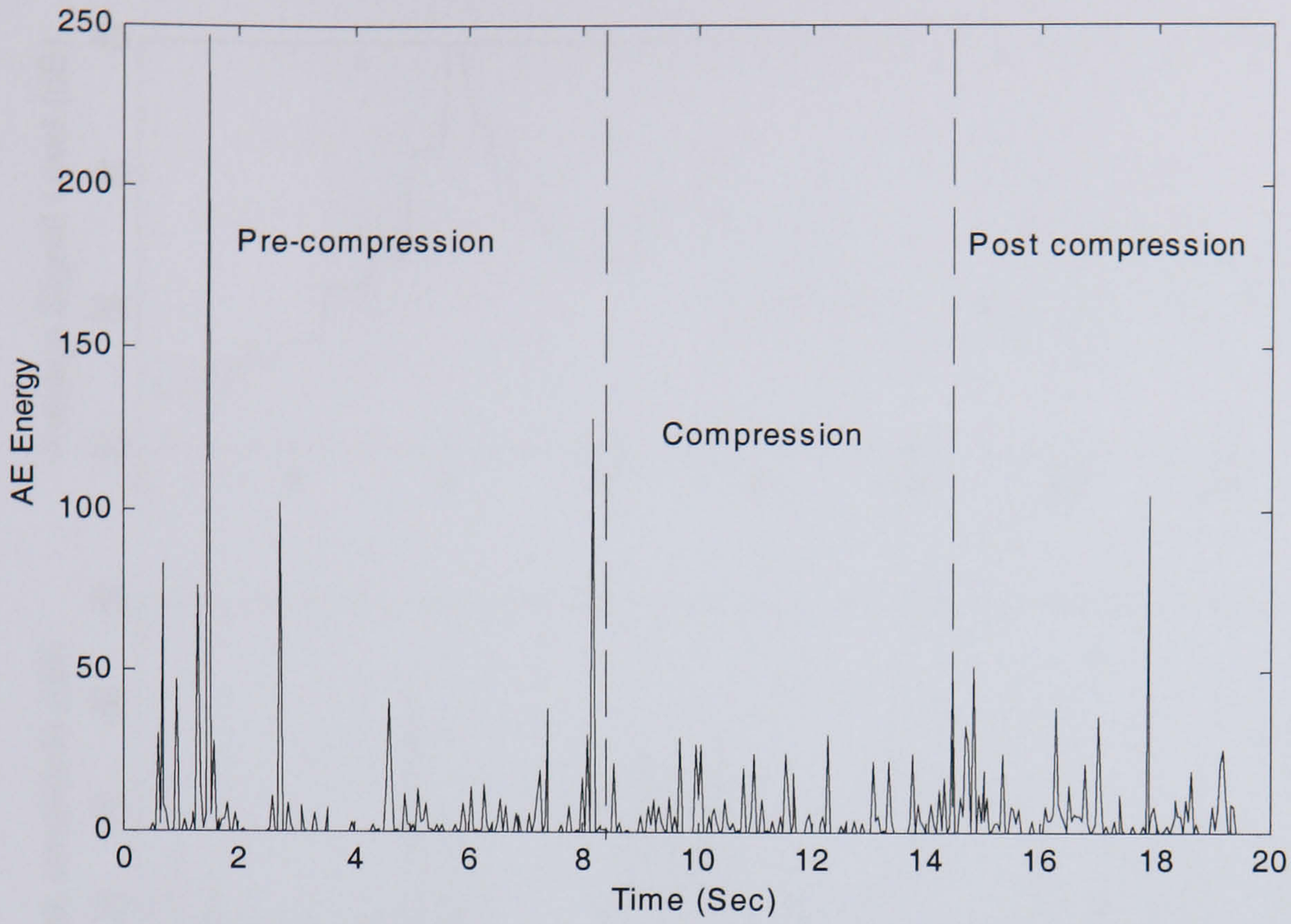

Figure 5.7 AE energy from compression Avicel powder at 10mm/min compression speed.

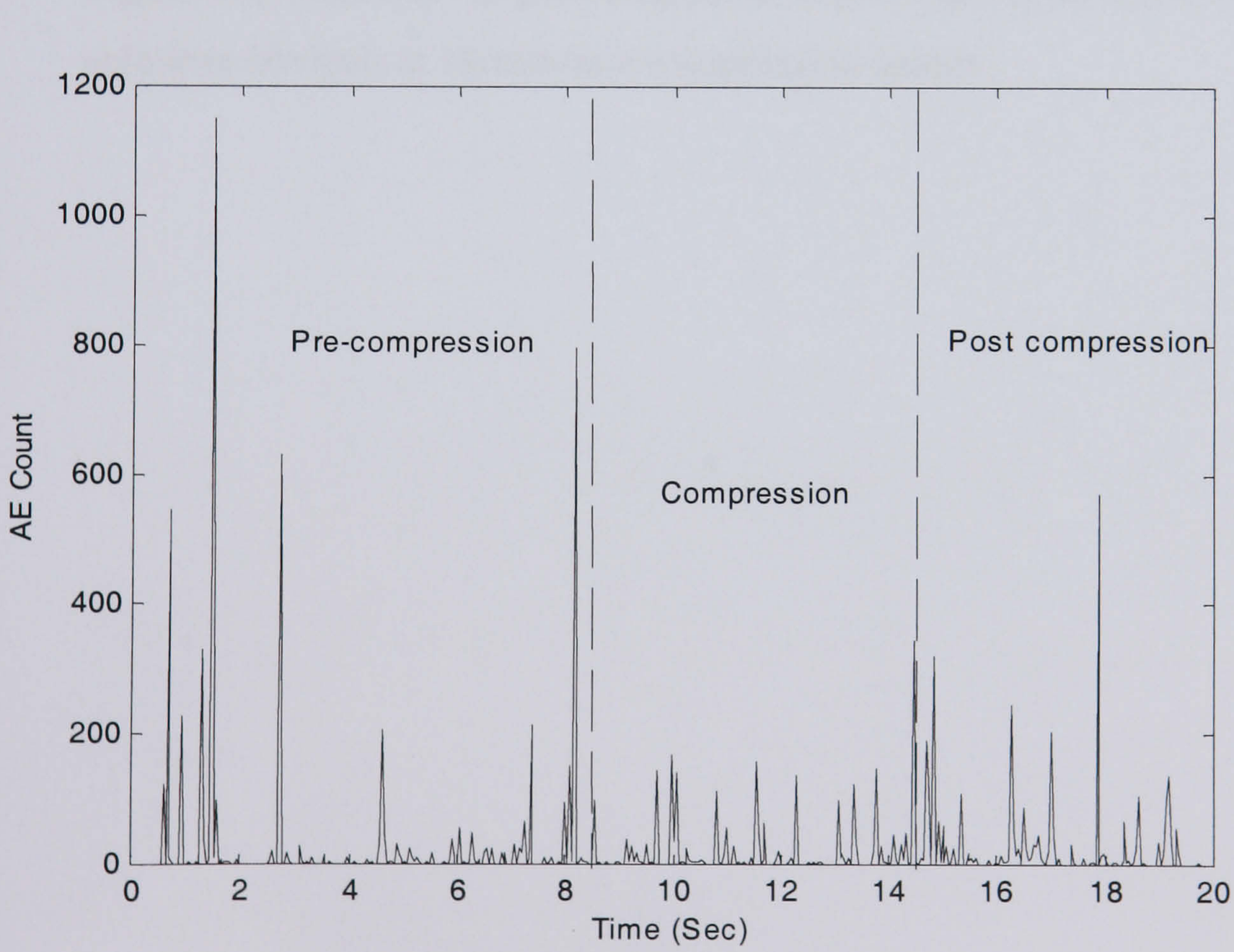

Figure 5.8 AE count from compression Avecil powder at 10mm/min compression speed.

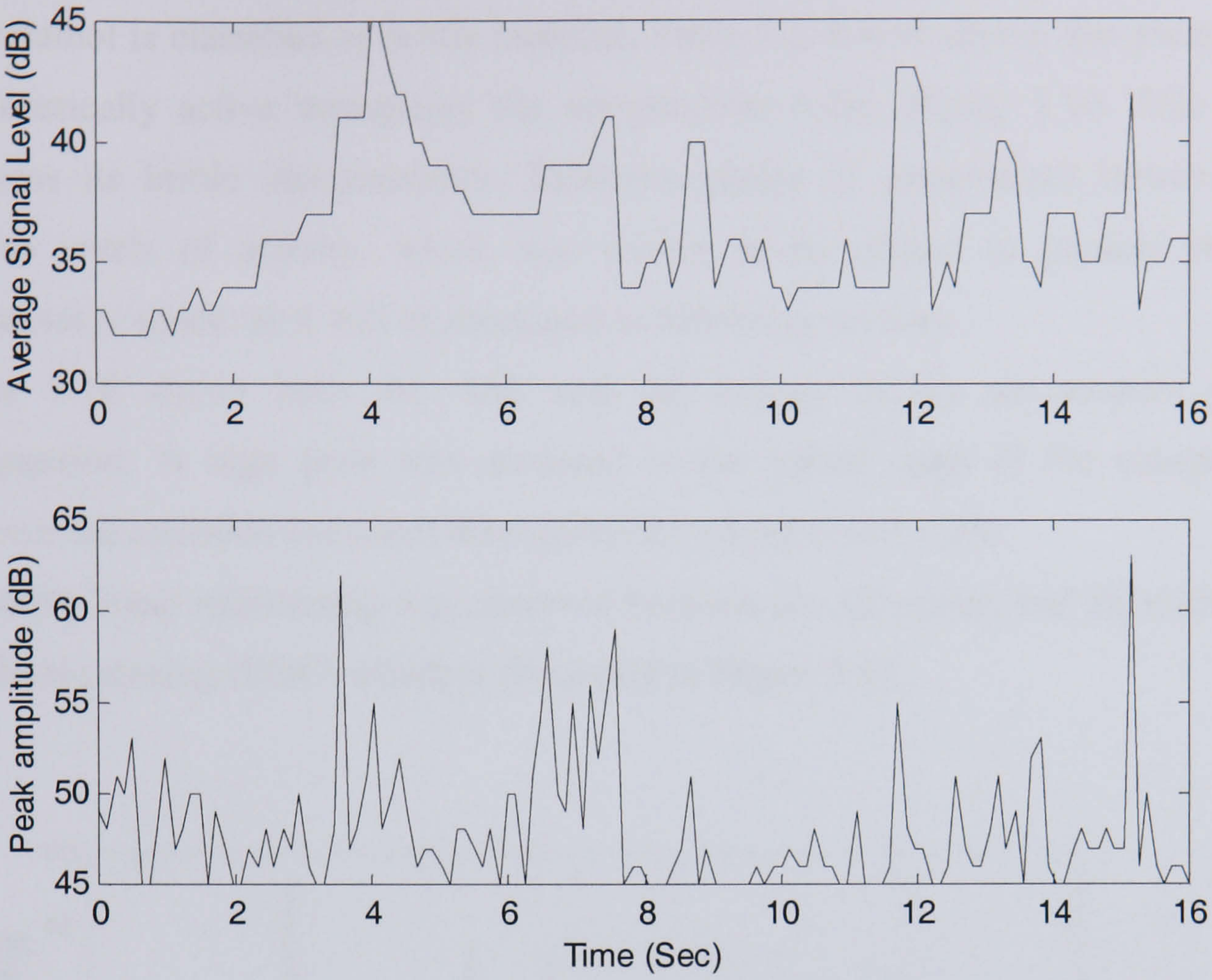

Figure 5.9 ASL and AE peak amplitude from compression microcrystalline cellulose (Avicel) at 10-mm/min compression speeds.

5.5.3 Paracetamol

Paracetamol is classified as brittle material, Table 5.1. It was shown that paracetamol is acoustically active throughout the compression cycle, Figure 5.10. This indeed confirms its brittle characteristics. Different grades of paracetamol however, had various levels of activity, which was shown to be related to particle size and compression speed, as it will be discussed in following sections.

Figure 5.10 shows both the ASL and AE energy during paracetamol powder compression. A high peak was recorded in the initial stage of the compression, however the emission continues throughout the compression cycle.

A notable linear relationship was observed between the AE energy and the number of threshold crossing (RDC) which is illustrated in Figure 5.11.

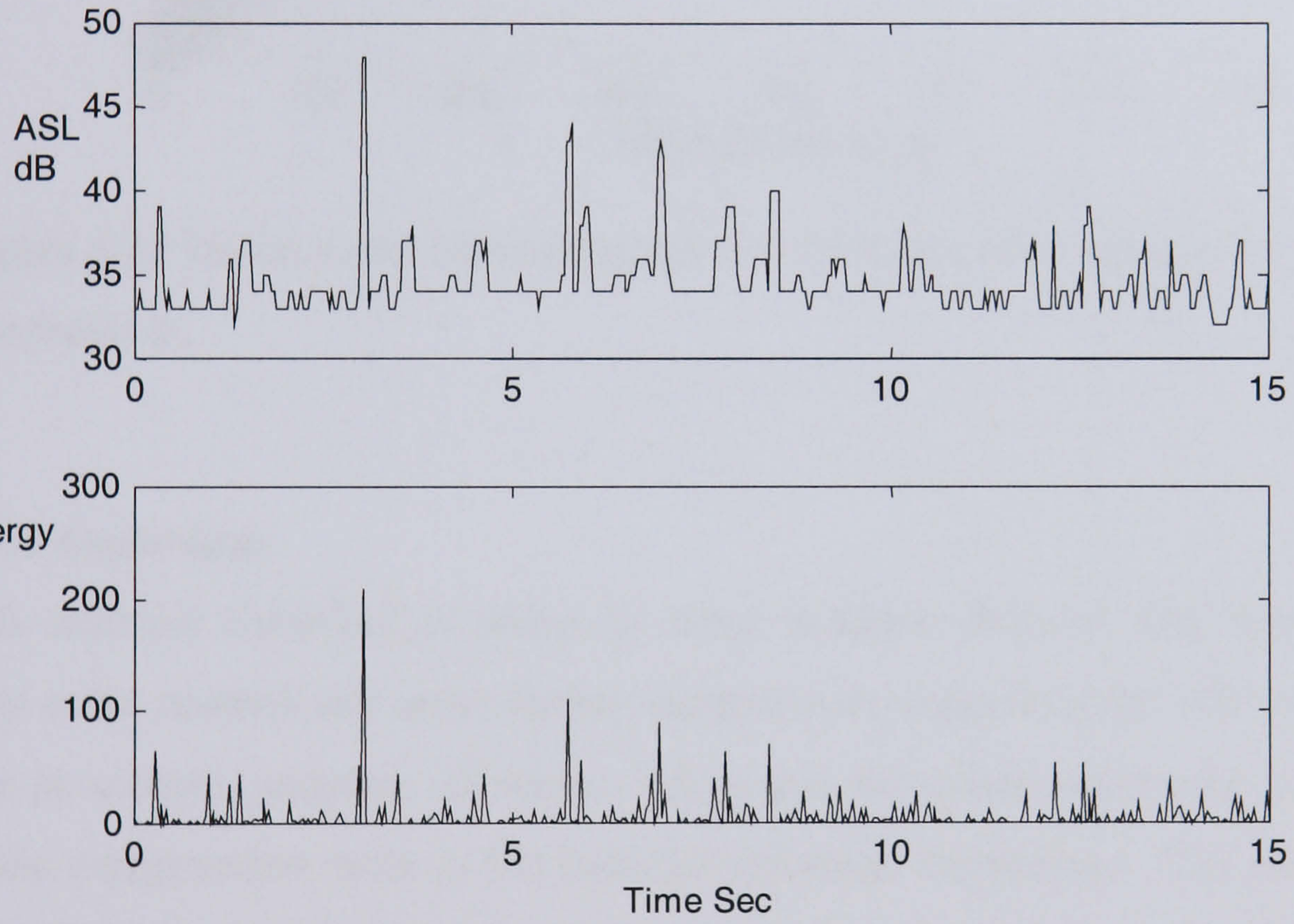

Figure 5.10 ASL and AE energy from compression paracetamol.

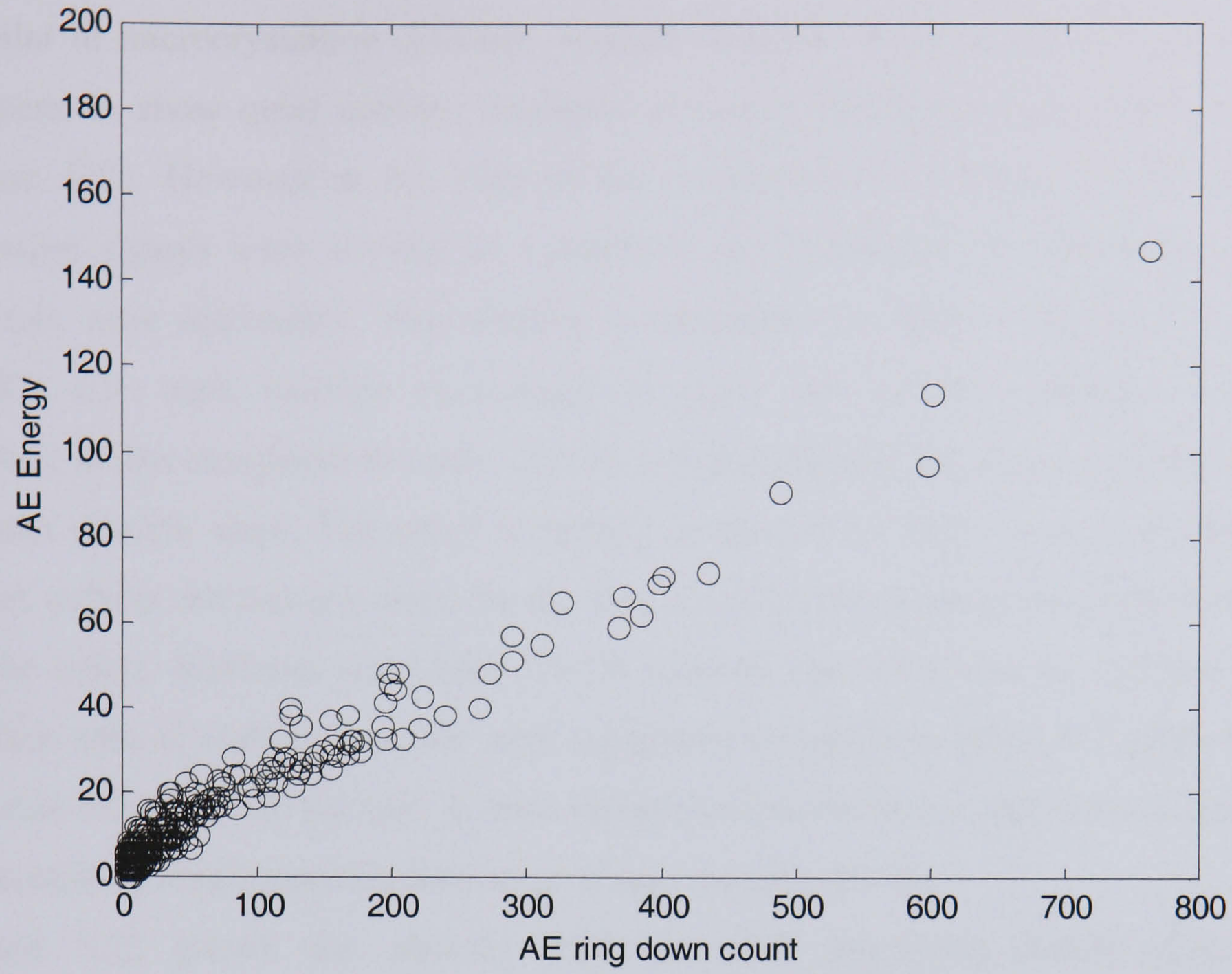

Figure 5.11 Relationship between ringdown count and AE energy from paracetamol compression.

5.5.4 Aspartame

This material classified as brittle by other workers (Roberts and Rowe, 1985) was seen to be acoustically quiet during compression suggesting the influence of particle size in acoustic response. However, AE events were detected during the initial phase of the compression cycle as the particles rearrange themselves. This material has low flowability characteristics in comparison with previous materials. See Appendix B2.

5.5.5 Calcium carbonate

Calcium carbonate was shown to be quiet during compression and post compression. However, a very low level of signal was recorded during the particle rearrangement stage. It is worth mentioning here that calcium carbonate did not compress well enough to hold as a good tablet. This material is widely used in most pharmaceutical formulation; however it requires a form of binding agent and is not suitable for direct compression. See Appendix B2.

5.5.6 Sodium Chloride

Similar to microcrystalline cellulose, sodium chloride, which is classified as plastic, happens to show quiet acoustic emission activities during the consolidation phase, Figure 5.12. However at the start of the compression at around 1.8kN, acoustic emission signals were emitted as a result of the brittle fracture mechanism as the crystals were rearranged. This finding is supported by work conducted by Down (1983) who used electron microscopy to show that sodium chloride underwent fracture at low compression loads. This is in fact evident as the emission reduced with smaller particle sizes. The novel technique developed by Down was to examine the tablet without removing it from the die thus avoiding the stresses involved in ejection of the tablet. Hardman and Lilley (1973), showed that there was no increase in the surface area of sodium chloride with increasing compaction force and proposed the absence of any brittle fracture. It must be pointed out, however, that they worked with an extremely small particles size range of less than 60 micron.

Figure 5.12 shows the acoustic emission peak amplitude profile during the compression cycle of NaCl. Typical force profile of NaCl powder compression is shown in Figure 5.13, an exponential rise in the force-time curve during compression is observed. This is followed by a rapid drop of the compression force. The area under the force-displacement curve is often referred to as compaction energy.

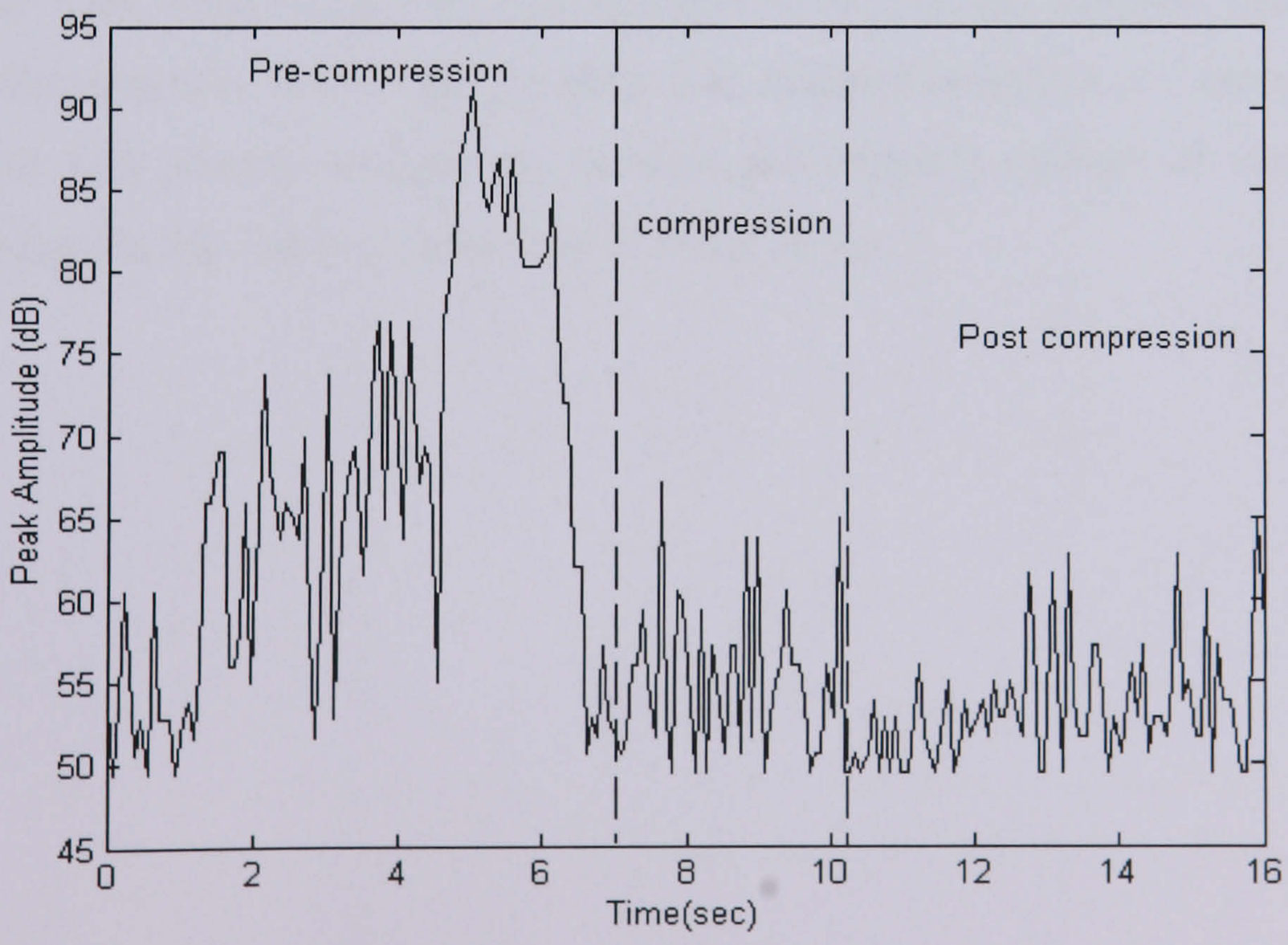

Figure 5.12 Acoustic-emission-peak amplitude profile of NaCl compression.

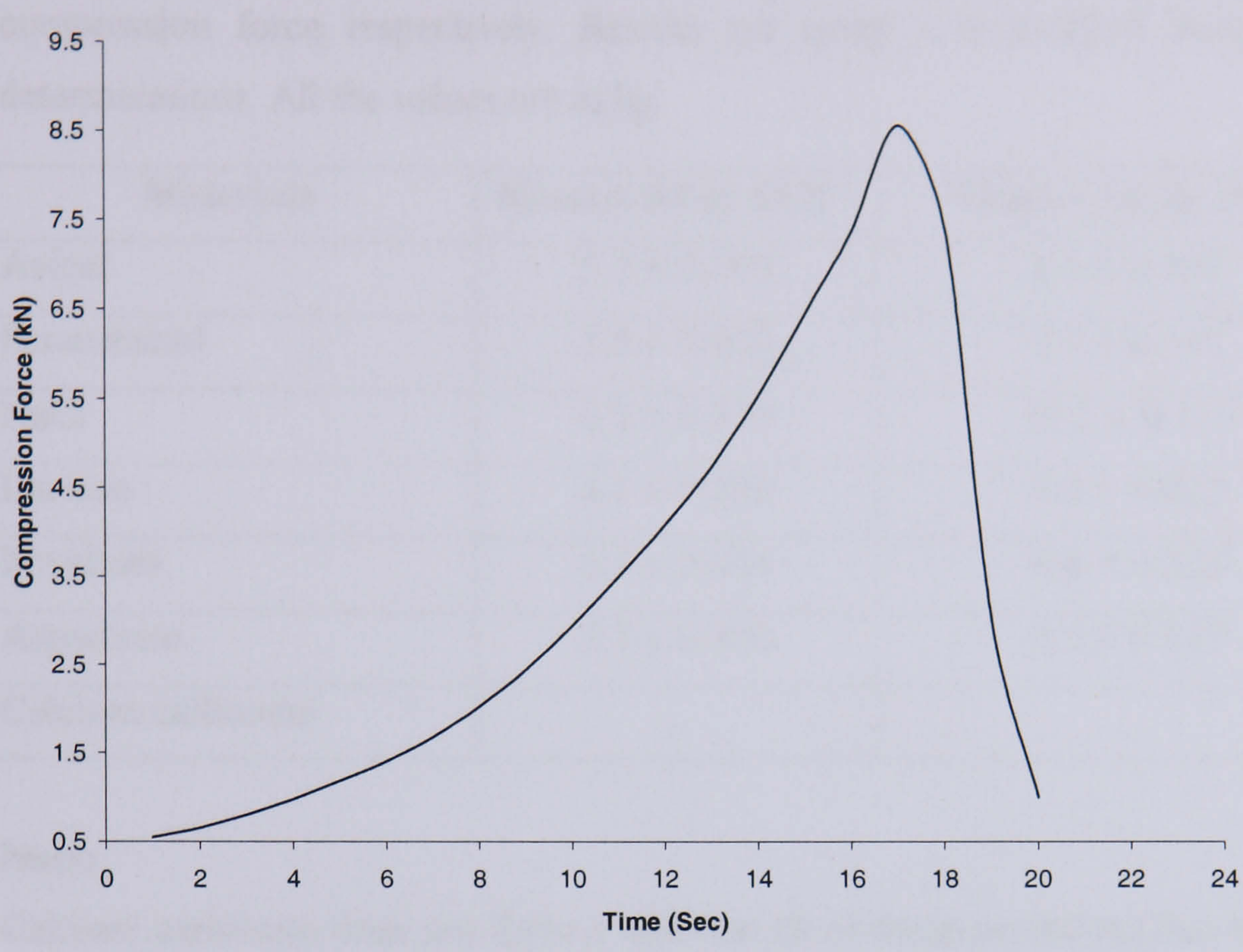

Figure 5.13. Compression force profile as function of time for NaCl.

5.6 Crushing strength measurement (hardness)

Hardness tests for all materials used in this study were measured using the tablet tester model C40. Table 5.2 shows a comparison of the average hardness values of various powder materials. Results are the mean and standard deviation of 6 measurements. Figure 5.14 presents comparison between the crushing strength of various materials tested at the tow loading conditions of 8 and 16 kN.

Table 5.2. Hardness test of different materials compressed at nearly 8 kN and 16 kN compression force respectively. Results are mean ± a standard deviation of 10 determinations. All the values are in kg.

Materials	Mean ± Sd @ 8kN	Mean ± Sd @ 16kN
Avicel	5.3 ± 0.008	8.5 ± 0.011
Paracetamol	5.8 ± 0.002	9.2 ± 0.141
NaCl	6.2 ± 0.133	10.2 ± 0.113
Lactose	6.1 ± 0.220	8.8 ± 0.025
Povidone	5.3 ± 0.044	8.4 ± 0.223
Aspartame	5.7 ± 0.450	8.5 ± 0.147
Calcium carbonate	–	–

Note:

Calcium carbonate does not form a tablet in all of these conditions due both to poor flowability and to insufficient binding forces between the particles.

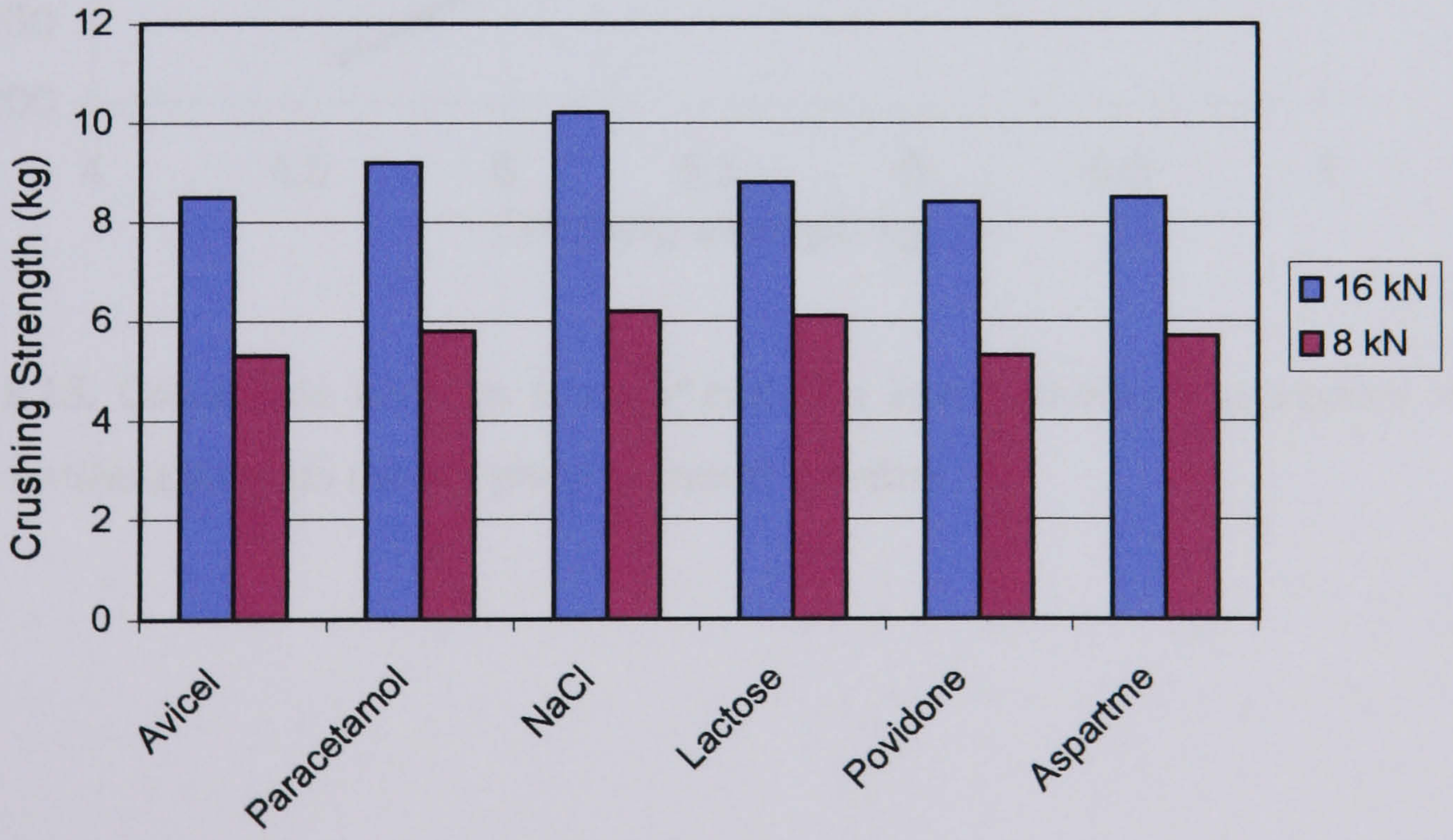

Figure 5.14 Crushing strength of different materials compressed at nearly 8 and 16 kN respectively. Results are mean and standard deviation of 6 determinations.

It was intended also to establish a relationship between some acoustic emission parameters and hardness measurement. Direct relationships have been found that tablets which exhibit high crushing strength are acoustically more active during the compression phase of formation. Figures 5.15 –5.18 show the relationships between AE energy, cumulative AE count and crushing strength. These relationships were noted to hold at two different compression forces of 8 and 16 kN.

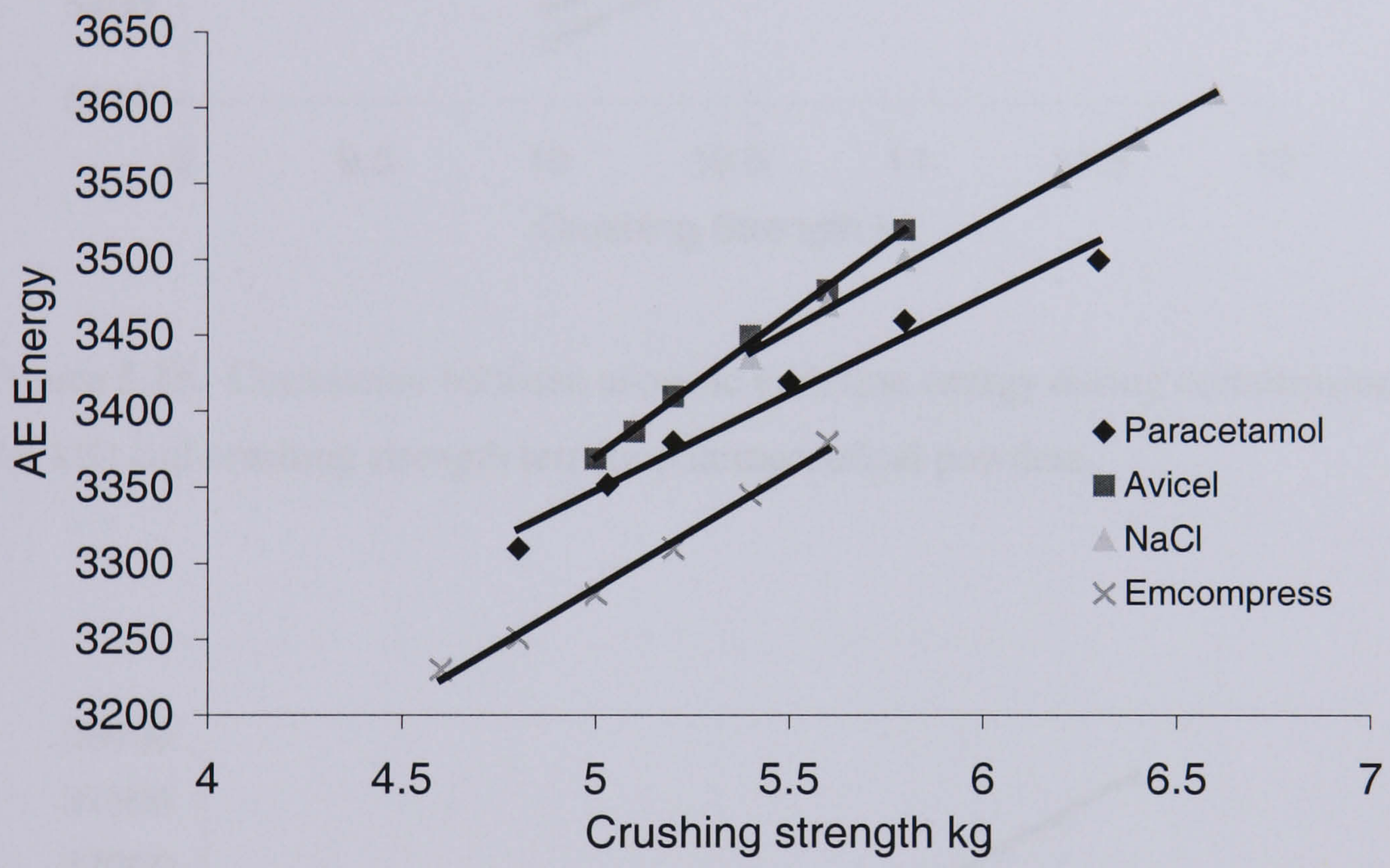

Figure 5.15. Correlation between acoustic emission energy during compression (8 kN) and crushing strength test for pharmaceutical powders.

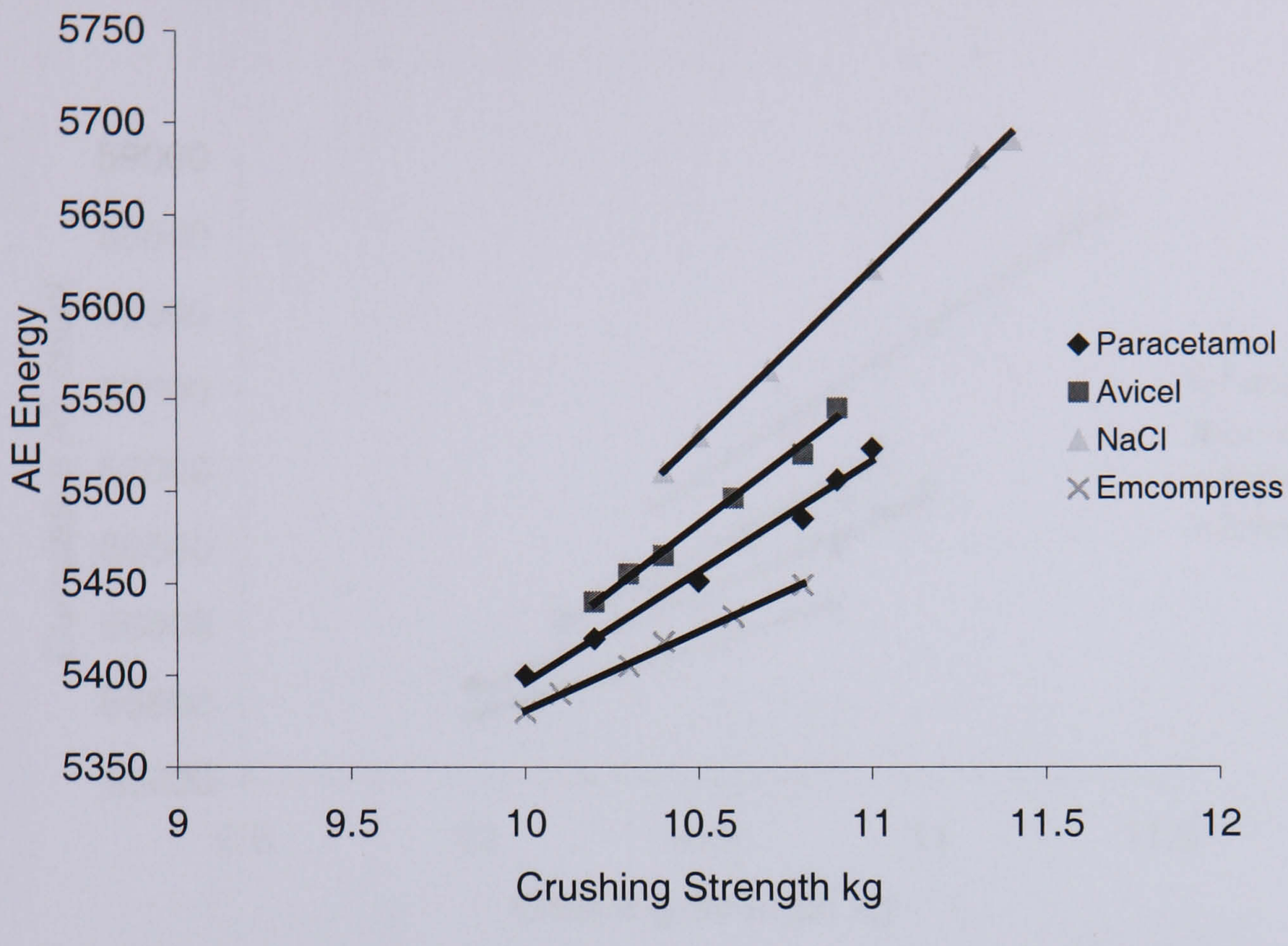

Figure 5.16. Correlation between acoustic emission energy during compression (16 kN) and crushing strength test for pharmaceutical powders.

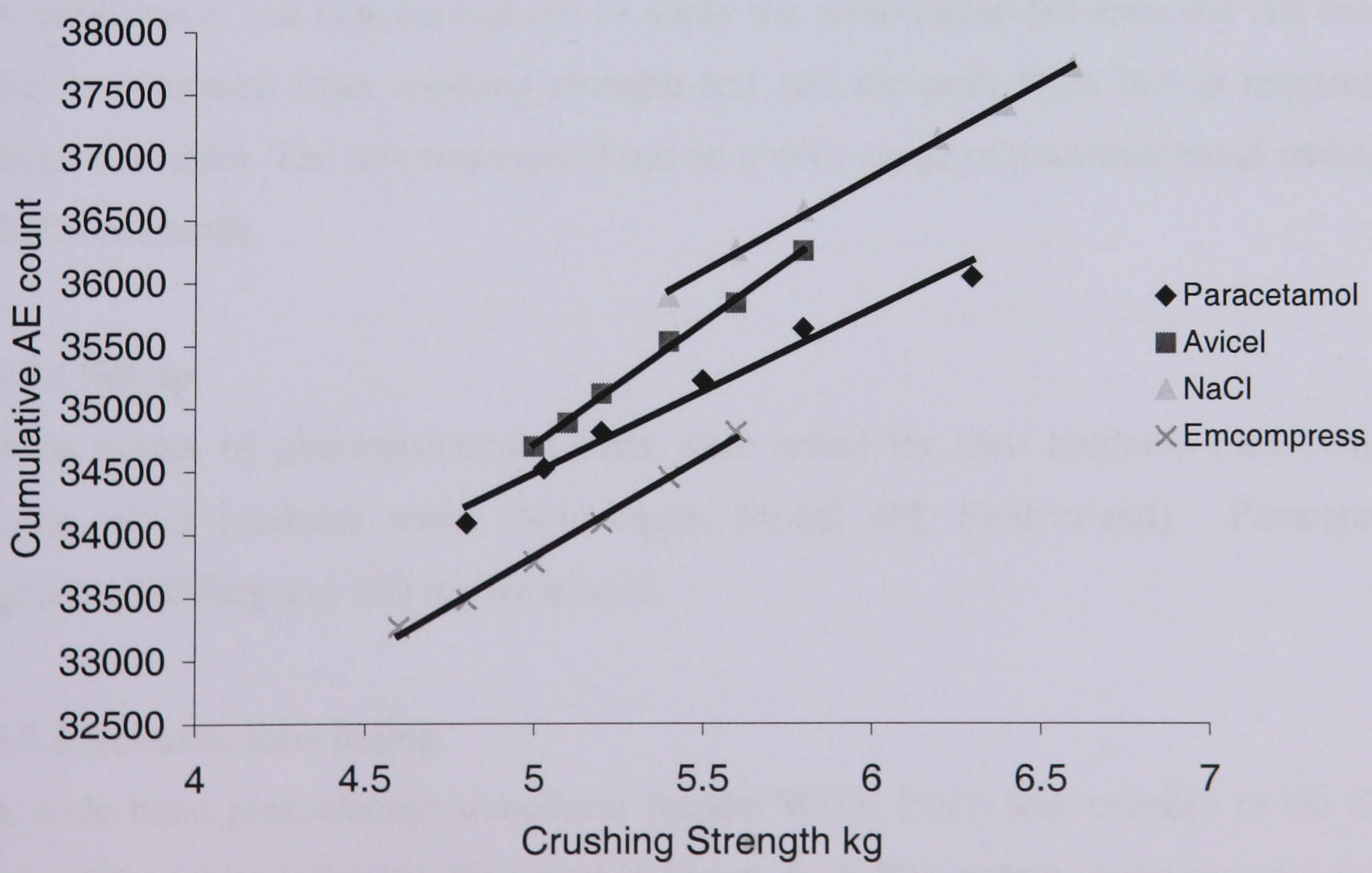

Figure 5.17. Correlation between acoustic emission cumulative count during compression (8 kN) and crushing strength test for pharmaceutical powders.

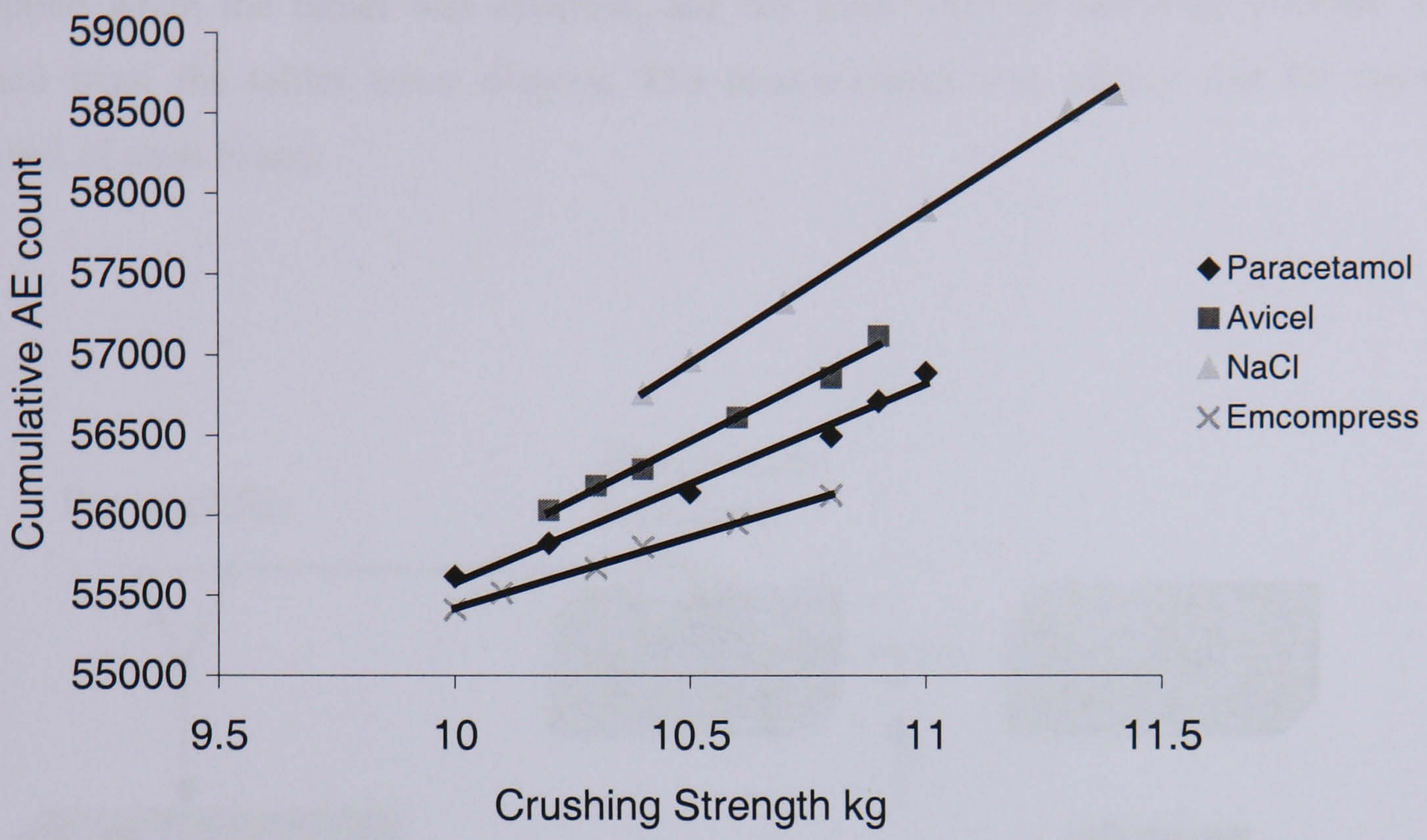

Figure 5.18 Correlation between acoustic emission cumulative count during compression (16 kN) and crushing strength for pharmaceutical powders.

5.7 Preliminary test on AE energy and crushing strength

A preliminary test was carried out to study the relationship between the AE energy that is generated from crushing strength test and the peak force that is required to break the tablet. The test was carried out on a wide range of pharmaceutical tablets of different brands.

5.7.1 Set up

Wide ranges of pharmaceutical tablets were tested for their hardness measurement using tablet hardness tester (Schleunger, Model 4M, Switzerland). Paracetamol tablets of 300mg and 500 mg were used.

5.7.2 Acoustic interfacing

A wide band piezoelectric transducer (model WD8, PAC) was coupled to the fixed jaw of the tablet tester, as illustrated in Figure 5.19. The output of the transducer was connected to the pre-amplifier with a filter built in. The sampling frequency was set at 4MHz. The output of the preamplifier was connected to the LabVIEW data

acquisition system programmed to record the raw signal that emanated from the tablet being crushed. The AE measurement started with the start of the crushing test and stopped when the tablet was crushed; and the peak force of crushing strength was noted from the tablet tester display. The measurement was carried out for twenty tablets of each brand.

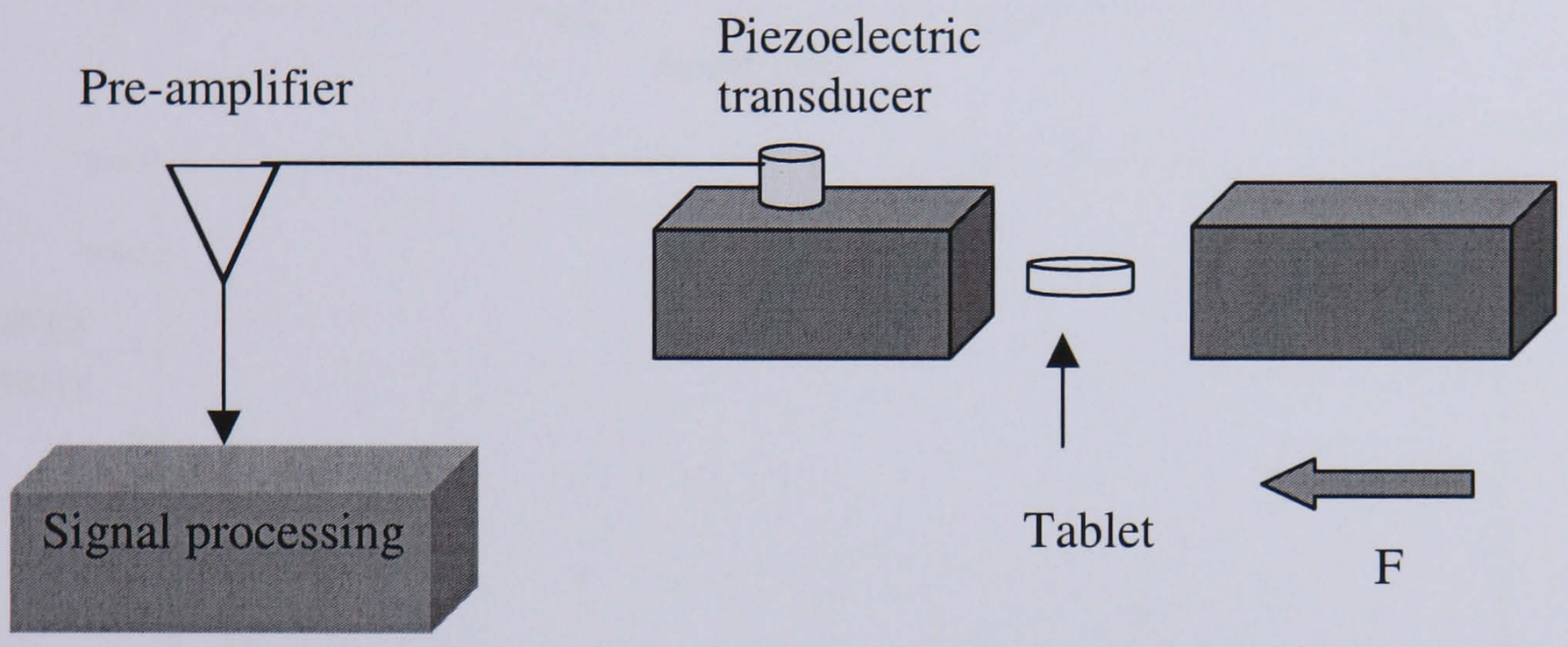

Figure 5.19 Experimental set up.

5.7.3 Relationship between crushing strength and AE energy

The AE signal generated from the crushing test was analysed in both the time and frequency domains.

Aspirin tablets from the same batch were used in the hardness test. Fig 5.20 shows the frequency plot of a raw AE signal produced when crushing a tablet; it was noticed that almost all AE energy was contained within the low frequency region from 50 kHz to 300 kHz. When plotting the AE energy in this frequency range against the peak crushing force as in Figure 5.21, it was found that they were linearly related with a certain amount of scatter. The AE energy was calculated by the integral of the time signal squared over the entire event duration.

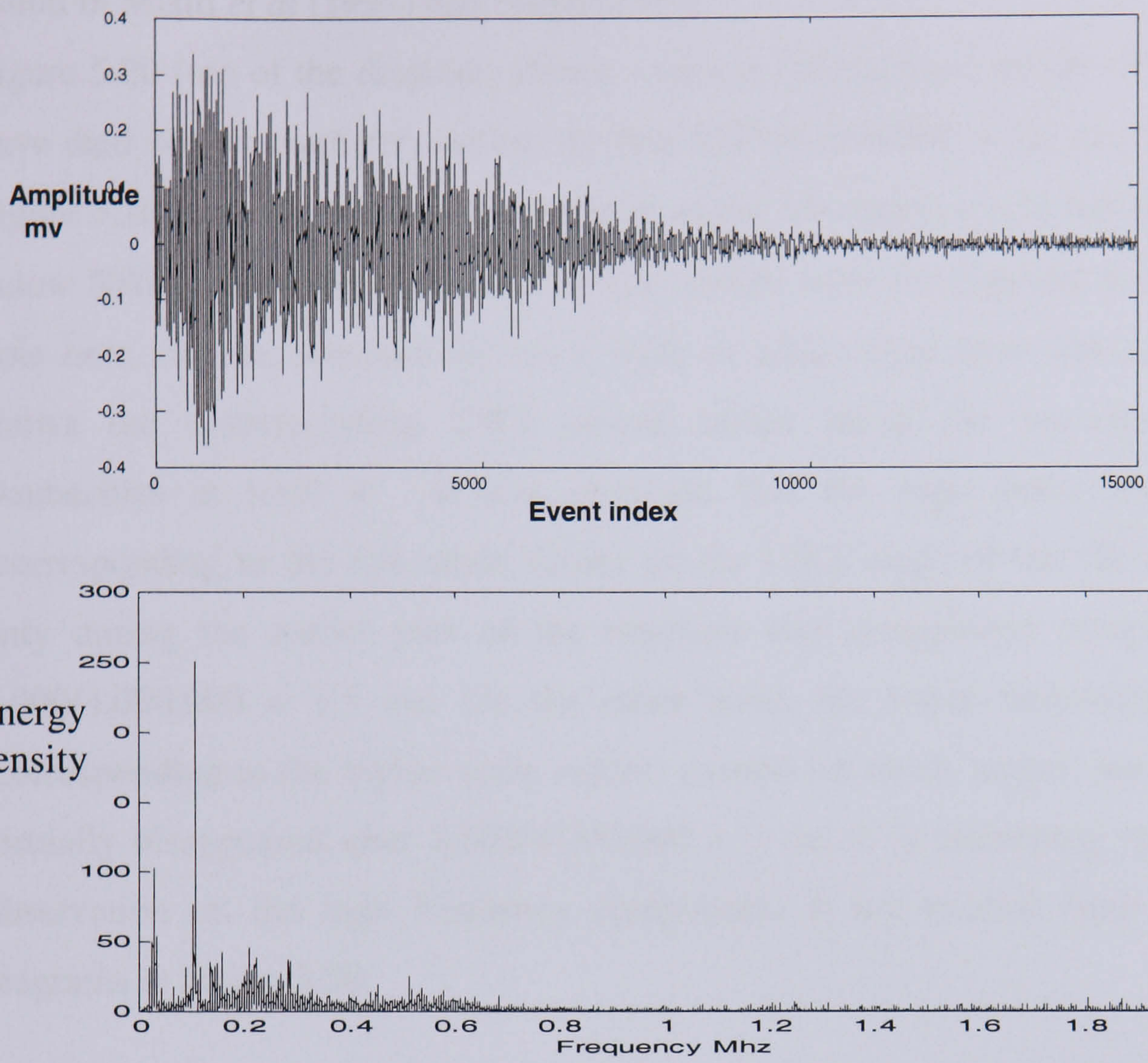

Figure 5.20 Top: AE transient signal obtained from tablet crushing (values of event index divided by 4 million to give a time in the unit of seconds), Bottom: Energy frequency spectrum of AE in tablet crushing.

A frequency spectrum such as Figure 5.20 is only suitable for signals that are periodic. A raw AE signal from tablet crushing is a transient, maybe, a number of transients with frequency components that grow, diminish or even disappear with time. The Continuous Wavelet Transform (CWT) is the tool for revealing not just the scale (inversely related to the frequency in spectral analysis) of the component of a signal but also the time of its occurrence. CWT produces a set of coefficients obtained by comparing the signal with a mother wavelet function at different positions along the time axis and at different scales of the mother wavelet function. The coefficient constitutes the results of a regression of the original signal performed on the mother wavelets. Typically these coefficients are displayed as a colour map with the x-axis and y-axis representing time and scale respectively while the magnitude of the coefficient at a particular time-scale combination is colour coded to appear as a

colour pixel. Details of mother wavelet and the theory of the wavelet transform can be found in Misiti *et al* (1997) and Meyer(1997).

Figure 5.20 (top of the diagram) shows a typical AE transient signal which appears to have died down completely within the first 8,000/4,000,000 = 2.0 ms. The bottom of Figure 5.20 shows the frequency spectrum of the AE signal, a very noticeable peaks at below 50kHz and at about 120kHz can be noticed from the diagram. It is important to note here that the preamplifier has a built in filter range from 20kHz. Figure 5.22 shows the corresponding CWT colour image using the wavelet function of Daubechies at level 4. It was observed that the high frequency components (corresponding to the low scale values on the CWT map) of the AE signal existed only during the earlier part of the transient and disappeared completely beyond 6,000/4,000,000 = 1.5 ms. On the other hand, the lower frequency components (corresponding to the higher scale values) existed for much longer; but most of them virtually disappeared after 8,000/4,000,000 = 2 ms. It is interesting to note that the observation on the high frequency components is not evident from either of the diagrams in Figure 5.20.

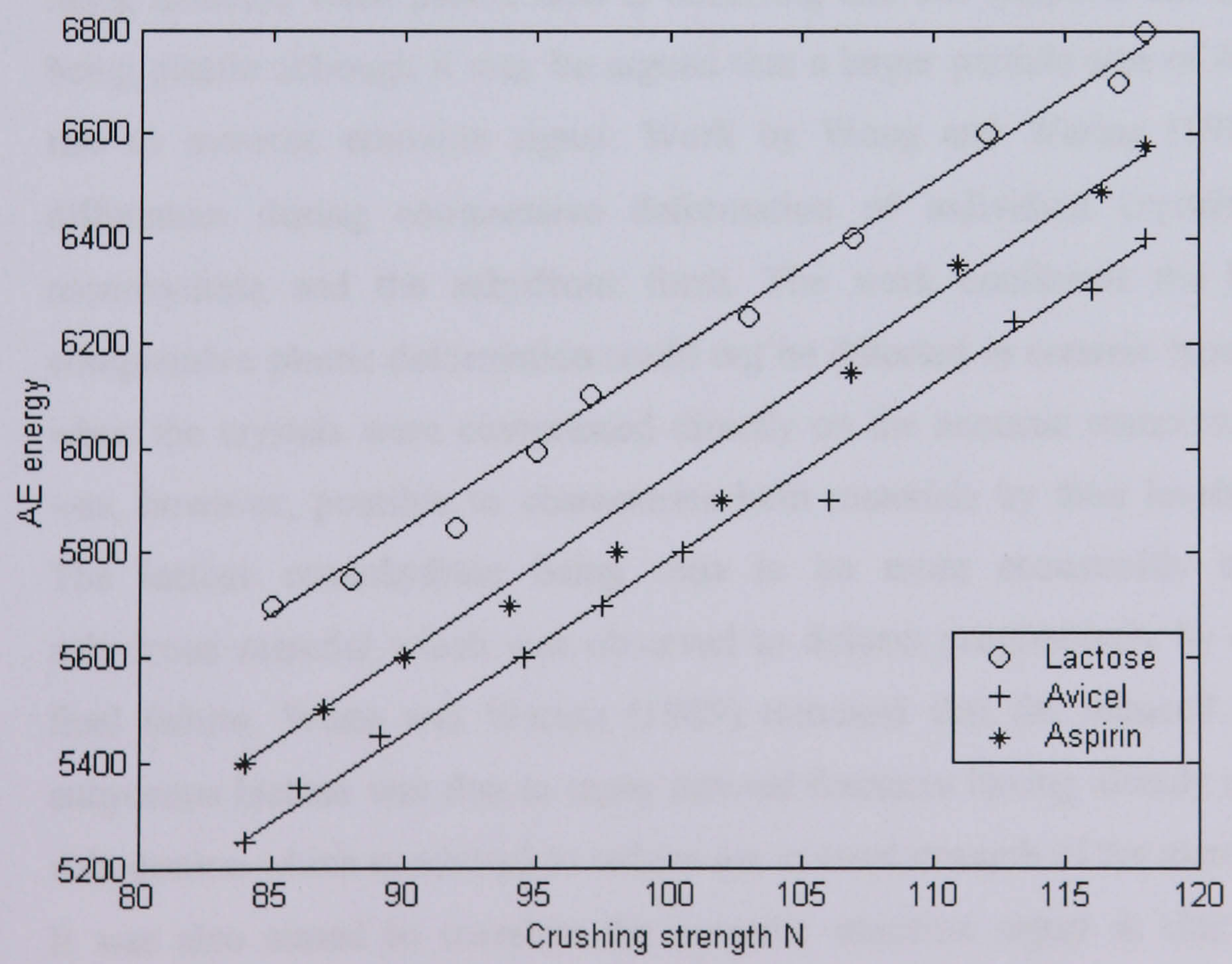

Figure 5.21 Relationship between AE energy and crushing strength

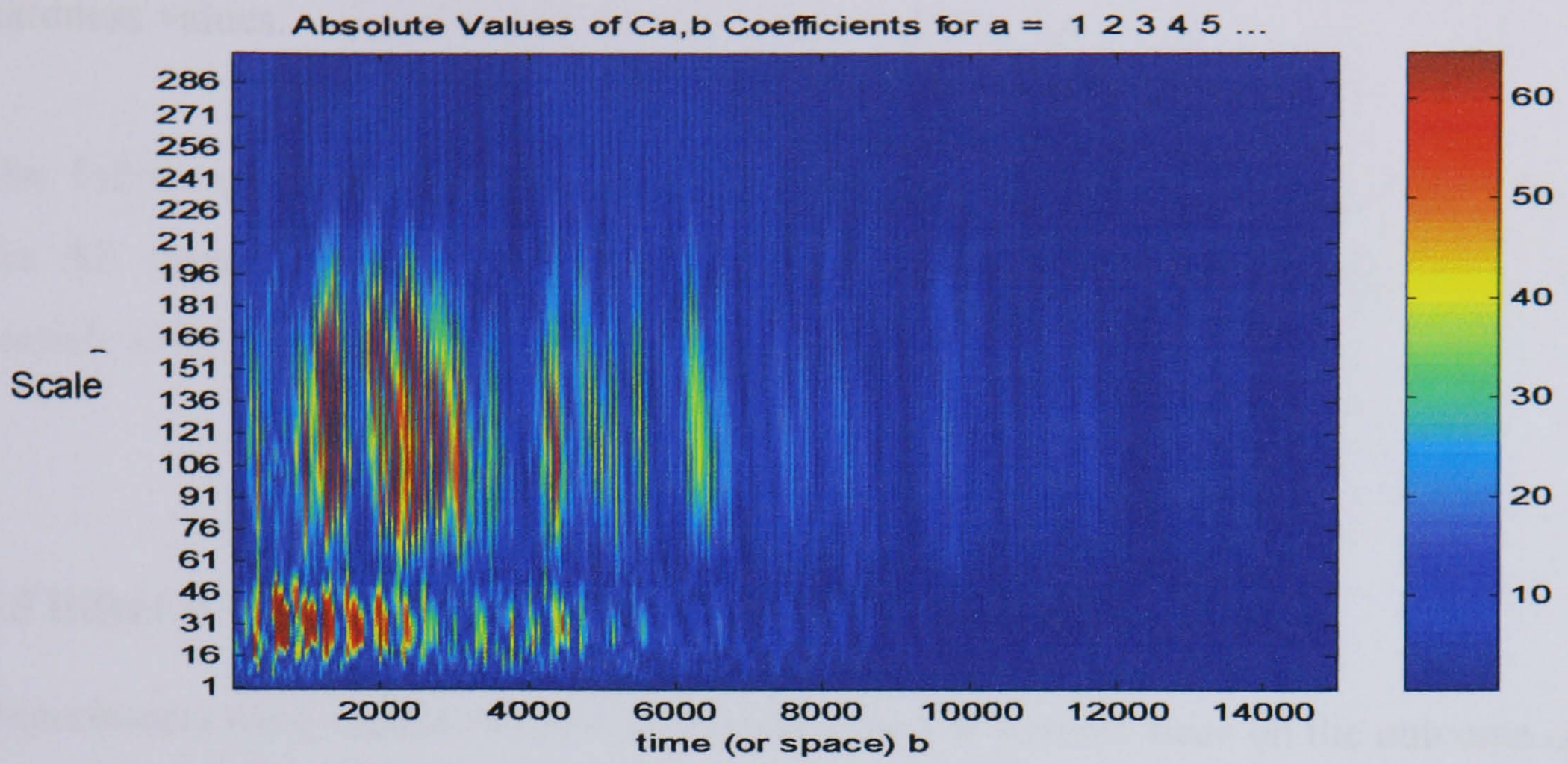

Figure 5.22 Continuous wavelet transform map of the AE transient

In summary, wide ranges of acoustic response were observed for different materials during compression. Brittle materials are particularly active although their level of acoustic activities appeared to be controlled by particle size. Plastic materials tend to be quiet during the consolidation phase. This suggest that acoustic emission is not being detected when plastic flow is occurring and this supports the claim for Avicel being plastic although it may be argued that a larger particle size of Avicel may give rise to acoustic emission signal. Work by Wong and Waring (1989) has shown differences during compressive deformation of individual crystals of α-lactose monohydrate and the anhydrous form. The work confirmed the hypothesis that compressive plastic deformation could not be detected in ceramic type materials even when the crystals were compressed directly on the acoustic emission transducer. It was, however, possible to characterise both materials by their levels of brittleness. The lactose monohydrate being seen to be more acoustically active than the anhydrous material which was observed to deform progressively by crumbling until final failure. Wong and Waring (1989) reasoned that the reduced activity for the anhydrous lactose was due to many internal fractures having already occurred during dehydration which combined to reduce the internal strength of the material.

It was also aimed to correlate the acoustic emission signal as characterised by its tradition features to the crushing test which represent the hardness of the tablet. It was

found that a good linear relationship exists between the AE measurement and hardness values.

The following section aims to investigate the effect of compression condition upon the AE signal generated during powder compression. This includes the effect of particle sizes, compression speed and tablet weight.

5.8 Effect of Particle Size

Experiments were carried out to examine the effect of particle sizes on the outcome of the acoustic emission signal during powder compression, (See Appendix B3 for particle size characterisation). Initial studies using the test rig demonstrated low acoustic emission for smaller particle sizes of the same material in comparison with larger particle sizes. In order to quantify this effect, a range of particle sizes were examined for lactose using the MISTRAS 2000 system for data recording and acoustic measurement. All materials were used as they are received. Materials were compressed at tablet the weight of 300 mg using 12mm diameter flat punches at a compression speed of 20 mm/min. the die being lubricated with a 10% solution of stearic acid in chloroform applied with a cotton bud.

Acoustic emission produced from this study was characterised by the peak amplitude and the total acoustic emission count occurring during the rearrangement phase of the compression cycle. Both parameters showed an increase as the average particle sizes increased. Figures 5.23 and 5.24 show the relationship between the particle sizes and the peak amplitude and total count respectively. The results obtained for sodium chloride confirms that the AE activities are associated with the size and quantities of fractures occurring during the rearrangement phase and enhance the mechanism that generates AE during compression as described in Section 5.3. It is noted that the R-square values in Figures 5.23 and 5.24 are very close to 1, which is a good fit of the line to the data. The results shown in Figures 5.23 and 5.24 are an average of five measurement for each material used in this study.

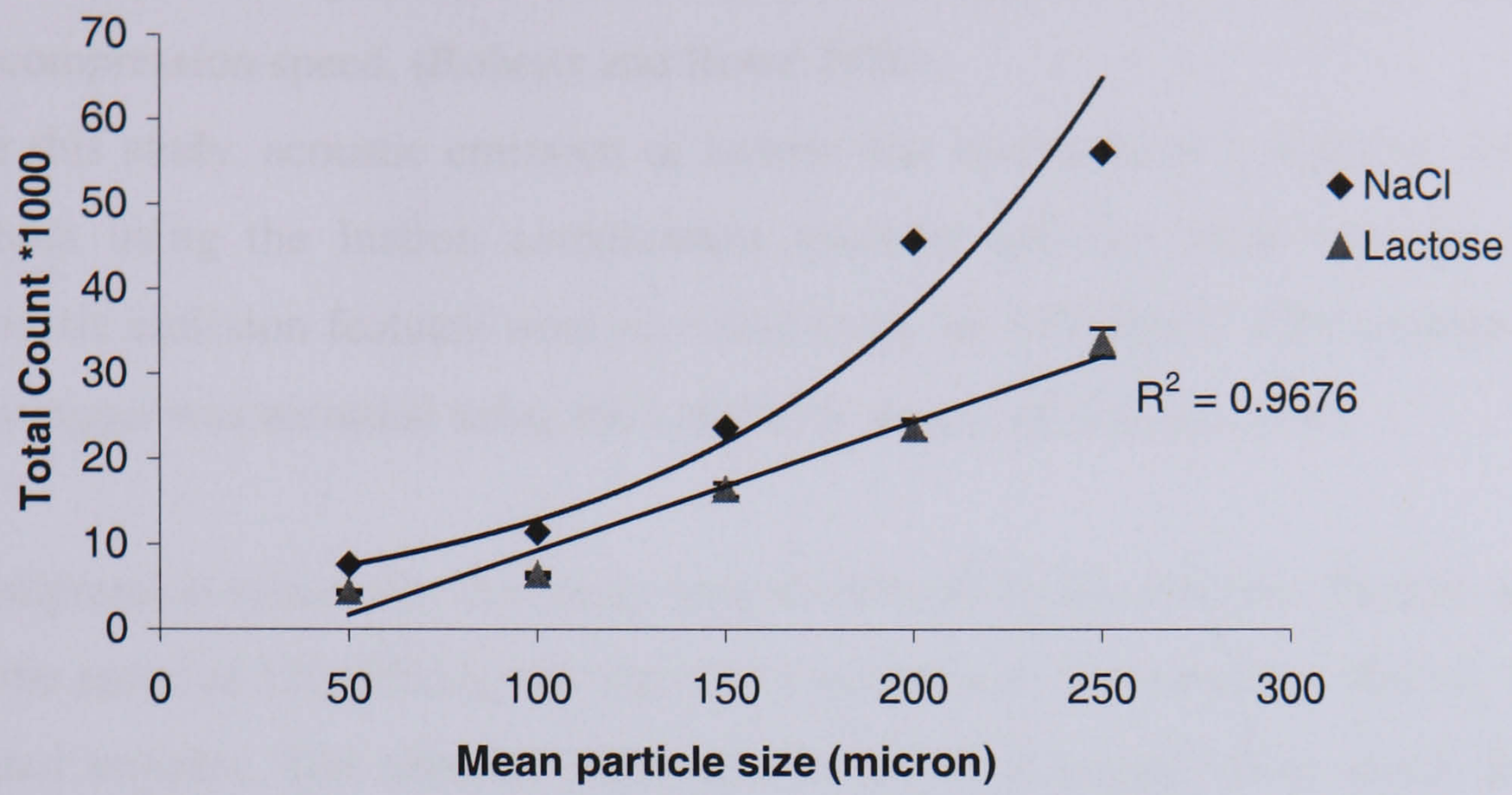

Figure5.23. Effect of lactose and NaCl particle sizes on AE count

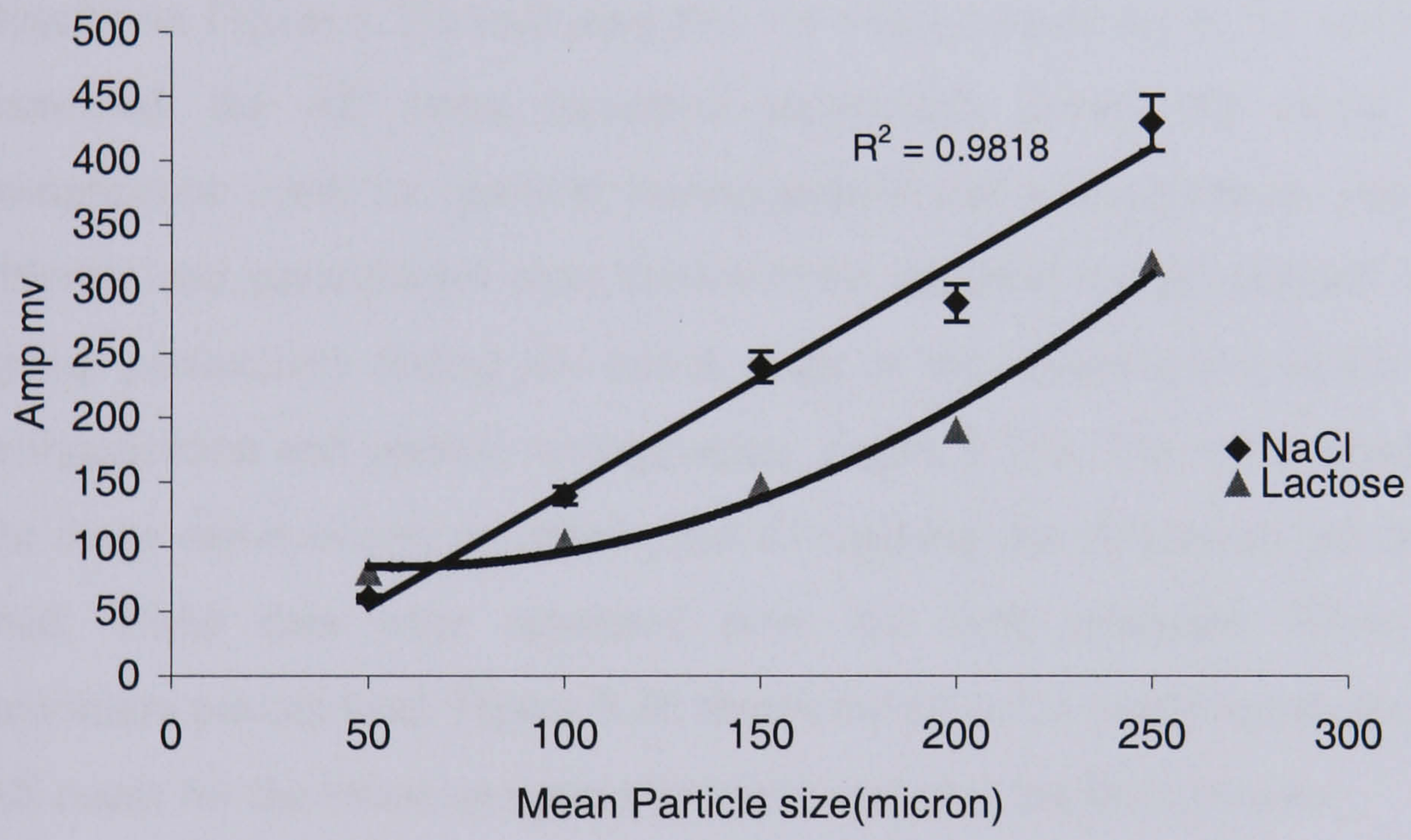

Figure 5.24. Effect of lactose and NaCl particle sizes on AE peak amplitude

5.9 Effect of Compression speed

The rate of pharmaceutical powder compression is a critical issue during tablet formation. This can be a particular problem during the development of tablet formulations which may result in a robust tablet at low compression speeds but will often cap or laminate at the higher speeds of production. Characterising the type of material as either brittle or plastic by the Heckle analysis at low speeds can assist in determining the properties of the tablets. The use of a compaction simulator with the

aid of Heckel analysis has now become the method of choice for predicting the effect of compression speed, (Roberts and Rowe 1986).

For this study, acoustic emission of lactose was examined at a range of compression speeds using the Instron compression machine and the same test rig. Similarly, acoustic emission features were recorded using the MISTRAS 2000 system. Also the raw signal was recorded using the LabVIEW data acquisition system.

Compression speeds for this study ranged from 10 to 60 mm/min. Particle sizes were in the range of 150-200micron. The tablet weight was maintained at 300 mg for all the tested samples. Ten samples were measured at each compression speed. Traditional AE features were recorded to examine the relationship between the AE signals and compression speed.

Results on Figure 5.25a indicated that for a lactose powder as the compression speed increased, the AE count increased particularly during the initial phase of the compression cycle i.e. particle rearrangement and reorganisation. Similarly, sodium chloride and paracetamol were shown to be sensitive to the increase in compression speed, particularly during the initial stage of the compression which comprises the reorganisation and particle arrangements, Figure 5.25b. The reorganisation phase data are those entire events recorded prior to reaching the maximum pre-set compression load. These data were separated from the time reference before reaching the maximum pre-set load. Figure 5.26 shows the effect of compression speed on the total AE count for the entire compression cycle included the three phases.

Similar to AE count, the peak amplitude increased as the compression speed increased. See Figure 5.27.

Waring *et al*, (1989) indicated in their study to examine the compression speed on the compression and ejection that the compression and ejection energies were not influenced by changes in compression speed. These two energy values are calculated from the area under the force-displacement curve. Although material changes in the powder they used were not detected using AE monitoring. With the aid of compactor simulator it is possible to examine the effect of compression speed in a wide range of brittle material on the AE parameters.

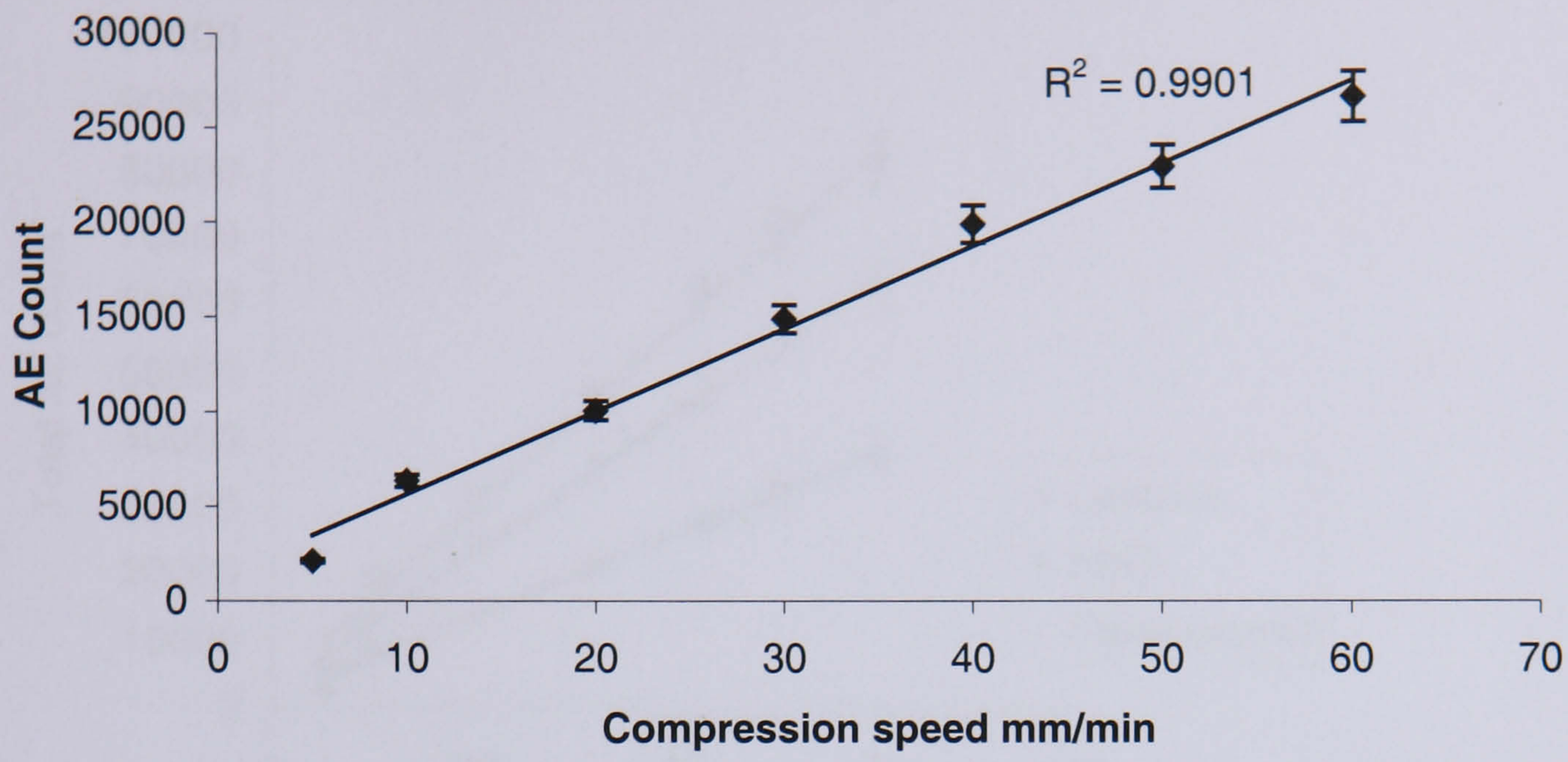

Figure 5.25a. Relationship between the compression speed and the acoustic emission count during the reorganisation phase of lactose compression.

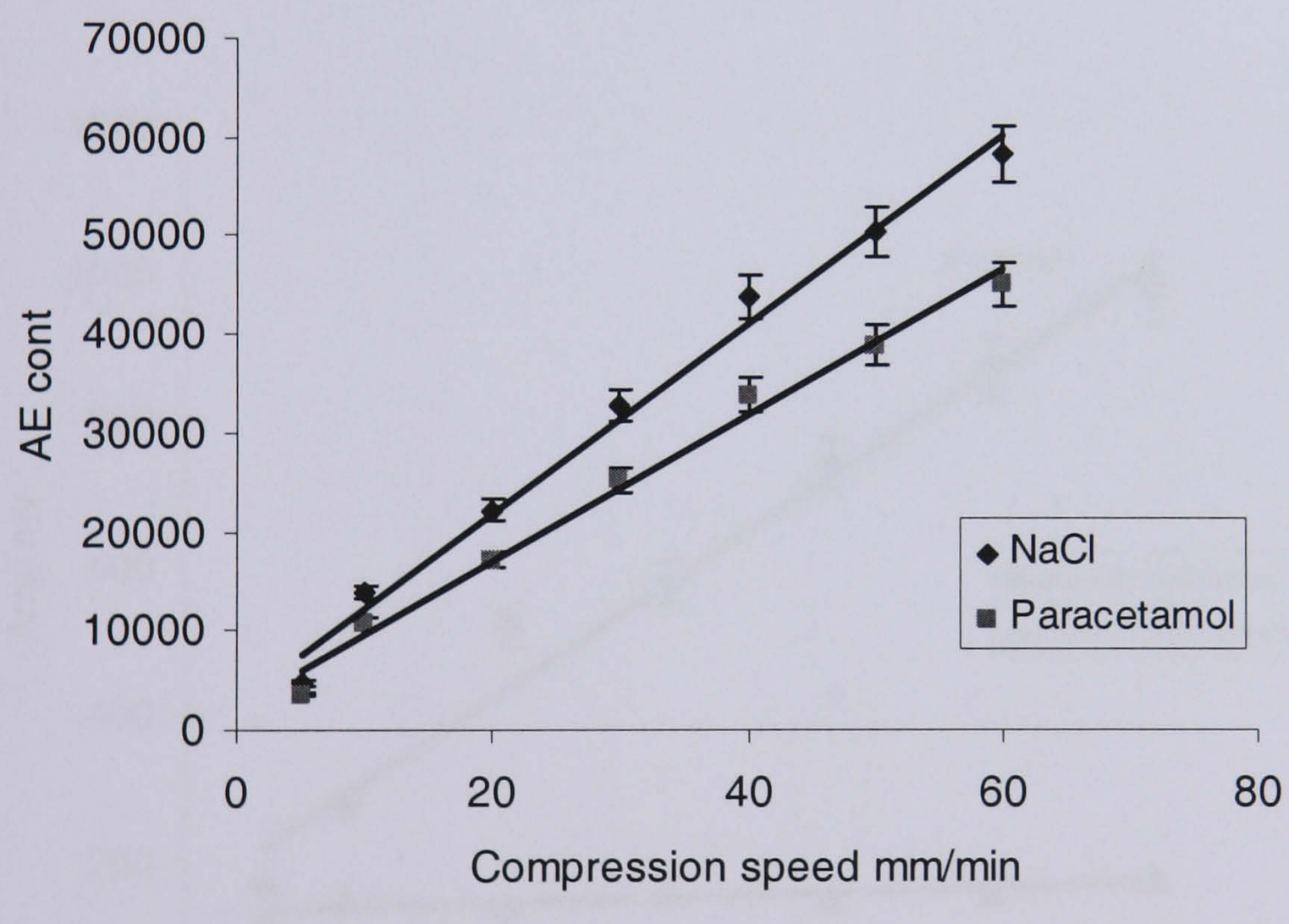

Figure 5.25b. Relationship between the compression speed and the acoustic emission count during the reorganisation phase of NaCl and paracetamol compression.

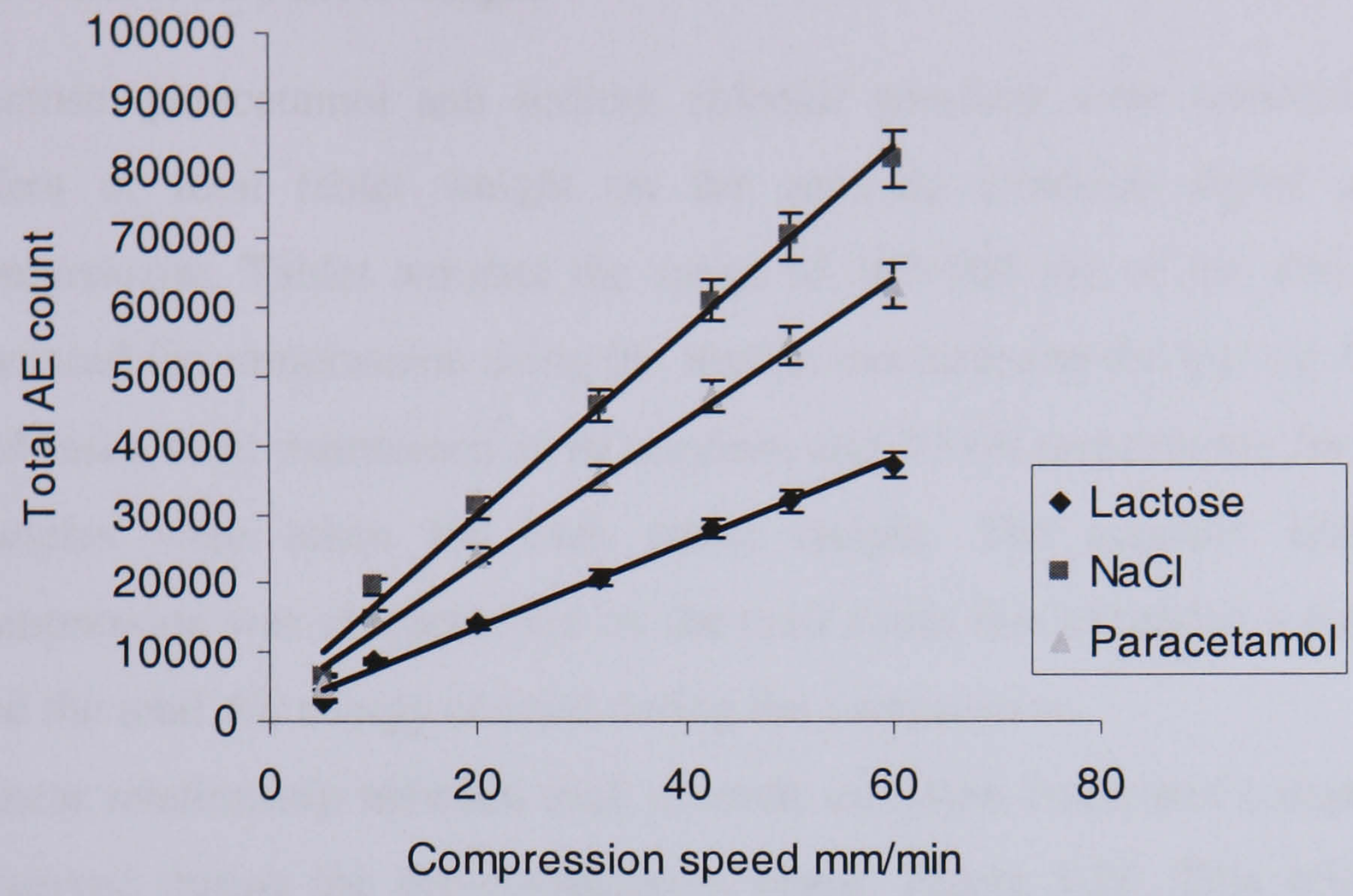

Figure 5.26 Effect of compression speed on total AE count.

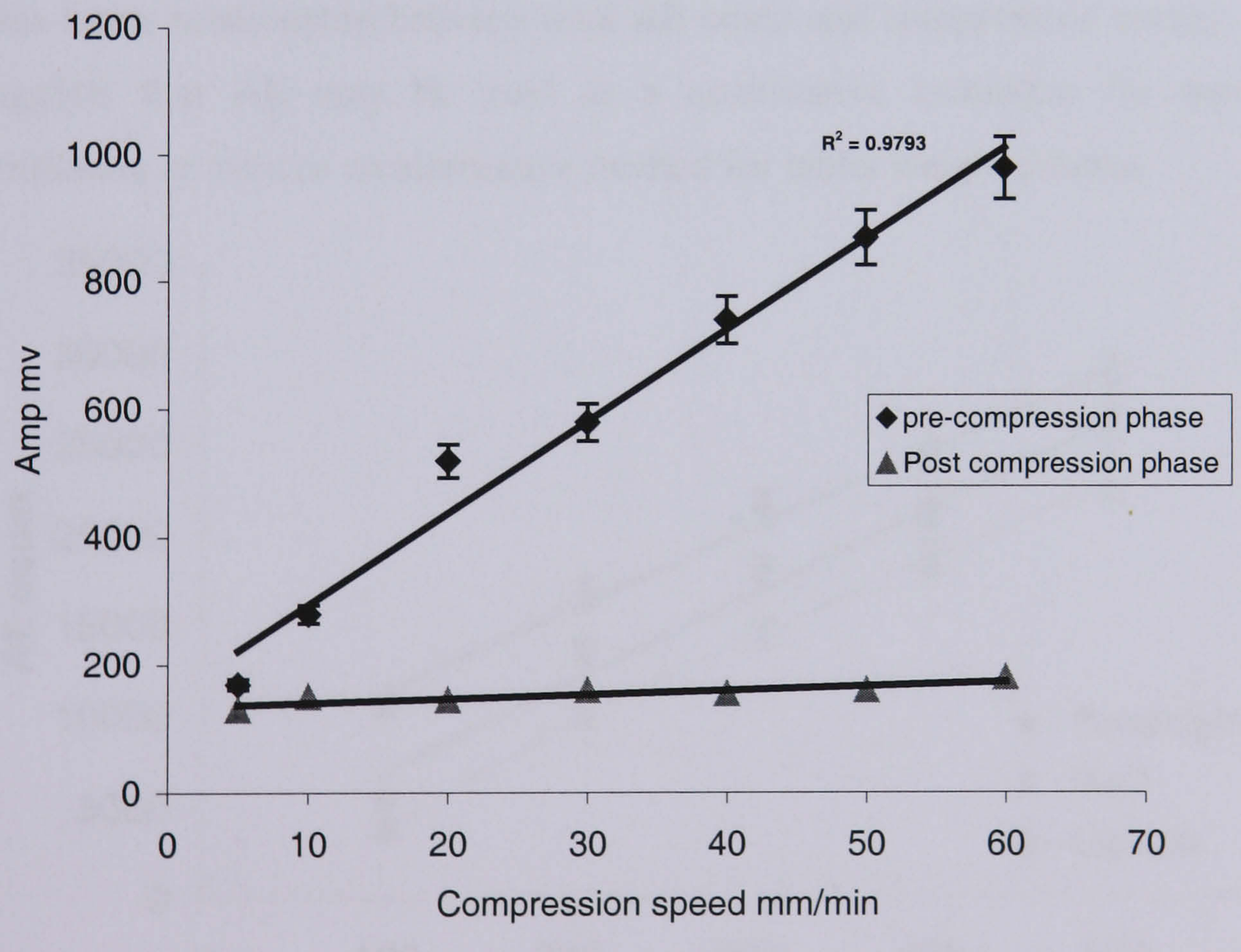

Figure 5.27 Relationship between the compression speed and the peak amplitude AE signal from lactose compression

5.10 Effect of Tablet weight

Lactose, paracetamol and sodium chloride powders were selected to examine the effect of total tablet weight on the acoustic emission signal generated during compression. Tablet weights the range of 100-500 mg of the above material were prepared for compression using the Instron machine and the test rig. Compression rate and force were maintained at 10 mm/min and 10 kN respectively for all samples. Ten samples were taken for each tablet weight. The acoustic emission signal of compression was characterised by the total count that exceeded a particular threshold and the total AE energy emitted during the compression.

Linear relationship between total acoustic emission count and compression weight is observed during the pre-compression phase, Figure 5.28. This relationship may be extended to the compression energy measured from the integration on the Instron force-displacement. It was also observed that the tablet weight of this pharmaceutical material did not appear to significantly affect the AE during the post-compression phase, Figure 5.29.

This linear relationship between total AE count and compression energy, Figure 5.30, suggests that AE may be used as a quantitative technique for measuring total brittleness or even as an alternative method for tablet weight control.

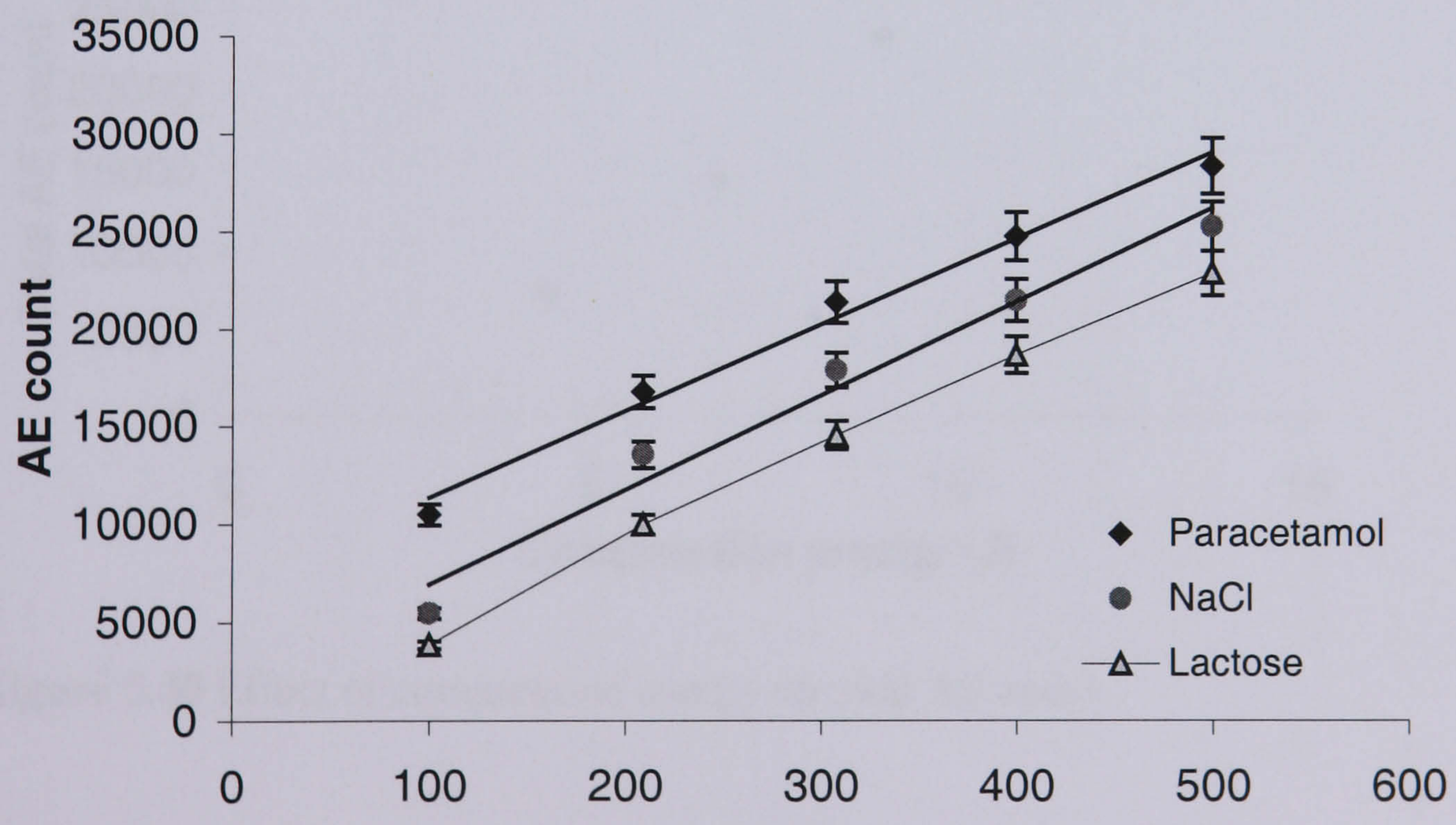

Figure 5.28. Effect of tablet mass on AE signal.

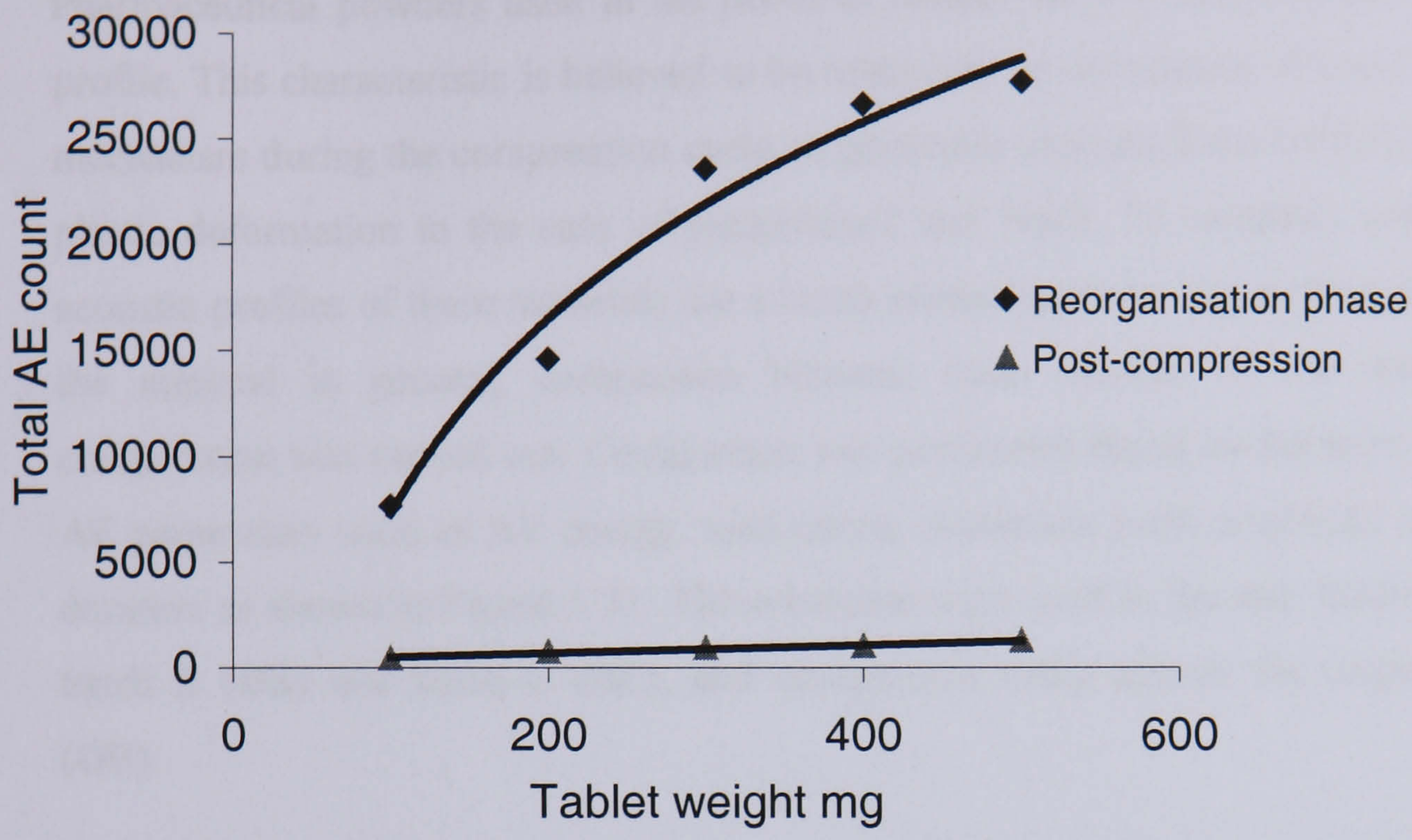

Figure 5.29 Effect of tablet weight on AE signal during both reorganisation phase and post-compression phase of lactose compression.

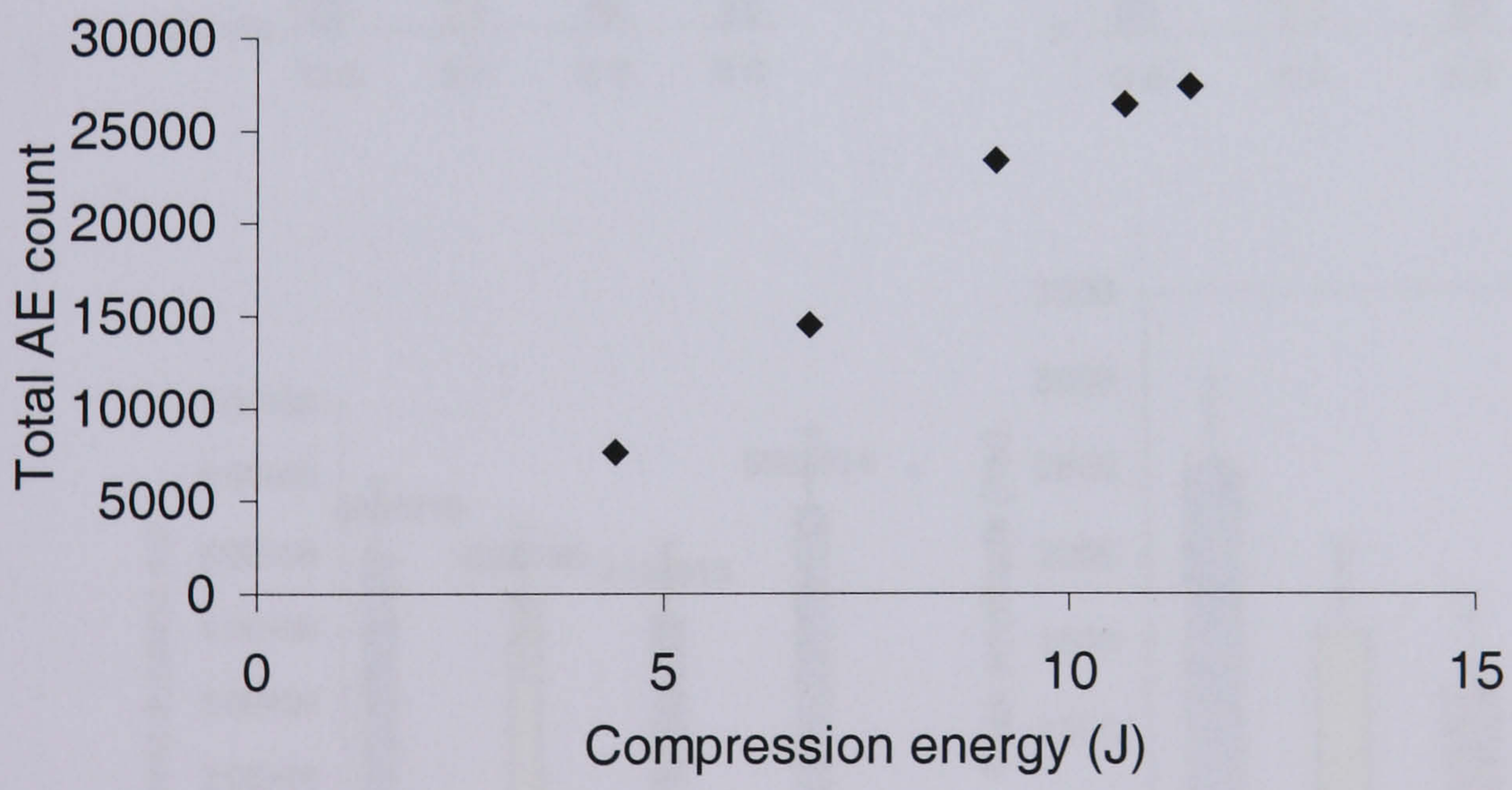

Figure 5.30 Effect of compression energy on total AE count.

5.11 Batch to Batch comparison of powder compression

Pharmaceutical powders used in the previous studies show a characteristic acoustic profile. This characteristic is believed to be related to the occurrence of more than one mechanism during the compression cycle, in particular changes from brittle fracture to plastic deformation in the case of paracetamol and NaCl. To establish whether the acoustic profiles of these materials are a batch phenomenon or it is a characteristic of the material in general, comparison between three batches of the material in compression was carried out. Comparison was performed based on the most sensitive AE parameters such as AE energy, total count, maximum peak amplitude and event duration as shown in Figure 5.31. Three batches were used in the test: batch A (BA), batch B (BB) and batch C (BC), and comparison made against the original batch (OB).

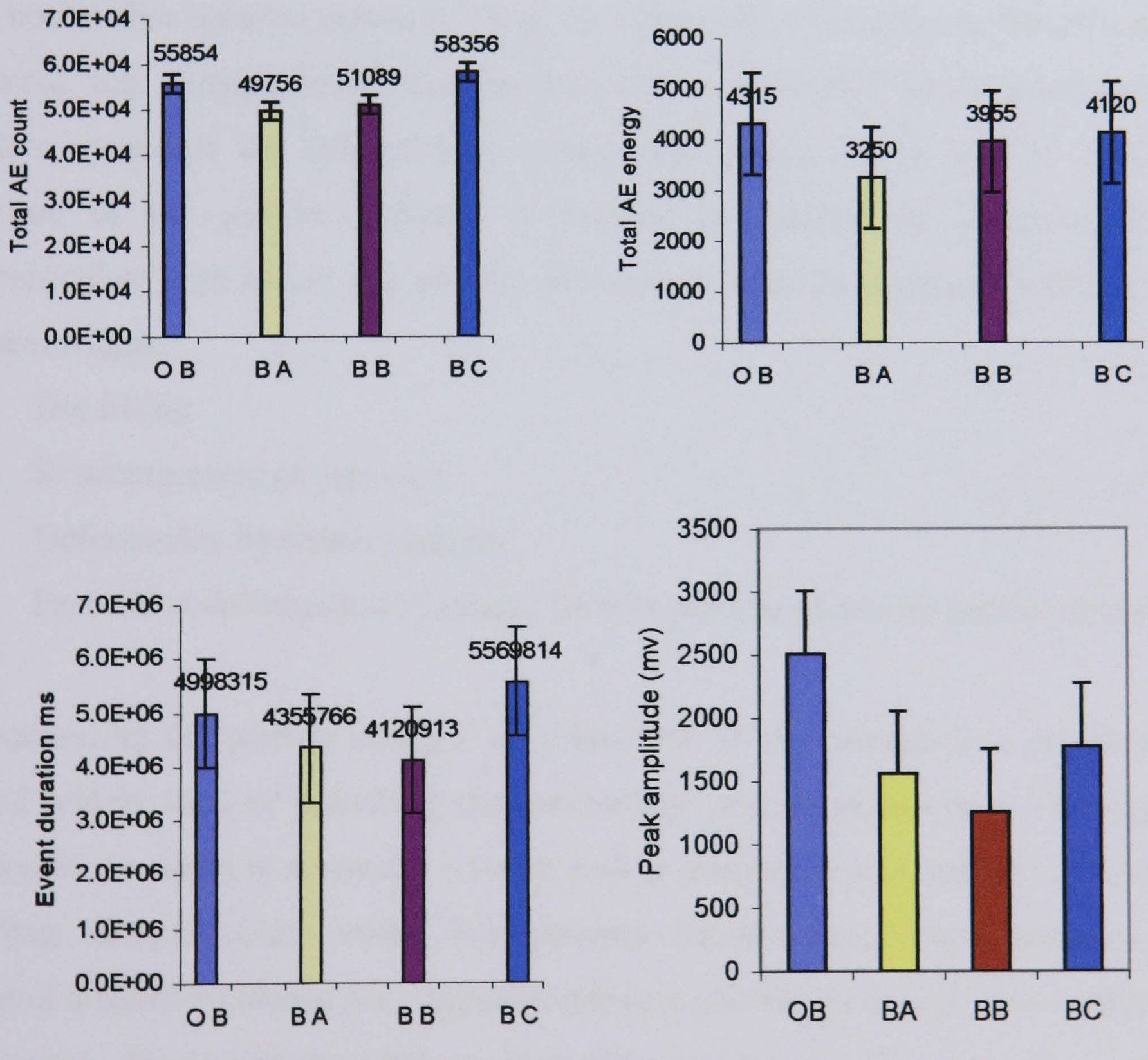

Figure 5.31 Batch to batch comparison for AE parameters. Error bars indicate ± 1 SD.

The results obtained in Figure 5.31, shows that there are small variation within AE parameters for different batches of the same material. This in particular, confirms that the results obtained earlier are a characteristic of the material rather than a batch phenomenon.

5.12 Porosity-Pressure Function

The powder column in a heterogeneous system consists of solid particulate material and air (interparticulate voids). The physical nature of a powder column is different from that of a solid body, as powder can flow and have rheological properties typical of liquids. On the other hand, permanent deformation (plastic flow), reversible deformation (elasticity), and brittle fracturing of particles are typical phenomena for solid bodies that occur in powders. Thus, the behaviour of powders in pharmaceutical processes, e.g. during compression, is often very complicated. In die compaction of powders, materials are subjected to compressive forces which lead to a volume reduction of the powder column. A volume is reduced by decreases in the interparticulate pore space. The process of volume reduction is generally divided into different stages:

Die filling

Rearrangement of particles

Deformation by elastic changes

Permanent deformation by plastic flow or particle failure by brittle fracturing.

The measuring of porosity changes as a function of the compression pressure is a method widely used in describing the compaction process of powders. Porosity is a function of the voids in a powder column, and in general all pore space is considered, including intreparticulate voids. For porosity measurements, the dimension and weight of a powder column (i.e., apparent density) and the particle density (referred to often as true density) of the solid material should be known. The porosity, ε , can be expressed by the following equation:

$$\varepsilon = 1 - \frac{\rho_A}{\rho_T} \qquad (5.1)$$

where ρ_A is the apparent density of a powder column (which can be obtained by dividing the weight by the apparent volume of the powder compact) and ρ_T is the particle density of the compressed material. The ratio ρ_A / ρ_T, also referred to as D, is regarded as the relative density or the packing fraction, which describes the solid fraction of a porous powder column (Paronen and IIKKA, 1997). A value for the applied pressure, P, while loading a powder column under pressure is a function of the compressional force, F, and the punch tip area, *a*

$$P = \frac{F}{a} \tag{5.2}$$

The volume of a powder column, and its corresponding porosity, can be measured either during compression or after ejection of the compact from a die. Instrumentation used in this project, including the universal testing machine, enables continuous monitoring of punch displacement. Hence, the method in which the density was determined employ "in die" or "at pressure" volume determination.

5.12.1 Estimation of powder compressibility using Heckel analysis

Heckel (1961) equation and its parameter for the densification phenomenon were described in Section 2.2.11.1. The equation is:

$$\ln \frac{1}{1-D} = kP + A \tag{5.3}$$

See appendix B3 for derivation.

A schematic diagram of a Heckel plot based on the Heckel equation is shown again here in Figure 5.32. Discribtion of the plot was given in Section 2.2.11.1.

From the intercept of the linear portion of the Heckel plot, A, the total densification of a powder bed due to die filling and particle slippage and rearrangement D_a may be obtained from the following equation:

$$A = \ln \frac{1}{1 - D_0} + B \qquad (5.4)$$

where B describes a volume reduction purely by particle rearrangement (Heckel, 1961a,b).

The relative densities can be related by the equation

$$D_a = D_0 + D_b \qquad (5.5)$$

and D_A may be calculated from

$$A = \ln \frac{1}{1 - D_a} \qquad (5.6)$$

The slope was also related to the yield strength, *Y*, of the material by the equation:

$$k = \frac{1}{3} Y \qquad (5.7)$$

Compressibility of a solid material is related to the bulk elastic properties of that material. The bulk elastic properties determine how much the material will compress under a given amount of external pressure. The ratio of the change in pressure to the fractional volume compression is called the bulk modulus of the material as in Equation 5.8:

$$Bulk \bmod ulus\ B = \frac{\Delta P}{\Delta V / V} \qquad (5.8)$$

where P is the pressure and V is the volume.

The reciprocal of the bulk modulus is called the compressibility of the material.

The extent of particle slippage and rearrangement, D_b, is determined by subtracting D_0 from D_a. The values of D_0 , D_a and D_b may be dependent on the shape and size of the

particles (Heckel, 1961-b; York, 1978), the rate of force application (Roberts and Rowe, 1987; Bateman, 1988) and moisture content (Nokhodchi, 1996).

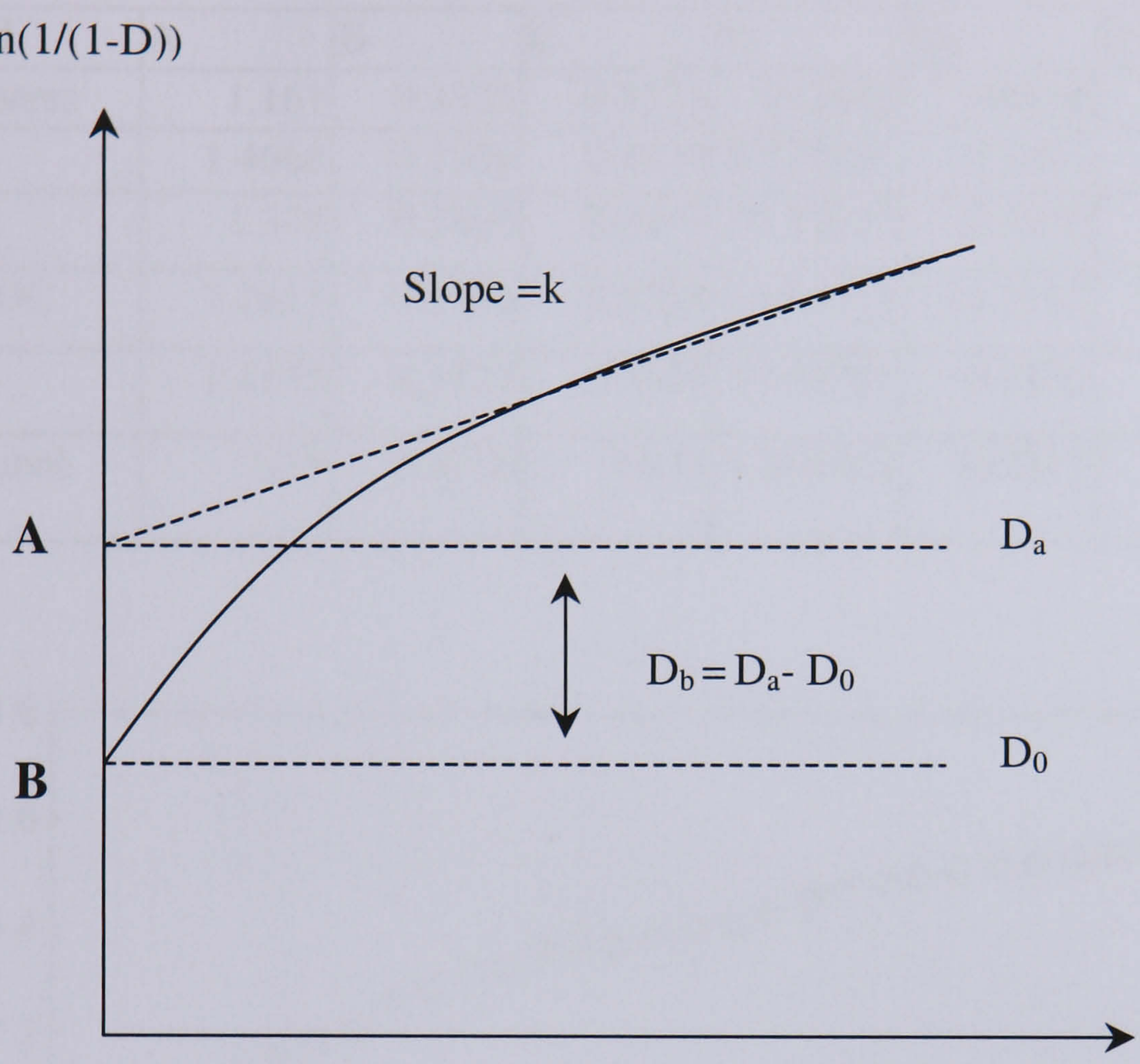

Figure 5.32 Schematic representation of Heckle plot.

The constant *k* is the slope of the straight line region of the Heckel plot and the reciprocal of the slope k is known as the mean yield pressure, which is related to the ability of a material to deform plastically under pressure (Hersey and Rees, 1970). Low values of mean yield pressure reveal the ability of material to deform plastically and high values are indicative of brittle materials (Humbert-Droz 1983).

Figure 5.33 shows Heckel plot of Emcompress powder calculated using Equation 5.3. the Figure shows a curved region which is due to powder densification as a result of particle slippage and rearrangement. Then, it followed by a linear region at higher pressures as a result of particles deformation. Figure 5.34 shows only the linear part of the plot to estimate the Heckel parameters described in Section 2.2.11.1. Table 5.3 list the parameters of Heckel plot for number of pharmaceutical powders during compression test using Instron universal testing machine.

Table 5.3 parameters of Heckel plot for number of pharmaceutical powders during compression test using Instron Universal testing machine, under the application of the maximum applied force of 16 kN and the force rate of 0.5 kN/Sec.

Material	A	B	k	P_y	D_a	D_0	D_b
Emcompress	1.161	0.4329	0.0275	36.3618	0.6814	0.3514	0.33
Avicel	1.4668	0.2306	0.1139	8.779631	0.7693	0.2059	0.5634
Zeparox	1.378	0.3863	0.0497	20.12072	0.7479	0.3204	0.4275
Isomalt DC	1.2611	0.4554	0.0724	13.81215	0.7167	0.3658	0.3509
Isomalt	1.4155	0.5727	0.0767	13.03781	0.7572	0.436	0.3212
Paracetamol DC	1.39	0.4716	0.832	1.201923	0.7517	0.376	0.3757

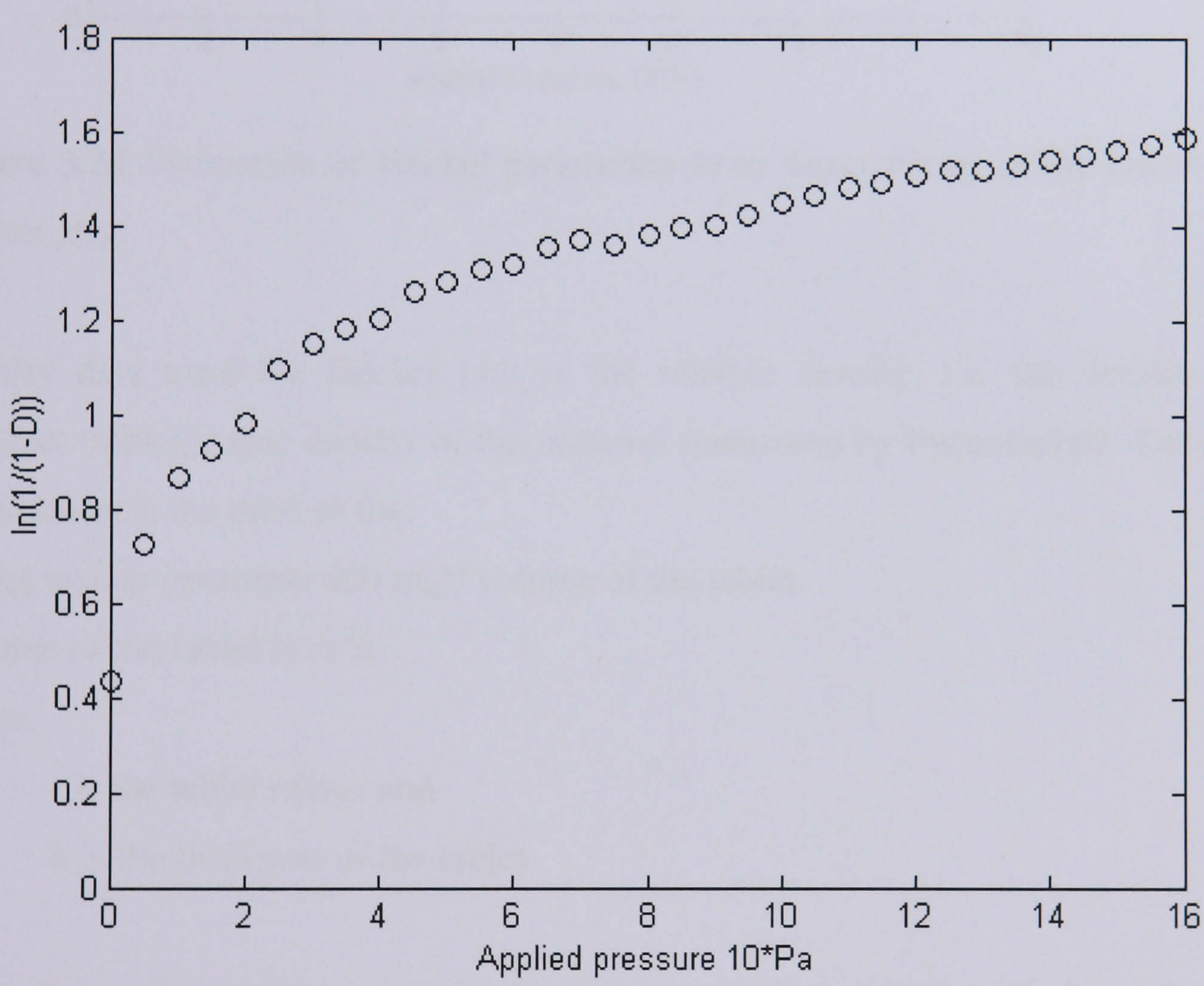

Figure 5.33 Heckel plot of Emcompress.

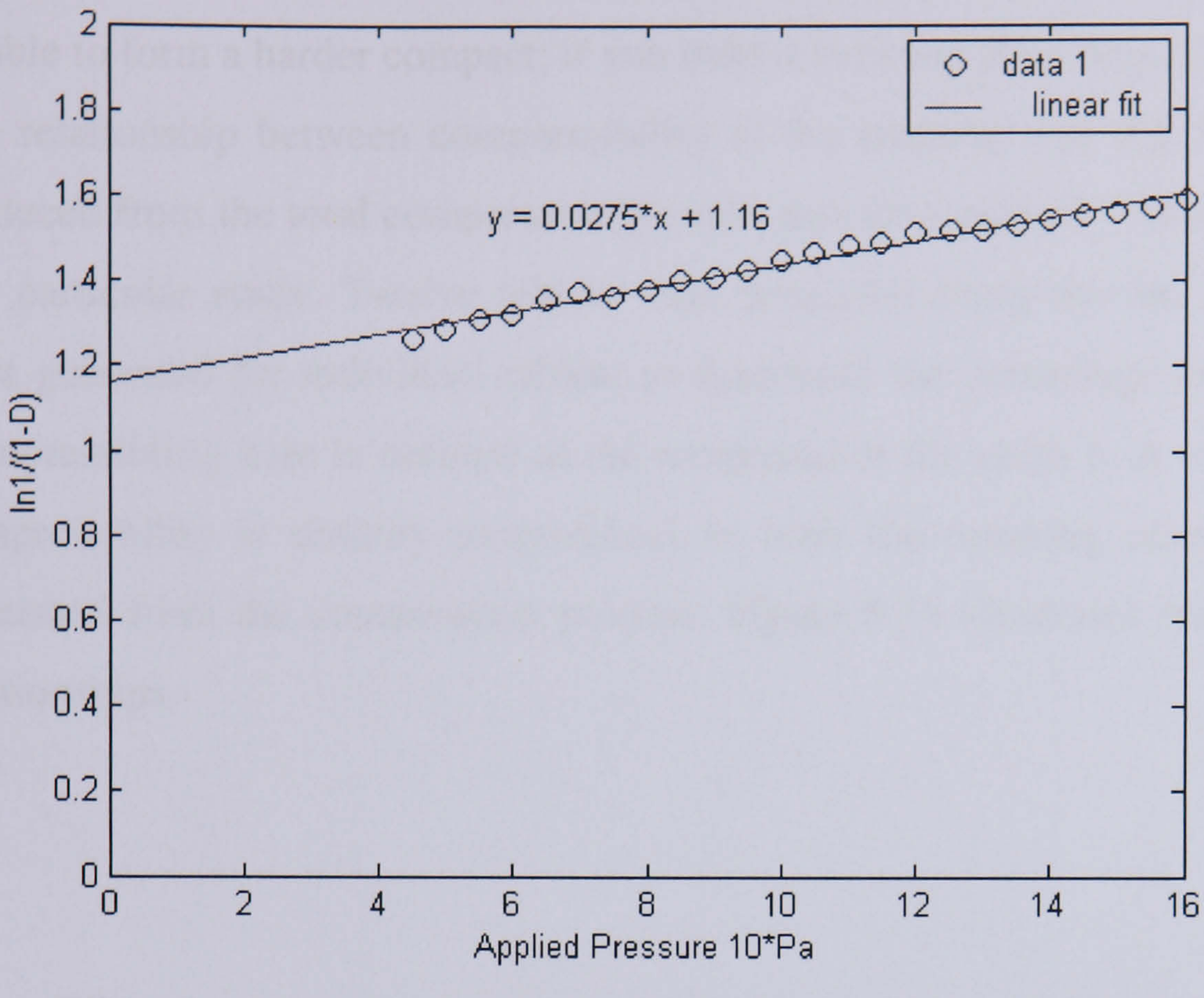

Figure 5.34 Estimation of Heckel parameters from linear fitting of the linear part of Heckel plot.

Density data used for Heckel plot is the relative density, i.e. the density of the compact (tablet) / true density of the material (measured by Pycnometer). The density of the tablet is the ratio of the:

Tablet weight (example 400 mg)/ volume of the tablet.

Volume of the tablet is $\pi r^2 h$

where,

r is the tablet radius and

h is the thickness of the tablet

The volume of the tablet was calculated at any applied compression force during the compression cycle, so was the relative density. In this thesis, the relative density is reported and D is always less than one, i.e. the density of the compact is less than the true density of the material and thus, it does not matter what compression force is used because a porosity of zero is never reached. Compressibility is the reduction in tablet or compact volume. Upon the application of the compression force, the material may reduce its volume, but may not form a compact (Harder mass). An example is

sand: you can reduce the volume of the sand if you apply a force, but you will never be able to form a harder compact; if you hold it between your finger it will collapse.

The relationship between compressibility of the material and the AE energy that is produced from the total compression process was investigated. Avicel was chosen for this particular study. Twelve tablets were produced using the test rig. Heckel plots were generated for individual tablets to determine the percentage of compressibility. Compressibility here is defined as the reciprocal of the slope *k*. It was found that the compressibility is directly proportional to both the crushing strength and the AE generated from the compression process. Figure 5.35 illustrates three plots of these relationships.

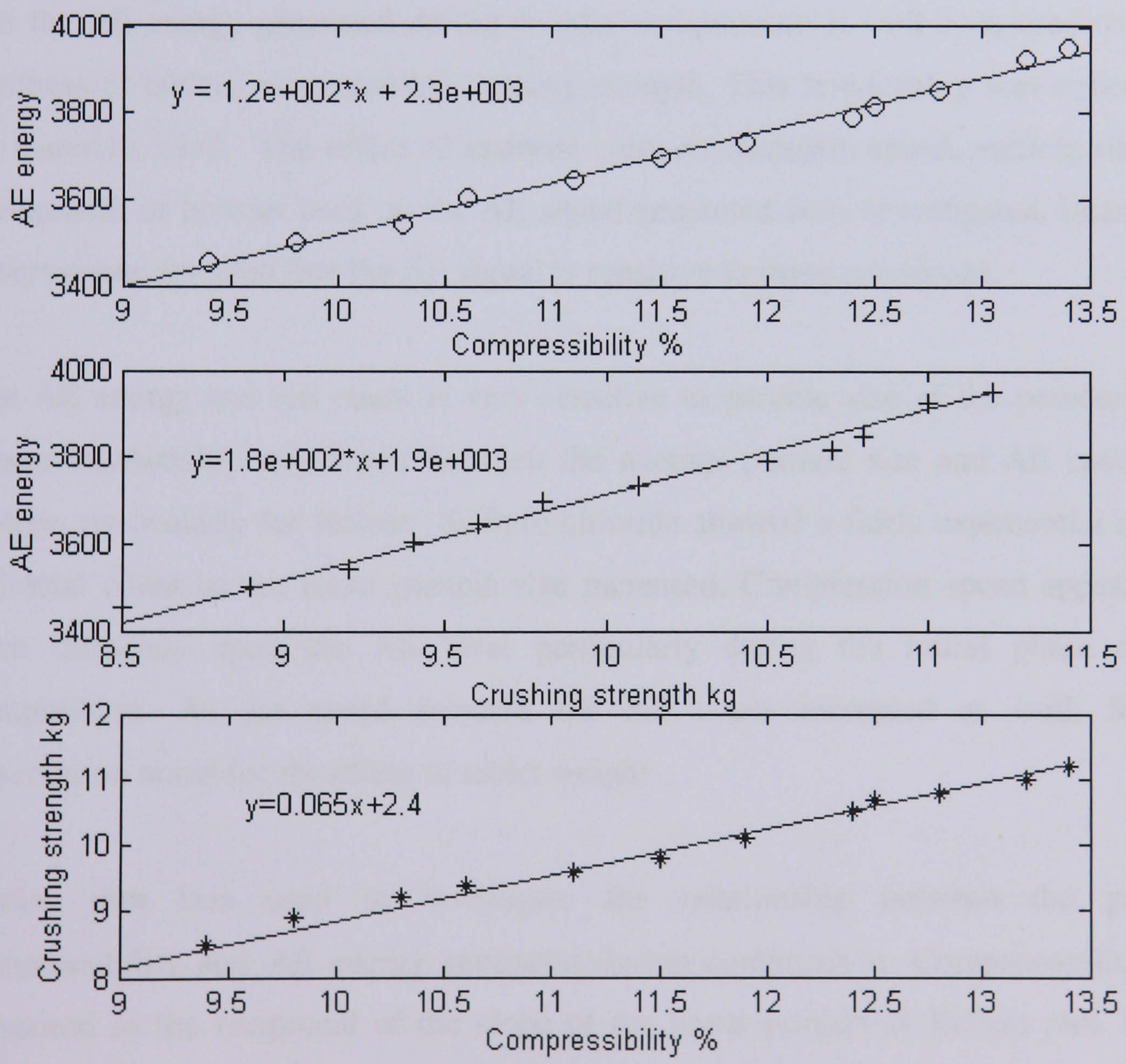

Figure 5.35 Relationships compressibility, AE energy and crushing strength.

5.13 Conclusion

This chapter dealt with several issues that are related to the AE monitoring of powder compression during tabletting. Initially, it was shown that the compression cycle can be characterised by three stages namely pre-compression and particle arrangement, followed by consolidation of powder and finally post-compression. There are various mechanisms which gave rise to the AE signal. These could be mechanical contact between the upper punch and the die and particle slippage and arrangement at the early stage of the compression, also particle die friction during consolidation. It was noticed that the AE energy peaks and peak amplitude increased exponentially as the load continued to increase. This observation was noticed to most material. This is because the mechanism that generate AE here is the particle arrangements and friction with the die as the load building up inside the die. Most material and in particular those classified as brittle are acoustically active during the initial stage. It was noticed that the AE energy generated during powder compression is well correlated with the hardness of tablets, measured by crushing strength. This relationship was noticed for all materials used. The effect of material type, compression speed, particle size and the amount of powder used on the AE signal generated were investigated. Interesting observations revealed that the AE signal is sensitive to these conditions.

The AE energy and AE count is very sensitive to particle size of the powder used. Linear relationship was found between the average particle size and AE count and energy, particularly for lactose. Sodium chloride showed a fairly exponential rise of AE total count as the mean particle size increased. Compression speed appeared to have influence upon the AE level particularly during the initial phase of the compression. As the speed increase the AE count increased as well. Similar observation noted for the effect of tablet weight .

Heckel plot was used to investigate the relationship between the powder compressibility and AE energy generated during compression. Compressibility was measured as the reciprocal of the slope of the linear portion of Heckel plot. It was found that AE energy is linearly related to powder compressibility which is also linearly related to crushing strength of the final tablet.

References

Armstrong N.A. and Haines-Nutt R.F. (1972) Elastic recovery and surface area changes in compacted powder systems. J. Pharm. Pharmacol. 24, 135.

Brown C. R (1979) Acoustic emission as a quantitative technique, Proc. Of Acoustic Emission and Materials Evaluation, Inst. of Acoustics, London.

Down G. R (1983) Localised particle fracture during compression of material expected to undergo plastic deformation. Powder Technology, **35**, 167-169.

Hardman J. S and Lilley B. A. (1973), Mechanisms of compaction of powdered materials. Proc. R. Soc. London, 333, 183-199.

Hersey J. A., Cole E. T. and Rees J. E. (1972) Powder consolidation during compaction, **4**, 165-172.

Humbert-Droz P., Gurny R., Mordier D and Doelker E. (1983) Densification behaviour of drugs presenting availability problems, Int. J. Pharm. Tech. And Prod. **4** (2), 29-35.

Meyer Y, (1997) 'Wavelet algorithms & application', published by the Society for Industrial and Applied Mathematics (1997).

Misiti M., Misiti Y, Oppenheim G and. Poggi J. M (1997) Wavelet Toolbox for use with MATLAB, published by the Math Works, Inc.

Roberts R.J and Rowe R. C. (1985) The effect of punch velocity on the compaction of variety of material, J. Pharm. Pharmacol. **37**, 377-384.

Roberts R.J and Rowe R. C. (1985) The effect of the relationship between punch velocity and particle size on the compaction behaviour of materials varying deformation mechanism. **38**, 567-571.

Swindlehurst W. (1974) Acoustic Emission 5-11, I. P.C. Science and Technology Press Ltd, Guildford, England.

Wade, A. & Weller, P. J. (1994): Handbook of Pharmaceutical Excipients. 2nd ed. Ajoint publication of London; The pharmaceutical Press& Washington; American Pharmaceutical Association. P5 6-56-59, 84-86, 252-259 & 392-398.

Wong D. Y. T., Waring M. J., Wright P. and Aulton M.E (1989). Analysis of the deformation of alpha-lactose monohydrate and anhydrous alpha-lactose monocrystals by acoustic emission. 8th Pharmaceutical technology conference, Monte Carlo.

Chapter 6: AE monitoring of industrial tabletting

6.1 Introduction

This chapter describes the acoustic emission studies conducted at GlaxoSmithKline using the industrial tablet press Manesty F3. It summarises the important relationship between acoustic emission parameters and physical properties of tablets such as disintegration time, hardness and homogeneity in binary mixtures. This chapter presents acoustic emission data that was generated from continuous powder compression of various tablet excipients. The materials chosen are very popular pharmaceutical powders used as common tablet fillers to form the final tablet compact.

6.2 Acoustic emission monitoring using Manesty F press.

The materials listed in Table 6.1 were compressed using the Manesty F-press. All the materials were used as received. The press was set to produce 50 tablets per minute. Both the upper and lower punches together with the die were lubricated with Acetone. The Manesty F3 is a single-stroke, power-driven tablet machine capable of producing tablets up to 22mm in diameter with a maximum output, using single-tip punches, of 85 tablets per minute (5,100 per hour). The tablet weight was adjusted by means of the lower plunger collars mounted below the die-table.

AE monitoring was performed using the MISTRAS system. The monitoring was carried out using the miniature transducer, Model nano 30 from Physical Acoustic Corporation, PAC. The transducer was attached to the upper punch using an acoustic coupling gel to facilitate signal transmission. The output of the transducer was connected to a 40 dB preamplifier, model 214/6 (28Volts DC, Filter 100-1200 kHz, from PAC). Data were sampled at 10MHz. For every material used in the test, twenty tablets were formed and AE data of these tablets were recorded. Traditional AE parameters such as energy, RDC, ASL, RT, and peak amplitude were collected.

Table 6.1 Pharmaceutical powder used in the F- press

Material	**Batch No**
Lactose	W04726
Aspartame	E006090
Povidone 30	BU7062
Povidone 90	21-6939
Microcrystalline Cellulose	2970024*

*All materials were supplied by GSK except for microcrystalline cellulose which was supplied by SIGMA

6.3 Mechanism of the F-Press

The mechanism is a sliding crank mechanism. Figure 6.1 shows a schematic representation of the mechanism.

The angular velocity

$\omega = \dot{\varphi} = constant$ (6.1)

The crank radius is *r* and the connecting rod length PC is *l*, usually between three and four times as large as *r*. For the Manesty press the ratio was in the order of magnitude of 106. The position, velocity and acceleration of the piston, point P can be calculated as follows:

For the analysis two auxiliary quantities were introduced into the Figure 6.1: $\angle CPO = \psi$ and CD, the normal on OP. The point O was taken to be the origin and OP=x, positive to the left of O. The angle φ is measured from the line OP and $\varphi = \omega t$.

$$x_p = OP = OD + DP = r\cos\varphi + l\cos\psi \quad (6.2)$$

To eliminate the auxiliary angle φ, the length CD can be written as a side of the triangles OCD and of PCD.

$$CD = r\sin\varphi = l\sin\psi \quad (6.3)$$

Hence

$$\sin\psi = \frac{r}{l}\sin\varphi = \frac{r}{l}\sin\omega t \tag{6.4}$$

And

$$\cos\psi = \sqrt{1-\sin^2\psi} = \sqrt{1-\frac{r^2}{l^2}\sin^2\omega t} \tag{6.5}$$

Substitute this into the expression for x_p,

$$x_p = r\cos\omega t + l\sqrt{1-\frac{r^2}{l^2}\sin^2\omega t} \tag{6.6}$$

The above expression represents the position of the piston as a function of the time t. When differentiating this expression twice, both the velocity v(t) and acceleration a(t) can be found.

$$x_p \simeq r\cos\omega t + l - \frac{r^2}{2l}\sin^2\omega t \tag{6.7}$$

$$\frac{\partial x}{\partial t} = -r\omega(\sin\omega t + \frac{r}{l}\sin\omega t\cos\omega t) \tag{6.8}$$

$$v(t) = -rw(\sin\omega t + \frac{r}{2l}\sin 2\omega t) \tag{6.9}$$

The approximation in Equation 6.7 justified as the ration r/l is more than 4.

Differentiating Equation (6.9) once more to obtain the acceleration of the piston

$$a(t) = -r\omega^2(\cos\omega t + \frac{r}{l}\cos 2\omega t) \tag{6.10}$$

Equation 6.7, 6.9 and 6.10 have been used to calculate the instantaneous displacement, velocity and acceleration of the upper punch respectively.

For the F-press r =5mm and l=206mm.

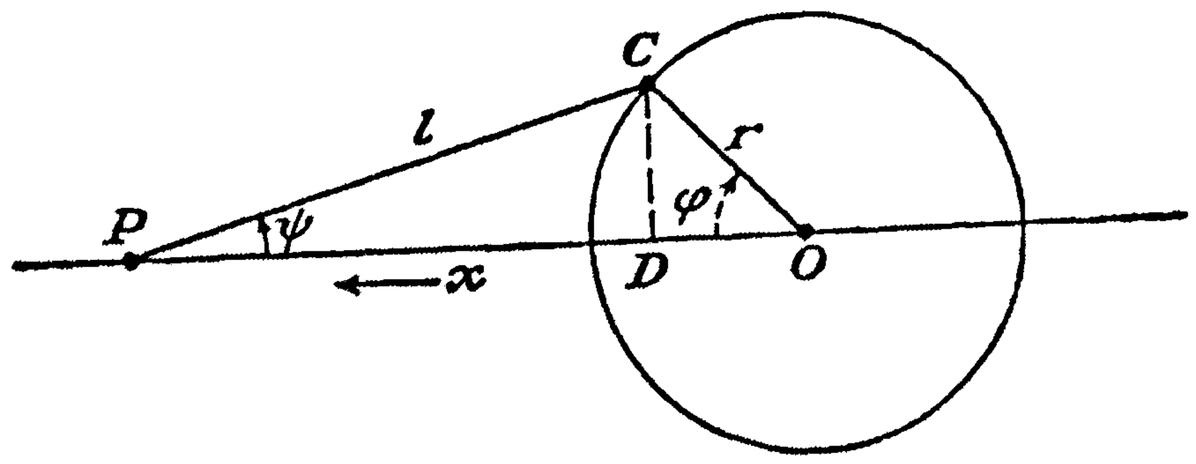

Figure 6.1 Schematic representation of mechanism which drives the F-Press.

6.4 Tabletting cycle phases in the F-press

The tabletting cycle in the F-press has four phases depending on the position of the upper punch. These phases are summarised as follows:

Phase 1: from top dead centre to the punch just before entering the die.

Phase 2: compression during which the punch is in contact with the powder.

Phase 3: punch at bottom dead centre and about to retract.

Phase 4: punch retraction.

6.5 Monitoring powder compression

Normal concave punches were used in the experimental work. The punch diameter was 10 mm, the radius of curvature at the punch tip 12.7 mm (½ inch) and the depth was 1.09 mm (0.0431 inch). Figure 6.2 a shows sketch of the punch dimensions. The maximum allowable load on the punch tips is 6.5 tons.

The weight of the tablet is determined by the depth of fill and hence by the position at which the lower regulating collars are set. Adjustment can be made to obtain any depth of fill from zero to maximum by rotating the collar.

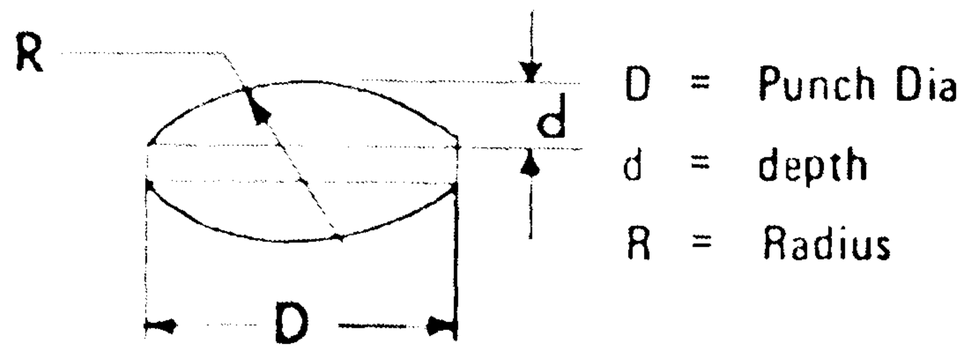

Figure 6.2 A sketch of the punch dimensions

6.5.1 Powder flowabilities

Powders flowabilities were determined by a direct method for the entire batch used in the test. A flow tube clamped to a retort stand was fitted with an orifice and closed with a rubber stopper. The powder was poured into the tube and the orifice was opened allowing the powder to flow out. Flow rate was measured by weighing the amount of powder escaping from the orifice in a specific time. The rate of flow for each powder was measured using the orifice size of 1.1 cm.

Table 6.2 shows the flowability indices for the all powders used as calculated by the following relationship:

$$Flowability\,(g/s) = \frac{Mass(g)}{Time(s)} \qquad (6.11)$$

Table 6.2 Flowabilities of powders used

Powder	Flowability (1) (g/s)	Flowability (2) (g/s)	Flowability (3) (g/s)	Mean value (g/s)
Lactose	15.4	16.3	15.8	15.83
Cellulose	14.5	13.6	14.3	14.13
Povidone 30	11.3	11.4	10.8	11.16
Povidone 90	10.2	9.6	10.7	10.16

Note:
The other powders (in particular Aspartame) do not give any flowability by using this method even when the orifice of 1.6 cm diameter was used.

6.5.2 Lactose

Lactose exhibits very good flowability characteristics. The die was filled with lactose powder after suitable adjustment from the lower regulating collar which also controls the position of the lower punch. The press was run to produce a few tablets to check both the tablet weight and crushing strength variability. Initial experiments aimed to produce tablets with a crushing strength of 5 kg. This was an indirect method of

controlling the applied load and the method maintained consistency of tablets produced.

The press was then run to produce continuously 20 tablets at a production rate of 50 tablets per minute. The acoustic emission measurement was start as soon as the press started running. Data were collected using the MISTRAS 2000 system. A wide band piezoelectric transducer was coupled to the upper punch. The output of the transducer was connected to the preamplifier which provided amplification and signal filtering. The traditional acoustic emission features were collected using the DISP software integrated in the MISTRAS 2000 system. Table 6.3 list the AE features, their descriptions and their resolution for this test.

Acoustic emission data were recorded continuously for all 20 tablets. Five tablets were then chosen for the crushing test and another 5 for the disintegration test.

The press then was run to produce 5 singular tablets for capping analysis and similarly AE data were recorded for each individual tablet produced.

Table 6.3 AE features and their resolutions

AE Feature	**Resolutions**
Ring down count	I count
Rise time	1 μs
Peak amplitude	1 dB
Event duration	1 μs
Absolute energy	1 count
AE rms	0.15 mv
Average signal level	1 dB

Figure 6.3 shows the AE energy and count as a function of the compression time in seconds. Twenty cycles were shown during which 20 tablets were produced. All tablets produced were in the good state. Five tablets were selected at random for the disintegration time test, results shown in Table 6.4 and another five for the weight examination, Table 6.5. Five tablets from the remaining ten tablets were subjected to the crushing strength test for their hardness, Table 6.6. Figure 6.3 clearly demonstrates three types of AE events that occur in every compression cycle as they were identified in the AE count profile. Data were processed against the cycle time. It was found that at three major groups of AE events are repeated at every compression cycle. These AE events correspond to different mechanisms that generate AE during the compression cycle.

Careful examination of these events was conducted. It is interesting to note that the events that scored the highest AE energies as seen in Figure 6.3 are emanated from the contact between the punch and the powder during the compression cycle. These particular events are related to the mechanism of compaction and they provide a valuable information about the state of the tablets i.e. whether good ones or bad. However the objective of this test is to relate these events to the physical properties of the tablets such as their hardness, disintegration and weight. Figure 6.3 shows quantitatively similar levels of the AE energy peak and AE count of all tablets produced. Both hardness and disintegration evaluation of these tablets reveals similarity of these characteristics for all tablets produced. This direct relationship between AE energy and disintegration and hardness confirms our previous finding about this relationship. Hence one can monitor the process in-situ by examining the peak energy that is generated from the compression of powder. First three points in of Figure 6.3 (bottom) can be ignored for the fact that these events are to do with other electronic setting which caused error in the measurement.

Figure 6.4 shows the typical AE rms for a single tablet produced using the industrial F-press. The figure shows AE events from one compression cycle of approximately 1.2 sec. This time was calculated based on the fact that the press was running at 50 revolution per minute i.e. 60/50=1.2s. At the start of the compression, the upper punch is at zero displacement, AE events due to mechanical and background noise showed a low value of rms. As soon as the punch was in contact with the powder, the

level of AErms rose to a higher value. The contact time was approximately 0.09628 s. This time is also referred to as the dwell time when describing a compression cycle. Once the tablet was formed, the punch returned to its original position and the level of AE rms also returned to its lower value. It was evident during the experiment that there are various mechanisms, which gave rise to acoustic emission. It is worth mentioning here that the initial AErms magnitudes before and after compression are different. This suggests that the two events are coming from two different mechanisms in the process cycle. This in fact supports the result obtained from the test rig, Section 5.3, which showed different levels of AE signals. Also the AE produced from the compression came from different mechanism.

Figure 6.5 shows the profile of peak amplitude during the compression cycle, a distinguished peak can be noticed at the instant of maximum punch displacement.

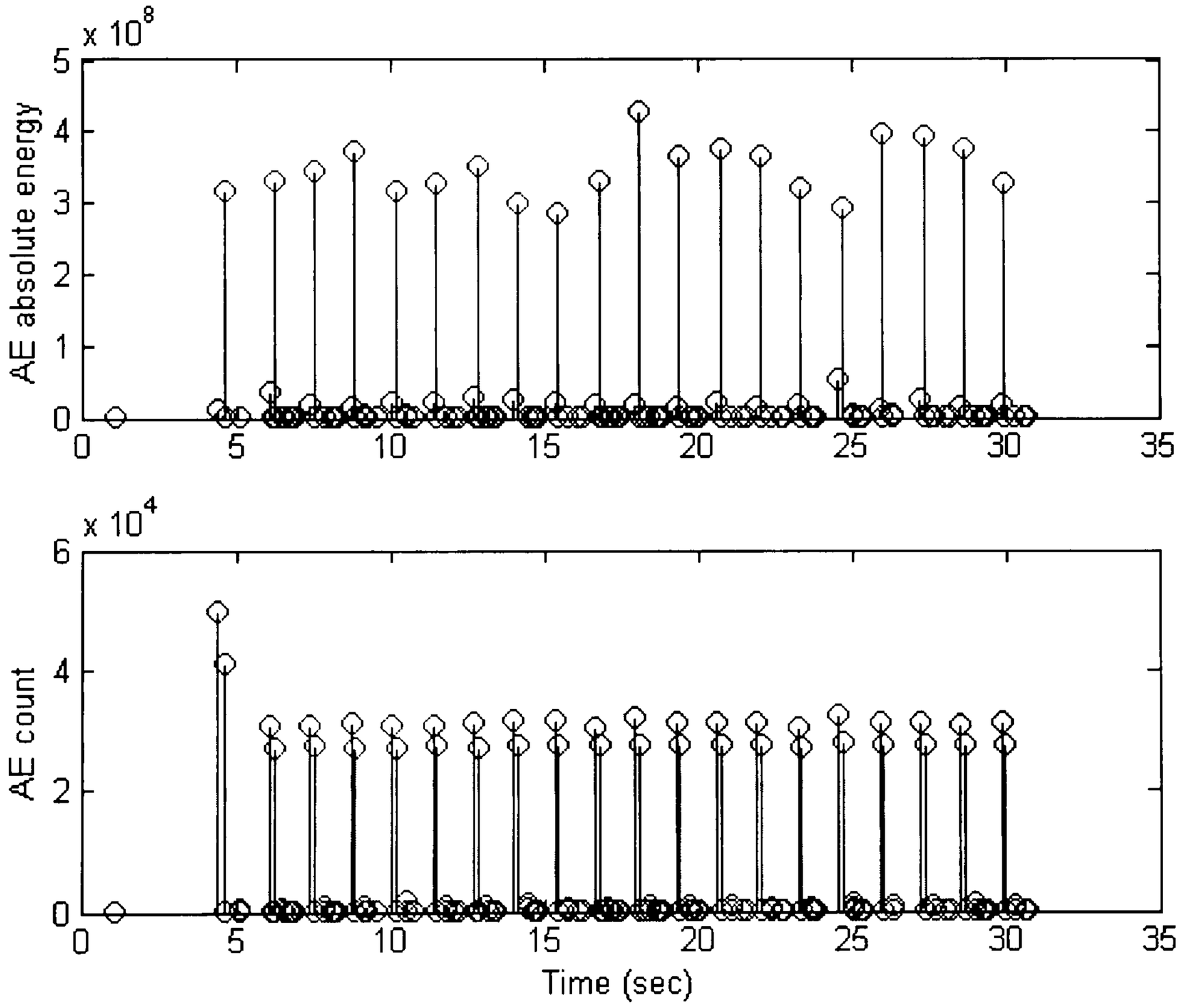

Figure 6.3 Stem plot of AE energy and count from lactose compression.

Table 6.4 Disintegration time for the selected tablet.

	Disintegration Time/ min				
	Tablet 1	Tablet 2	Tablet 3	Tablet 4	Tablet 5
Aspartame	19.32	26.12	18.29	7.25	15.27
Povidone 90	35.09	39.17	40.36	38.42	41.4
Povidone 30	13.55	13.38	14.17	13.34	14.03
Lactose (5Kg)	4.16	4.34	4.27	4.59	4.08
Lactose (10Kg)	2.21	2.26	2.17	2.27	2.12
Cellulose (5Kg)	~150.0				
Cellulose (10Kg)	>180				

Note: Due to fault in the equipment, no data for cellulose is presented in the above table.

Table 6.5 Tablet weight data for all materials

Material	Tablet weight (mg)							
	Tablet 1	Tablet 2	Tablet 3	Tablet 4	Tablet 5	Mean	SD	%RSD*
Aspartame	154.7	231.8	208.3	176.8	212.9	196.9	30.8	15.7
Povidone 90	176.6	174.4	177.2	177.5	172.5	175.6	2.1	1.2
Povidone 30	114.7	114.6	115.6	113.3	115.3	114.7	0.89	0.78
Lactose (5Kg)	222.8	242.1	201.1	207.8	188.4	212.4	20.7	10
Lactose (10Kg)	207.5	196.4	206.4	183.6	189.3	196.6	10.5	5.3
Cellulose (5Kg)	155	154.9	144.4	156.6	156.5	153.5	5.1	3.3
Cellulose (10Kg)	156.7	156.6	156.1	156.7	156.4	156.5	0.25	0.16

$$^{*}RSD = \frac{SD}{Mean} \times 100$$

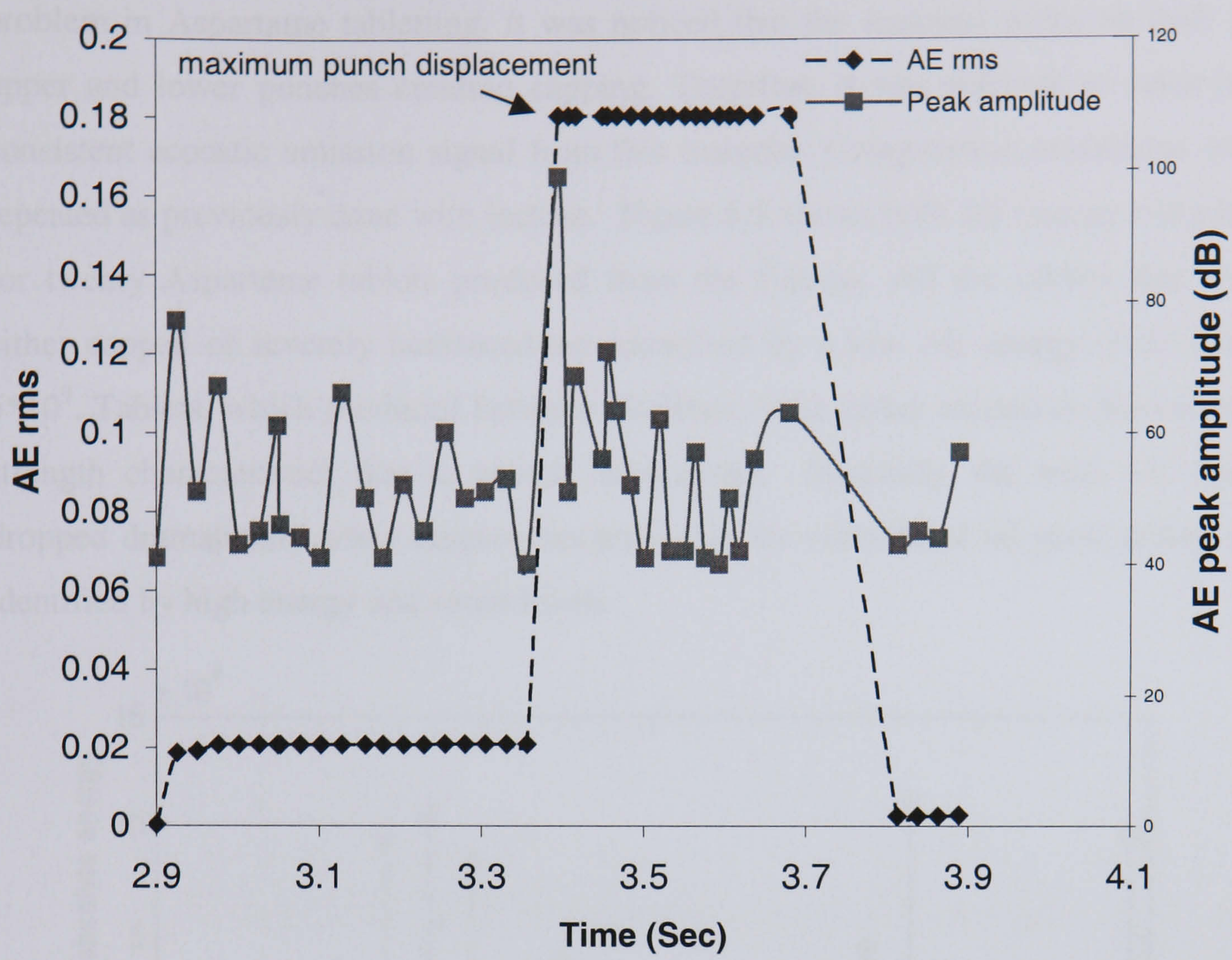

Figure 6.4 AE RMS and peak amplitude recorded for compression lactose tablet.

Table 6.6 Crushing strength data for material used in the F-press

Material	**Crushing strength (kg)**							
	Tablet 1	Tablet 2	Tablet 3	Tablet 4	Tablet 5	Mean	SD	%RSD
Aspartame								
Povidone 90	6.8	6.72	7.9	6.9	6.8	7.03	0.4906	6.97866
Povidone 30	6.89	6.83	6.83	6.23	6.92	6.79	0.333	4.90427
Lactose (5kg)	4.95	5.12	5.12	5.39	5.56	5.27	0.2413	4.57875
Lactose (10 kg)	10	9.35	9.35	9.3	9.6	9.65	0.339	3.51295
Ceullulose (5 kg)	5.51	4.94	4.94	5.25	5.56	5.22	0.3224	6.17625
Ceullulose (10 kg)	10.19	10.28	10.28	10.15	10.48	10.17	0.2632	2.588

6.5.3 Aspartame

Aspartame is widely used as a sweetening agent in a number of pharmaceutical tablets. However this material has low flowability. This was evident particularly during the continuous press run to produce large quantities of Aspartame tablets. Because of this major problem as well as its high brittleness, capping was a common

problem in Aspartame tabletting. It was noticed that the material sticks on both the upper and lower punches creating capping. Therefore it was difficult to achieve a consistent acoustic emission signal from this material. Compression conditions were repeated as previously done with lactose. Figure 6.5 shows both AE energy and count for twenty Aspartame tablets produced from the F-press. All the tablets that were either capped or severely laminated are identified by a low AE energy level below $5*10^9$. Tablets, which produced between 10-20sec, were either capped or showed low strength characteristics due to severe laminations. Similarly, the total AE count dropped dramatically when capping occurred. On the other hand all good tablets are identified by high energy and count levels.

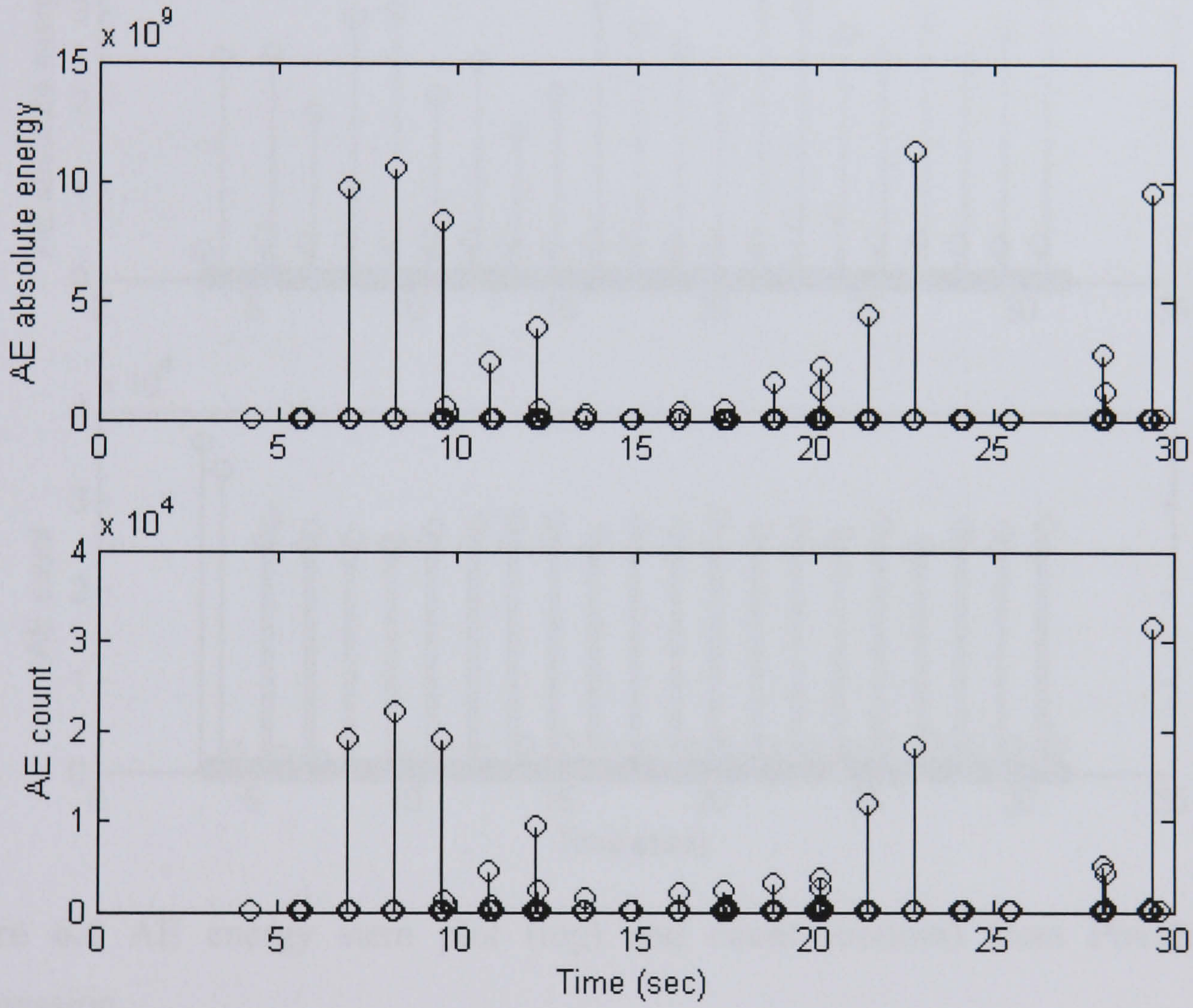

Figure 6.5 Stem plot of AE energy and count from Aspartame compression.

6.5.4 Povidone 30

Povidone class 30 powders produced relatively good tablets in general. No capping was identified in the press run. However tablets number 2,5,6,7,8 and 12 when examined for their crushing strength were slightly less hard than the other tablets produced. However, a value of less than 5% of relative standard deviation (RSD) was

achieved, which is an acceptable level. Note that the first point was ignored as the twenty tablets count started from the second point in Figure 6.6. Figure 6.6 shows both the AE absolute energy and count during Povidone 30 tabletting. It can be noticed that the AE energy (top diagram of Figure 6.6) is more a sensitive parameter in comparison with the total AE count (bottom diagram of Figure 6.6) as the AE energy can be related to the tablet's final hardness measured by the crushing strength, Table 6.7 and this relationship shown in the right-hand diagram of Figure 6.11.

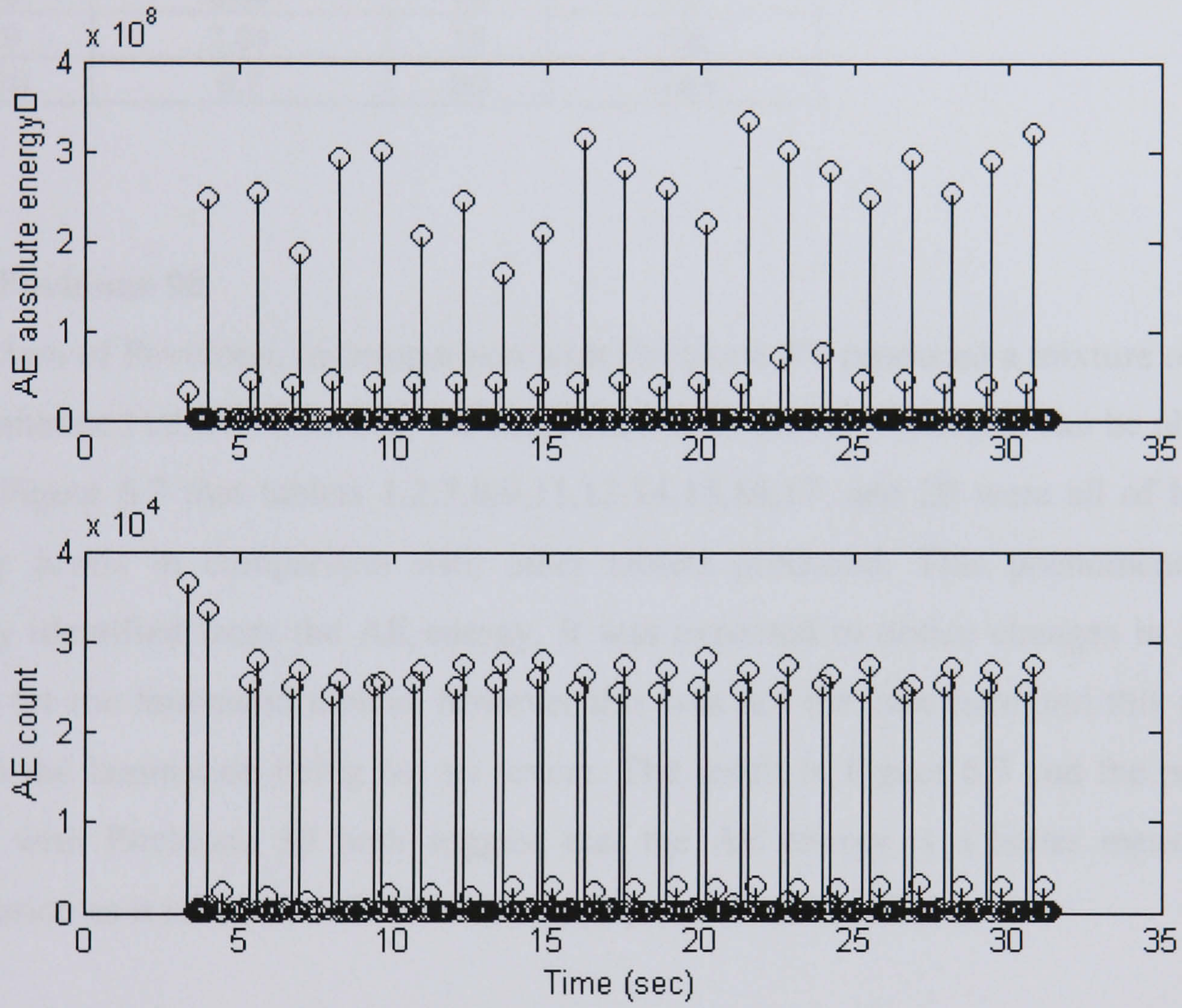

Figure 6.6 AE energy stem plot (top) and count (bottom) from Povidone 30 compression.

Table 6.7 Crushing strength data for twenty tablets produced from Povidone 30 compression.

Tablet No	Crushing strength (kg)	Tablet No	Crushing strength (kg)
1	6.75	11	6.75
2	6.2	12	6.41
3	6.92	13	7.15
4	6.95	14	6.85
5	6.32	15	6.75
6	6.35	16	6.7
7	6.3	17	6.75
8	6.33	18	6.7
9	7.01	19	6.8
10	6.7	20	6.85

6.5.5 Povidone 90

This class of Povidone, in comparison with Povidone 30, produced a mixture of good and laminated tablets. However the lamination was not very strong. It can be observed from Figure 6.7 that tablets 1,2,7,8,9,11,13,14,15,16,17, and 20 were all of low AE energy levels in comparison with other tablets produced. This phenomenon was clearly identified from the AE energy. It was expected to notice changes in the AE count for the laminated tablets, however this was not the case here and this may be due to the lamination being not so severe. The result in Figure 6.7 and the previous result with Povidone 30 both suggest that the AE energy is a better measure for lamination as it is sensitive to the tablet's physical characteristics.

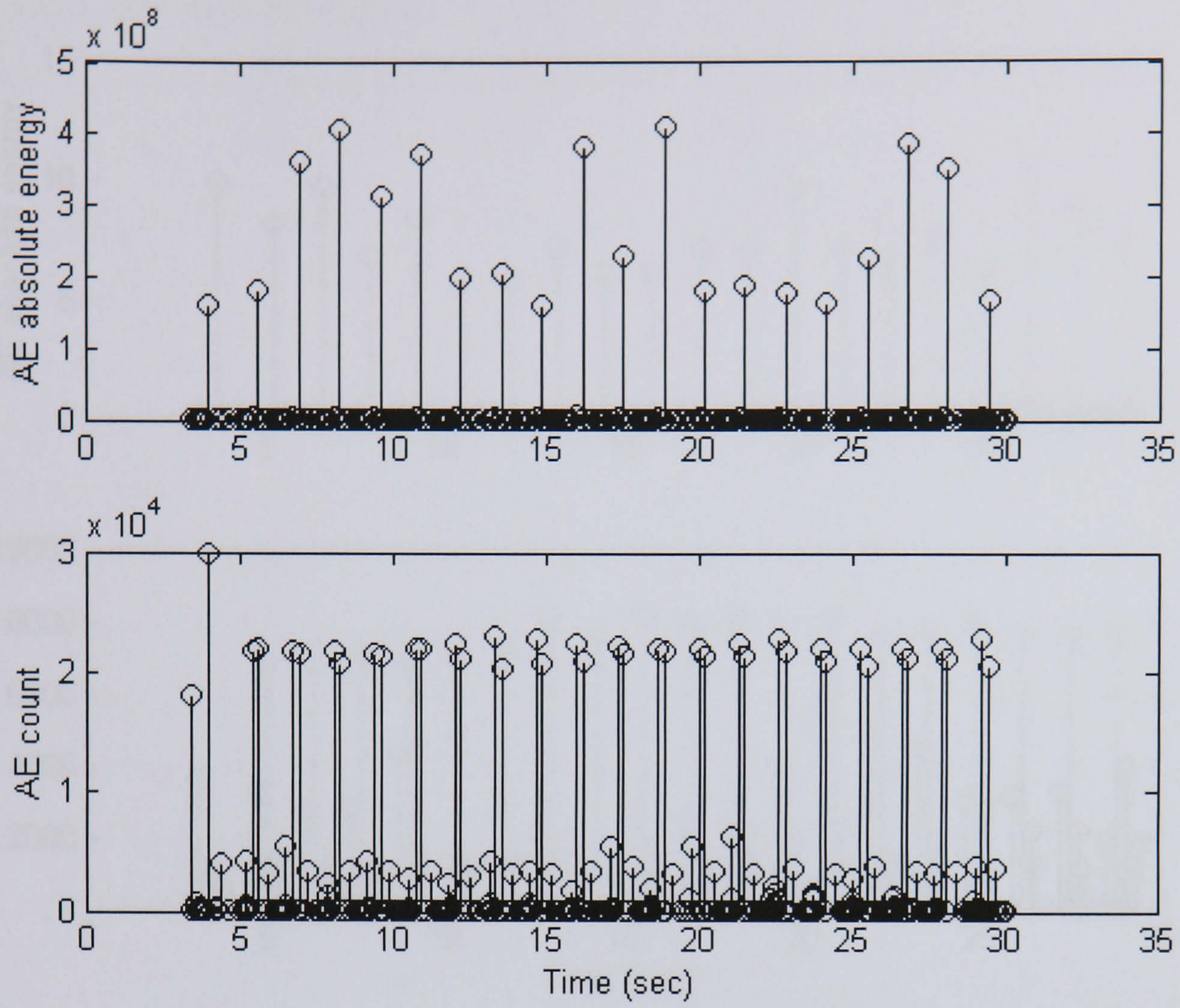

Figure 6.7 AE energy stem plot (top) and count (bottom) from Povidone 90 compression.

6.5.6 Microcrystalline cellulose

Microcrystalline cellulose in general produced very good tablets. No capped or laminated tablets were noticed. This is confirmed by the level of AE energy produced and the AE count. The subsequent crushing strength test further reveals that all sampled tablets are in a very good state and an RSD of 1.5% was achieved.

Figure 6.8 shows the AE energy and count for microcrystalline cellulose produced from twenty compression cycles.

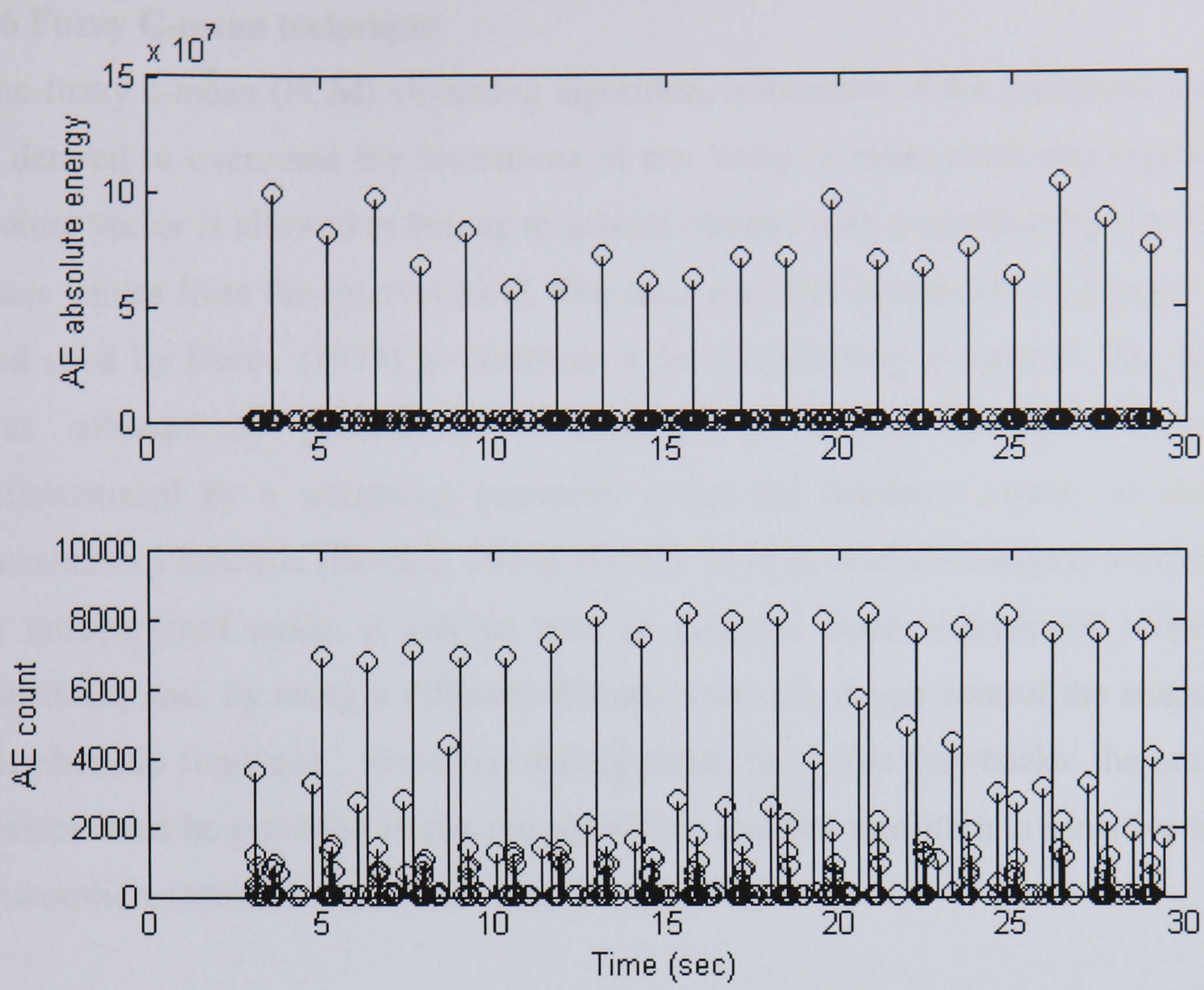

Figure 6.8 AE energy stem plot (top) and count (bottom) from microcrystalline cellulose compression.

6.6 Fuzzy C-mean technique

The fuzzy c-mean (FCM) clustering algorithm, a member of the partitional category, is derived to overcome the limitations of the 'crisp' c-mean clustering algorithm. A feature vector is allowed to belong to several clusters with a membership function that takes values from the interval [0,1]. The idea was first introduced by Ruspini (1969) and used by Dunn, (1974) to construct a fuzzy clustering algorithm. The approach was subsequently generalised to embrace an infinite family of algorithms differentiated by a weighting exponent, called the fuzziness index, on the fuzzy membership function (Bezdek, 1981). (FCM) have several advantages: it can be used in unsupervised mode; it can be used to generate multi-dimensional membership functions; and, by using a different distance measure, it can control the shape of the membership functions. However, the algorithm has some drawbacks: the number of classes must be provided to run the algorithm; and the algorithm is sensitive to noise and outliers (Mesadani, 1998).

AE signals from twenty compression cycles were recorded. The duration of each recording is twenty-five seconds. From each recording seven AE parameters, namely, rise time, ring down count, event duration, peak amplitude, average signal level, AE RMS and energy were recorded. The data were processed as follows:

(1) Data, which correspond to events that occurred once or twice in the compression cycle, are removed; these are due to the variation in the powder particle sizes and other mechanical sources. This is done by plotting all the event from the twenty cycles against the cycle time 1.2 sec. Some events repeated itself for every cycle and they appeared to cluster at a particular time. Those that only appeared once or twice within the time span are removed.

(2) The first ten AE events which come from the first compression cycle are discarded as they are likely to be outliers.

(3) Each set of features was normalised to a zero mean and unit standard deviation.

(4) AE features clustering using the fuzzy C-mean algorithm was performed.

Fuzzy c-mean clustering algorithm

Let X = $\{x_j \in \Re^p, j = 1, ...,n\}$ a finite set of n unlabelled feature vectors. Given a number of clusters c, FCM finds a fuzzy c-partition of X by minimising the following objective function

$$J_m(X,U,V) = \sum_{i=1}^{c}\sum_{j=1}^{n} u_{ij}^m d^2(x_j, v_i) \qquad (1)$$

subject to the constraints

$$0 \le \sum_{j=1}^{n} u_{ij} \le n \quad \forall i \qquad (2)$$

$$0 \le u_{ij} \le 1 \qquad \forall i,k \qquad (3)$$

$$\sum_{i=1}^{c} u_{ij} = 1 \qquad \forall j \qquad (4)$$

$m \in [1,\infty)$ *is* the fuzziness index, $n = |X|$ is the cardinality of X, i.e. is the number of feature vectors , and $d(x_j,v_i)$ is a similarity measure between the feature vector x_j and the prototype i . U is $c \times n$ matrix of memberships (U_{ij} is the degree of membership of x_j to the cluster i), $V = \{v_1,...,v_c\}$ is a set of prototype parameters (centroids).

The fuzziness index, also called the fuzziness exponent weight in the fuzzy logic literature, is an important parameter in the FCM algorithm. As a theoretical basis for an optimal selection for the value of m is lacking, the selection is usually, performed according to the specificities of problem under consideration. When $m \to 1$, the fuzzy partition tends toward the crisp partition, i.e. u_{ij} equals 0 or 1. Conversely, when $m \to \infty$ all the clusters tend to the centroids, i.e., $u_{ij} \to 1/c$. That is, the higher m, is the fuzzier the partition, and, conversely, the smaller m, the crispier the partition is. The most common choice of the fuzziness index is $m = 2$ and this value is used in this paper.

The similarity measure d is any measure induced by an inner product on $\mathbb{R}^p$. A variety of fuzzy clustering methods, based upon different distance measures, have been proposed and (Dubes (1993). In our context, a weighted Euclidean distance is used.

$$d^2(x_j, v_i) = (x_j - v_i)^T A(x_j - v_i) \qquad (5)$$

A is a $p \times p$ positive definite weight matrix.

The FCM algorithm, described below, is guaranteed converge to a local minimum (Bezdeck, 1980). Its performance, however, depends on a number of *a priori* user-selected parameters: the number of clusters, the initial values of the proximity matrix, the error threshold for the stopping criterion and the number of iterations (Bezdeck, 1980). A different initial guess of the parameters may lead to different local minimum.

Fuzzy c-mean algorithm

The fuzzy c-mean (FCM) clustering algorithm (Bezdek) is the fuzzy equivalent of the nearest mean 'hard' clustering algorithm (Duda and Hart), which minimises the following objective function with respect to fuzzy membership μ_{ij} and cluster centroid V_i.

$$J_m = \sum_{i=1}^{c} \sum_{j=1}^{n} (\mu_{ij})^m d^2(X_j, V_i) \qquad (6.12)$$

where

$$d^2(X_j, V_i) = (X_j - V_i)^T A(X_j - V_i) \qquad (6.13)$$

A is a $p \times p$ positive definite matrix, p is the dimension of the vectors X_j (j=1, 2,…,n), c is the number of clusters, n is the number of vectors (or data points), and m >1 is the fuzziness index (Bezdek). The FCM algorithm is executed in the following steps:

1. Initialise the membership μ_{ij} of X_j belonging to cluster i such that

$$\sum_{i=1}^{c} \mu_{ij} = 1 \qquad (6.14)$$

2. Compute the fuzzy centroid V_i for $i = 1, 2, \ldots, c$ using

$$V_i = \frac{\sum_{j=1}^{n} (\mu_{ij})^m X_j}{\sum_{j=1}^{n} (\mu_{ij})^m} \qquad (6.15)$$

3.Update the fuzzy membership μ_{ij} using

$$\mu_{ij} = \frac{\left(\frac{1}{d^2(X_j, V_i)}\right)^{\frac{1}{m-1}}}{\sum_{i=1}^{c} \left(\frac{1}{d^2(X_j, V_i)}\right)^{\frac{1}{m-1}}} \qquad (6.16)$$

4. Repeat steps (2) and (3) until the value of J_m is no longer decreasing.

The FCM algorithm always converges to strict local minima of J_m (Bezdek, 1981) starting from the initial guess of μ_{ij}, but different choices of initial μ_{ij} might lead to different local minima

6.6.1 Signal pre-processing

Signal pre-processing is an important step in clustering. Properly processed data makes the clustering task easier and more efficient; while improperly pre-processed data may render the clustering task very difficult. A major problem with pre-processing is the apparent lack of universal methodology applicable to every situation. Knowledge of the field of application, engineering judgement and empirical experimentation usually provides useful guidance. However, once a particular method is adopted, it is often difficult to be certain in advance with regard its optimality.

6.6.2 Signal clustering

Extensive exploration of the collected data suggested that three groups of events are repeated within each cycle at fixed punch displacement. This suggests the existence of three clusters which correspond to different AE generation mechanisms.

All the AE events that occurred during the compression cycle are plotted against the cycle time. A preliminary investigation revealed that the three major AE events are

repeated for almost every compression cycle. These events are generated from three different mechanisms:

Mechanism 1: when the punch enters the die just prior to compression

Mechanism 2: mechanical friction inside the die during compression and

Mechanism 3: when the punch leaves the dies during post-compression. This was established by tracing back the occurrence time to the punch displacement; taking into account that the duration of each compression cycle is approximately 1.2 s.

New data sets were generated from typical conditions of powder processing. These data were pre-processed as described previously. The resulting features were then inputted into a fuzzy C-mean algorithm implemented in MATLAB Fuzzy Logic Toolbox (Mathworks). Clustering was initialised by setting the number of cluster to three.

The results that emerged from the application of the fuzzy C-mean clustering algorithm are shown in Figure 6.9. Three clusters were identified in the AE data. Cluster 1 represents the entire set of AE events when the upper punch is at its maximum displacement inside the die, i.e. the entire set comes purely from the powder compression. Cluster 2 represents the AE events due to friction during the retraction of the punch from the die. Cluster 3 corresponds to the events that originate from the contact as the punch enters the die. Clusters validation was achieved throughout correlation of the AE event with the correspondent punch displacement taking into account that the compression cycle time was constant throughout the tablet production.

Figure 6.10 shows the changes in the objective function values with the progress of clustering. It can easily be noticed that the algorithm exhibits a fast convergence. The optimal solution is reached in a few iterations. After only 4 iterations the change in the objective function becomes marginal, attesting to the efficiency of the clustering algorithm.

The obtained results show a reasonably good clustering of the AE data generated from the powder compression. Events which belong to cluster 1 which is generated by mechanism 1, i.e. those which originate from pure compression appear to be tightly

clustered around the cluster centre. AE energy, peak amplitude and average signal level seem to be good features for clustering. The level of scattering around the cluster centres are different amongst the three clusters. In particular, for clusters 2 (generated by mechanism 2) and cluster 3 (generated by mechanism 3), the scattering is much higher. This is likely to be due to the high variability in the mechanism which generates the AE events.

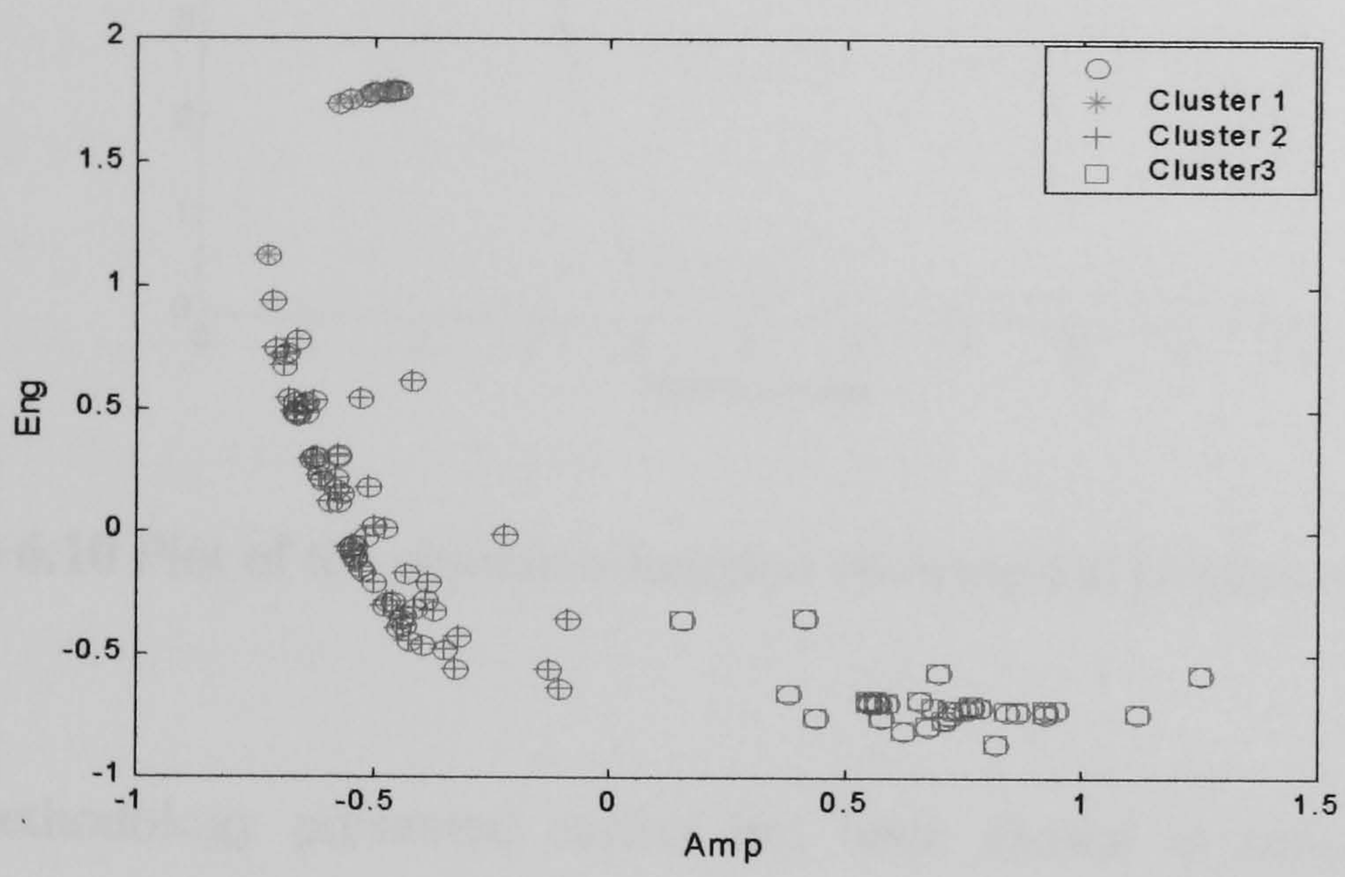

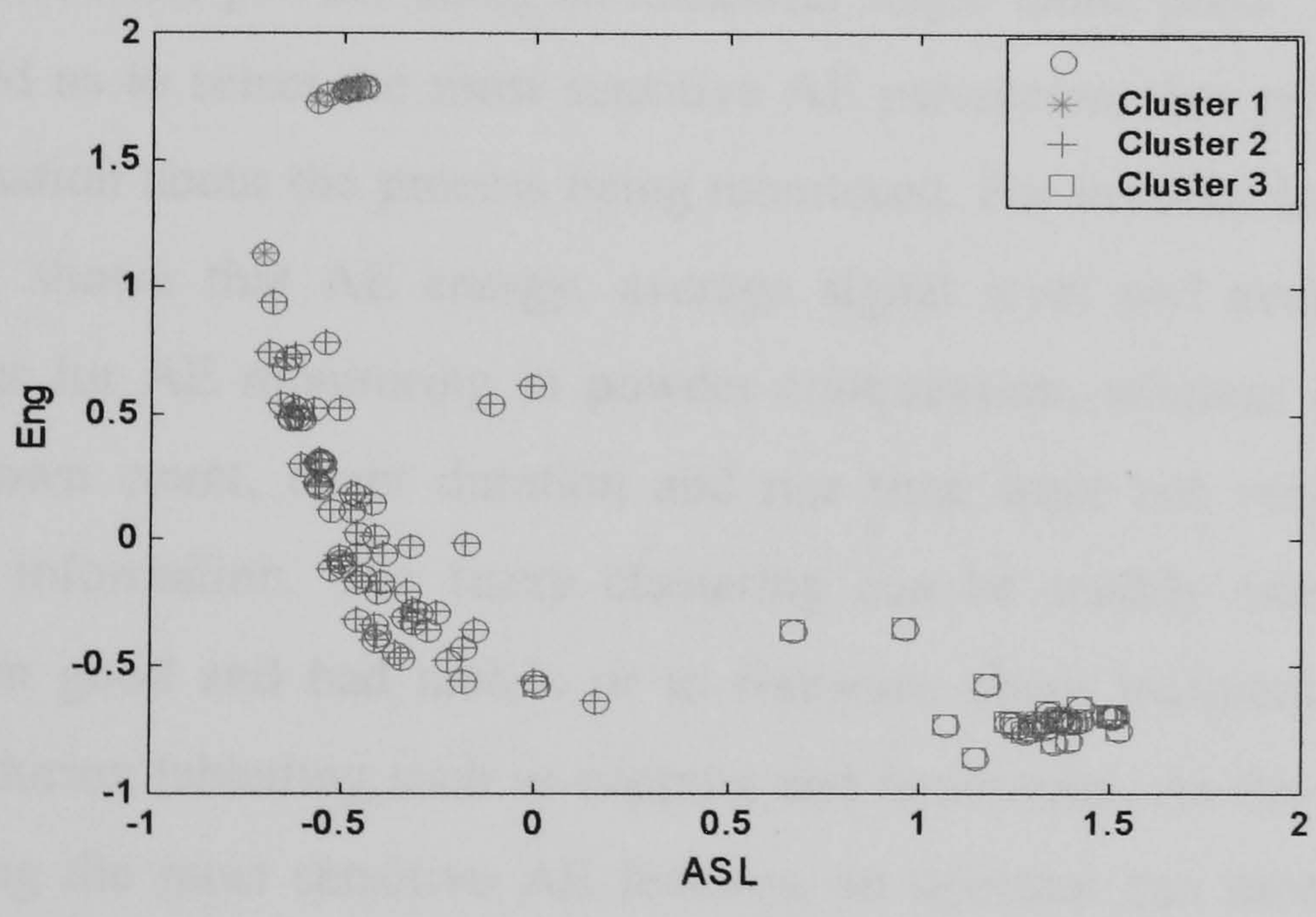

Figure 6.9 AE events clustered into 3 groups as projected onto the normalised energy-amplitude plane and the normalised energy-ASL plane.

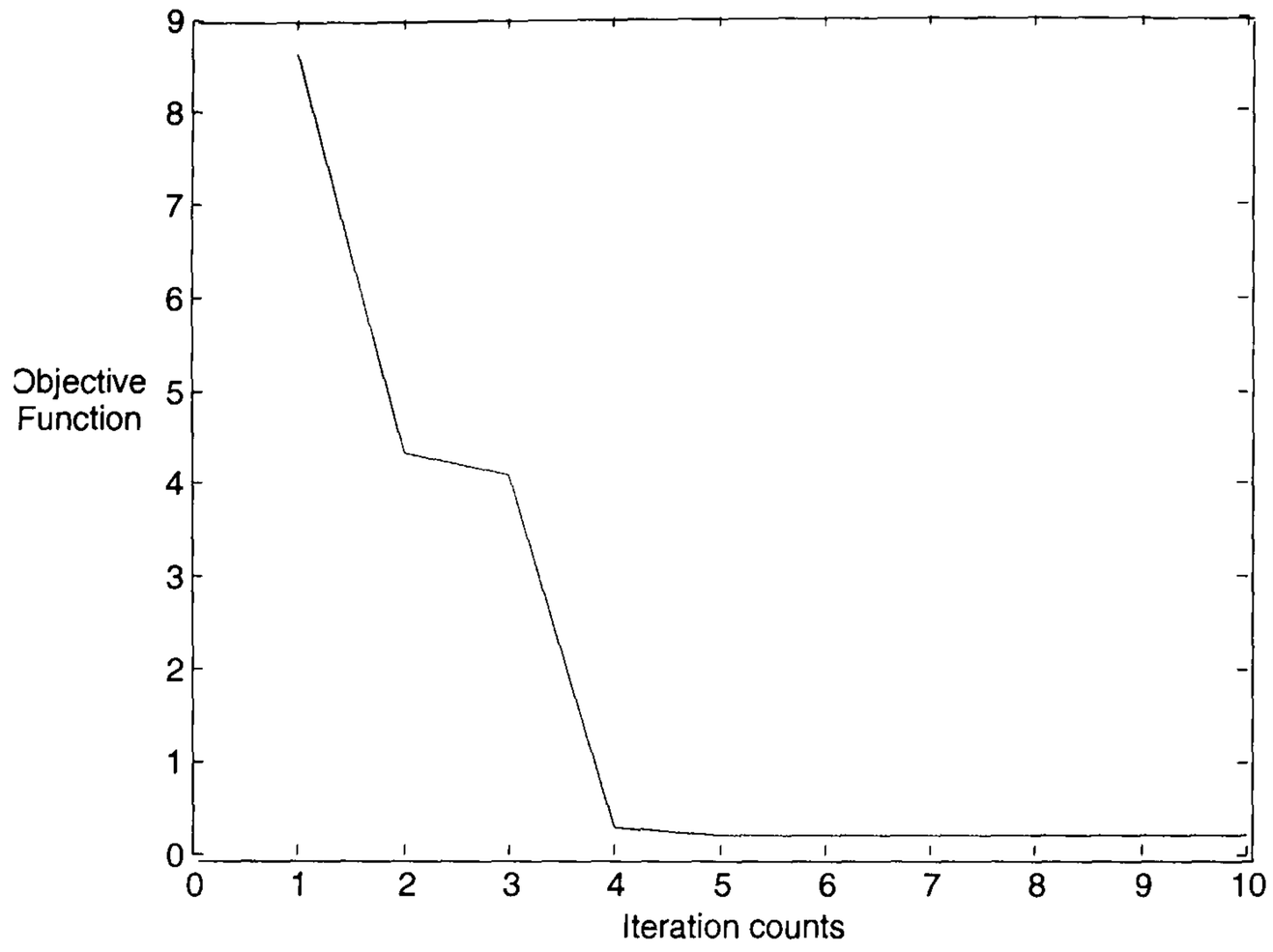

Figure 6.10 Plot of the objective function showing the progress of the clustering

The methodology presented earlier has been shown to satisfactorily discriminate various mechanisms, which generate AE events during the compression of pharmaceutical powder using an industrial single tablet press. This methodology also enabled us to select the most sensitive AE parameters that provide us with valuable information about the process being monitored. For instance in our previous analysis it was shown that AE energy, average signal level and peak amplitude are good features for AE monitoring in powder compression, whereas other features such as ring down count, event duration and rise time were not very sensitive to provide useful information. The fuzzy clustering can be readily extended to discriminate between good and bad tablets or to forewarn about incipient problems that might occur during tabletting such as capping and lamination. As the technique can help in selecting the most sensitive AE features, an operator can monitor those features to observe any changes within the tabletting. It was evident from previous findings that the AE energy, for instance is a good feature.

6.7 Relationship between AE and physical properties of tablets

This section deals with the relationship between AE energy produced from powder compression in tabletting and both disintegration time and crushing strength characteristics of the final tablet produced. As was mentioned earlier, 10 samples of the produced tablets from each material were randomly selected for both crushing strength and disintegration analysis.

Generally, it was found that the AE energy that emanated from only the powder compression during the F-press tabletting cycle, i.e. phases 2 and 3 was directly proportional to the disintegration time and crushing strength. The whole AE signal generated from the continuous compression was subjected to data pre-treatment as described earlier to separate the AE events that were generated from the compression i.e. when the punch is in contact with the powder from those due to other mechanical and noise effects during the tabletting cycle. Figures 6.11a,b shows this relationship for the povidone powder. It can be seen that a linear relationship exists between the AE energy produced from phases 2 and 3 from the compression cycle and both the disintegration time and crushing strength.

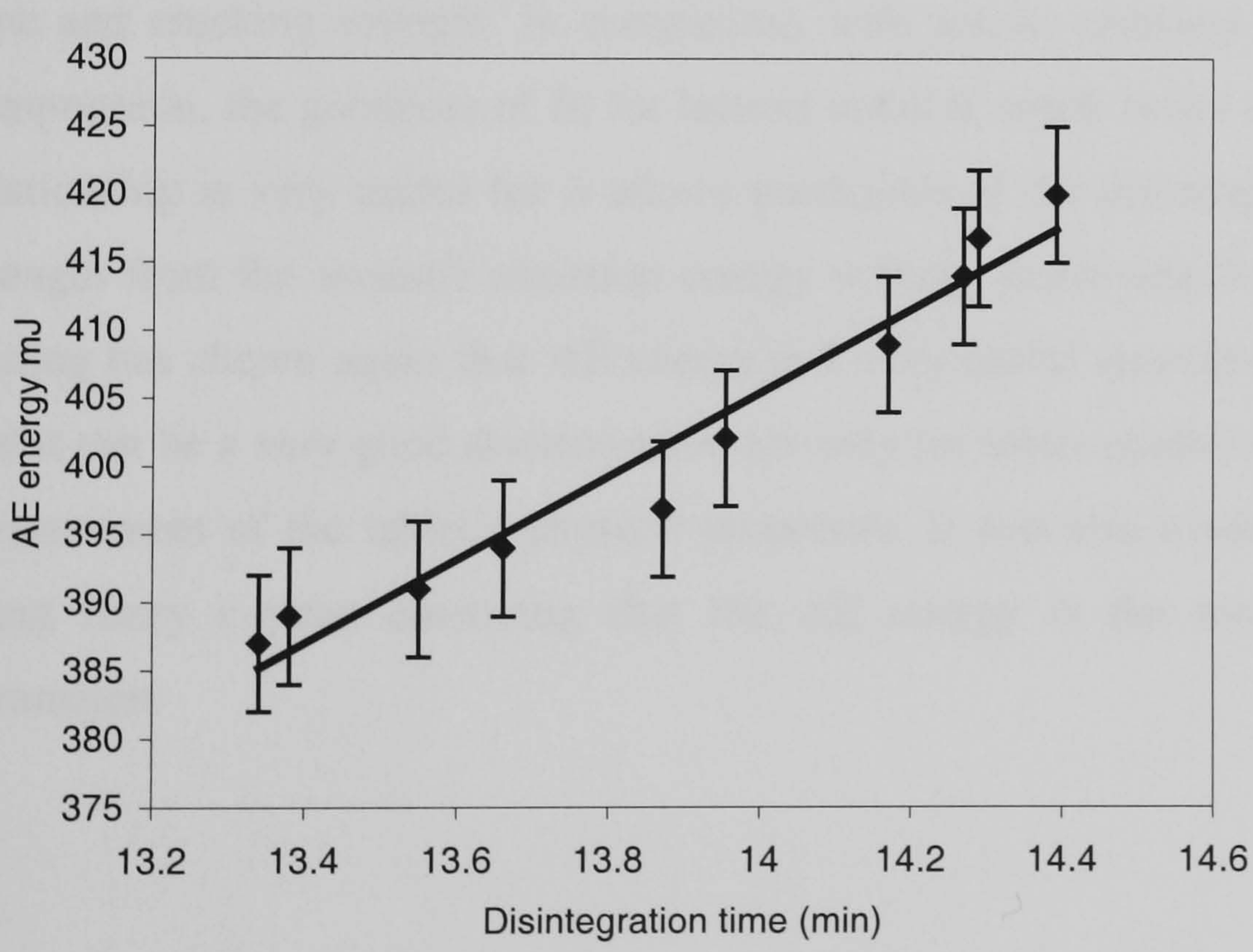

Figure 6.11a Relationship between AE energy and both disintegration time (top) and crushing strength (bottom) of Povidone tablet.

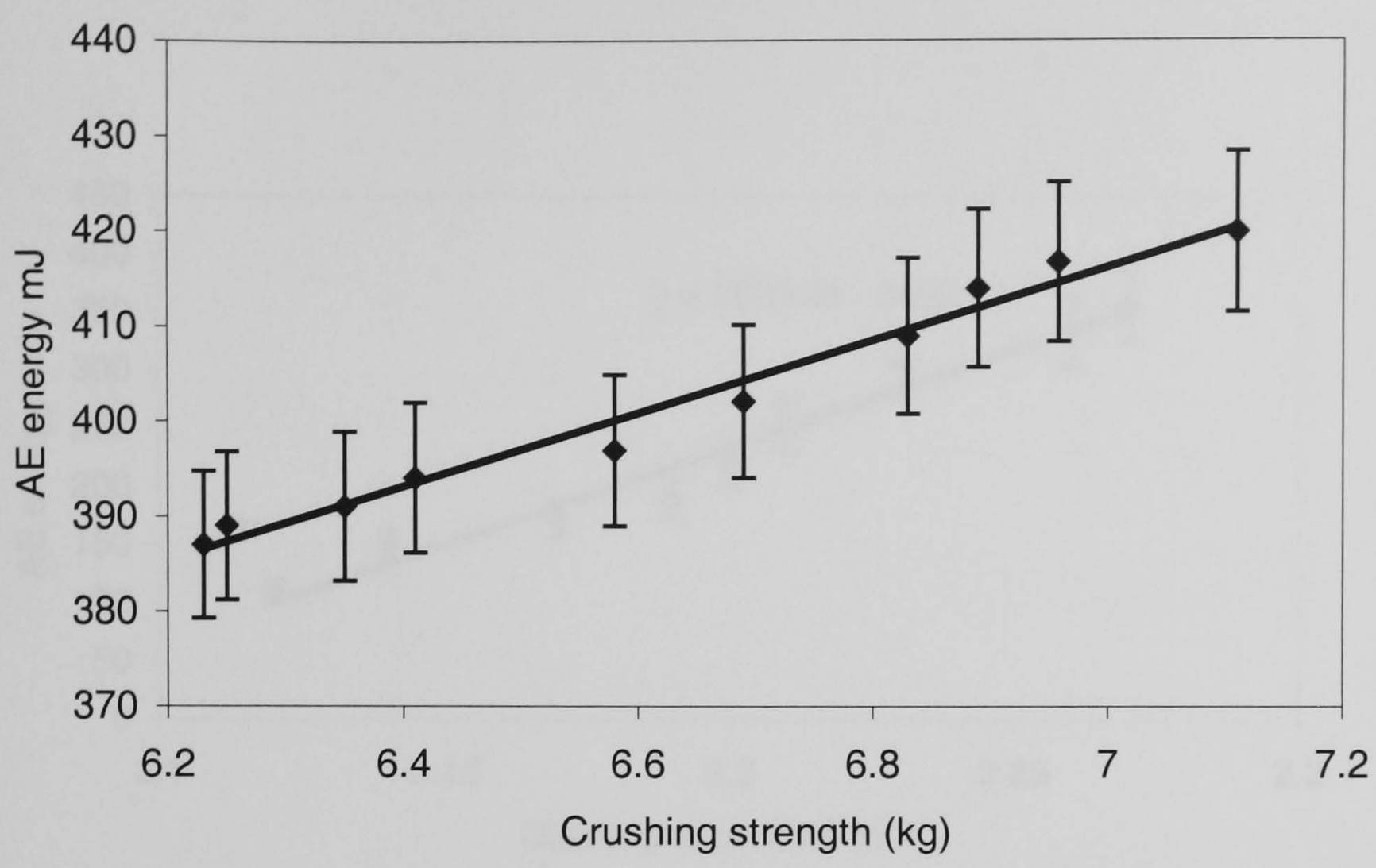

Figure 6.11b Relationship between AE energy and both disintegration time (top) and crushing strength (bottom) of Povidone tablet.

Similar results were obtained for lactose compression. This relationship was also obtained when the loading increased i.e. the compression force increased. Figure 6.12 and 6.13 illustrate the relationship between AE energy and both the disintegration time and crushing strength. In comparison with results obtained from the Povidone compression, the goodness of fit for lactose result is much better than Povidone. This relationship is very useful for it allows prediction of the disintegration and crushing strength from the acoustic emission energy without destroying the tablet. The above finding has shown again that AE energy is a very useful descriptor of the AE signal and it can be a very good discriminator not only for tablet quality but also for indirect measurement of the tablet's physical properties. It was also evident from Figure 6.9 using fuzzy c-mean clustering that the AE energy is the most informative AE parameters

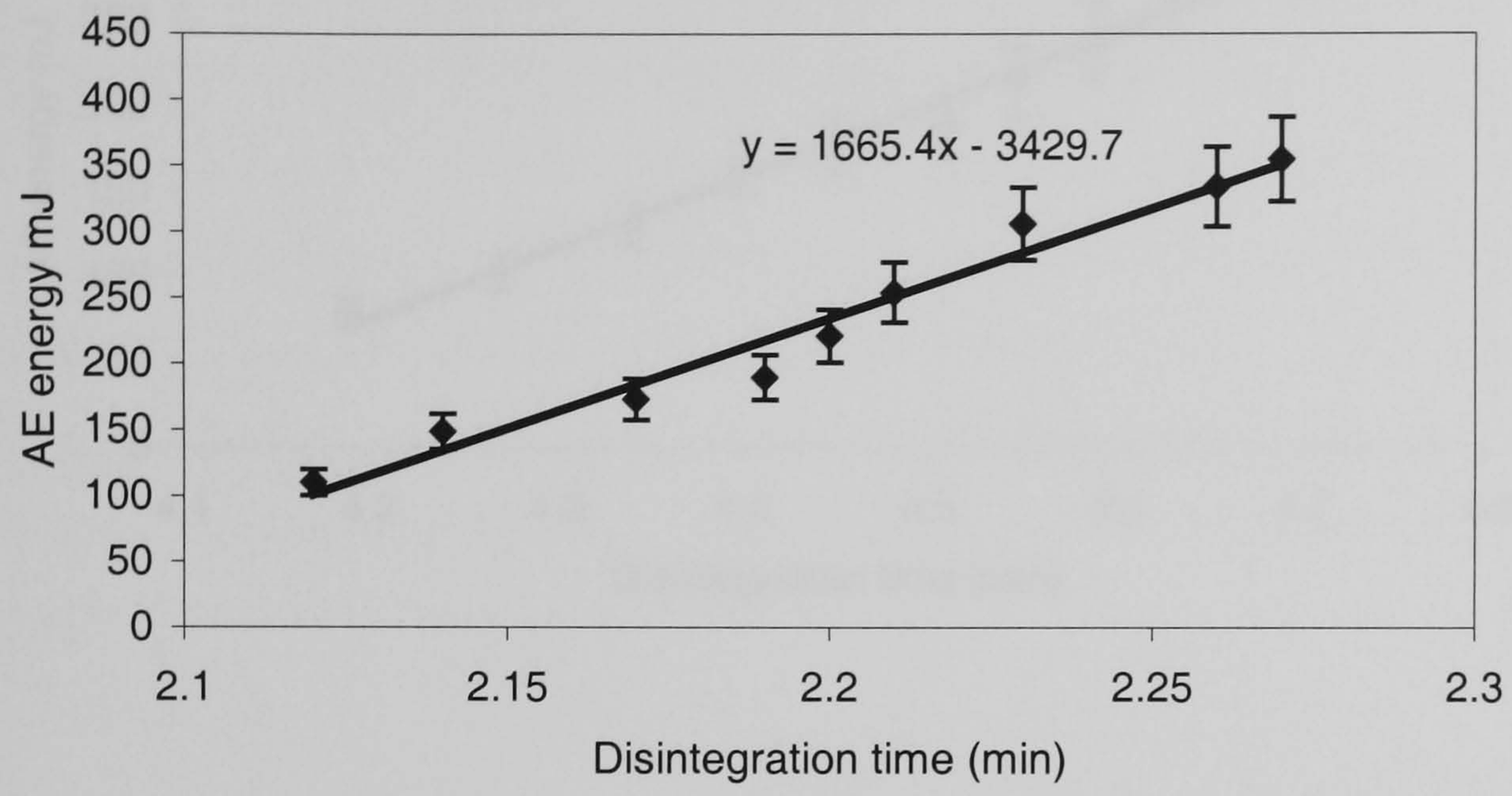

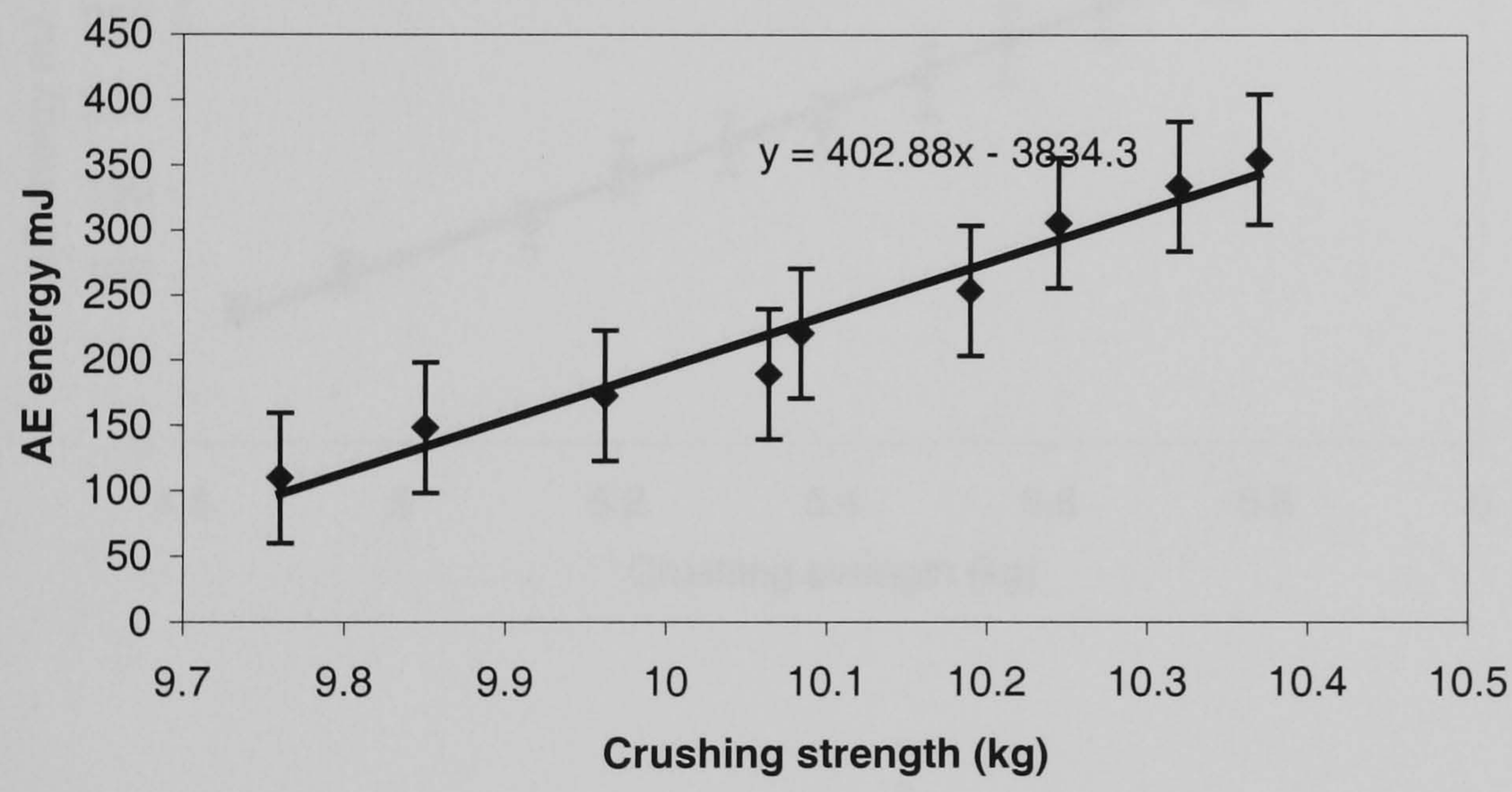

Figure 6.12 Relationship between AE energy and both disintegration time (top) and crushing strength (bottom) of Lactose_10 tablets.

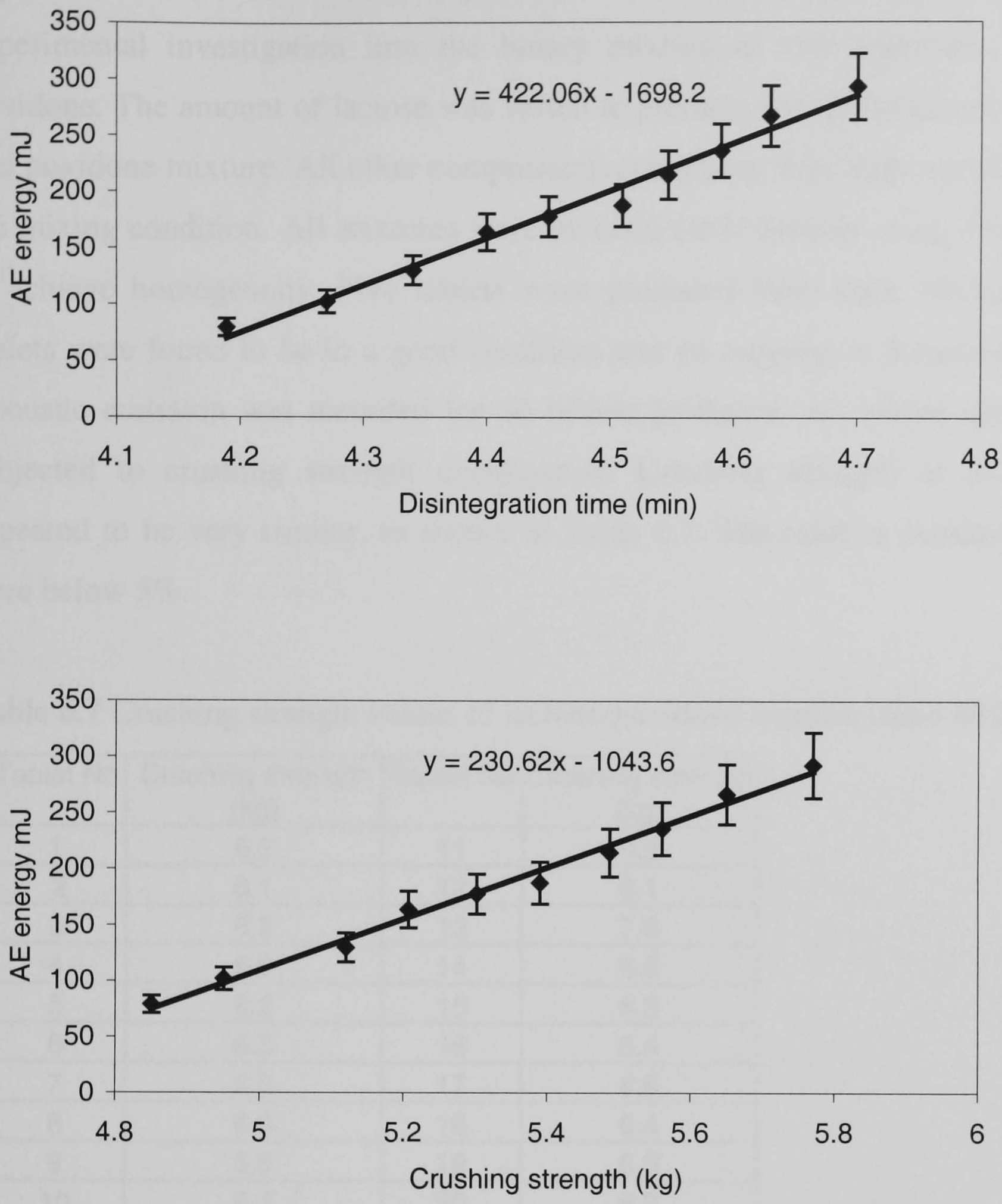

Figure 6.13 Relationship between AE energy and both disintegration time (top) and crushing strength (bottom) of Lactose_5 tablets.

6.8 Monitoring compression of binary mixtures

Previous experimental studies were carried out on a number of pharmaceutical powders on their own. These powders represented the bulk mass of a pharmaceutical tablet. However pharmaceutical tablets comprise various other ingredients including the active materials. As has been shown some of the materials used in this research

appeared to be more acoustically active than other. This section discusses an experimental investigation into the binary mixture of two materials: lactose and povidone. The amount of lactose was varied to produce five different ratios of lactose and povidone mixture. All other compression conditions were kept constant including the mixing condition. All mixtures were blended for 6 minutes using a turbula mixer to achieve homogeneity. Five tablets were produced from each mixture ratio. All tablets were found to be in a good condition and no capping or lamination occurred. Acoustic emission was recorded for all tablets produced. All tablets produced were subjected to crushing strength examination. Crushing strength of all the tablets appeared to be very similar, as shown in Table 6.7. The relative standard deviations were below 5%.

Table 6.7 Crushing strength values of lactose-povidone mixture (ratio 80:20).

Tablet No	Crushing strength (kg)	Tablet No	Crushing strength (kg)
1	6.3	11	6.5
2	6.1	12	6.1
3	6.2	13	7.5
4	6.5	14	6.5
5	6.2	15	6.3
6	6.5	16	6.4
7	6.0	17	6.6
8	6.0	18	6.4
9	6.5	19	6.3
10	6.4	20	6.2

It was found that as the amount of lactose in the mixture increased, the AE energy also increased. Particle slippage and friction with the die wall as well as the fragmentation of lactose particulates were the main mechanisms that generated AE during the compression. The more lactose particles present in the die, the more AE was generated as characterised by the AE energy and cumulative count. Figure 6.14 illustrates these relationships as the mean AE parameters were plotted against the fraction of lactose components in the binary mixture. All data were pre-processed to extract the AE events that were generated from the powder compression phase inside the die.

Figure 6.15 shows the relationship between the AE energy, crushing strength (hardness) and the fraction of lactose present.

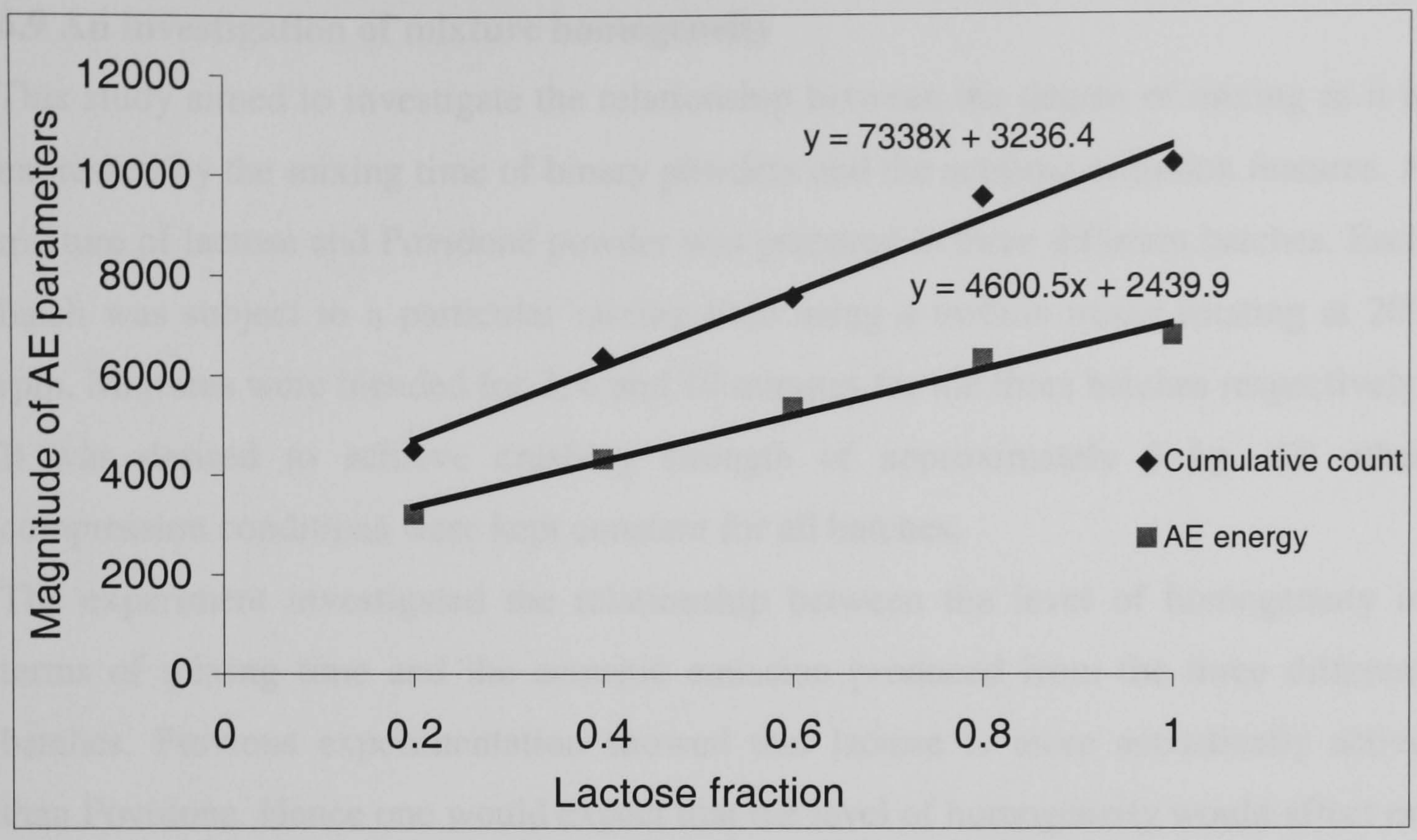

Figure 6.14 AE energy and count as a function of lactose fraction in binary mixture.

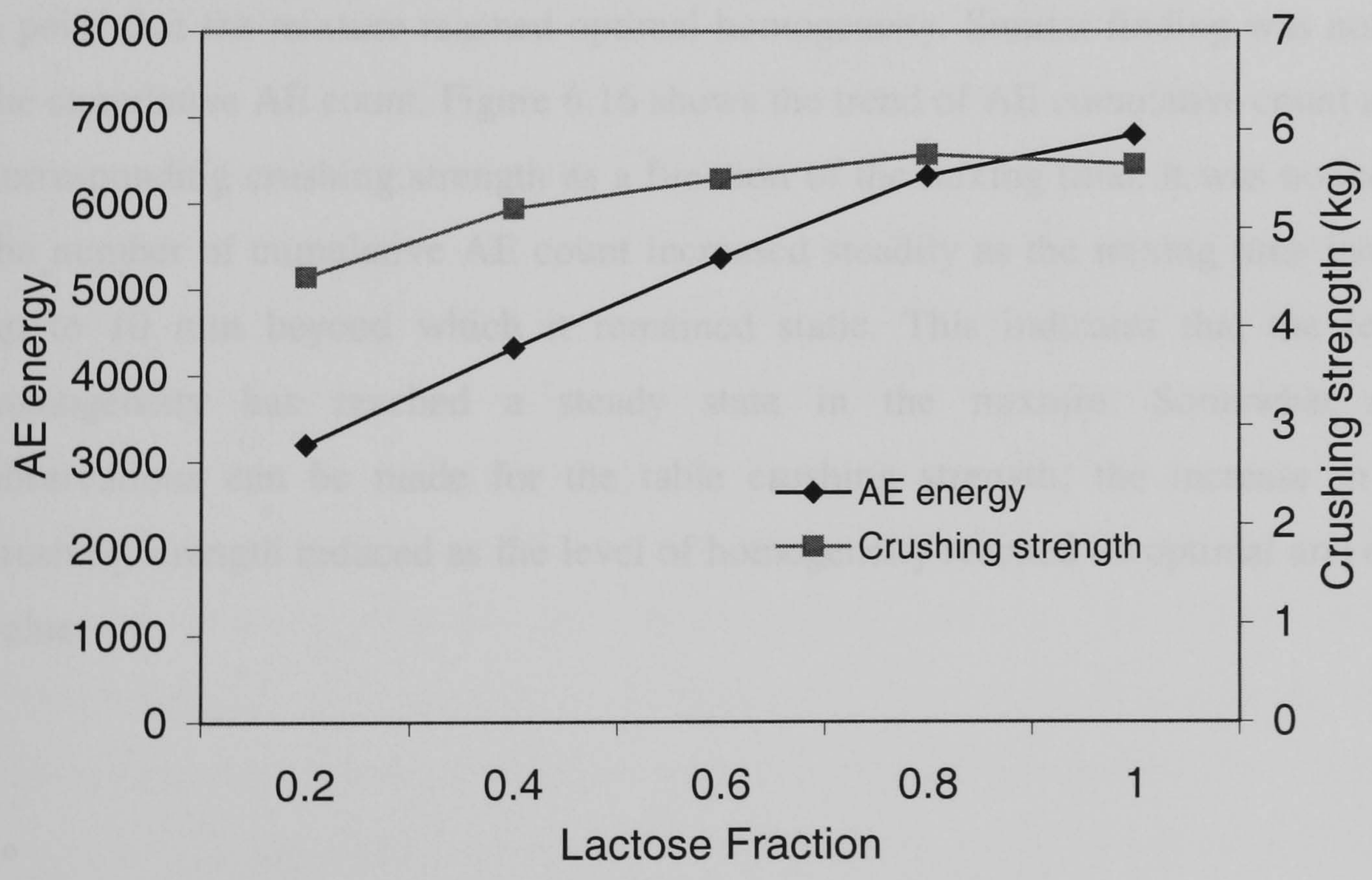

Figure 6.15 Crushing strength and AE energy as function of lactose fraction.

6.9 An investigation of mixture homogeneity

This study aimed to investigate the relationship between the degree of mixing as it is expressed by the mixing time of binary powders and the acoustic emission features. A mixture of lactose and Povidone powder was prepared in three different batches. Each batch was subject to a particular mixing time using a turbula mixer rotating at 200 rpm. Mixtures were blended for 2, 6 and 10 minutes for the three batches respectively. It was desired to achieve crushing strength of approximately 5 kg. All other compression conditions were kept constant for all batches.

The experiment investigated the relationship between the level of homogeneity in terms of mixing time and the acoustic emission produced from the three different batches. Previous experimentation showed that lactose is more acoustically active than Povidone. Hence one would expect that the level of homogeneity would affect on the AE signal produced during compression.

Acoustic emission signals were recorded in the same manner as in previous experiments. The AE signal was characterised by its traditional features. It was found that the AE energy increased as the mixing time for the binary mixture increased up to a point that the mixture reached optimal homogeneity. Similar finding was noted for the cumulative AE count. Figure 6.16 shows the trend of AE cumulative count and the corresponding crushing strength as a function of the mixing time. It was noticed that the number of cumulative AE count increased steadily as the mixing time increased up to 10 min beyond which it remained static. This indicates that the level of homogeneity has reached a steady state in the mixture. Somewhat similar observations can be made for the table crushing strength; the increase in tablet crushing strength reduced as the level of homogeneity reached its optimal and desired value.

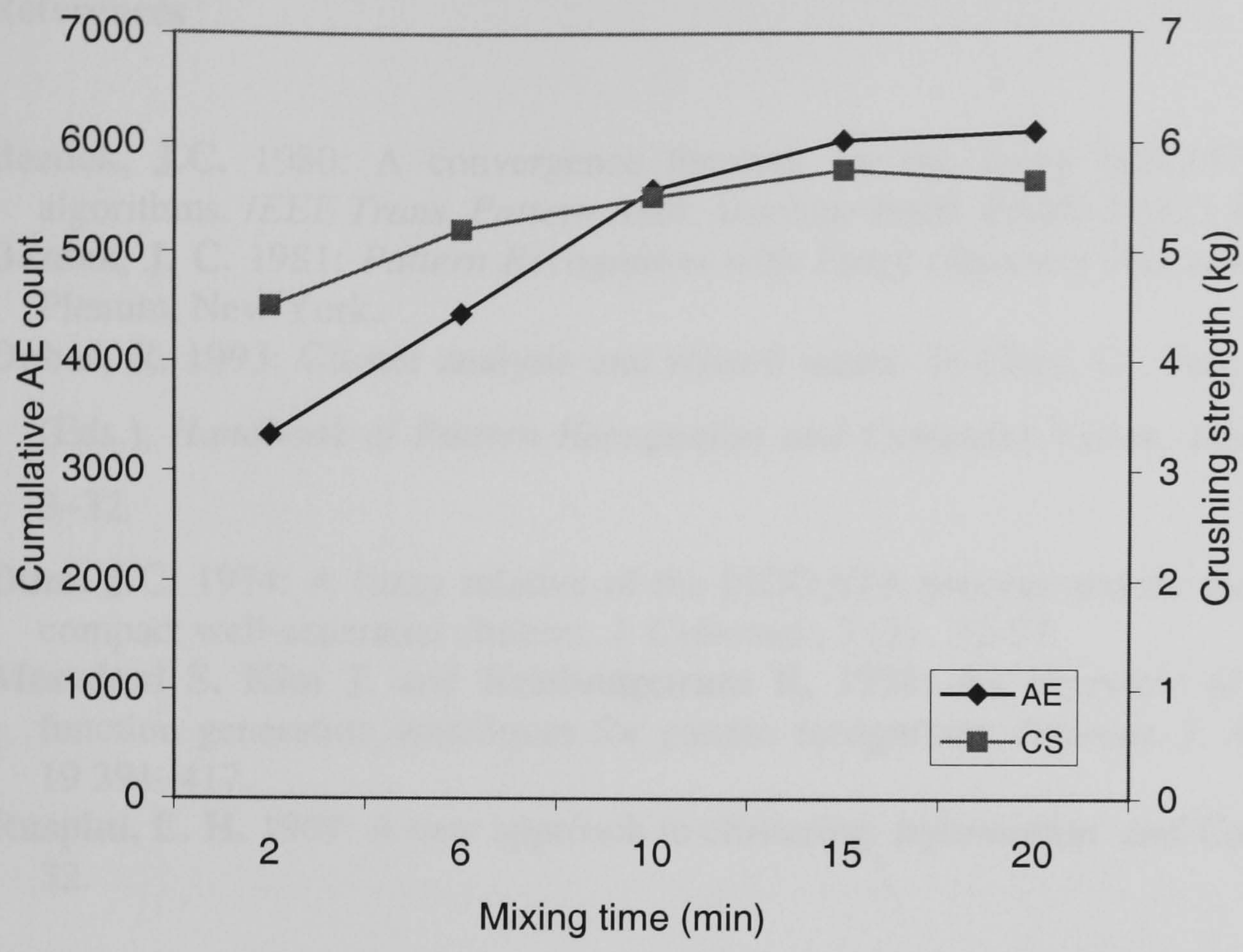

Figure 6.16 Cumulative AE count and crushing strength as a function of mixing time.

6.10 Conclusion

This chapter dealt with the experimental investigation conducted on powder compression using industrial tablet press Manesty F type. Various materials were compressed using normal concave punches. Acoustic emission from the compression was monitored continuously for twenty compression cycles to produce 20 tablets for every run. Traditional AE features were collected. Tablets produced were examined for their crushing strength (hardness) and disintegration characteristics. It was found that the AE energy generated during the compression phase is well correlated with both the crushing strength and disintegration time of the tablets produced. Furthermore, it was possible to identify the capping phenomenon by the AE monitoring technique. Capped tablets appear to be characterised by a low AE energy level whereas non-capped tablets have a higher energy level. Pharmaceutical powders exhibit different acoustic emission activities. Lactose previously classed as acoustically active was used to form binary mixtures with povidone. It was shown that as the amount of lactose increased in the binary mixture, the AE energy and cumulative AE count also increased. Finally, it was shown that the AE signal is very sensitive to the degree of homogeneity as measured by the mixing time in the binary mixture.

References

Bezdek, J.C. 1980: A convergence theorem for the fuzzy ISODATA clustering algorithms. *IEEE Trans. Pattern Anal. Machine Intell.* PAMI-2 (1),1-8.

Bezdek, J. C. 1981: *Pattern Recognition with Fuzzy Objective Function Algorithms.* Plenum, New York.

Dubes, R. 1993: Cluster analysis and related issues. In Chen, C., Pau, L., Wang, P. (Eds.), *Handbook of Pattern Recognition and Computer Vision*, Academic Press, 3–32.

Dunn J.C. 1974: A fuzzy relative of the ISODATA process and its use in detecting compact well-separated clusters. *J. Cybernet.*, 3 (3) , 32-57.

Mesadani S. Kim J. and **Krishnapuram R.** 1998: An overview of membership function generation techniques for pattern recognition. *Internat. J. Approx. Reas.* 19 391–417.

Ruspini, E. H. 1969: A new approach to clustering. *Information and Control*, 15, 22-32.

Chapter 7

In situ monitoring of capping and lamination occurring during Tabletting

7.1 Introduction

This chapter presents a novel approach for condition monitoring of pharmaceutical tablet production using the acoustic emission method for detection of problems associated with tabletting. Capping and lamination have been problems for as long as tablets have been compressed. Detailed description of these phenomena and their causes were presented in Section 3.4.8. This chapter describes the condition monitoring system in terms of its subsystem following extensive experimental results on tabletting using the industrial tablet press at GSK. The system relies on acoustic emission measurement which provides useful information about the tablet's final quality in terms of its hardness. A novel approach to process monitoring which employs the technique known as the receiver operating characteristic (ROC) is presented in this chapter. This chapter also provides some guideline on implementing the proposed condition monitoring with regard to maximising its cost effectiveness.

7.2 Monitoring capping and lamination during powder compression

Lactose, paracetamol and microcrystalline cellulose were chosen as the classic materials for producing capped tablets. Tablets were compressed to approximately 10 kN using normal concave punches fitted in the Manesty F-Press. The compression speed was maintained at 50 tablets per minute. The concave punches were chosen because of their high tendency to produce a capped tablet in comparison with flat punches. However, capping is also material dependent and in most practical situations it is an unpredictable phenomenon. The compressions were characterised acoustically using the MISTRAS 2000 system to record the traditional AE features of rms, absolute energy, peak amplitude, count and average signal level.

Twenty tablets were produced for each material and AE was recorded continuously. It was possible to see the capping on the top layer of a tablet before it was fully ejected; this in fact indicates that capping can occur during the compression thus confirming the findings by Ritter and Sucker (1980).

Of the twenty tablets produced from the compression of paracetamol, only three tablets were seen to have capped. Tablets were labelled for crushing and disintegration tests and weight analysis. However the aim of this study was to investigate whether a capped tablet can be distinguished from an uncapped tablet using AE monitoring. It was noticed, Figure 7.1 that a capped tablet has low rms values compared with non-capped tablets. Similar observations can be made for averaged signal level, Figure 7.2. The AE data shown are only from a the powder compression after filtering out all other AE events from mechanical noise.

The number of peaks in these diagrams is the number of tablets produced i.e. twenty. Capping occurred for tablets 4, 13 and 20, whereas tablet number 14 was laminated. The laminated tablet was shown to have a low crushing strength in comparison with good tablets. Five good tablets randomly selected from the good ones were subjected to crushing strength test. Crushing strength data suggested that these tablets are of a good quality. The test was carried out using tablet tester (Model C40). Crushing strength is a measure of the hardness of the tablets as explained in Section 4.2.5. A hardness value in the range of 9.85 kg ± 0.453 kg (±1 standard deviation) was achieved. This gives a relative standard deviation RSD value of 4.59%, which is very acceptable in pharmaceutical practice (desirably <5%). The hardness for the laminated tablet was 6.8kg.

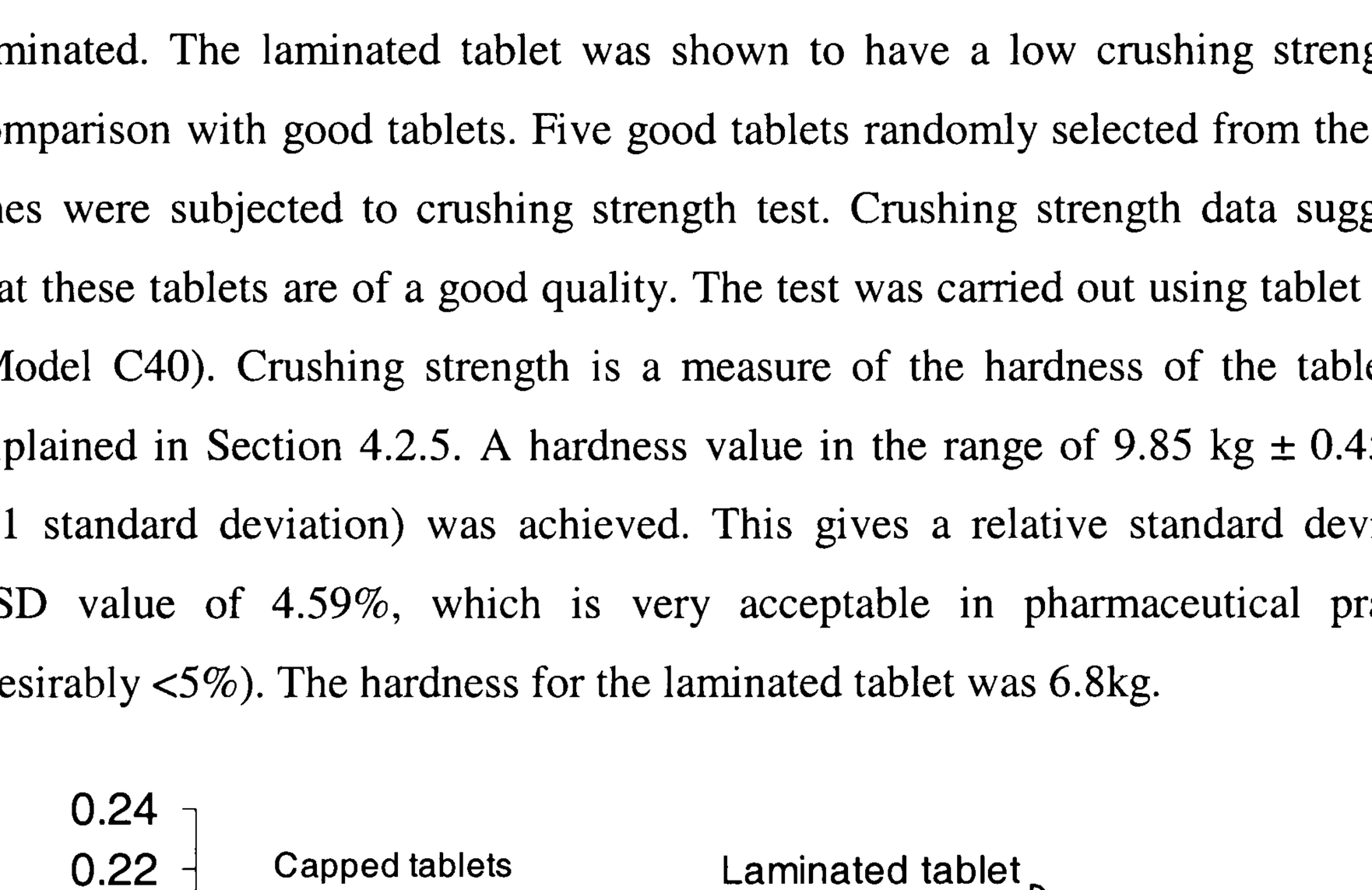

Figure 7.1 Acoustic emission rms of twenty Paracetamol tablets in which arrows indicated capped tablets.

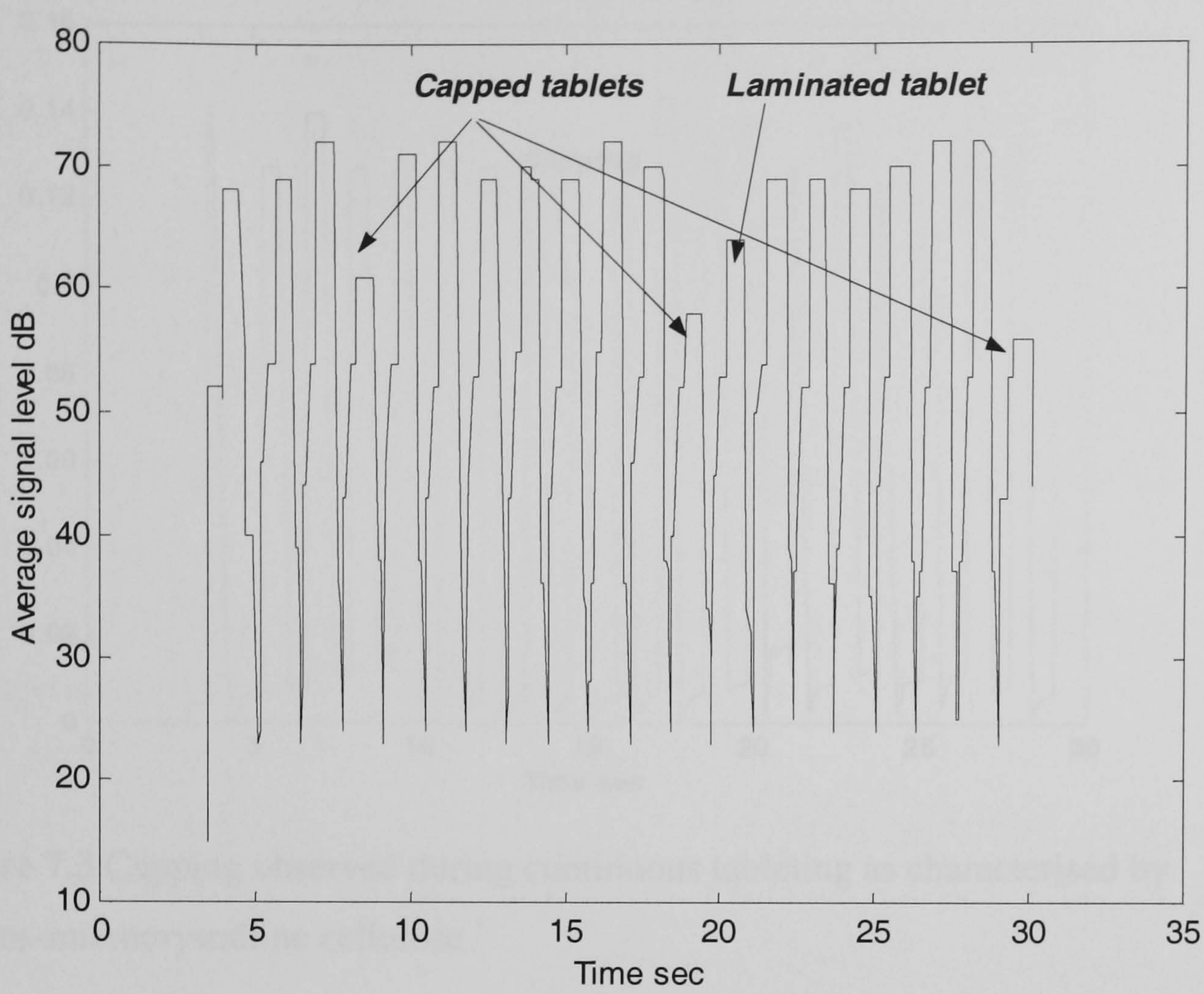

Figure 7.2 Acoustic emission ASL of twenty Paracetamol tablets in which arrows indicated capping

AE monitoring of capping was also investigated during the compression of microcrystalline cellulose powder. Compression conditions were the same as that for paracetamol tablets. No lamination was observed during this test. However, out of twenty tablets produced, capping was observed on only one tablet. AE monitoring was based on AErms and average signal level as shown in Figures 7.3 and 7.4 respectively.

The mean AErms value of good tablets was around 0.133 whereas the capped tablet has an AErms value below 0.1. Similarly, five good tablets were tested for hardness measurement. Their mean hardness value was approximately 9.5kg ± 0.35 kg (±1 standard deviation) which give an RSD value of 3.68%.

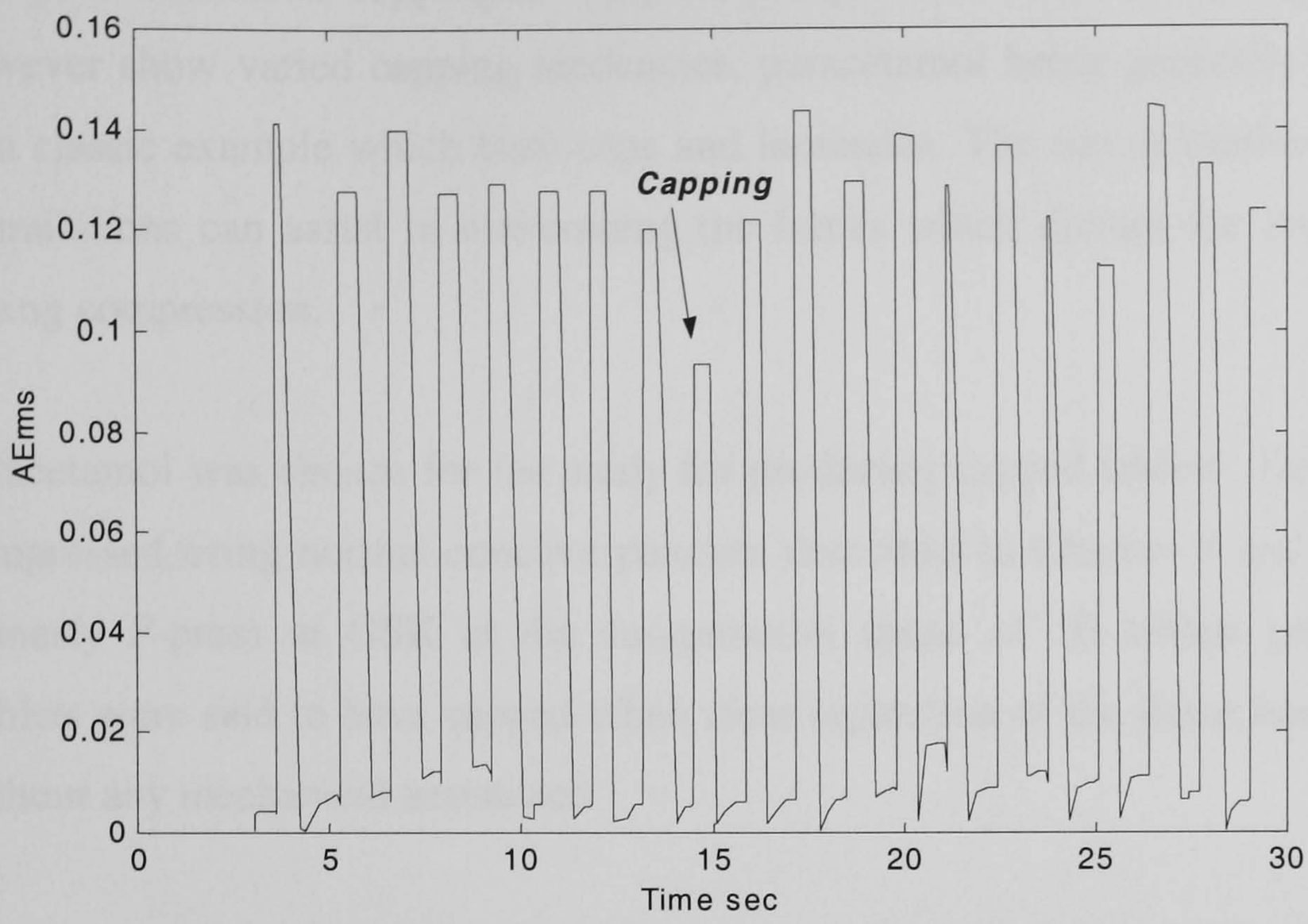

Figure 7.3 Capping observed during continuous tableting as characterised by AErms-microcrystalline cellulose

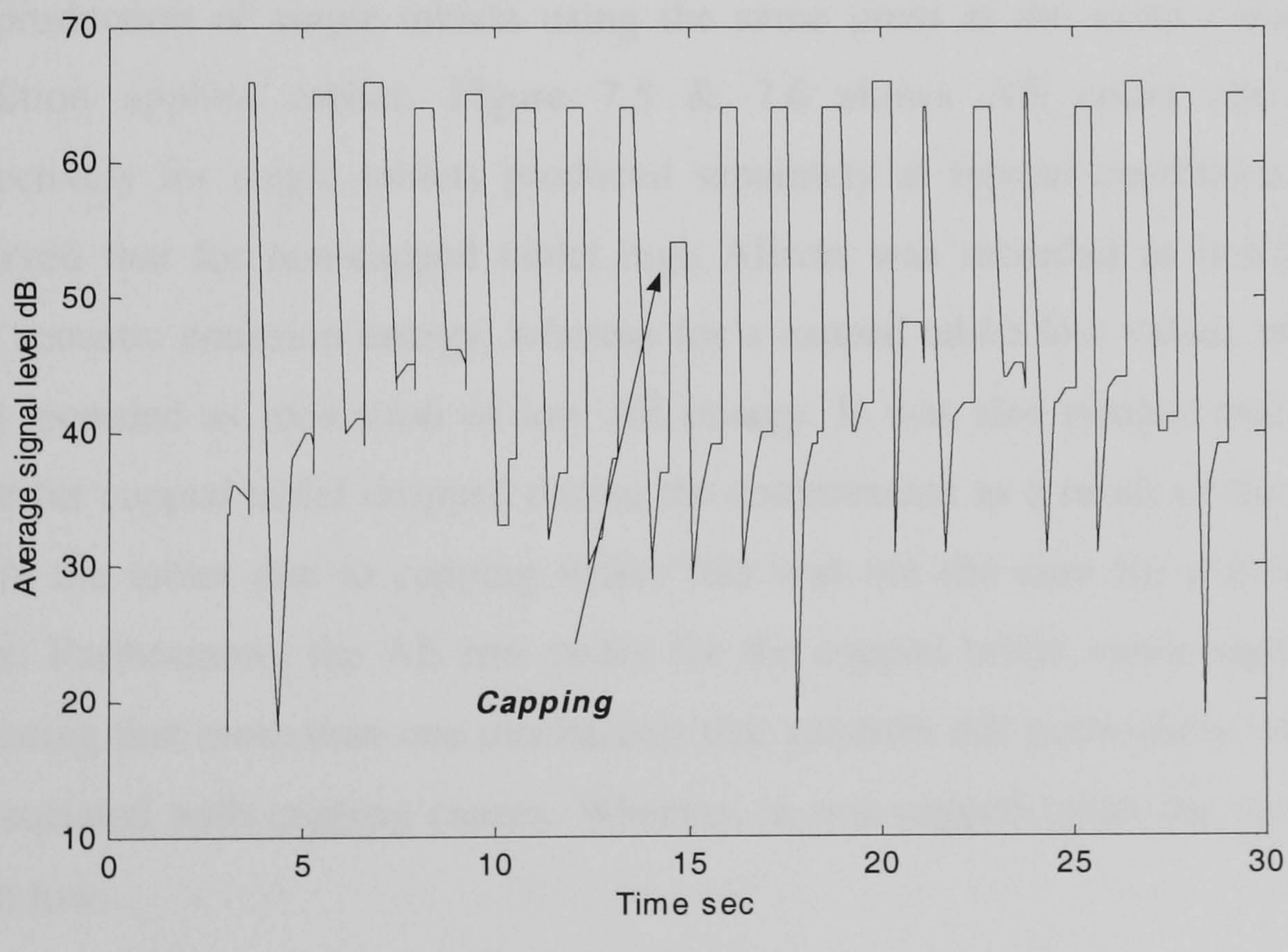

Figure 7.4 Capping observed during continuous tableting as characterised by average signal level- microcrystalline cellulose

The phenomenon of capping is completely unpredictable. Different materials do however show varied capping tendencies, paracetamol being generally described as a classic example which both caps and laminates. The use of binders in tablet formulations can assist in overcoming the forces which disrupt the bonds made during compression.

Paracetamol was chosen for the study for producing capped tablets. Tablets were compressed using normal concave punches described in Chapter 4 and using the Manesty F-press at GSK at the compression speed of 50 tablets per minute. Tablets were said to have capped when clear separation of the dome has occurred without any mechanical assistance.

The cap of the tablet was seen to fall out of the die before movement of the tablet in the die had been initiated, indicating that capping had occurred post compression but before ejection.

The differences between capped and non-capped tablets were also shown during the production of single tablets using the same press at the same compression condition applied earlier. Figure 7.5 & 7.6 shows AE count and AErms respectively for single tablets produced separately at typical conditions. It was observed that for non-capped tablet high AErms was recorded as indication of high acoustic emission energy, whereas for a capped tablet low values of AErms were recorded as indication of low AE energy. It was also noticed that the AE count for capped tablet dropped during the compression as a result of the fracture within the tablet due to capping where this was not the case for a non-capped tablet. Furthermore, the AE rms peaks for the capped tablet varies significantly indicating that more than one mechanism that generate AE particularly one which is associated with capping causes. Whereas, in non-capped tablet the variation is much low.

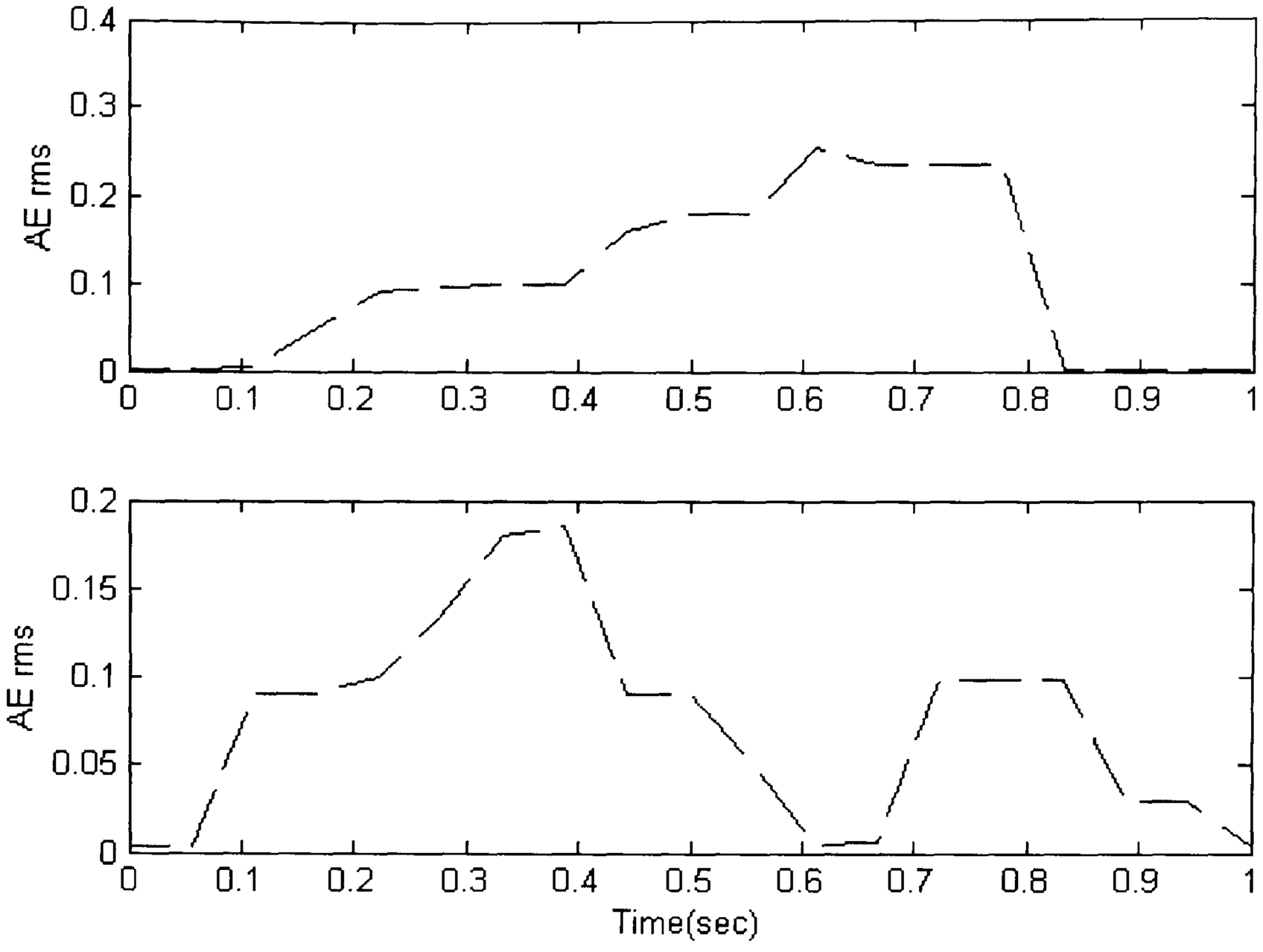

Figure 7.5 AE RMS of two tablets capped (bottom) and non-capped (top) produced from compression of paracetamol powder.

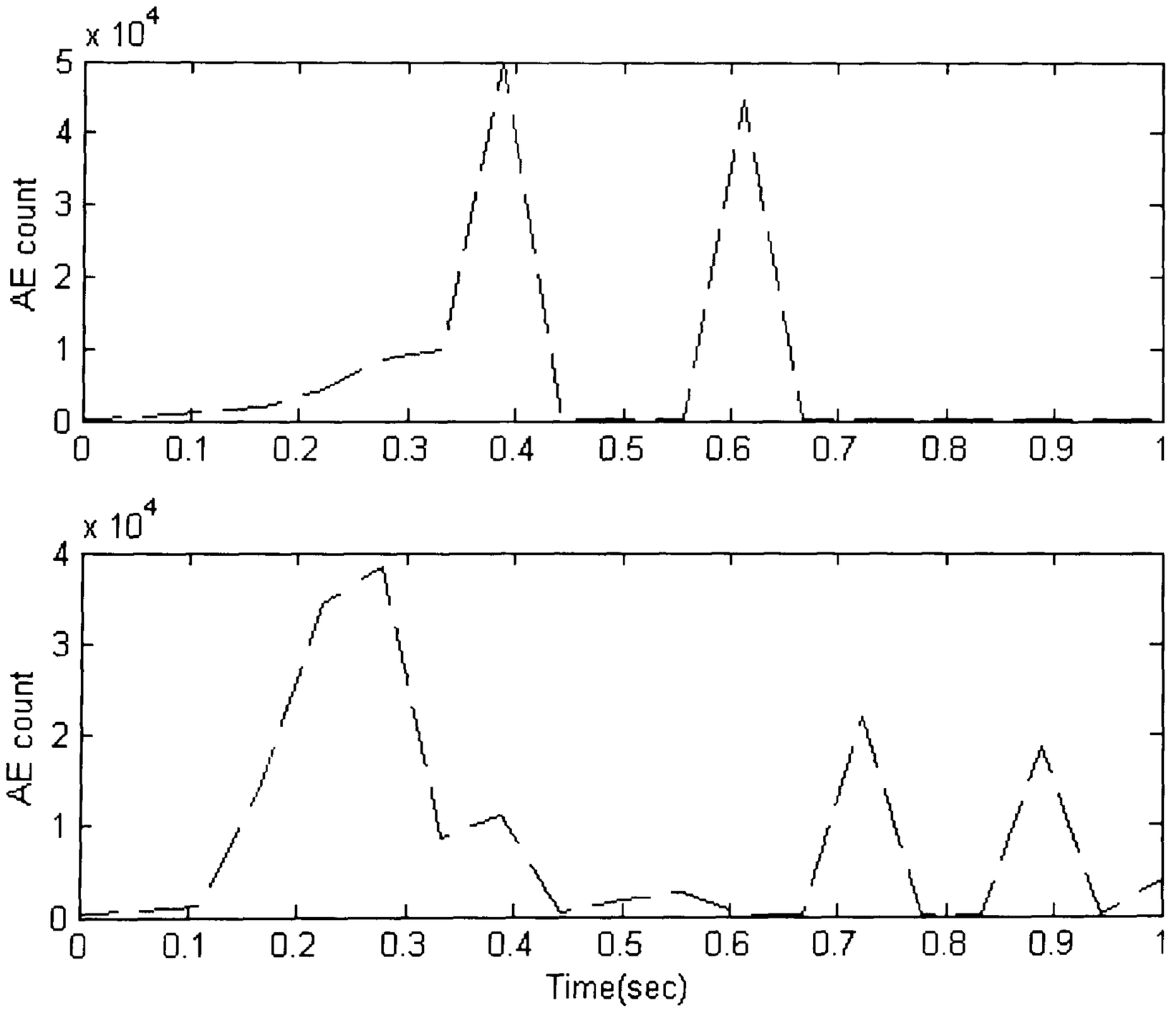

Figure7.6 AE count of two tablets capped (bottom) and non-capped (top) produced from compression of paracetamol powder

7.3 Capping in binary mixtures

The phenomenon also existed during the compression of the binary mixture of lactose and Povidone. The binary mixture at ratio of 80:20 for these two materials respectively was prepared and was mixed for two minutes. Tablets were prepared using the same press and at exactly the same compression condition outlined earlier. The signal was characterised by the average signal level (ASL) and AE energy. Figure 7.7 illustrates the ASL profile of the 20 compression cycles of the binary mixture. Of the twenty tablets produced two tablets were capped, Figure 7.7. It was observed that the AE generated from the production of capped tablets appears to have a low ASL of 57-60 dB, whereas good tablets produced higher peaks in the range of 63-68 dB. Capping was noticed before the tablets were fully ejected from the die. Capping in this test was also characterised and identified by the MISTRAS AE energy as shown in Figure 7.8, a great drop in the AE energy was noticed when capping occurred for tablets 12 and 19.

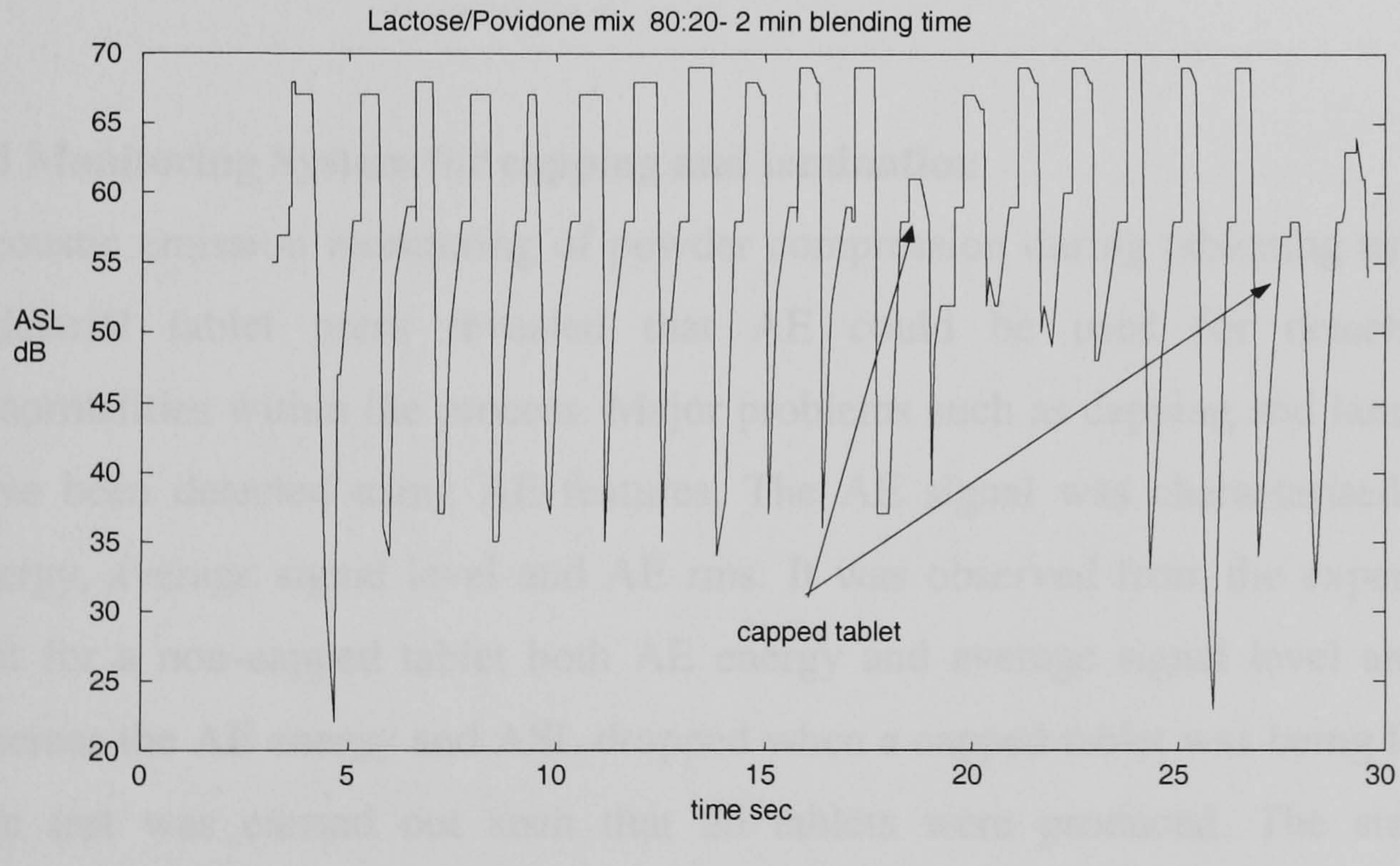

Figure 7.7 Average signal level of twenty tablets produced from binary mixture of Lactose/Povidone. Arrows indicate the occurrence of capping during tabletting

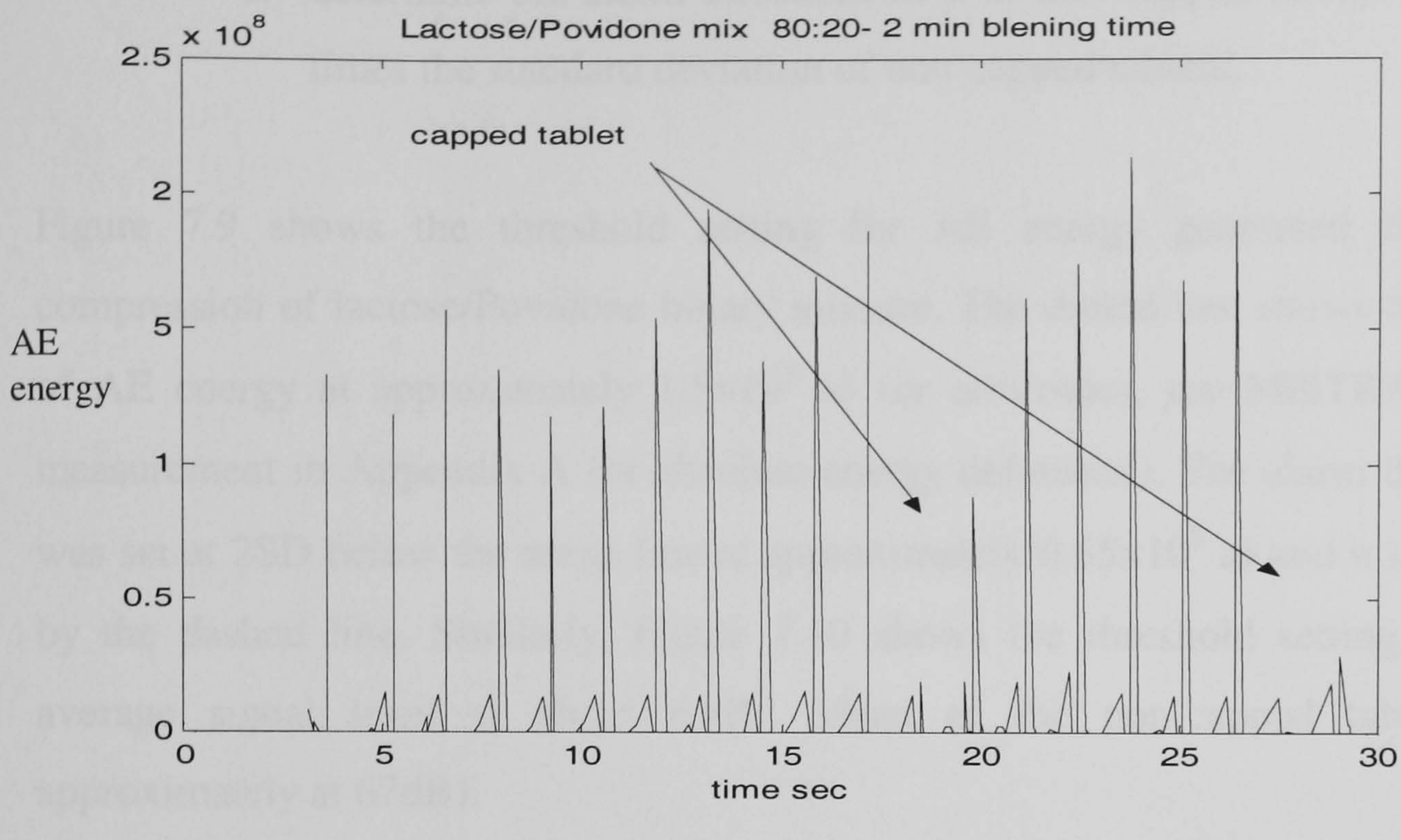

Figure 7.8 Absolute AE energy of twenty tablets produced from binary mixture of Lactos/Povidone. Arrows indicate the occurrence of capping during tableting

7.4 Monitoring System for capping and lamination

Acoustic emission monitoring of powder compression during tabletting using the industrial tablet press revealed that AE could be used for detection of abnormalities within the process. Major problems such as capping and lamination have been detected using AE features. The AE signal was characterised by its energy, average signal level and AE rms. It was observed from the experiments that for a non-capped tablet both AE energy and average signal level are high, whereas the AE energy and ASL dropped when a capped tablet was being formed. The test was carried out such that 20 tablets were produced. The statistical characteristics of data distribution for both non-capped tablets and capped tablets were examined. The mean and standard deviation of both distributions were determined so that an alarm threshold can be set to detect abnormalities. The threshold was determined as follows:

a. calculate the mean μ and standard deviation sd of the non-capped tablets.
b. calculate the mean μ and standard deviation sd of the capped tablets.

c. determine the alarm threshold as μ of non-capped tablets minus 2 times the standard deviation of non-capped tablets.

Figure 7.9 shows the threshold setting for AE energy generated from the compression of lactose/Povidone binary mixture. The dotted line shows the mean of AE energy at approximately 1.5×10^8 aJ (or attoJoules, see MISTRAS 2000 measurement in Appendix A for absolute energy definition). The alarm threshold was set at 2SD below the mean line at approximately 0.65×10^8 aJ and it is shown by the dashed line. Similarly, Figure 7.10 shows the threshold setting for the average signal level at about 63dB. Mean of the non-capped tablet was approximately at 67dB).

Figure 7.11 and Figure 7.12 show both the AE energy and ASL generated from microcrystalline cellulose which is slightly less acoustically active than lactose. Threshold for capping detection was set at 2× (standard deviation, SD) below the mean of the non-capped tablets.

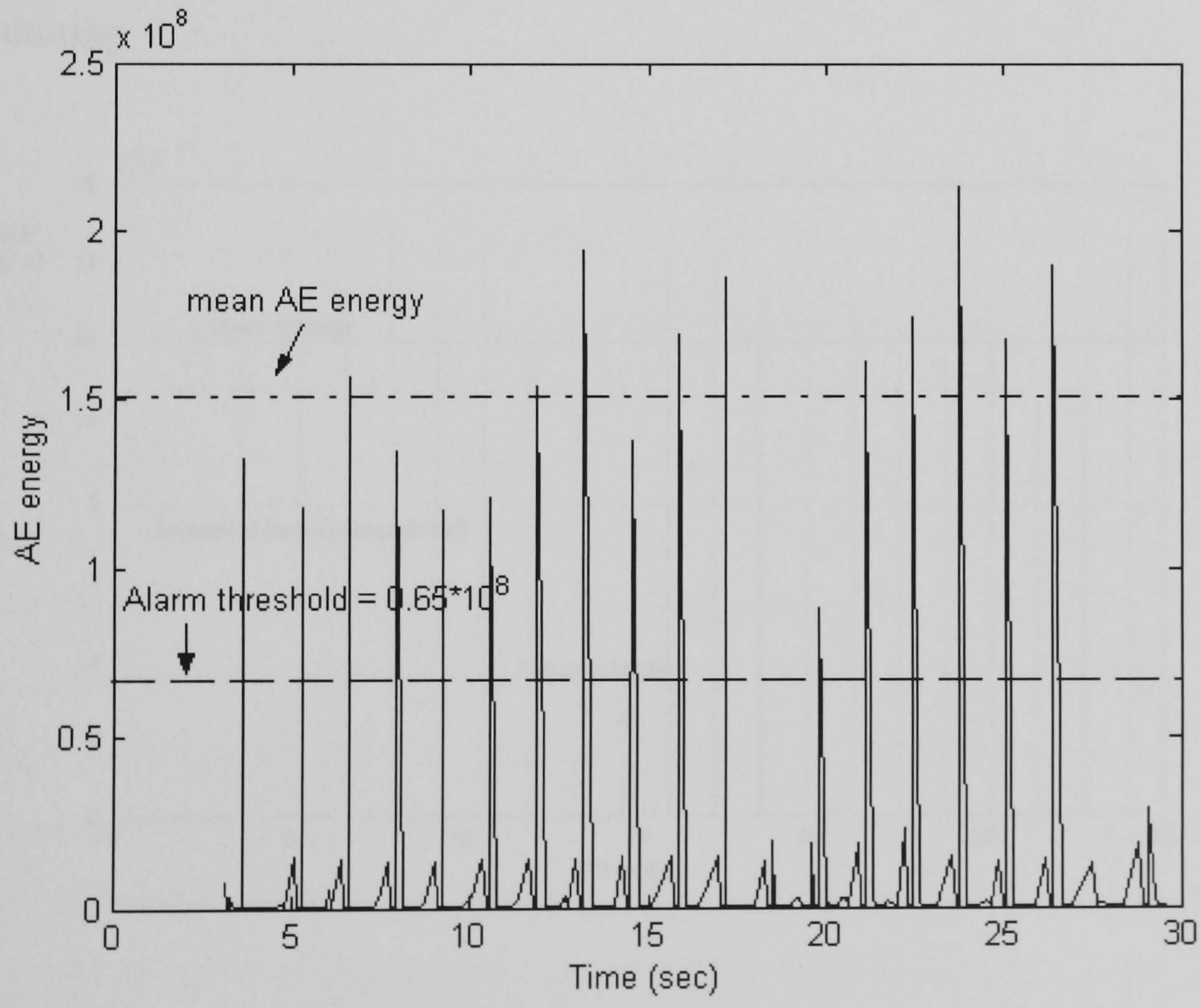

Figure 7.9 Threshold of binary mixture tablet quality detection based on absolute energy monitoring

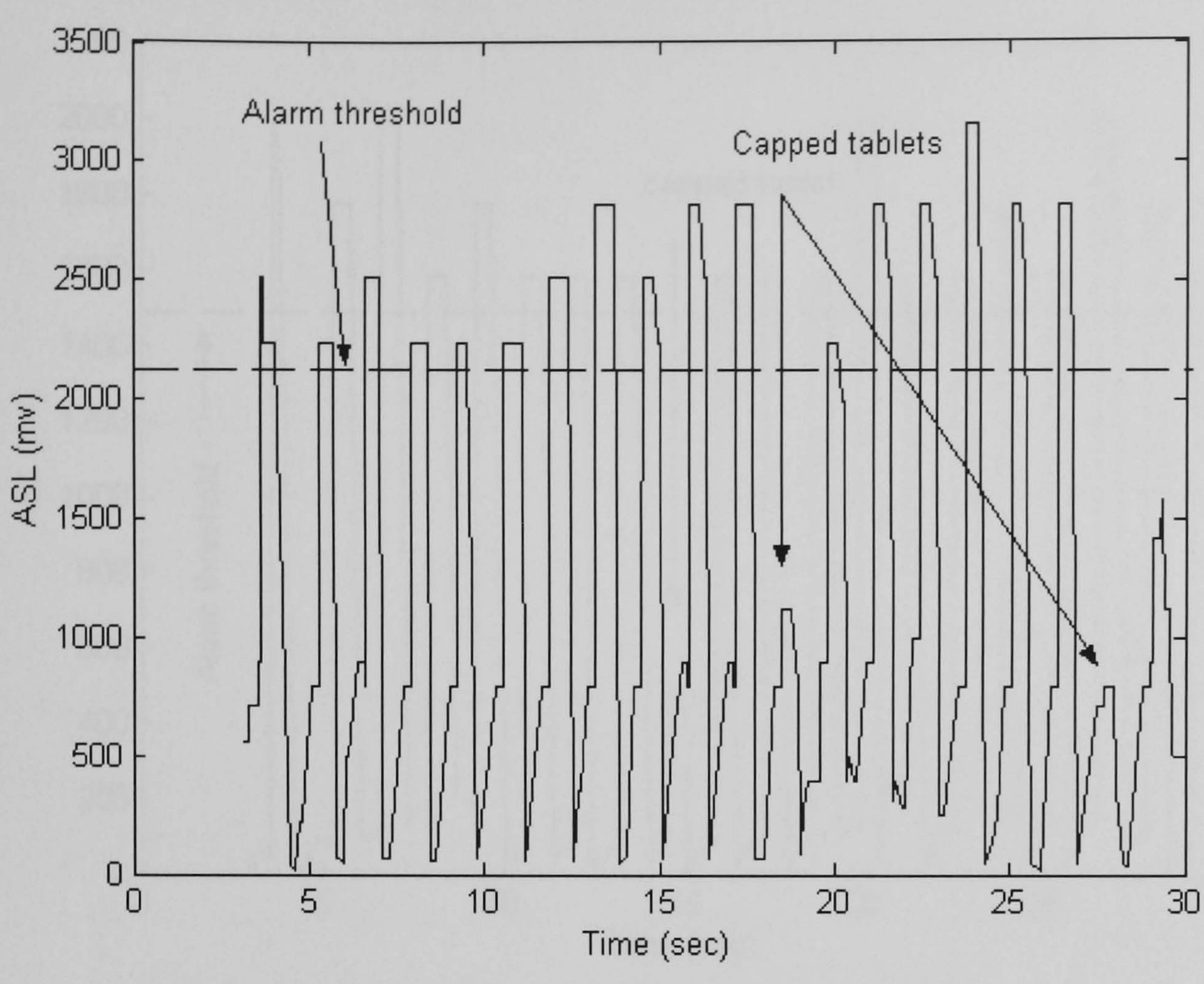

Figure 7.10 Threshold of binary mixture tablet quality detection based on ASL monitoring

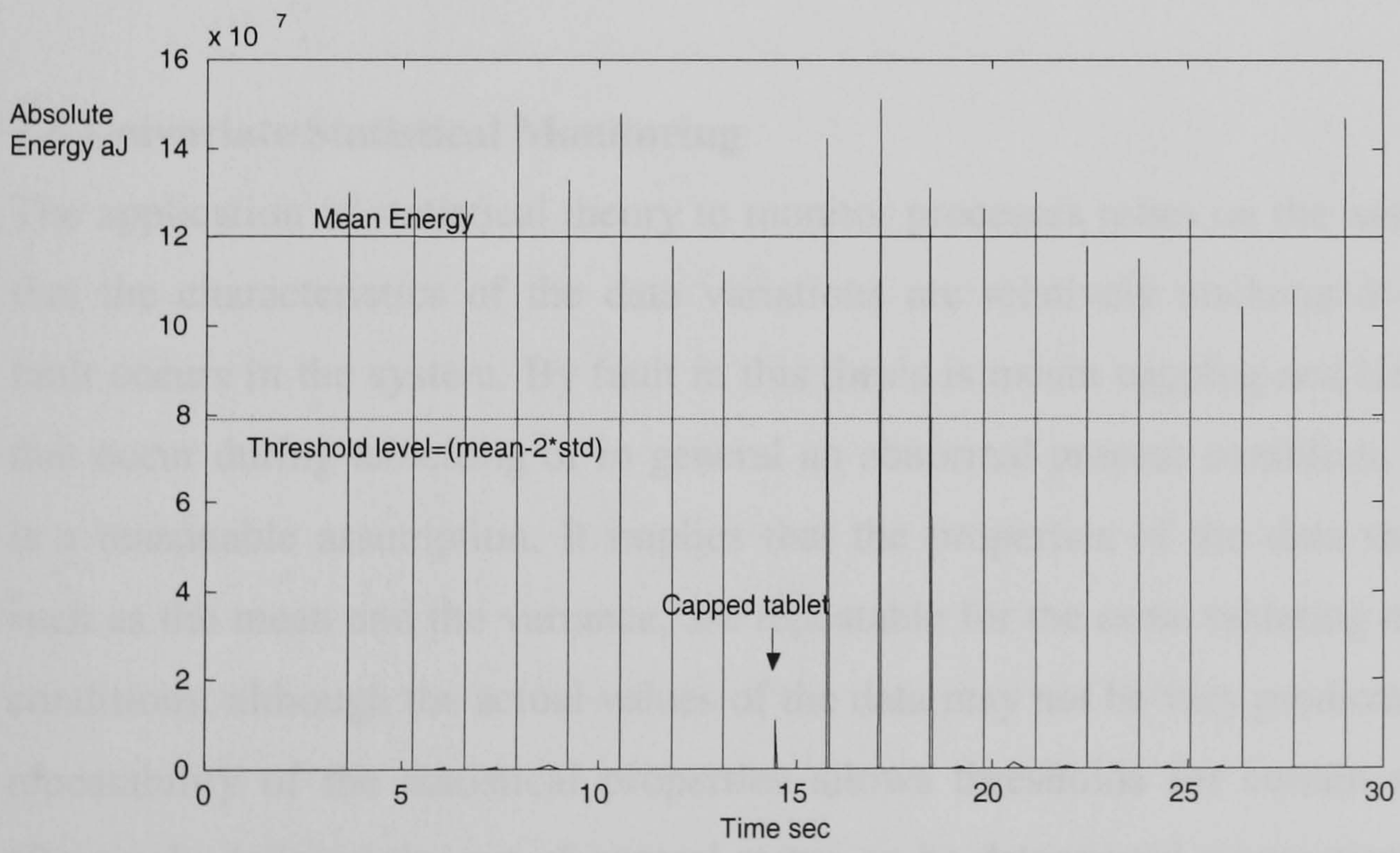

Figure 7.11 AE energy of twenty tablets produced from microcrystalline cellulose compression. Arrows indicate the occurrence of capping during tabletting.

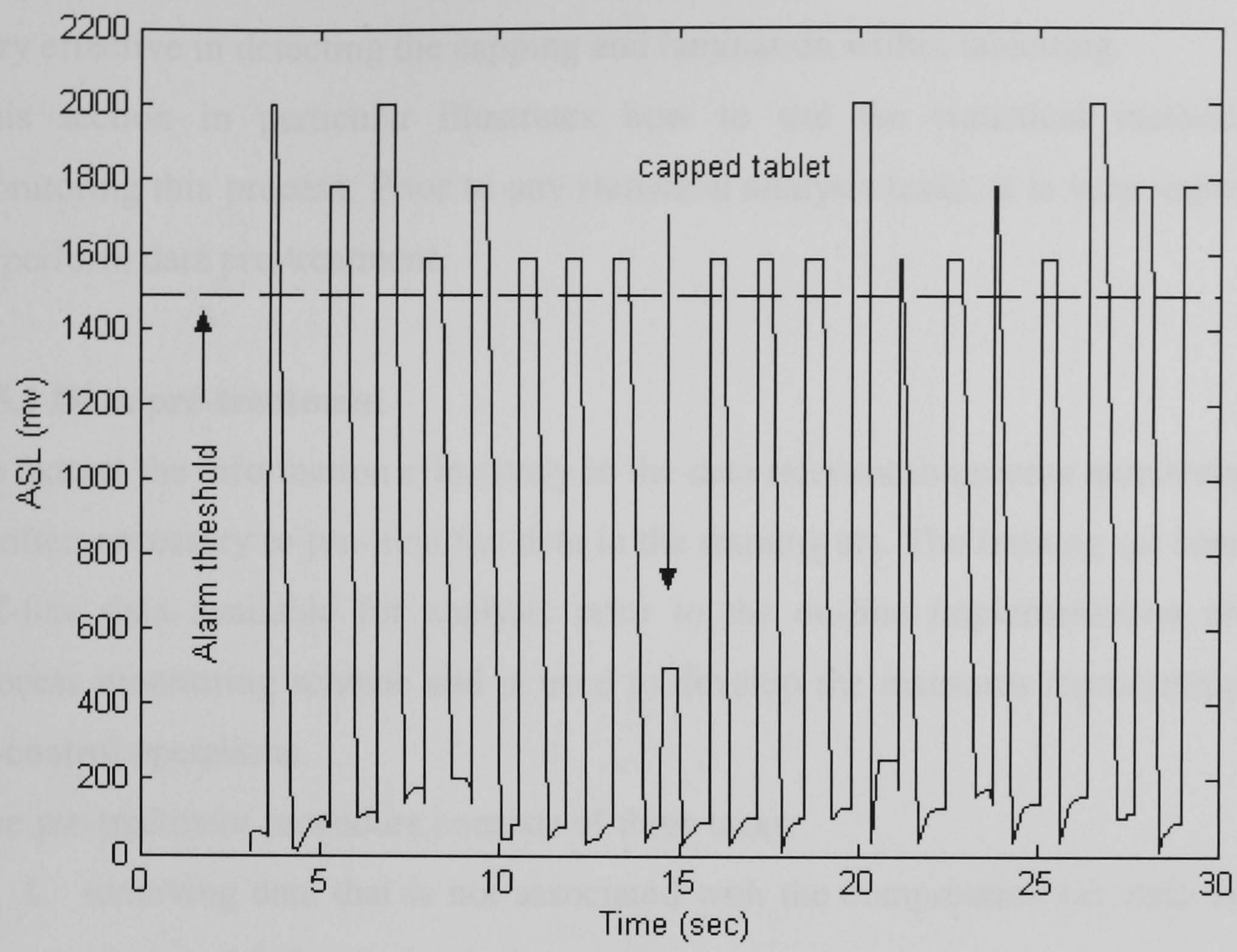

Figure 7.12 Average signal level of AE generated from cellulose compression.

7.5 Univariate Statistical Monitoring

The application of statistical theory to monitor processes relies on the assumption that the characteristics of the data variations are relatively unchanged unless a fault occurs in the system. By fault in this thesis is meant capping and lamination that occur during tabletting or in general an abnormal process condition, and this is a reasonable assumption. It implies that the properties of the data variations, such as the mean and the variance, are repeatable for the same tableting operating conditions, although the actual values of the data may not be very predictable. The repeatability of the statistical properties allows thresholds for certain measure, effectively defining the out-of-control status, to be determined automatically. This is an important step to automating a process monitoring scheme.

The purpose of the remaining sections of this chapter is to describe a condition monitoring system for powder compression during tablet processing based upon the statistical measures of AE parameters. It was already established that certain

AE parameters such as AE energy, average signal level and peak amplitude were very effective in detecting the capping and lamination within tabletting.

This section in particular illustrates how to use the statistical method for monitoring this process. Prior to any statistical analysis tasks, it is very important to perform data pre-treatment.

7.5.1 Data pre-treatment

To extract the information effectively in the data relevant to process monitoring, it is often necessary to pre-treat the data in the training set. The training set contains off-line data available for analysis prior to the on-line implementation of the process monitoring scheme and is used to develop the measures representing the in-control operations.

The pre-treatment procedure consists of three tasks:

1. removing data that is not associated with the compression i.e. data that is generated from mechanical contact.
2. removing outlier in particular events which are generated at the start of the measurement during the turning on of the press, and which are events associated with the end of data recording.
3. removing irrelevant variables i.e. variables that do not give meaningful information about the process such as the event duration and rise time.

A univariate statistical approach to limit sensing has been used to determine the thresholds for each observation variable (a process variable observed through a transducer e.g. AE energy), where these thresholds define the boundary from in-control operations and a violation of these limits with on-line data would indicate a fault. The objective is to minimise the rate of **false alarms** and the rate of **missed detections**. A false alarm in this context is an indication of a capping or lamination in the processing, when in fact more of these has occurred; a missed detection is no indication of a fault, though a fault has occurred. The false alarm is called the type I error (alpha), and the missed detection of a fault is the type II error (beta). This is illustrated graphically in Figure 7.13.

Given certain threshold values, statistical hypothesis theory can be applied to predict the false alarm and missed detection rates based on the statistics of the data in the training sets. Increasing the threshold (shifting the vertical line to the right

in Figure 7.13) increases the false alarm rate but decreases the missed detection rate. Attempts to lower the false alarm rate are usually accomplished with an increase in the missed detection rate, with the only ways to get around this trade off being to monitor sample mean instead of individual values or to use a more precise method of measurement.

Process variability can be described by a normal distribution with the mean μ and standard deviation σ:

$$p(x) = \frac{1}{\sigma\sqrt{2\pi}} \exp\left[-\frac{(x-\mu)^2}{2\sigma^2} \right] \tag{7.1}$$

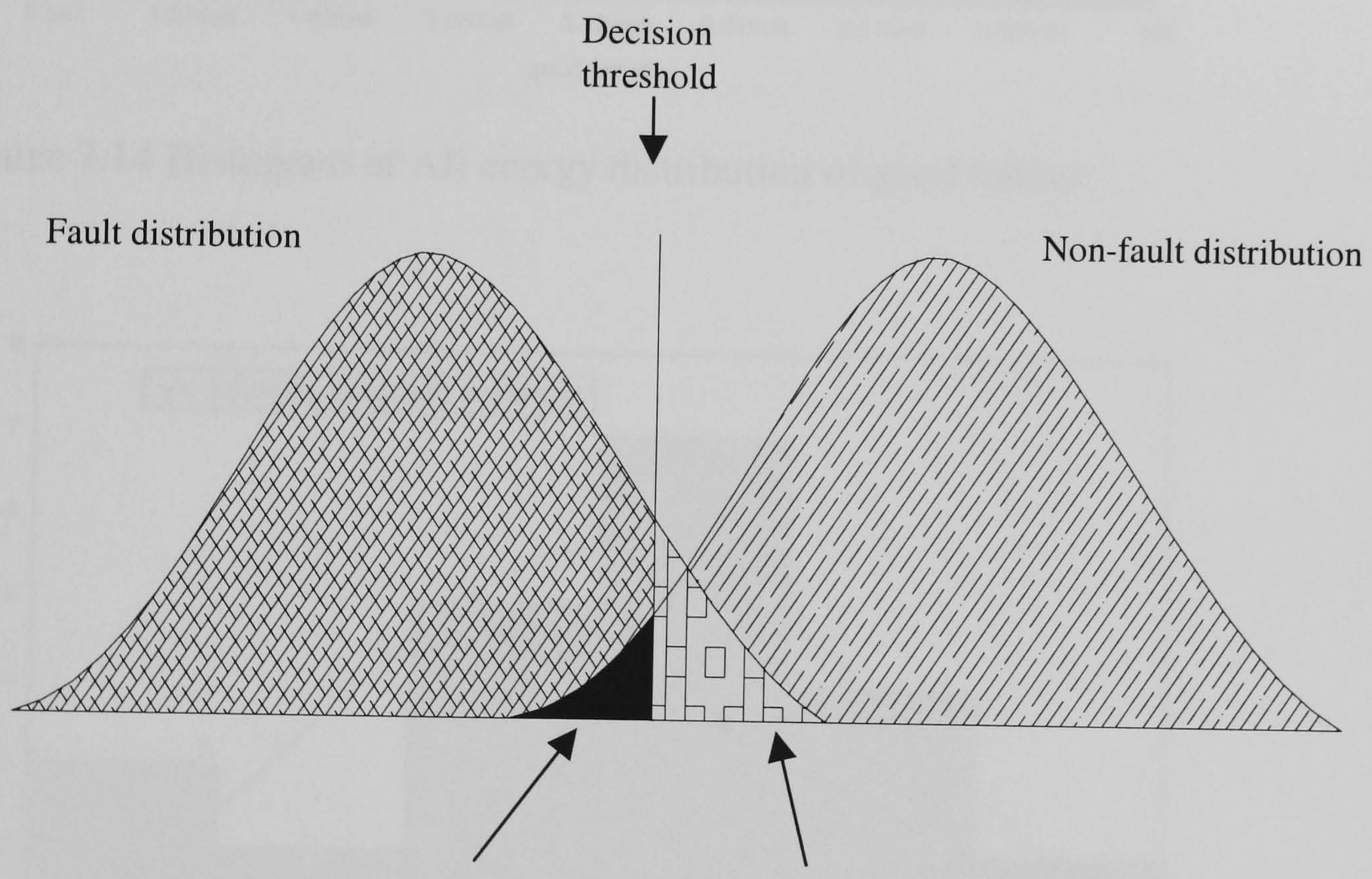

Figure 7.13 The Type I and Type II error regions for the null hypothesis.

Two distributions of both non-capped tablets and capped tablets have been produced and they appear to be following normal distribution. Figures 7.14 and 7.15 show the histograms with normal distribution curves fitting to the non-capped and capped tablets.

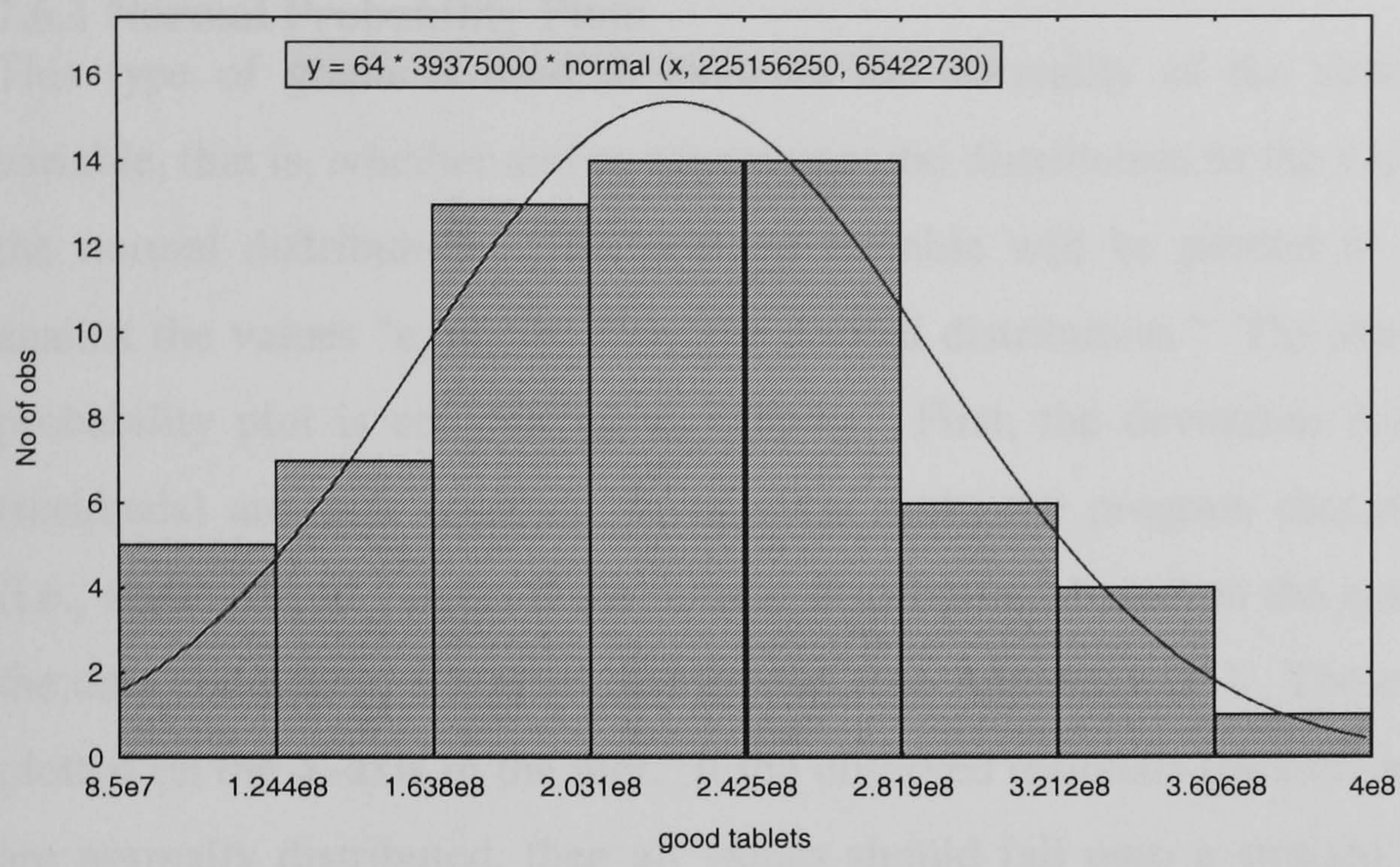

Figure 7.14 Histogram of AE energy distribution of good tablets

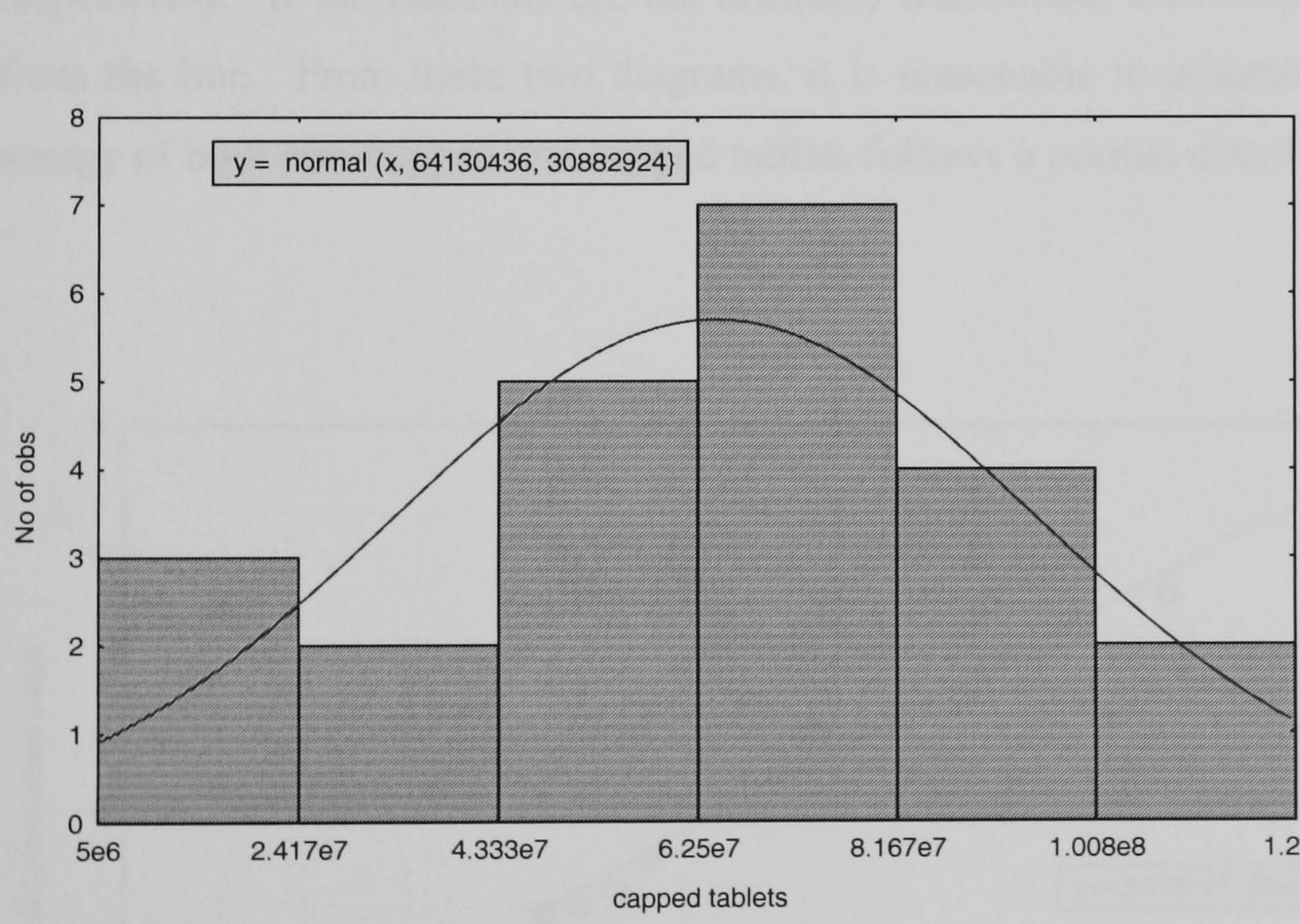

Figure 7.15 Histogram of AE energy distribution of capped tablets.

7.6 Normality testing

Normality testing of the data was carried out using normal probability plots implemented in the STATISTICA software package.

7.6.1 Normal Probability Plots

This type of graph is used to evaluate the normality of the distribution of a variable, that is, whether and to what extent the distribution of the variable follows the normal distribution. The selected variable will be plotted in a scatterplot against the values "expected from the normal distribution." The standard normal probability plot is constructed as follows. First, the deviations from the mean (residuals) are rank ordered. From these ranks the program computes z values (i.e., standardized values of the normal distribution) based on the assumption that the data come from a normal distribution (see Appendix D1). These z values are plotted on the Y-axis in the plot. If the observed residuals (plotted on the X-axis) are normally distributed, then all values should fall onto a straight line; Figures 7.16 and 7.17 shows normality plot for both non-capped tables and capped tablets respectively. If the residuals are not normally distributed, then they will deviate from the line. From these two diagrams, it is reasonable to assume that the AE energy of both non-capped and capped tablets follows a normal distribution.

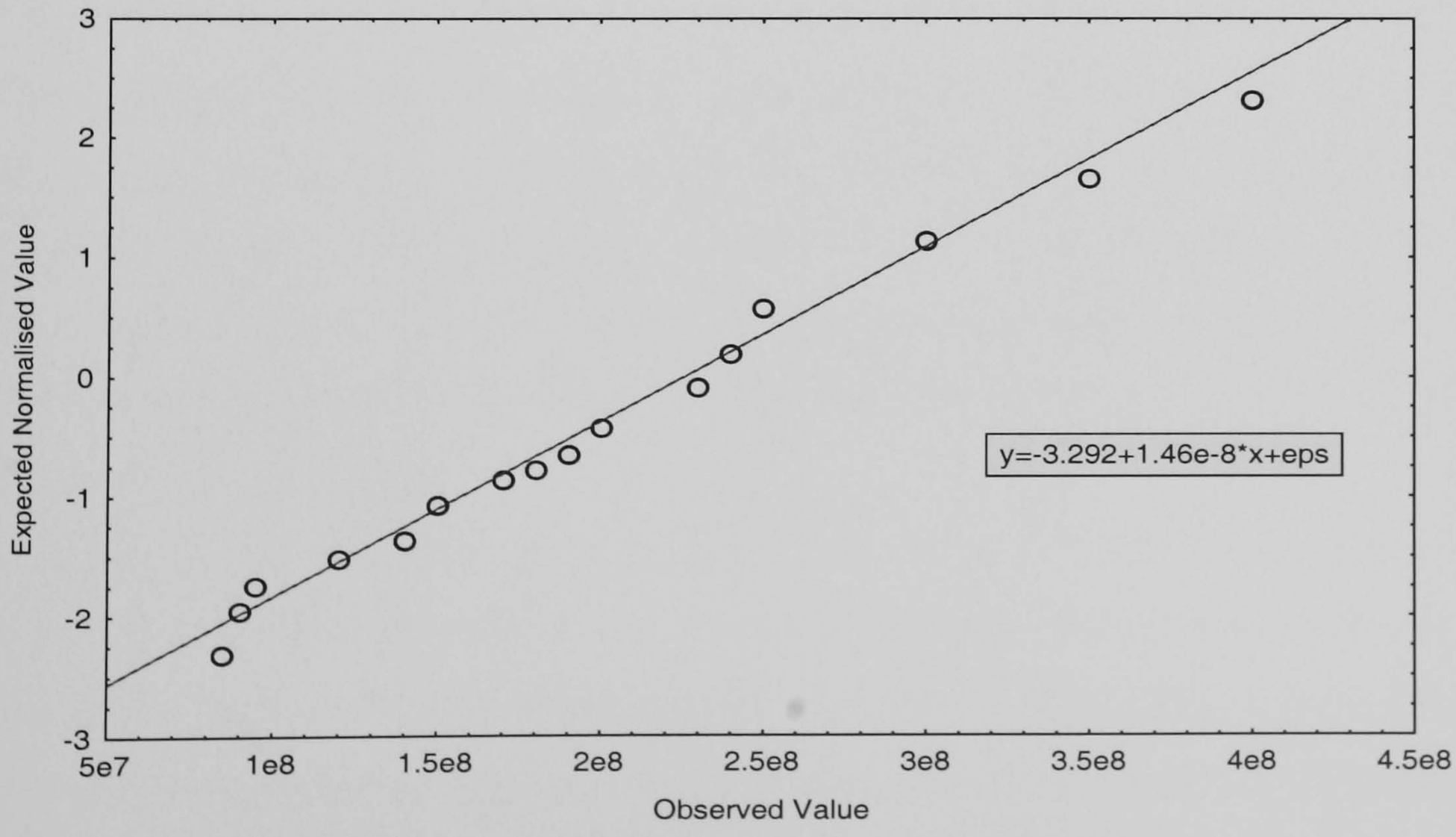

Figure 7.16 Normality plot of AE energy of non-capped tablet.

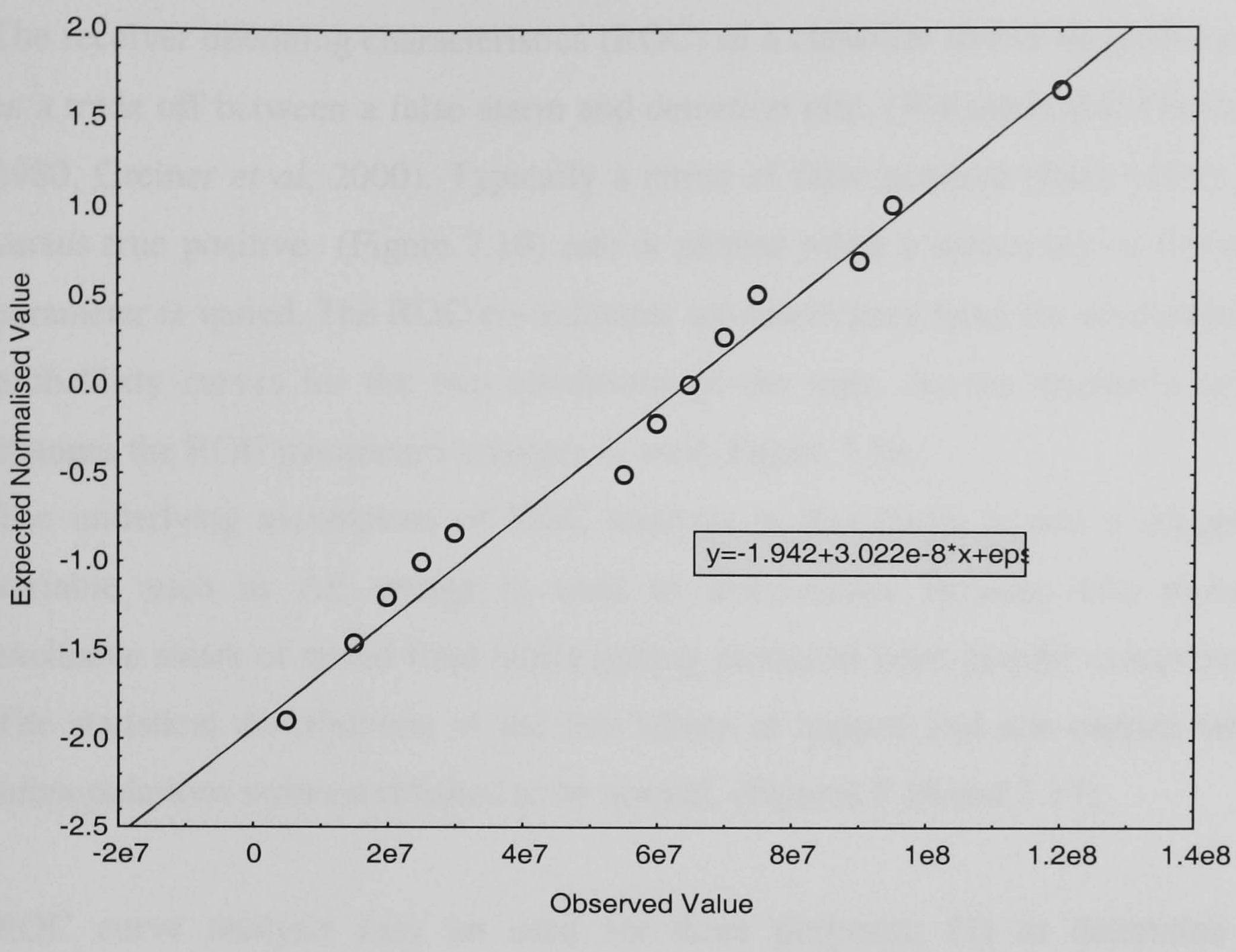

Figure 7.17 Normality plot of AE energy of capped tablet.

7.7 Receiver Operating Characteristics (ROC)

The receiver operating characteristics (ROC) of a classifier shows its performance as a trade off between a false alarm and detection rate, (Weinstein and Fineberge, 1980, Greiner *et al*, 2000). Typically a curve of false positive (false alarm) rate versus true positive (Figure 7.18) rate is plotted while a sensitivity or threshold parameter is varied. The ROC co-ordinates are determined from the area under the probability curves for the two conditions of the state. As the threshold setting changes the ROC parameters changes as well, Figure 7.18.

The underlying assumption of ROC analysis in this thesis is that a diagnostic variable such as AE energy is used to discriminate between two mutually exclusive states of tested final tablet quality produced from powder compression. The statistical distributions of the test values of capped and non-capped tablets subpopulations were established to be normal, (Figures 7.16 and 7.17).

ROC curve analysis may be used for three purposes: (1) to determine the discriminative ability of a diagnostic test, (2) to compare the discriminative abilities among several different diagnostic tests in order to identify the preferred one and (3) to determine the optimal threshold of a diagnostic test. The remaining sections of this chapter focus on the third purpose, (Greiner et al, 1995).

For all diagnostic tests, a value of the monitoring parameter, for example, AE energy, is selected as a decision threshold (cut-off value) to define positive (capped) and negative (non-capped) test outcomes. Comparison of the AE monitoring results against the true status for individual tablets (as determined by crushing strength and dissolution characteristics) allow estimation of the diagnostic sensitivity Se, the probability of positive test outcome in capped tablets and specificity, Sp, the probability of negative test outcome in non-capped tablets, (Figure 7.18).

It can be seen from the ROC curve as shown in Figure 7.19 that Se & Sp are inversely related depending on the choice of threshold value. When increasing values of a measurement are associated with non-capping, higher threshold values are generally associated with higher Se and lower Sp, (Figure 7.18). This relationship has two important implications. First, when an operator would like to

select a threshold value such that the desired operating characteristic, (Se, 1-Sp) in Figure 7.19, is achieved. Second, it is realised that Se and Sp at a single threshold value do not describe the test performance at other potential threshold values. The latter also implies that the effect of the selected cut-off value should be taken into account when comparing diagnostic tests.

The diagnostic Se and Sp are a function of the selected threshold value. ROC analysis assesses the diagnostic performance of the system in terms of Se and (1-Sp) for each possible cut-off value of the test. The terms Se and (1-Sp) in this context are also referred to as "true-positive fraction" and "false-positive fraction", respectively.

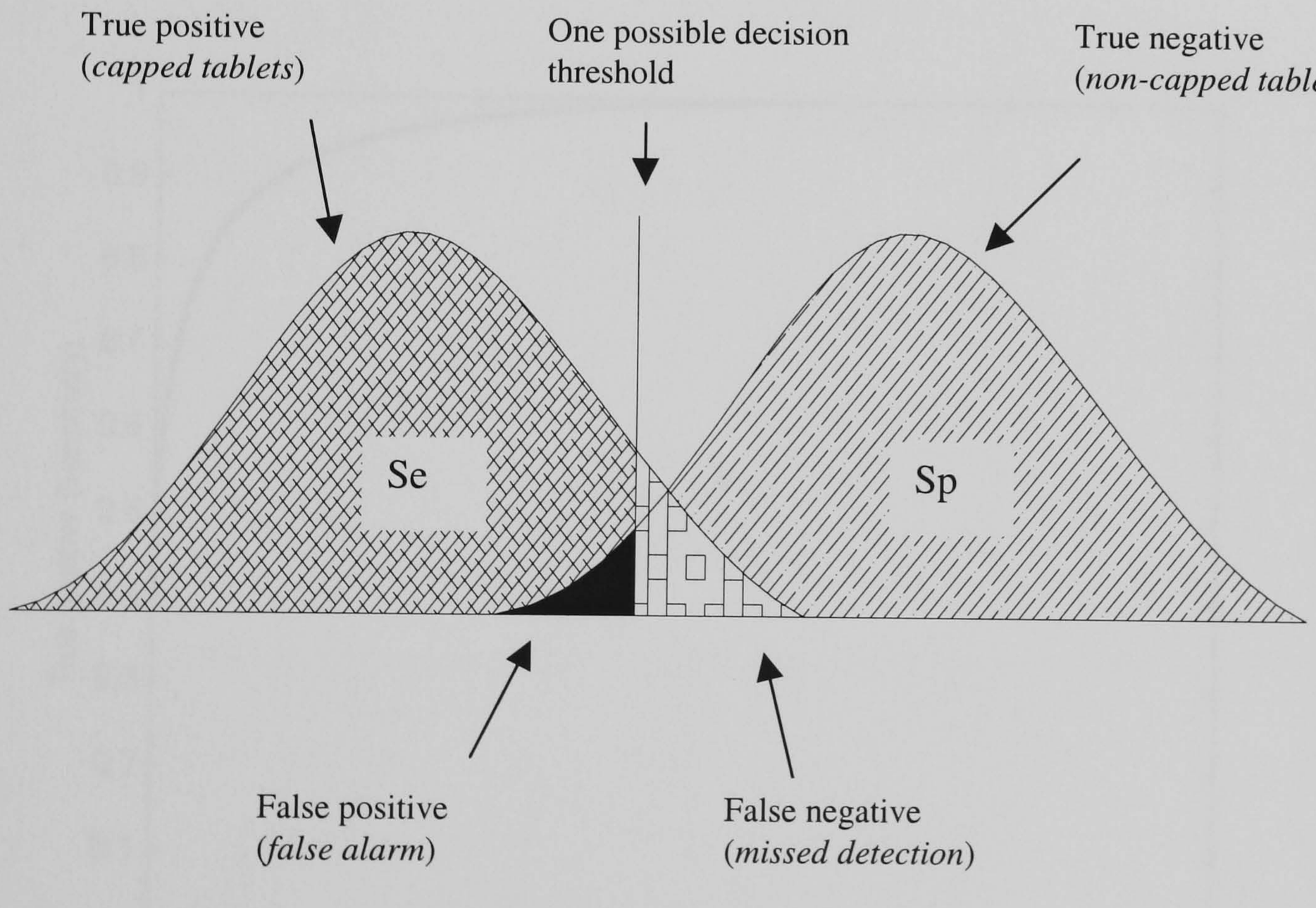

Figure 7.18 Two hypothetical distributions of AE energy on which decisions are based, showing one possible decision threshold. The conditional probability of

each kind of decision is equal to the area under a distribution on one side of the threshold.

The ROC curve always goes through two points (0,0 and 1,1), Figure 7.19, the first point (0,0) is where the classifier finds no positives (detect no alarms). In this case it always gets the negative cases right but it gets all the positive cases wrong. The second point is (1,1) where everything is classified as positive. So the classifier gets all positive cases right but it gets all negative cases wrong i.e. it raises a false alarm on each negative case.

The ROC curve can be used to choose the best operating point. The best operating point might be chosen so that the classifier gives the best trade off between the costs of failing to detect positives against the costs of raising false alarms. These costs need not be equal, however this is a common assumption. Cost benefit analysis will be discussed in Section 7.8.

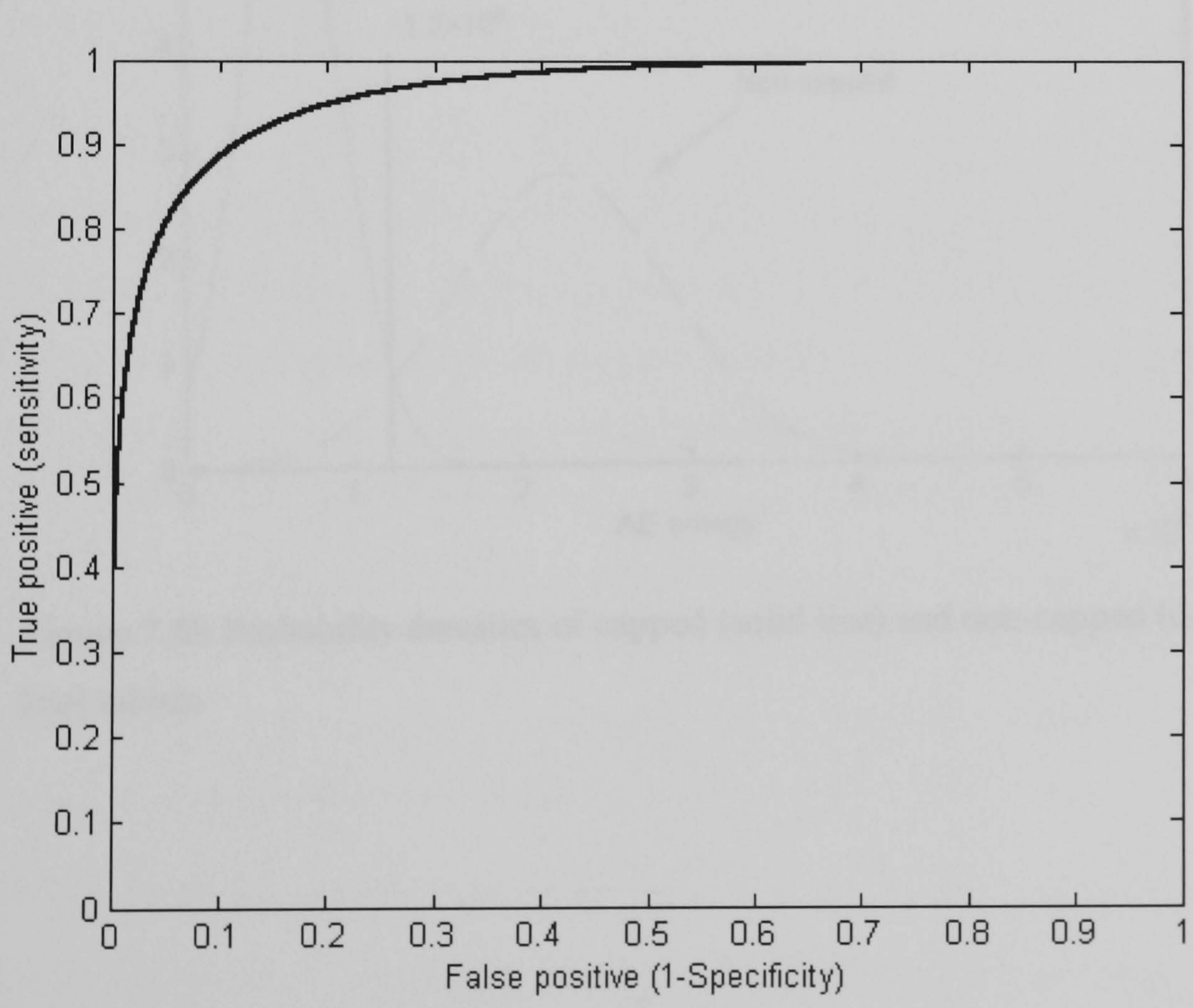

Figure 7.19 Typical ROC curve

Figure 7.20 shows the probability densities of AE energy for both good (blue curve) and capped tablets (red curve). It was established that both curves behave as normal distribution. Sample means and standard deviations were calculated from the data distribution. The two distribution curves overlapped over AE energy values as shown in the probability plot, Figure 7.20. The task is to set a threshold x for detection of the capped tablets from the non-capped ones. The ROC curve in Figure 7.21 shows a plot of false positive rate i.e. false alarm rate (x-axis) against true positive rate i.e. detection rate (y-axis). A very high detection rate of 95% was achieved at minimum false alarm rate. Specifically, if the energy threshold value (x) is set at 1.2×10^8 the false alarm probability is approximately 5% and the detection rate is 95%.

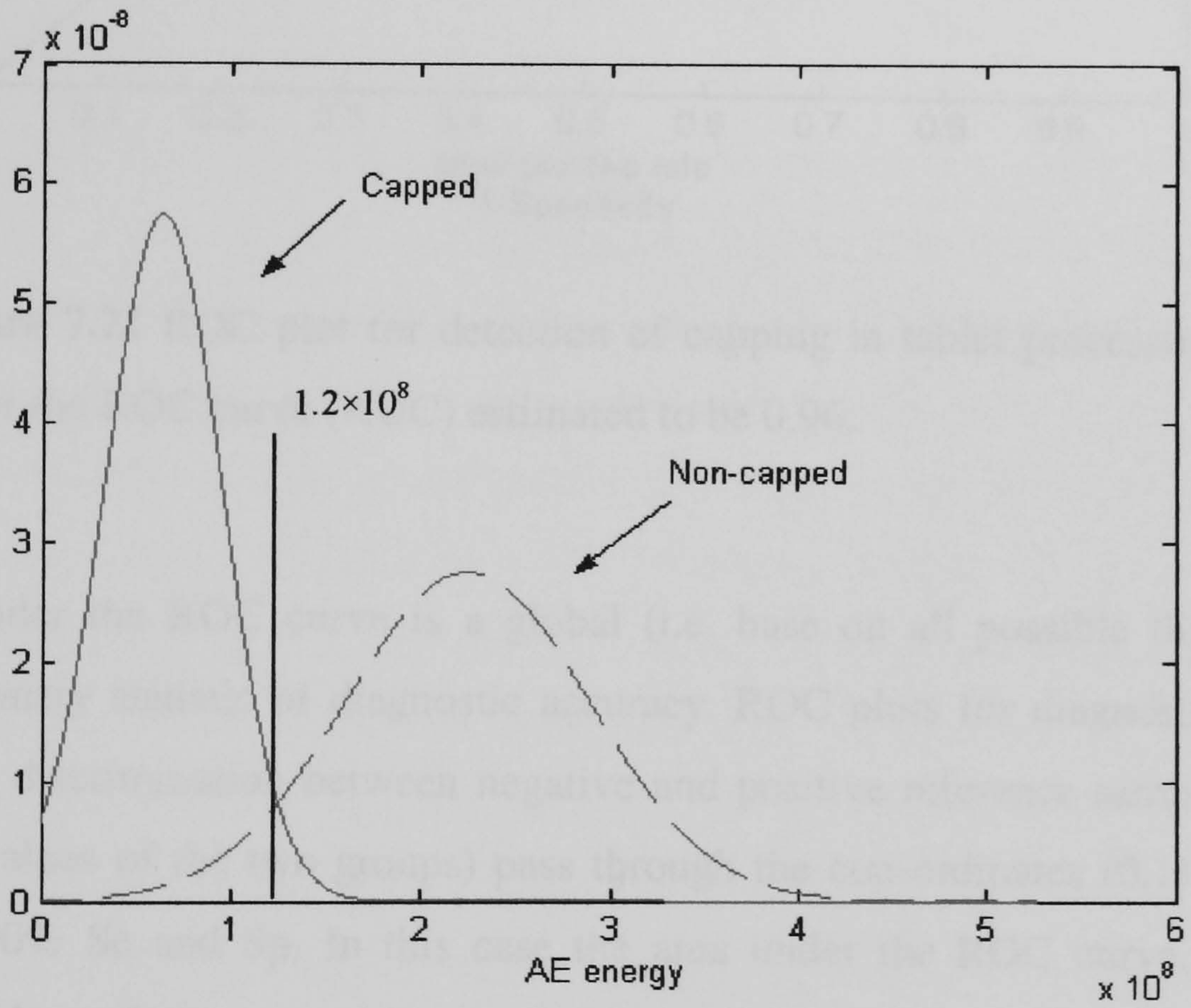

Figure 7.20 Probability densities of capped (solid line) and non-capped (dashed line) tablets

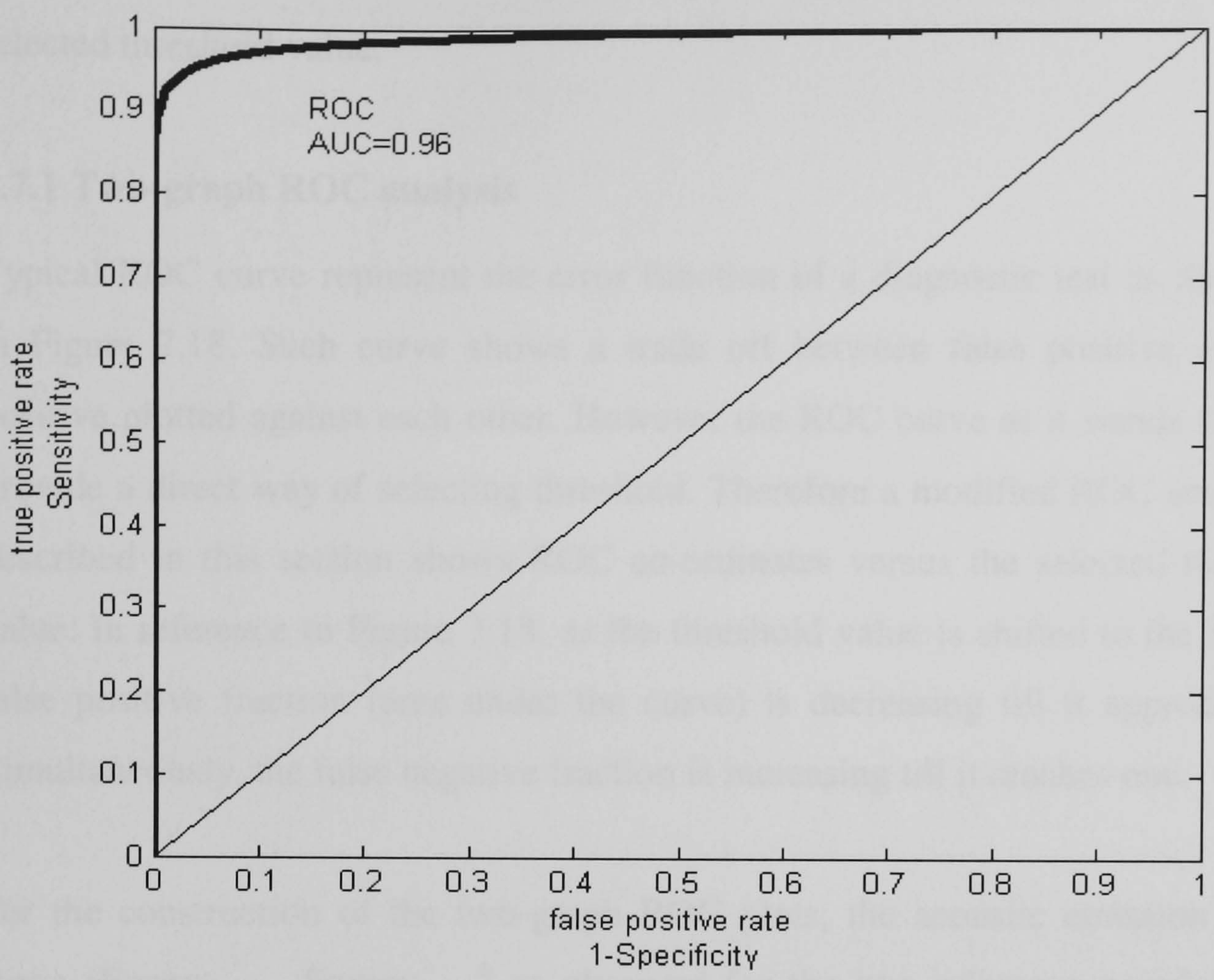

Figure 7.21 ROC plot for detection of capping in tablet processing; area under the ROC curve (AUC) estimated to be 0.96.

The area under the ROC curve is a global (i.e. base on all possible threshold values) summary statistic of diagnostic accuracy. ROC plots for diagnostic tests with perfect discrimination between negative and positive reference samples (no overlap of values of the two groups) pass through the con-ordinates (0,1) which represent 100% Se and Sp. In this case the area under the ROC curve, AUC, would be 1. According to an arbitrary guideline (based on a suggestion by Swets, 1988), one could distinguish between non-informative (AUC=0.5), less accurate ($0.5<AUC\leq0.7$), moderately accurate ($0.7<AUC\leq0.9$), highly accurate ($0.9<AUC<1$) and perfect test (AUC=1).

The diagnostic parameters Sp and Se can be described as a function of the selected threshold by receiver operating characteristic ROC as it has been shown. However, it is not possible to read any threshold value for a selected combination of Se and Sp directly from an ROC plot. Therefore, a modified ROC analysis is

described in this thesis, which depicts both test parameters separately versus the selected threshold value.

7.7.1 Two-graph ROC analysis

Typical ROC curve represent the error function of a diagnostic test as illustrated in Figure 7.18. Such curve shows a trade off between false positive and true positive plotted against each other. However the ROC curve as it stands does not provide a direct way of selecting threshold. Therefore a modified ROC analysis is described in this section shows ROC co-ordinates versus the selected threshold value. In reference to Figure 7.18, as the threshold value is shifted to the left, the false positive fraction (area under the curve) is decreasing till it approaches 0. Simultaneously, the false negative fraction is increasing till it reaches one.

For the construction of the two-graph ROC plots, the acoustic emission energy range (Energy $_{min}$, Energy $_{max}$) as observed for the two reference populations is divided arithmetically into 5000 intervals with the resulting limits termed thresholds (x_j). Se_j and Sp_j obtained with each threshold value are calculated as the proportion of positive results in the positive and negative results in the negative reference populations, respectively. The resulting matrix of x_j and the corresponding fraction Se_j and Sp_j (j= 1, …, 5000) are displayed as a multiple x-plot, representing the two observed parameters over the specified range of AE energy value. The threshold (x_0) that realises equal test parameters $Se_j = Sp_j$ can be read from the intersection point of the two graphs (point of equivalence).
Figure 7.22 shows the representation of the ROC co-ordinates as a function of the selected threshold over the entire range of AE energy.

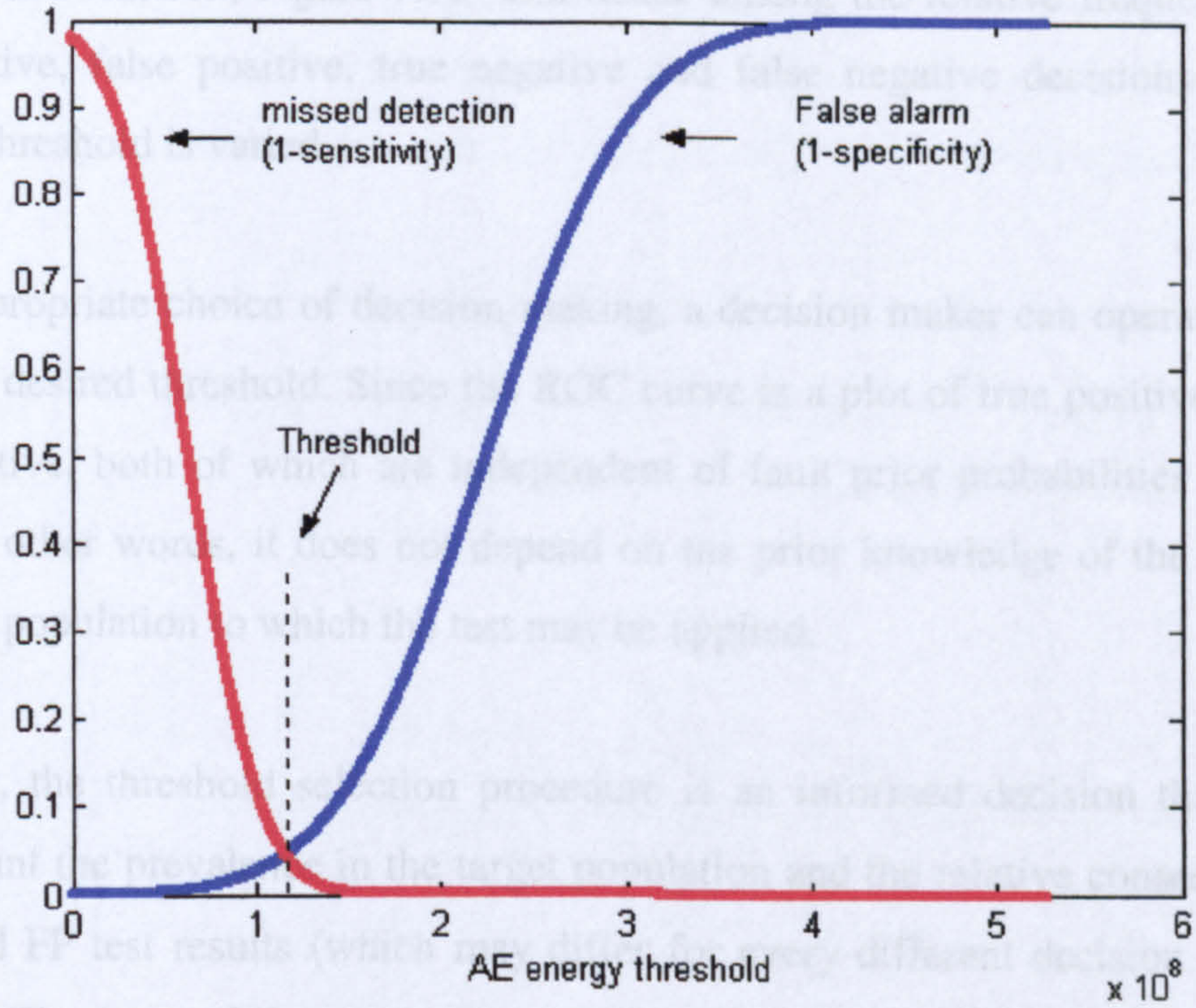

Figure 7.22 Plot of diagnostic sensitivity (Se) and specificity (Sp) of tablet production as a function of selected threshold.

7.8.2 ROC analysis and threshold selection

Threshold values for diagnostic test can be derived using different methods. In this present work it was shown that a threshold value is defined as the mean minus two standard deviation (2SD) of the negative reference sample.

Two parameters (Se and Sp) are necessary to fully describe the probabilities of the four possible test outcomes (TP= true-positive, TN=true-negative, FP= false-positive and FN=false-negative). A plot of Se and Sp as a function of the threshold values provides an useful visualization and can also be used to derive two threshold values for the definition of intermediate test results (i.e. test results that are considered non-negative and non-positive) as the case in lamination, particularly when the lamination is not so severe. However the present studies has shown that for the capping it is much easier to distinguish between capped tablet and non-capped tablet.

Essentially, a conventional ROC curve as the one shown in the present studies describes the compromises that can be made between true positive fraction and

false positive fraction, Figure 7.18- and hence among the relative frequencies of true positive, false positive, true negative and false negative decisions- as the decision threshold is varied.

By an appropriate choice of decision-making, a decision maker can operate at (or near) any desired threshold. Since the ROC curve is a plot of true positive versus false positive, both of which are independent of fault prior probabilities (Swets, 1978). In other words, it does not depend on the prior knowledge of the fault in the actual population to which the test may be applied.

Optimally, the threshold selection procedure is an informed decision that takes into account the prevalence in the target population and the relative consequences of FN and FP test results (which may differ for every different decision making situation). The issue of choosing an optimal operating point will be dealt with in a later section of this chapter, but a few comments seem appropriate here. As an example, given a pharmaceutical powder processing of low capping prevalence and high cost of false-positive diagnoses, it may be advisable to choose a threshold at the lower part of the curve to maximise Sp and to keep false positive fraction small. Otherwise almost all positive decisions will be false positive decisions. Also, if the consequences of false positive decision are overridingly bad, false positive must again be kept small. In either or both situations, the decision maker should operate on the lower left part of the ROC curve to keep the false positive small.

If on the other hand, the capping occurs at high prevalence and missing any capped tablet has serious consequences, a threshold value towards the upper part of the curve would be selected to maximise Se and the decision maker should adjust his decision threshold to operate higher on the curve, accepting a higher false positive in order to keep the true positive fraction high and the false negative fraction low.

Table 7.1 shows the effect of threshold setting on the ROC curve parameters sensitivity and specificity. Shifting the threshold to the right hand side in Figure 7.20 would result in increase in the percentage of sensitivity (true positive).

Youden's index (Youden , 1950), J=Se+Sp-1, at a given threshold value is a useful measures for minimising the total number of misclassifications. Figure 7.23 shows Youden's index as a function of the entire range of threshold values.

Table 7.1 Assessment scores for threshold setting

Case 1	Threshold	Sensitivity %	Specificity %	Youden index
1	1	90	97	.85
2	1.2	93	95	.88
3	1.4	97	91	.91
4	1.6	98	88	.86
5	1.8	99	78	.74
6	2	99	70	.65

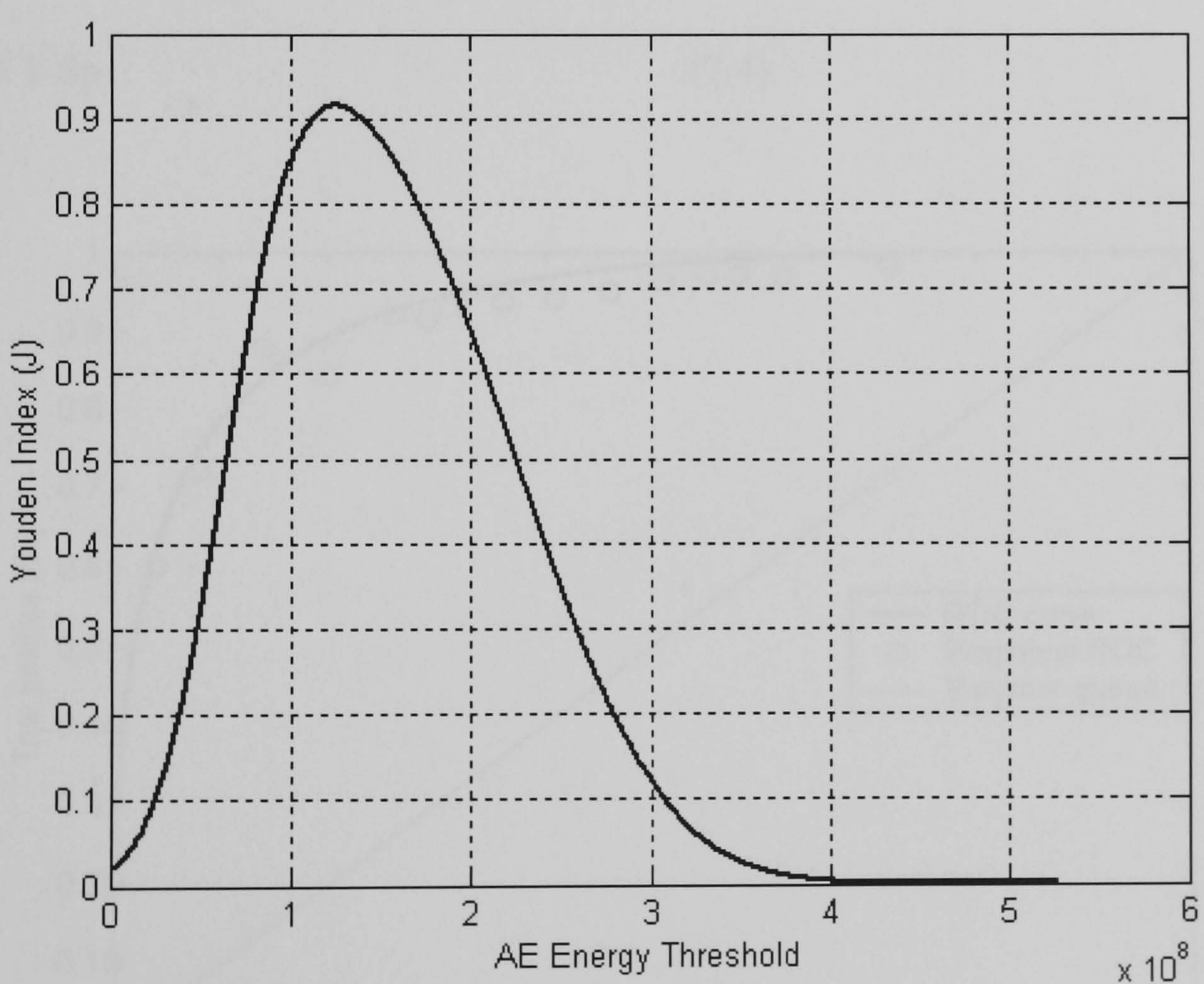

Figure 7.23 Youden's index as function of threshold

Figure 7.24 shows the ROC curve generated from the compression of microcrystalline cellulose powder. The solid line shows the theoretical ROC curve

based on only the mean and standard deviation of the data. The area under the ROC curve is AUC= 0.85; this area was computed with a MATLAB programas described in Appendix D.

Similarly Figure 7.25 shows similar analysis for Aspartame compression. This material showed high tendency toward capping, as the flowability of the material is very poor in comparison with lactose and microcrystalline cellulose. Hence capping occurred more frequently during continuous tabletting. The area under the curve is now, AUC = 0.8167.

The theoretical ROC co-ordinates were calculated using equation 7.1 as follows:

$$\text{TN} = \text{Se} = \int_{-\infty}^{x} Pp(x)dx \qquad (7.2)$$

where P_p (x) has mean μ_p and standard deviation σ_p

$$\text{Sp} = \int_{x}^{\infty} Pn(x)dx \qquad (7.3)$$

where P_n (x) has mean μ_n and standard deviation σ_n

$$\text{FP} = 1\text{-Sp} \qquad (7.4)$$

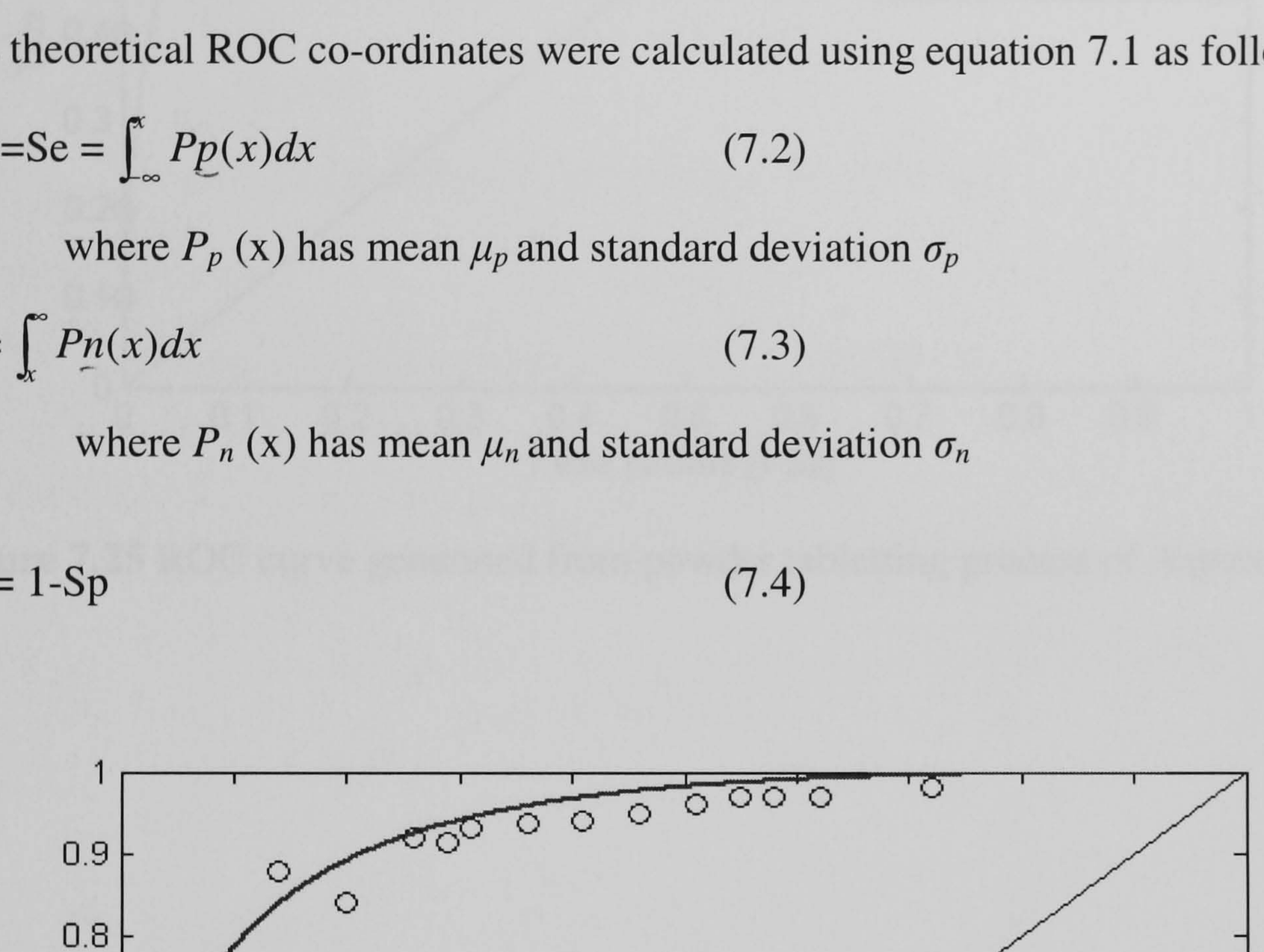

Figure 7.24 ROC curve generated from powder tabletting process of microcrystalline cellulose.

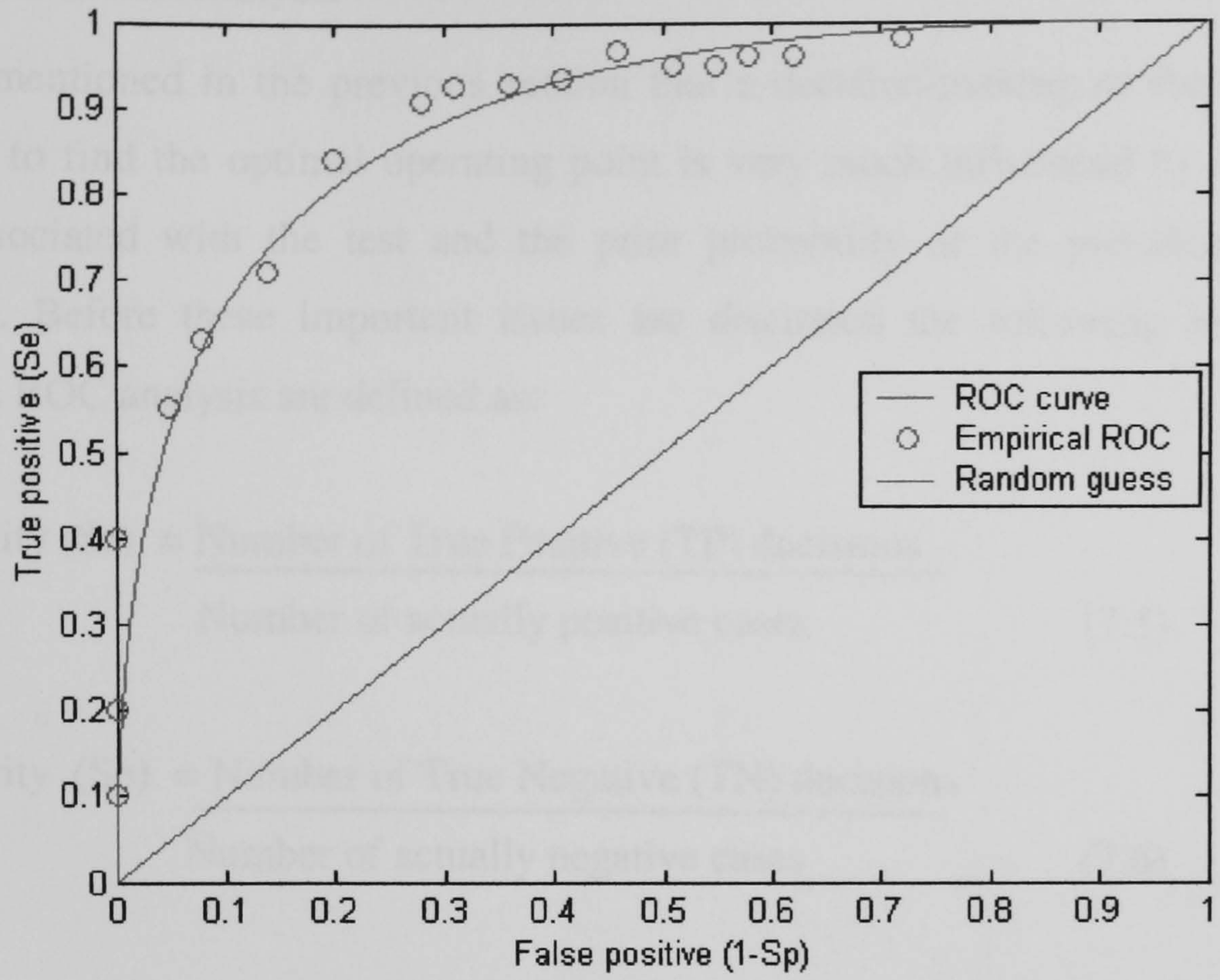

Figure 7.25 ROC curve generated from powder tabletting process of Aspartame.

7.8 Cost Benefit Analysis

It was mentioned in the previous section that a decision-making of the capping process to find the optimal operating point is very much influenced by both the cost associated with the test and the prior probability or the prevalence of a capping. Before these important issues are discussed the following important terms in ROC analysis are defined as:

$$\text{Sensitivity (Se)} = \frac{\text{Number of True Positive (TP) decisions}}{\text{Number of actually positive cases}} \quad (7.5)$$

$$\text{Specificity (Sp)} = \frac{\text{Number of True Negative (TN) decisions}}{\text{Number of actually negative cases}} \quad (7.6)$$

In effect, sensitivity and specificity represent two kinds of accuracy: the first for actually positive cases and the second for actually negative cases. One must note carefully that the term "positive" and "negative" in these definitions concern some particular state, which must be specified clearly in calculating and quoting sensitivity and specificity values. In our case positive means a capped-tablet and negative means a non-capped tablet.

Accuracy, or the fraction of the study population that is decided correctly, is related to sensitivity and specificity by the simple formula:

$$\begin{aligned}\text{Accuracy} = {} & \text{Se} \times (\text{fraction of the study population that is actually positive}) \\ & + \text{Sp} \times (\text{fraction of the study population that is actually negative})\end{aligned} \quad (7.7)$$

True positive fraction (TPF), Figure 7.26, is simply the same thing as sensitivity, and true negative fraction (TNF) is simply the same as specificity. These two terms suggest another two definitions.

False positive fraction (FPF), Figure 7.26, is the ratio between the number of false positive decisions and the number of actually negative cases. Also, False negative fraction (FNF) is the ratio between the number of false negative decisions and the

number of actually positive cases. Therefore FPF and FNF represents respectively, the factions of actually negative cases and of actually positive cases that are decided incorrectly.

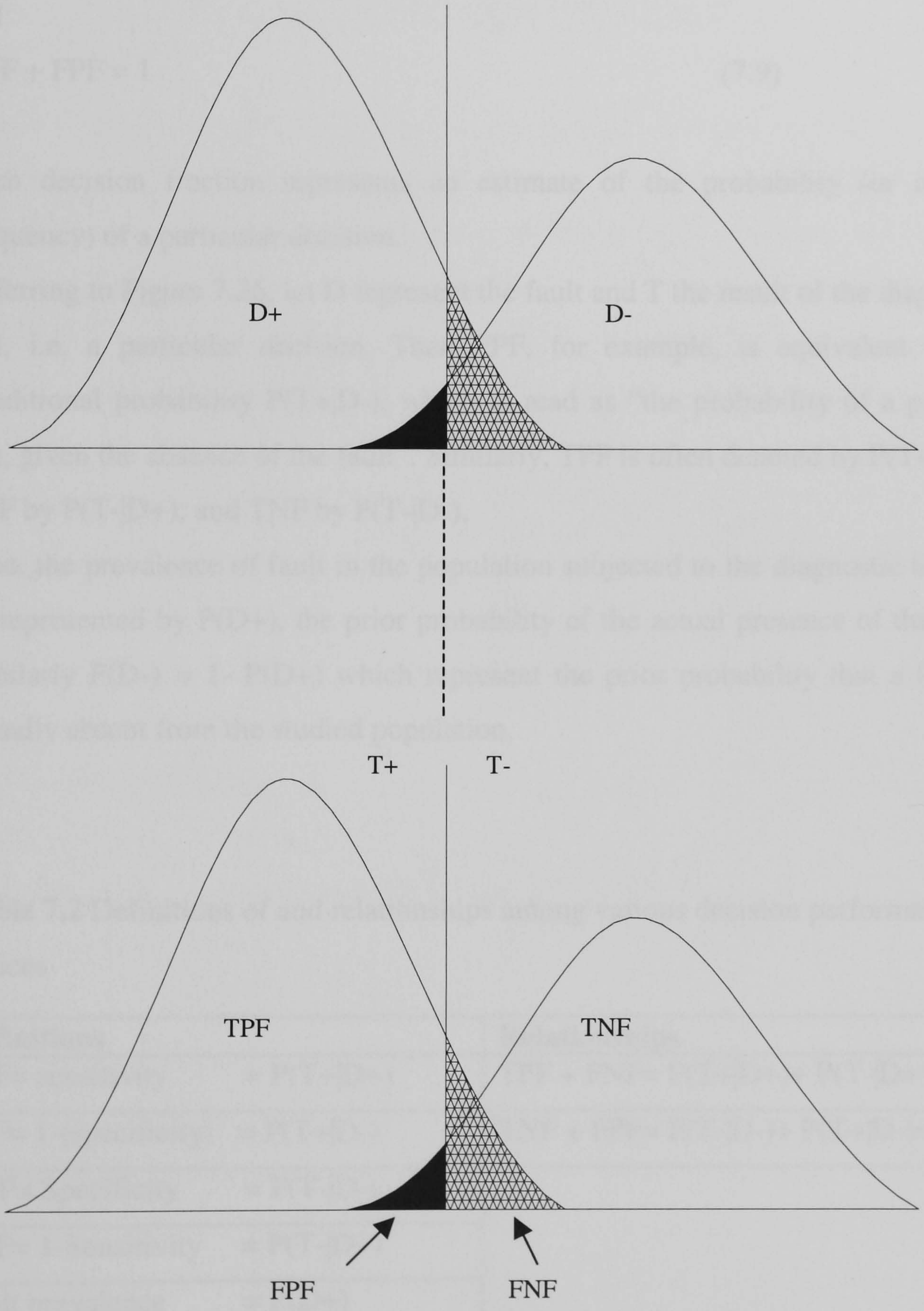

Figure 7.26 Diagram illustrates the four outcomes of a diagnostic test.

Now during a test, all cases are diagnosed as either positive or negative (with respect to a specified fault). Hence the fraction of correct decision plus the fraction of incorrect decisions must equal one. Thus it is easy to show that the various fractions defined above must be related by:

$$TPF + FNF = 1 \qquad (7.8)$$

and

$$TNF + FPF = 1 \qquad (7.9)$$

Each decision fraction represents an estimate of the probability (or relative frequency) of a particular decision.

Referring to Figure 7.26, let D represent the fault and T the result of the diagnostic test, i.e. a particular decision. Then FPF, for example, is equivalent to the conditional probability P(T+|D-), which is read as "the probability of a positive test, given the absence of the fault". Similarly, TPF is often denoted by P(T+|D+) ; FNF by P(T-|D+); and TNF by P(T-|D-).

Also, the prevalence of fault in the population subjected to the diagnostic test can be represented by P(D+), the prior probability of the actual presence of the fault. Similarly P(D-) = 1- P(D+) which represent the prior probability that a fault is actually absent from the studied population.

Table 7.2 Definitions of and relationships among various decision performance indices

Definitions	**Relationships**
TPF= sensitivity = P(T+|D+)	TPF + FNF= P(T+|D+)+ P(T-|D+)=1
FPF= 1-(specificity) = P(T+|D-)	TNF + FPF= P(T-|D-)+ P(T+|D-)=1
TNF= Specificity = P(T-|D-)	
FNF= 1-Sensitivity = P(T-|D+)	
Fault prevalence = P(D+)	

Let C_0 be the cost of performing a diagnostic test. Also the costs of outcome consequences of every decision need to be added. One must weigh each of the decision consequence costs by the probability that the type of decision in question occurs. Thus the average cost C resulting from the use of the diagnostic test can be expressed as:

$$C= C_0 + C_{TP} \times P(TP) + C_{TN} \times P(TN) + C_{FP} \times P(FP) + C_{FN} \times P(FN) \qquad (7.10)$$

where P(TP) is the probability that a true positive decision is made, and C_{TP} represents the average cost of the fault consequences of a true positive decision.
The probability of a true positive decision, P(TP), is equal to the probability that a case from the population studied is actually positive, P(D+), multiplied by the probability that an actually positive case will be diagnosed as positive using the test in question, P(T+|D+). Thus we can replace P(TP) by P(D+) P(T+|D+).
Similarly:

$$P(TN)= P(D-)\, P(T-|D-) \qquad (7.11)$$

$$P(FP)= P(D-)\, P(T+|D-) \qquad (7.12)$$

$$P(FN)= P(D+)\, P(T-|D+) \qquad (7.13)$$

And previously it has been established that

$$P(T-|D+)= 1- P(T+|D+)$$

and that

$$P(T-|D-)= 1- P(T+|D-)$$

Therefore, the average cost can be written as

$$\begin{aligned} C= C_0 &+ C_{TP} \times P(D+) \times P(T+|D+) \\ &+ C_{TN} \times P(D-) \times [1- P(T+|D-)] \\ &+ C_{FP} \times P(D-) \times P(T+|D-) \\ &+ C_{FN} \times P(D+) \times [1- P(T+|D+)] \end{aligned} \qquad (7.14)$$

Rearrange Eq (7.14) to give

$$C= -\{[C_{FN}-C_{TP}]\times P(D+)\}\times P(T+|D+)$$
$$+\{[C_{FP}-C_{TN}]\times P(D-)\}\times (T+|D-)$$
$$+\{C_0+C_{TN}\times P(D-)+C_{FN}\times P(D+)\} \qquad (7.15)$$

The average diagnostic cost depends on both P(T+|D+) and P(T+|D-), which are the same as TPF and FPF respectively and are the coordinates of an ROC curve. The average cost depends on the decision threshold used and usually can be made larger or smaller. Thus, in terms of cost benefit analysis, the best operating point that minimises average cost and accordingly maximise average benefit in a particular applied diagnostic situation.

The above average cost expression is in the form of:

$$C= k_1 P(T+|D+) + k_2 P(T+|D-) + k_3 \qquad (7.16)$$

where ,

$k_1= -\{[C_{FN}-C_{TP}]\times P(D+)\}$,

$k_2= -\{[C_{FP}-C_{TN}]\times P(D-)\}$ and

$k_3= \{c_0+C_{TN}\times P(D-)+C_{FN}\times P(D+)\}$

By differentiating and setting dC = 0, the optimal operating point must occur where the ROC curve slope is given by:

$$dC= k_1[dP(T+|D+)] + k_2[dP(T+|D-)] = 0$$

Therefore,

$$\frac{dP(T+|D+)}{dP(T+|D-)} = -\frac{k_2}{k_1} = R, \text{ the slope on the ROC curve}$$

$$R = \frac{P(D-)}{P(D+)}\times\frac{[C_{FP}-C_{TN}]}{[C_{FN}-C_{TP}]} \qquad (7.17)$$

The above expression shows the slope of the operating line at the optimal condition. This would achieve the minimum cost of classification. Investigating the above expression reveals that the slope is dependent on both the cost of consequences associated with choosing a threshold and the prior knowledge of fault occurrence. If the ratio of prior knowledge is known this will make the

decision making much easier, however in many condition monitoring situations this ratio on the occurrence of a fault is not always easy to determine due to process variation and other aspects related to the process itself. In such a situation the operator faces a much more difficult challenge in decision making.

In our application, the pharmaceutical powder compression, it is assumed that the prior knowledge of the fault occurrences is known for at least a specific condition.

The second ratio in Eq. 7.17 can be dissected into its component parts regarding the eventual outcomes of the test result. Two perspectives for evaluating the net costs to net benefits are available, depending on whether one wants to view outcomes as either 'costs' (in a negative frame) or as 'utilities' (in a positive frame). In the first perspective, cost is a negative outcome measure, referring to the negative effects in terms of monetary cost, adverse health risks, or combination of the two. The following is the framework developed by Metz and Weinstein and Fineberg. In general:

$$C/B = (C_{TN}-C_{FP})/C_{TP}-C_{FN}) \qquad (7.18)$$

where

C_{TN} cost of a true negative result; typically best outcome of not having capping

C_{FP} cost of false positive alarm result

C_{TN} cost of true positive result

C_{FN} cost of false negative result; typically worst outcome of missed case

In the second perspective, outcomes can be viewed in terms of utilities, 'utility' being a positively framed outcome measure that refers to monetary savings, health benefits, or a combination of the two. It should be noted that utility refers to a generally positive outcome measure and not necessarily a utility defined in the Von Neumann-Morgenstern (1953) framework as an outcome evaluated using the standard gamble method. The paradigm of using utilities in the ratio of net costs to net benefits was developed by Sox *et al* (1988):

$$C/B= (U_{TN}- U_{FP})/(U_{TP}- F_{TN}) \qquad (7.19)$$

where

U_{TN} utility of a true negative result; typically best outcome of not having fault

U_{FP} utility of a false positive result

U_{TP} utility of a true positive result

F_{TN} utility of a false negative result; typically worst outcome of missed case

Consider the effect of prior probability or the prevalence of capping. For a process of low capping occurrences which typically result in more false positive (false alarm) than true positive and for a condition in which a false positive would result high cost of dealing with capping, the operator should select a threshold that yield a fewer false positives, such segment in the ROC as in the lower left of the ROC curve. A tangent line therefore has steep slope.

In other words, P(D+) would be much less than 1.00 and P(D-) =1-P(D+) will be near to 1. Thus the ratio P(D-)/P(D+) will be large for the case of lactose and Avicel powders. The decision maker should operate towards the lower left portion of his ROC curve (where TPF is small but FPF is much smaller) by using a relatively strict decision threshold. Because otherwise almost all positive decisions will be false positive decisions.

Conversely, when the capping in the test is so common so that P(D-) is small, the best operating point is towards the upper right part of the ROC curve where TPF is high and FPF is high also. Otherwise, in this situation almost all negative decisions would be false negative decisions.

The issue of prevalence can also be viewed as one that affects the relative sizes of the two distributions shown in Figure 7.20. Thus if capping occurs on average say, one every ten times, then, the distribution for capped tablets has an area which is 1/10 that as the non-capped tablets. Then a plot of the missed detection and false alarm curves from these two distributions similar to Figure 7.22 will give the required threshold.

To consider the effect of the various decision consequences costs, note that the difference between the costs of false positive and of a true negative decision C_{FP}-C_{TN} is much greater than the difference between the costs of a false negative and of a true positive decision C_{FN}-C_{TP} (which might be the situation if capping cost or

further consequences were high. Then the optimal curve slope is large. Thus, both TPF and FPF are best kept small, because otherwise more loss would be incurred by the FP decisions than benefit would be done by true positive decisions.
Conversely, if C_{FP}-C_{TN}<< C_{FN}-C_{TP} as would be true if capping cost and further cost are relatively small, then the decision maker should be operating high and to the right on the ROC curve, and TPF should be kept large even at the expense of large FPF.

If the penalty cost is the same for FP and FN, then the threshold should be set such that the areas for FPF and FNF are equal. Likewise, differential penalty costs can be handled by adjusting the areas of the distributions.

Let

α = cost of a false positive (false alarm)

β = cost of missing a positive (false negative)

p = proportion of positive cases

Then the average expected cost of classification at point (x, y) in the ROC space is

$$C= (1\text{-}p)\ \alpha x + p\ \beta (1\text{-}y) \qquad (7.20)$$

The following are various scenarios that are possible during a diagnostic test:

Scenario one

Isocost lines (lines of equal) costs are parallel and straight. Their gradients depend upon the cost ratio and prior probabilities ratio as shown in Figure 7.20. If the costs are equal (α =β) and the proportion of positive cases is 50% i.e. p =0.5, the gradient is 1 and the isocost lines are at 45 degrees.

Scenario two

If the cost of missing negative cases outweighs the cost of missing positive cases by ten to one. (e.g. p=0.5, α = 1,β =10), then the gradient would be much steeper.

Scenario three

If the cost of missing a positive case outweighs ten fold the cost of raising a false alarm, that is when it is much more important to maintain a high true positive rate and the negative case has little impact on the total costs, then the gradient would be nearly horizontal.

If the costs associated with classification are a simple sum of the cost of misclassifying positive and negative cases then all points on a straight line (whose gradient is given by the importance of the positive and negative examples) have the same cost. If the cost of misclassifying positive and negative cases are the same, and positive and negative cases occur equally often then the line has a slope of 1, that is, at 45 degrees. The best place to operate the classifier is the point on its ROC which lies on a 45-degree line closest to the north-west corner (0,1) of the ROC plot.

The misclassification cost term (MCT) can be found from the following expression:

$$MCT = \frac{C_{FN}}{C_{FP}} P(D+)(1 - Se) + P(D-)(1 - Sp) \qquad (7.21)$$

Efficiency is represented as

$$Ef = P(\mathrm{D+})\, Se + P(\mathrm{D-})\, Sp \qquad (7.22)$$

where P(D+) is the percentage of fault occurrence. Figure 7.27 shows the efficiency as a function of the threshold value that discriminates between capped and non-capped tablets over the range of theoretical prediction of capping occurrences for the example as described in Figure 7.25. The above expression for determining the efficiency is dependent on the prevalence or the occurrence of capping during tablet processing.

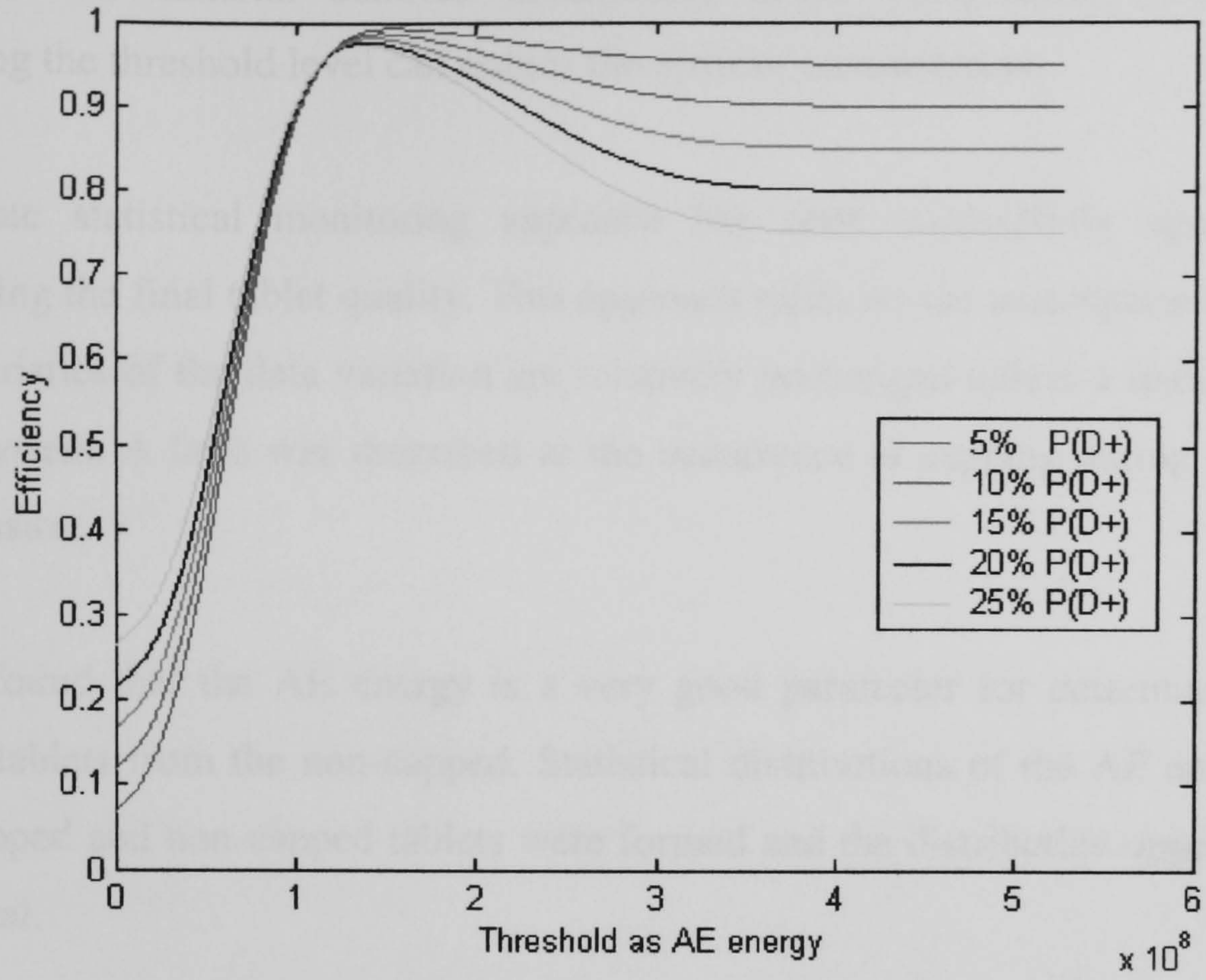

Figure 7.27 Efficiency measure as function of threshold setting for a range of proportions of capping occurrence (%).

7.10 Conclusions

This chapter described condition monitoring of powder compression during tabletting with emphasis on capping and lamination as the major problem associated with this tablet processing. Initial investigation revealed that AE monitoring is useful for detecting abnormalities within tablet manufacturing. AE monitoring based on recording the traditional features such as count, average signal level, peak amplitude, AErms and absolute energy was shown to be a good approach for detection of problems such as capping and lamination. A condition monitoring system was proposed based on setting an alarm threshold for abnormalities detection. Initially it is desirable to establish the distribution of AE parameter for good tablets and bad tablets. A threshold can be determined as a level below the mean plus 2 to 3 standard deviations of the good tablets. However, the threshold level can be adjusted based on initial measurement and knowledge

about how a material behaves acoustically under compression conditions. Adjusting the threshold level can reduce the error of measurement.

Univariate statistical monitoring approach has been successfully applied to monitoring the final tablet quality. This approach relies on the assumption that the characteristics of the data variation are relatively unchanged unless a fault occurs in the system. A fault was described as the occurrence of capping during powder compression.

It was found that the AE energy is a very good parameter for determining the capped tablets from the non-capped. Statistical distributions of the AE energy of both capped and non-capped tablets were formed and the distribution appeared to be normal.

The monitoring system employs a threshold setting to determine the detection rate and the false alarm rate. A plot of true positive fraction versus false positive fraction was constructed for a number of pharmaceutical material. This plot is called the receiver operating characteristic (ROC) curve for the diagnostic test, since it describes the inherent detection *characteristics* of the test and since the *receiver* of the test information can *operate* at any point on the curve by using an appropriate decision threshold. The decision-making process was discussed in this chapter based upon prior knowledge of capping and cost benefit analysis.
The data showed a very good detection rate of 95% of good tablet against 5% of false alarm rate. A modified ROC curve was also proposed as it shows the ROC parameters as a function of the entire range of threshold values.

Two method of threshold setting were presented. The first, based on the area under the two distributions of the two tablets conditions. This assumed equal penalty cost for both capped and non-capped tablet. The modified two-graph ROC curve enable setting a threshold directly from the point of intersection between the two errors curves i.e. false alarm and missed detection. The second method requires prior knowledge of capping prevalence and penalty costs. This information enable an operator to determine the slope of the ROC curve which reflect the optimal operating point.

References

Funakoshi Y. (1975), Some observation on the capping properties detected in the tablet making compaction process, Zairoyo **24** 673-676.

Funakoshi Y., Kajuira T. And Asogowa T. (1969) Ruling factors of cappping in the compressing process and the method of preventing capping, Zairyo **18** 547-553.

Galen, R. S (1986) Use of predictive value theory in clinical immunology. In: N. R. Rose, H, Friedmann and J.L Fahey (Eds), Manual of Clinical Laboratory Immunology. American Society of Microbiology, Washington, DC, pp. 966-970.

Greiner M, Pfeiffer D, and Smith R. D, Principles and practical application of the receiver-operating characteristic analysis for diagnostic tests. Preventive Veterinary Medicine **45**, 23-41.

Jarosz P. J and Parrot E. L. (1982) Factors influencing axial and radial tensile strengths of tablets.

Jones T. M. (1983) Tablets, Tabloids ... and Tabloids. Pharm. J,. Sept 17 301-307.

Little A and Mitchel K.A. (1951), Tablet Making, Northern Publishing Co.

Metz C.E (1978) Basic principles of ROC analysis. Semin Nucl Med, **8**: 283-298.

Nystrom C., Alex W and Malmqvist K. (1977) New Approach to tensile strength measurement of tablets. Acta. Pharm. Suec. **14** 317-320.

Nystrom C., Malmqvist K., Mazier J., Alex W., and Holzer A. W. (1978) Measurement of axial and radial tensile strength of tablet and their relation to capping.

Ritter A and Sucker H. B, (1980) Studies of Variables that effect Tablet Capping, Pharm. Tech. March 57-65 and 128.

Seitz J A and Flessland G. M (1965), Evaluation of the physical Properties of Compressed Tablet 1: Tablet Hardness and Friability, J. Pharm. Sci. (54) **9** 1353-1357.

Shatter, H, (1989). Constructing a cut-off point for a quantitative diagnostic test. Stat. Med. **8**, 1381-1391.

Smith, R.D. (1991) Evaluating of diagnostic tests. In: R.D. Worth-Heinemann, Stoneham, pp. 29-43.

Vizard, A., Anderson, G.A and Gasser, R.B (1990) Determination of the optimum cut off value of a diagnostic test. Prev. Vet. Med. **10**, 137-143.

Von Neumann J, Morgenstern O (1953). Theory of Games and Economic Behavior. Princeton: Princeton University Press.

Weinstein MC, Fineberg HV1980. Clinical Decision Analysis. Philadelphia: W.B. Saunders.

Youden , D. (1950) Index for rating diagnostic tests. Cancer 3, 32-35.

Chapter 8 Proposed tablet condition monitoring system

8.1 Introduction

This chapter provides a description of the AE condition monitoring system for powder compression during tabletting. It describes the proposed condition monitoring system which includes both AE and non-AE measurements. This chapter also provides guidelines about how to implement this system in tablet production environment.

8.2 Acoustic emission measurement and data collection

Figure 8.1 shows a block diagram of the proposed tablet condition monitoring based upon acoustic emission and non-acoustic emission measurements. Acoustic emission is performed to record the AE signal that is generated from powder compression during the production of a pharmaceutical tablet. The AE measurement is for capturing the raw signal, extract traditional AE features such as the ring down count (RDC), peak amplitude (PA), rise time (RT), AE energy, average signal level (ASL) and other features of interest that the operator would like to monitor. Details of acoustic emission measurement and requirements were discussed in Chapter 4. There are a wide range of commercial software packages which are user friendly and which can be programmed for AE data recording and analysis as well. It is very important to maintain the sensor location at a fixed position throughout all measurements.

8.3 Trend analysis of AE data

The first level of AE data analysis aims to observe trends in the AE traditional features. For example, to observe changes in RMS level, ASL, Energy peak level and highest peak amplitude. Certain features maybe respond to physical changes in tabletting much more than others. The operator will be interested to observe changes or trends within the individual AE features in a real time situation. This research has shown that acoustic emission energy is a good feature for monitoring the final quality of a pharmaceutical tablet and in detecting capping phenomenon in tabletting. As the AE energy is sensitive to various mechanisms that are generate AE during compression cycles. It is important to mention here again that signal pre-processing is a very important step prior to any further

analysis. The pre-processing is performed to remove unwanted AE events that are not of interest such as mechanical noise, friction and events produced at the beginning of the monitoring such as those emanated from the first compression cycle.

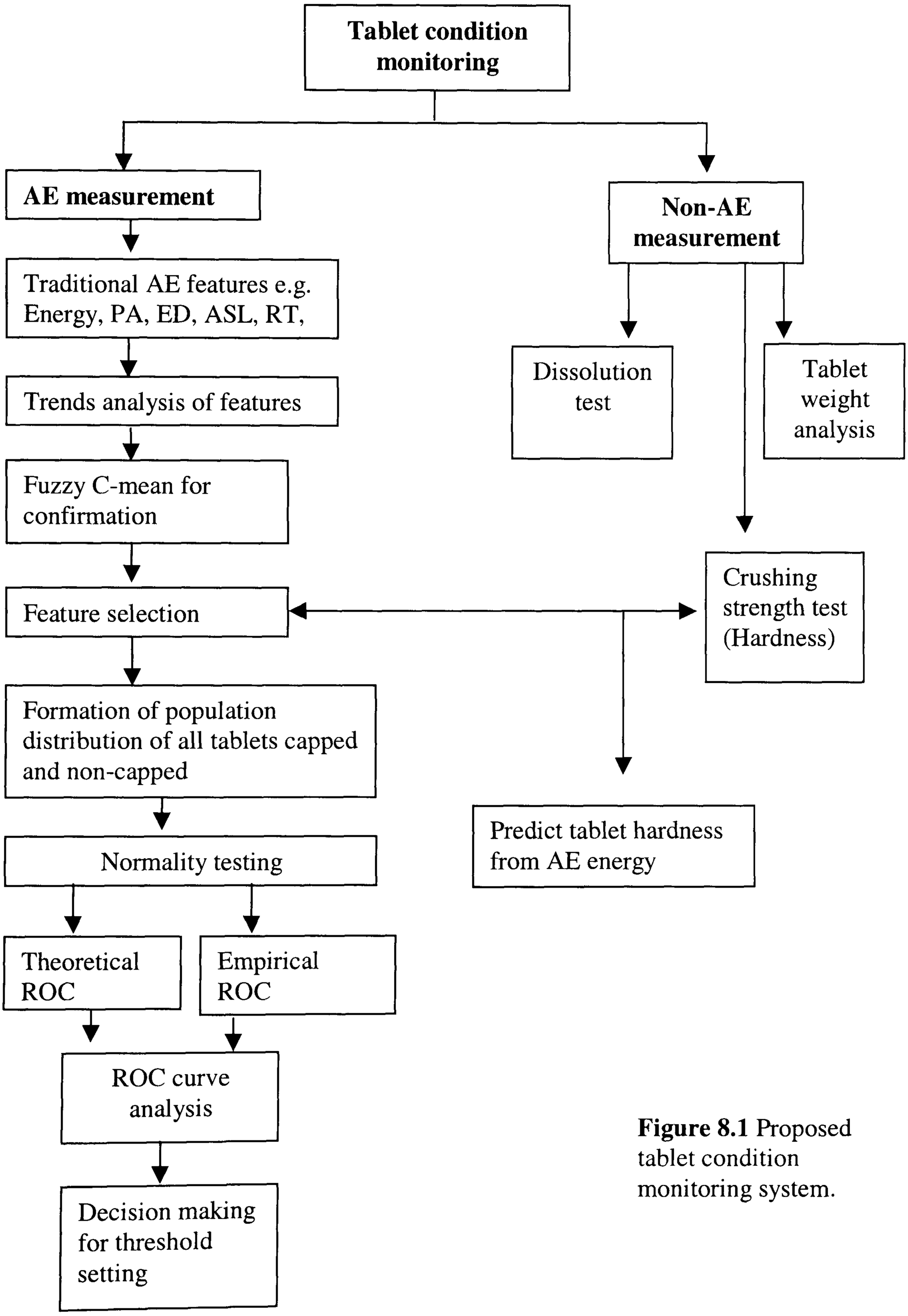

Figure 8.1 Proposed tablet condition monitoring system.

8.4 Classification

This can be performed to serve more than one purpose. One reason is to distinguish between various mechanisms that give rise to AE signal. Fuzzy C-mean clustering was used in this study to distinguish between various mechanisms that generate AE during powder compression. The technique also confirmed that the features selected in our trend analysis are good ones, particularly AE energy and average signal level. It was shown in this research that there are three major events groups that exist during a typical compression cycle using the single tablet press.

8.5 Statistical analysis of distribution

The operator needs to keep track of AE data from the process for both capped and non-capped tablets. This can be followed by forming two distributions of both types. Statistical analysis of the data would suggest whether there is normality in any of the two distributions. Testing for normality can be done as outlined in Appendix D.

8.6 Construction of receiver operating characteristic (ROC)

If the distribution of capped or non-capped or both tablets are normal then a theoretical ROC curve can be constructed based upon the mean and standard deviation of the data and using the equations of two error types outlined in Section 7.8. If one or both distributions are of different forms other than normal, an empirical ROC curve can be generated with appropriate curve fitting.

8.7 ROC analysis

Receiver operating characteristic curve describes the inherent detection *characteristics* of the test and since the *receiver* of the test information can *operate* at any point on the curve by using an appropriate decision threshold. ROC analysis shows the trade off between the true positive (sensitivity) cases versus the false positive cases (1-specificity).

8.8 Decision making (threshold selection)

The final stage of this proposed system is to select a threshold level for detecting capping. The process of selecting threshold depends on both prevalence of capping as well as the various decision consequences.

Figure 8.2 in conjunction with Figure 8.3 illustrate various decisions to different operating conditions. For instance, for a process of low capping occurrences such that more false positive than true positive, it is in the operator interest to select a threshold within region B in Figure 8.2. Such a choice would results a fewer false positives. Conversely, when the capping in the test is so common it is desirable to operate in region C in Figure 8.2 where TP is high but FP is high also.

The diagram in Figure 8.3 summarises the effect of various decision consequences costs on threshold selection. If the difference between the costs of false positive and of a true negative decision C_{FP}-C_{TN} is much greater than the difference between the costs of a false negative and of a true positive decision C_{FN}-C_{TP}. Then the optimal curve slope is large. Thus, both TPF and FPF are best kept small. Conversely, if C_{FP}-C_{TN}<< C_{FN}-C_{TP}, then the decision maker should be operating high and to the right on his ROC curve, and TPF should be kept large even at the expense of large FPF.

If the penalty cost is the same for FP and FN, then the threshold should be set such the area for FPF and FNF are equal. Likewise, differential penalty costs can be handled by adjusting the areas of the distributions.

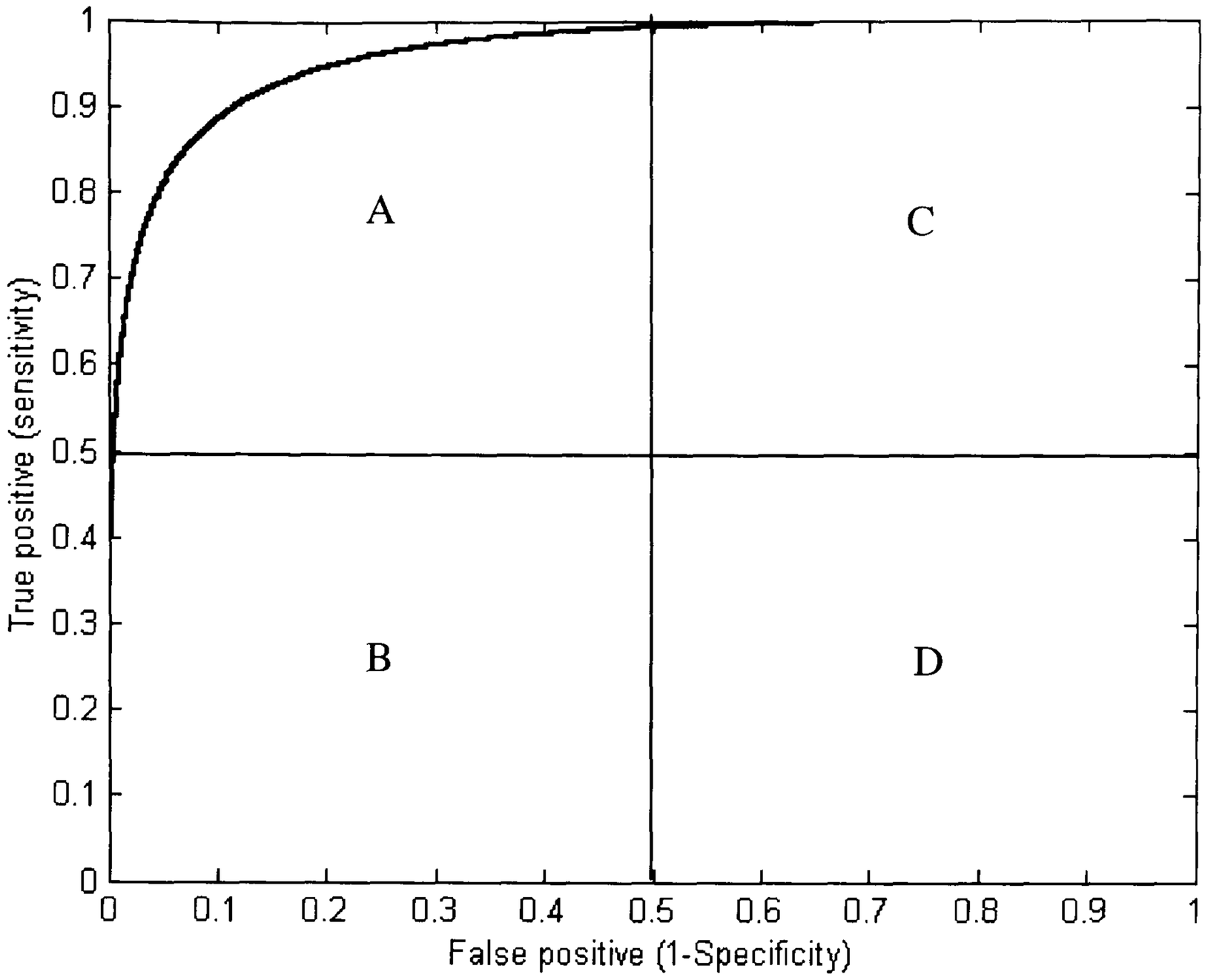

Figure 8.2 ROC curve divided into 4 quadrants for different operating conditions.

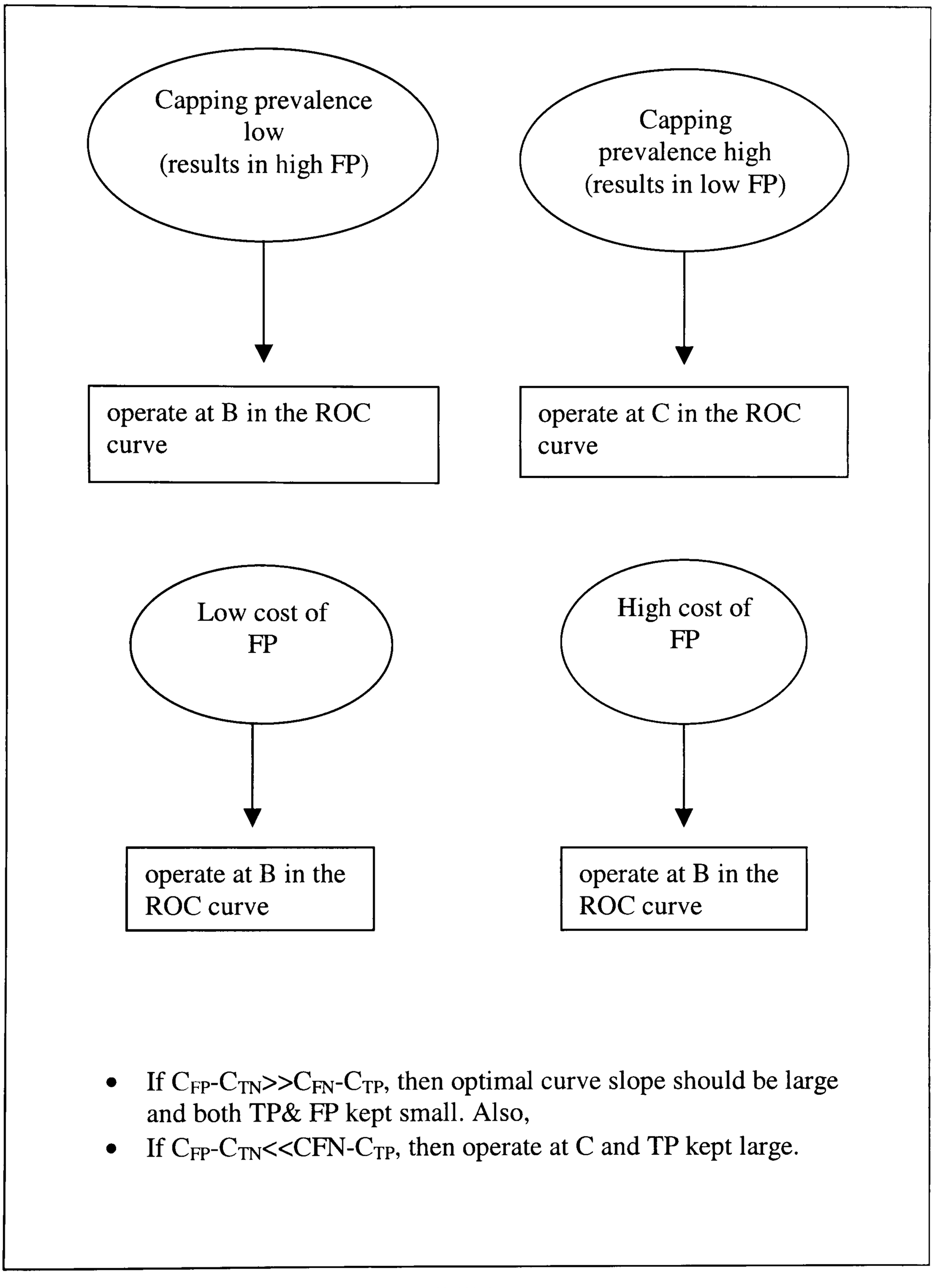

Figure 8.3 Decision making possibilities

8.9 Non-Acoustic emission measurement

This involves recording tablets weight, dissolution test, disintegration test and tablet crushing strength (hardness analysis). The purpose of doing these tests in the proposed system is to investigate possible relationships between AE measurements. It was already shown in this research that the AE energy that is produced from powder compression is proportional to the hardness of the tablets as it is measured by crushing.

8.10 Relationships between AE data and non-acoustic measurement

This research has shown a linear relationship between the AE energy that is emanate from powder compression during tabletting and the hardness of these tablets as it is measured by its crushing strength. This relationship will enable the operator to predict tablet hardness by the non-destructive method using the AE energy (Section 6.7).

Conclusion

The system provided here relies on using traditional time signal features particularly AE energy. The results obtained in this project showed that the AE energy is a good feature for condition monitoring analysis and fault detection in tabletting e.g. capping. However, this is only limited to the data obtained from the industrial tablet press and the materials used in this study.

Although the AE and ROC approach for condition monitoring of tabletting seems to be very good way forward in tabletting control, it is important to note that the analysis was applied to a data generated from a single stroke tablet press and the results shown are limited to the given application detail. In a fast manufacturing environment, there are different types of tablet presses for tablet production, some which has multi-station running simultaneously. Therefore, the results obtained here is limited to Manesty-F-press which is single stroke press.

The advantage of using ROC analysis method here is that regardless of whether the fault and non fault's populations are normal or not, the method still working well. Furthermore, it suggests two ways of threshold setting. The first one is based upon the

area under the two distributions of the two tablet conditions. The second method is require prior knowledge of capping prevalence and penalty costs of capping. The two-graph ROC plot enables the operator to choose the desired threshold directly without prior sophisticated knowledge, an advantage which is not possible using the conventional ROC plot.

Chapter 9

Conclusions & Recommendations

9.1 Tablet condition monitoring

Powder compaction is the process by which material is compressed and compacted into a dense unit form called a tablet. Typically, the process employs punches to compress the material in a die to produce a solid body of a specified shape and size. This process is widely used in the engineering, food and pharmaceutical industries. A review of previous work conducted for powder compression and tablet assessment was provided. This included various techniques and methods used for tablet condition assessment. These techniques such as crushing strength, dissolution, work of failure and friability test are destructive in nature.

This research has shown that acoustic emission is a useful technique not only for characterising powder compression and complex physical changes but also a good condition monitoring technique that can be employed on-line for detecting problems within tabletting. Common problems associated with tabletting include capping and lamination. AE's main advantages appear to be that changes can be monitored during compression, unlike other techniques which have to rely upon post-compressional analysis such as force-displacement analysis, surface area, porosimetry and physical measurement on the compact.

Early investigations in this research revealed a direct relationship between the acoustic emission energy that emanates from the tablet crushing strength test and the peak force that is sufficient to break the tablet during the same tablet crushing test. This particular investigation led to acoustic emission studies conducted on powder compression and establishment of the relationship between the AE parameters and physical properties of a tablet such as its hardness, dissolution and disintegration and compressibility. Furthermore, the AE signal as characterised by the energy parameter was used as a discriminating factor between tablets of good conditions "*not-capped*"

and "*capped* " tablets. This was evident from clustering analysis conducted of 7 AE parameters using fuzzy c-mean technique. Also it was possible to identify the AE events which is generated from only pure powder compression. This particular group of events were used in the proposed condition monitoring between capped and non-capped tablets.

Capping and lamination are serious problems encountered during tabletting and are the phenomena where the tablet no longer retains its integrity. Capping and lamination can be caused by a number of factors but is primarily determined by the visco-elastic behaviour of the powdered materials comprising the tablet. As tabletting speed is increased, the relative elastic component of a given material also increases, giving rise to a higher incidence of capping and lamination. However, capping and lamination can occur randomly depending on the material used in tabletting. It was found in this research that material flowability has a great influence upon capping occurrences. A better flowability results in a more consistent filling of the die cavity, therefore creating tablets of uniform weight. A cavity that is not uniformly filled with powder would lead to tablets of varying hardness and capping tendency.

Experimental investigations on industrial tablet press at GSK site using acoustic emission technique for powder compression monitoring were conducted on a number of common tablets excipients. Traditional AE features such as AE energy, rise time, peak amplitude, event duration and average signal levels were recorded continuously for a repeated compression cycle of 1.2 second. AE energy was shown to be a good feature that enabled proposing a condition monitoring system for tablet condition detection. This is because its sensitivity to capping and lamination occurring during continuous tablet manufacturing performed using the industrial press described in this thesis. It was possible to identify a capped tablet from the drop of the AE energy peaks during on-line monitoring of continuous tabletting in comparison to non-capped tablet which scores higher energy level. A laminated tablets which exhibit low strength also was shown to have low energy level, however, this energy level is much higher than those which generated during capping.

A condition monitoring system was proposed that aimed for setting the AE energy threshold that can discriminate between capped and non-capped tablets based upon statistical distributions of AE energy values of both conditions. The proposed system also shows AE and non-AE measurements and how they are related. The information provided gained by AE monitoring enabled us to predict the hardness of the tablet, a relationship which has been established in this research.

Univariate statistical approach to limit sensing has been used to determine the thresholds for each observation variable (a process variable observed through a transducer e.g. AE energy), where the threshold defines the boundary for operation control. The system aims to minimise the rate of false alarms (indication of a capping when in actuality a capping has not occurred) and the rate of missed detection (an indication of non-capping, though a capping has occurred).

Receiver operating characteristics (ROC) plot was constructed to different materials. The plot can used as a trade-off between the true positive and false positive (false alarm). The co-ordinates of the ROC curve are generated from the areas under the distributions of the two tablet conditions, as shown in Figure 7.18. However the plot as its stand does not provide information about the threshold setting. Hence a modified two graph ROC curve was developed that would enable an operator to choose the condition's operating point. This plot shows the ROC co-ordinate as a function of the threshold value over the entire threshold (AE energy) range for all test outcomes. Two methods of selecting the threshold were presented. The first method was based upon the two-graph ROC curve where the two curves meet to determine the desired threshold. The second method was based on the penalties cost of capping and the prevalence of capping, hence the slope of the ROC curve can be calculated. Prior knowledge of capping occurrence and the costs associated, both have an affect on the decision threshold.

It is important to note that the this proposed condition monitoring system is limited to the type of press used which is single tablet press and the material used in this study. Different types of press, such as multi-stations of tablet production, require

different approaches and analysis and it may be that the system provided here will not be suitable. However, there is a good scope for research and further investigations in this area.

9.2 Summary of findings

The main findings in this research are summarised as follows:

9.2.1 Review of non-AE techniques for tablet evaluation

A literature survey has been conducted to provide a brief account of previous attempts made for tablet evaluations using non-AE techniques. It was concluded that all these techniques are destructive in nature. However, some of these techniques such as crushing strength and disintegration are still in use in the pharmaceutical industry.

9.2.2 Relationship between AE energy and crushing strength

Preliminary experimental investigation in this research showed that the AE energy that is emanated from the crushing strength test is directly proportional to the peak force required to break the tablet during the test (hardness). This relationship was shown to be material independent. This important finding was the motive to investigate the relationship between AE energy and fractures that exists during tabletting.

9.2.3 Acoustic emission monitoring of powder compression cycle

The compression cycle of a typical powder was characterised by the AE signal generated. Pre-compression is the first stage where all particles arrange themselves in the die vicinity. High AE energy level was recorded in this stage in comparison with compression. A noticeable AE peak was also noticed in the post-compression stage. However, these observations differ from one material type to another. Brittle material shows a higher level of emission than plastic material.

9.2.4 Effect of compression speed

Experimental results indicated that as the compression speed increased, the cumulative AE count increased particularly during the initial phase of the compression cycle i.e. particle rearrangement and reorganisation phase. However the total AE count did not show good relationship as the compression speed increased.

9.2.5 Effect of particle size

The particle size has a great influence on the AE signal during compression. This is particularly important during the reorganisation phase. It was evident that as the particle size increased the AE emission characterised by its peak amplitude and count also increased.

9.2.6 Effect of tablet weight

The sensitivity of acoustic emission to detect changes in the compression weight of acoustically active materials is unlikely to be of value for controlling the tablet weight as the simpler and cheaper alternative of force measurement would be preferable. However, it was noticed that as the material weight increased the AE energy emitted from the compressed material also increased. This finding is particularly important as it was established in this research that flowability of the material affected the hardness of the tablet. When the die is not uniformly filled with material, this weight variation can largely affect the hardness and solubility characteristics of a tablet.

9.2.7 AE from binary mixture

Typical tablet dosage contains more than one ingredient as it was described in this research. Furthermore, these ingredients differ in terms of their acoustic emission activities. Study on the binary mixture of lactose (very active) and povidone (less active) with different fractional proportion of lactose has revealed that as the fraction of lactose increased, the AE level also increased.

9.2.8 AE tablet capping and lamination monitoring

Acoustic emission monitoring has been successfully used to determine capping and lamination during compression. Capping was indicated by a low energy peak in comparison with high peaks for those tablets with no capping. The level of AE energy, also noted with a laminated tablet, is relatively higher than that in capping. AE energy has been shown to be a useful parameter in this study.

9.2.9 In-situ tablet condition monitoring

This research has shown that it is possible to implement in-situ condition monitoring of tablet condition using acoustic emission. Previous techniques of tablet assessment are often carried out at post compression whereas AE can be applied on-line for process condition monitoring and control. AE also provides in-situ way for non-destructive testing of tablet condition and its physical properties e.g. hardness.

9.2.10 Relationship between AE energy, crushing strength and disintegration time

The studies conducted on industrial tablet press showed that the AE energy that is generated during compression is proportional to the crushing strength of tablets and the disintegration time. This relationship was noted for two different loading conditions. It is important to note that these two physical properties of pharmaceutical tablet are related to each other.

9.2.11 Effect of mixture homogeneity on AE signal

It was found that the powder homogeneity as measured by mixing time greatly influences the AE signal generated during compression. AE as characterised by cumulative AE count was increased as the mixing time increased between lactose and povidone powder mix.

9.2.12 On-line monitoring of industrial tabletting

AE monitoring was successfully applied to industrial tabletting using Manesty F-press. Signals generated from this process were processed to identify various event groups in the compression cycle of the F-press. The fuzzy C-mean clustering technique was used to confirm the three different mechanisms that generate AE during a compression cycle.

9.2.13 Relationship between AE and tablets properties

It was found that the AE energy generated during the compression is well correlated with both crushing strength and disintegration time of the tablets produced. This relationship is very useful for it allows prediction of the disintegration and crushing strength from the acoustic emission energy without destroying the tablet. Furthermore it was possible to identify the capping phenomenon by AE monitoring technique based on AE energy.

9.2.14 Receiver operating characteristic (ROC)

Receiver operating characteristic analysis was constructed to enable determination of the threshold value to discriminate between capped and non-capped tablets. ROC analysis achieved 97% detection rate with a low false alarm rate below 5%. The area under the ROC curve is a good quantitative measure for various ROC classifiers.

9.2.15 Two-graph ROC curve

It is not easy to read off a desired threshold value from the conventional ROC curve. Therefore, a modified two-graph ROC was developed. The two-graph ROC is a representation of the test sensitivity (Se) and specificity (Sp) against the threshold value. This plot allows direct selection of the desired threshold value to achieve the desired detection and false alarm rates.

9.2.16 Cost benefit analysis

In receiver operating characteristic curve analysis, the optimal threshold value for a diagnostic test can be found on the ROC curve where the slope of the curve is a function of both cost ratio and fault prevalence. A set of guidelines was outlined for the decision making process. It takes into account the effects of capping cost and its prevalence. If capping is occurring at low rate, the decision maker should operate towards the lower left portion of his ROC curve. Also if the difference between the costs of a false positive and of true negative decision is much greater than the difference between the costs of a false negative and of a true positive decision, then both true positive (TP) and false positive (FP) are best kept small.

9.3 Contribution to Knowledge

The author considers the following to be a contribution to knowledge

9.3.1 Relationship between AE energy and tablet crushing strength

Linear relationship between the AE energy produced from powder compression during tabletting and both the hardness of the tablets as it is measured by crushing strength and disintegration time were established during this research. This relationship was noted for a number of common pharmaceutical powders using in tablet production. This relationship enables us to predict tablet final quality in terms of the AE energy observed during the compression.

9.3.2 Relationship between compressibility of powder, AE energy and crushing strength

A linear relationship was established between the AE energy generated during powder compression and the powder compressibility that was estimated based on Heckel analysis. Both correlate very well with tablet hardness as measured by the crushing strength.

9.3.3 AE energy for detecting capping and lamination in tabletting

Acoustic emission energy was found to be a good method for non-destructive testing and on-line detecting capping and lamination during tabletting. It was found that the level of AE energy dropped significantly when a capping or lamination occurs during tablet production performed on the industrial single press. Hence it was possible to set a threshold to distinguish between capped and non-capped tablets.

9.3.4 Application of receiver operating characteristic technique in tabletting

The receiver operating characteristic was successfully applied for threshold setting in the monitoring of tabletting. The analysis conducted was based on using AE energy as a discriminatory feature between capped and non-capped tablets. A modified two-graph ROC curve was also used to enable direct selection of a threshold level to discriminate between the two conditions.

9.3.5 Novel condition monitoring approach using receiver operating characteristic

This research resulted in a novel approach to a condition monitoring system for tablet production. The system comprised AE and non-AE measurements and evaluation which are interrelated. AE monitoring involves data collection, features extraction and advanced signal processing techniques. The extracted information is then, subjected to the ROC analysis to choose the best operation conditions. Non-AE evaluation includes measuring the hardness and disintegration of the final tablet. Relationships between the AE parameters (AE energy) and non-AE parameters were established.

9.4 Suggestion for further work

In the course of doing this research, the following ideas have occurred which may be worth further research and development:

9.4.1 Further work using the compactor simulator

The compactor simulator is capable of producing tablets of various shapes and sizes that mimic different pharmaceutical tabletting processes. Therefore, further work can be directed towards using the proposed system in this research on the compactor simulator. Its main advantages lie in its ease of controlling the tabletting parameters such as speed, load, depth of filling and hence will make the approach more widely applicable to other types of tablets. Furthermore, the compactor simulator enables more rapid data generation, collection and hence analysis.

9.4.2 Frequency analysis of AE data

This work is mainly focussed on the time domain analysis of the AE signal because it was believed that the AE energy would be good descriptor of the AE signal. Further study could be done on analysing the frequency component of the AE signal particularly in characterising the various mechanisms that generate AE signal during tabletting. The most common method of determining the frequency content of AE signals is to measure its power spectrum. Both swept-frequency spectral analysis and autocorrelation analysis have been employed by other researchers. Although particular features in the power spectrum may be characteristic of a specific source

and hence useful as a source signature, power spectral measurement destroys the phase information available in the AE signal. Fourier transform analysis, one the other hand, preserves phase and is thus potentially a better technique for source characterisation.

9.4.3 Utilisation of other traditional AE parameters

The current work on traditional AE parameters is concerned with capping. In this case, it is found that the AE energy is a good discriminatory feature. However, when other tablet failure types are considered, it is likely that other traditional AE parameters (such as rise time and ringdown count) may be more appropriate. Consequently further investigation should be conducted to explore the possibility. Further work could be directed toward carrying further experimentation on different type of presses using other AE features including frequency component. A novel method that employs using the statistical characteristic of interarrival time of successive AE event was developed at Brunel Center for Manufacturing Metrology may be used in further studies, (Kaewkonga, 2002).

9.4.4 Powder compaction modelling

An approach to minimizing capping and lamination is to design formulations that deform largely by plastic deformation. Despite extensive empirical studies of compaction, there is still incomplete understanding of the fundamental parameters that characterize this process. Experimentally, it is difficult to correlate the observed macroscopic deformational behaviour of a powder sample with the processes of particle packing, bonding and fragmentation that occur within the die in the very short timescale of tablet compression. An alternative is to model the powder compaction using finite element analysis. The model should treat the particles as a deformable body that may be mapped by a finite element mesh and the mechanical behaviour of the particles under loading is also included in the analysis. This approach allows the inclusion of failure at the particle level, due to either ductile or brittle mechanisms.

9.4.5 Force – displacement profile and AE monitoring

Further work can be directed toward using force-displacement profile of the compression and relate that to AE signal generated during compression. Punch displacement may be a better ordinate than time to investigate the progress of AE signal in relation to displacement. Also the material type and characteristics would be better informed by presenting the force displacement.

A1: Pycometer- density calculation

Pycnometer is derived from the Greek word pyknos, which has long been identified with volume measurements. The multipycnometer is an instrument specifically designed to measure the true volume of various quantities of solid materials. The technique employs Archimedes principle of fluid displacement to determine the volume. The displaced fluid is a gas, which can penetrate the finest pores to assure maximum accuracy. For this reason, helium is recommended since its small atomic dimension assures penetration into crevices and pores approaching one Angstrom (10^{-10} m).

The multipycnometer determines the true density of solid or powder samples by measuring the pressure difference when a known quantity of helium under pressure is allowed to flow from a precisely known reference volume (VR) into a sample cell containing the solid or powdered material (Multipycnometer Brochure). The true density, ρ, is:

$$\rho = \frac{m}{V}$$

where m is the mass of the sample and V is the true volume (defined as the space occupied by the powder exclusive of spaces greater than the intramolecular space (Ansel et al., 1995).

A2 Mistras 2001 data recording

At the C:\>

This indicates that the computer is ready to load a program and run.

MISTRAS then press <Enter> to boot up the MISTRAS program

The following are the steps that should be taken when carrying out the first AE test using the PAC supplied initialisation files:

1. Read the appropriate system initialisation (.INI) file into the system in order to set up the system to your desired operation and display conditions.
2. Enter the acquire menu.

3. Select the data file name which you want to save to disk.
4. Start acquisition.
5. Look at various screens, graphs and data listings during acquisition.
6. Exit data acquisition.

1. Set up measurement

From File menu select

Test Set-up menu: to add a test file, perform hardware set-up (such as gain, features selection, select channels to be on or off, etc)

Graphics menu: to set up the multiple graphs that will show up in data acquisition and replay.

Acquire menu: allow the user to start a test setting, set different (display) modes and carry out an Auto Sensor Test (AST).

Replay menu: to select and replay a data file and set up different (display) modes.

Option menu: select and execute the different optional software packages that are available for MISTRAS.

Utilities menu: to perform the utility function within the MISTRAS program without exiting.

Help menu: Provide on line help as to the operation of certain parts of the software.

2. Loading an Initialisation file into MISTRAS

Select Files from menu bar

Then select Read INI

Select MISTRAS.INI file from the list of INI files. This will select the MISTRAS.INI as the initialisation file that will set up the MISTRAS for a 2 channel AEDSP-32/16 board with a good, complete, default set-up.

To finish sequence

Move the mouse to OK and press <ENTER>

3. Entering Acquisition

From **Acquire** menu select **Mode, Normal**

Start ..F9 to get into acquisition

Autodump box on to save the data

Ok to begin acquisition

<ENTER>

4. Actions within Data acquisition

Use the function keys in order to examine other types of graphs representing the data acquired

F7 to see the previous graphs or screen in the list of desired graphs

F8 to the next graph or screen in the list of desired graphs

F2 to see a line dump of the AE data both for AE hits and for Timed data, **F2** again to go back to graph mode

F9 then <Enter> to pause test measurement

5. Exiting Data acquisition

F9 to Pause and exit data acquisition then <Enter>

F10 to stop the test then <Enter>

6. Operation sequence of Replaying AE data

Replaying an AE test is almost identical to that of acquiring data. The following are the steps which need to be done:

1. Read the appropriate system initialisation (.INI) file into the system in order to load the system to your desired set-up and display conditions.
2. Enter the Replay menu.
3. Select the data file name which you want to replay.
4. Start replay.

5. Look at various screens, graphs and data listings during and after replay.
6. Exit Replay and return to the main menu.

From menu bar, select Files then select Read INI...

Select MISTRAS.INI file from the list of INI files

Press **OK**

<Enter>

Entering Replay

From **Replay** menu select **Mode, Normal.**

OK

Now ready to enter the **Start... F10** to begin replay.

From the replay menu select a data file name for replay.

Then **OK.**

<Enter> to begin replay.

7. Action within replay

F7 to see the previous graphs or screen in the list of desired graphs.

F8 to the next graph or screen in the list of desired graphs.

F2 (while replay is reading data from the disk) to see a line dump of the AE data both for AE hits and for Timed data, **F2** again to go back to graph mode.

F9 then <Enter> to pause replay.

F9 again to resume replay.

F10 to exit replay

MISTRAS 2000 Measurement

AE Parameters definitions:

Absolute energy: absolute energy is 6 byte value whose units are aJ (or attoJoules). This feature is a true energy measure of the AE hit. Absolute energy is derived from the integral of the squared voltage signal divided by the reference resistance (10 kΩ)

over the duration of the AE waveform packet. Resolution is 0.000931 aJ per count (at 1MHz or greater sample rate).

Count: also referred to as AE threshold crossing counts. This AE hit feature simply counts the AE signal excursions over the AE threshold.

Duration: AE duration is defined as the time from the first threshold crossing to the end of the last thrshold crossing of the AE signal from the AE threshold.

ASL: average signal level is a measure of the continuously varying and "averaged" amplitude of the AE signal. This measurement is similar to that of RMS in that it is an averaged reading. The main difference is that the RMS is following the Toot Mean Square and is measured in volts, whereas the ASL is following the Amplitude variation and is measured in dB.

A3 Tablet hardness measurement

Tablet tester

Testing

1. Depress "RESET" before every series of tests.
2. Place the tablet to be tested in the middle to the left jaw of the test plate.
3. Depress "TEST" when the green light above it is on. At depression the light will go off.
4. After the tablet has been crushed the result is held on the main display (figure) until the next test is completed or another button is depressed.
5. The quantity of tests in a series is shown on the display (figure).
6. Clean the test plate of fragments before every test.

Appendix B

B1 Representation of compression cycle for various material

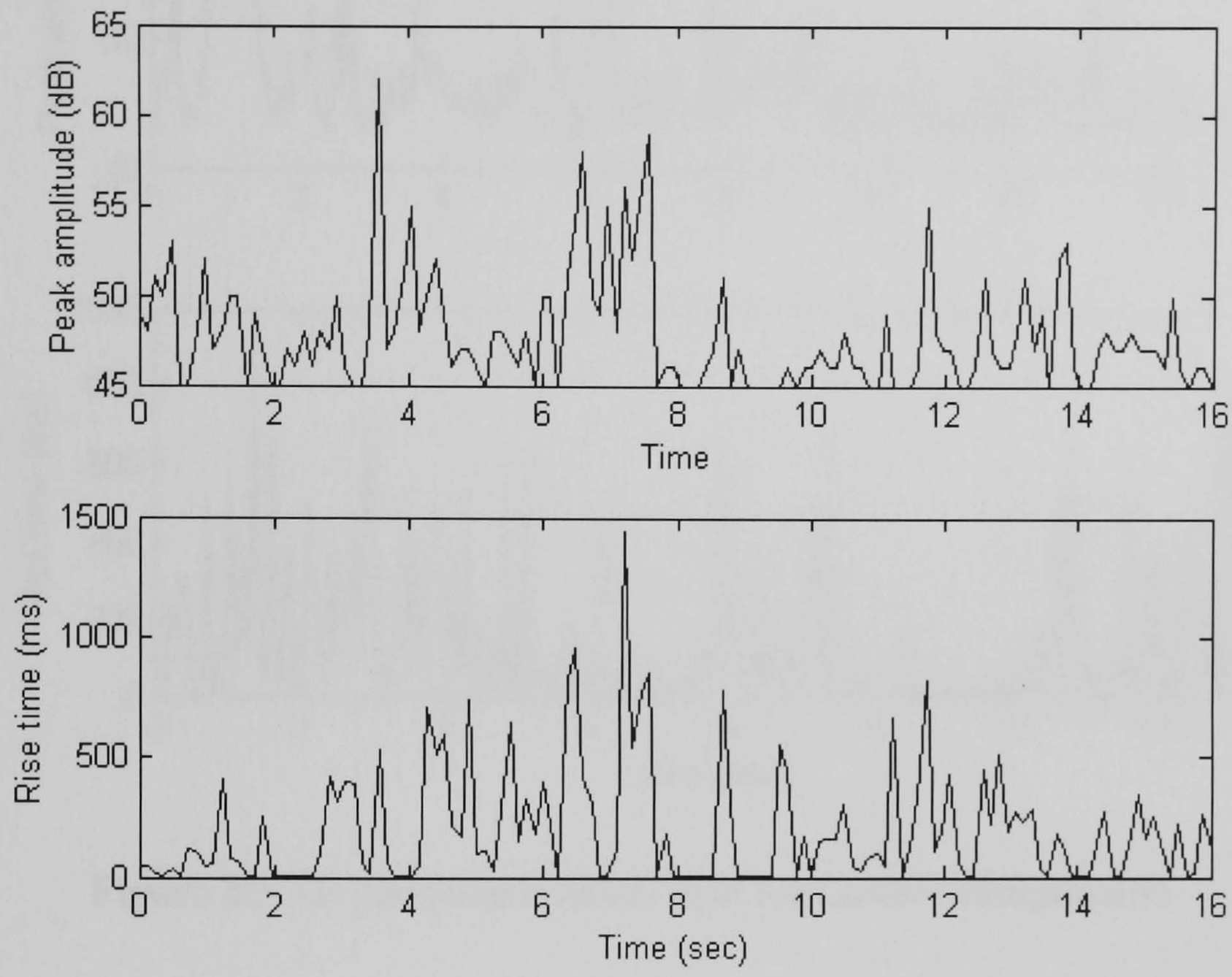

Figure B1 AE parameters versus time for microcrystalline cellulose (Avicel) compression

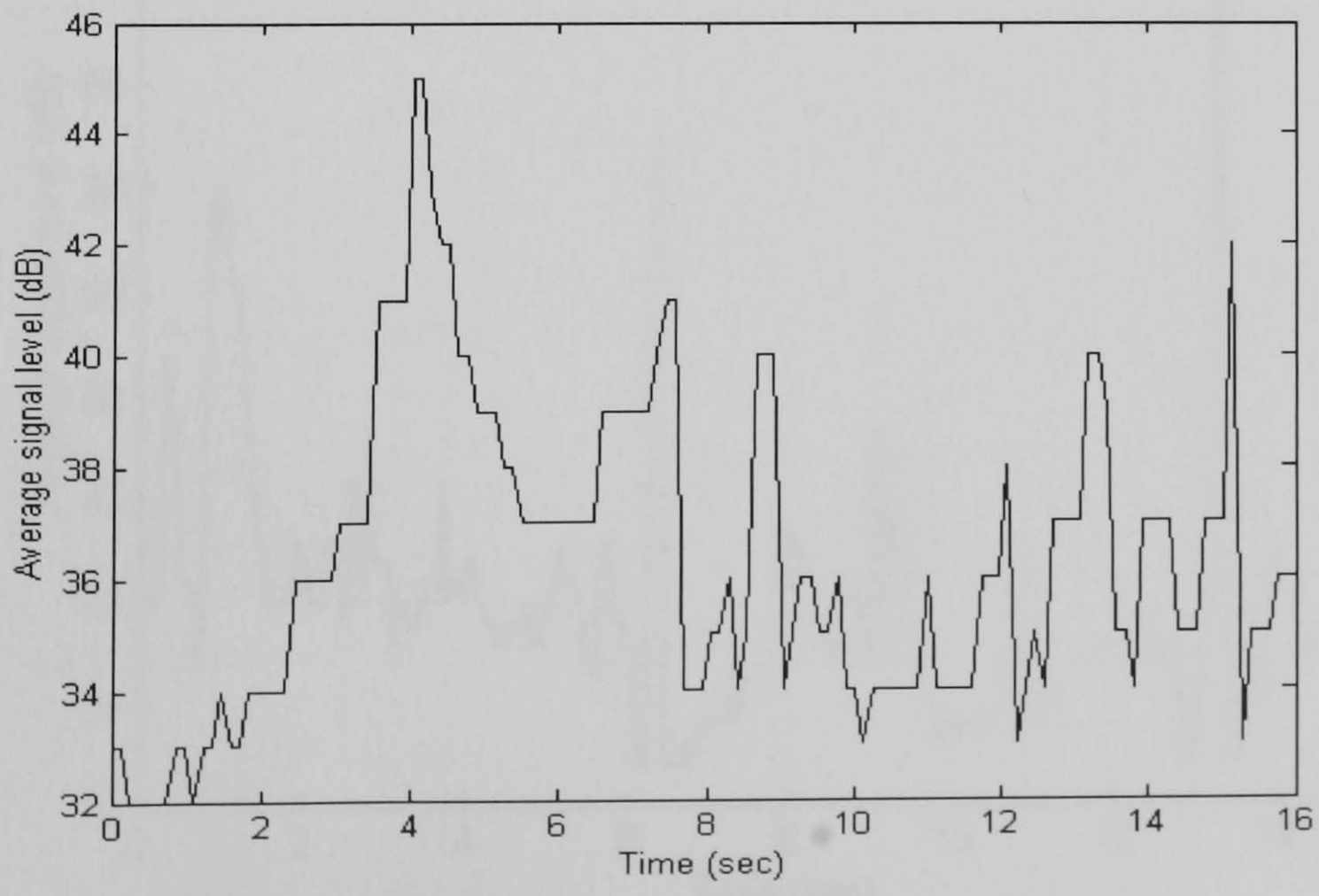

Figure B2 Average signal level for Avicel compression

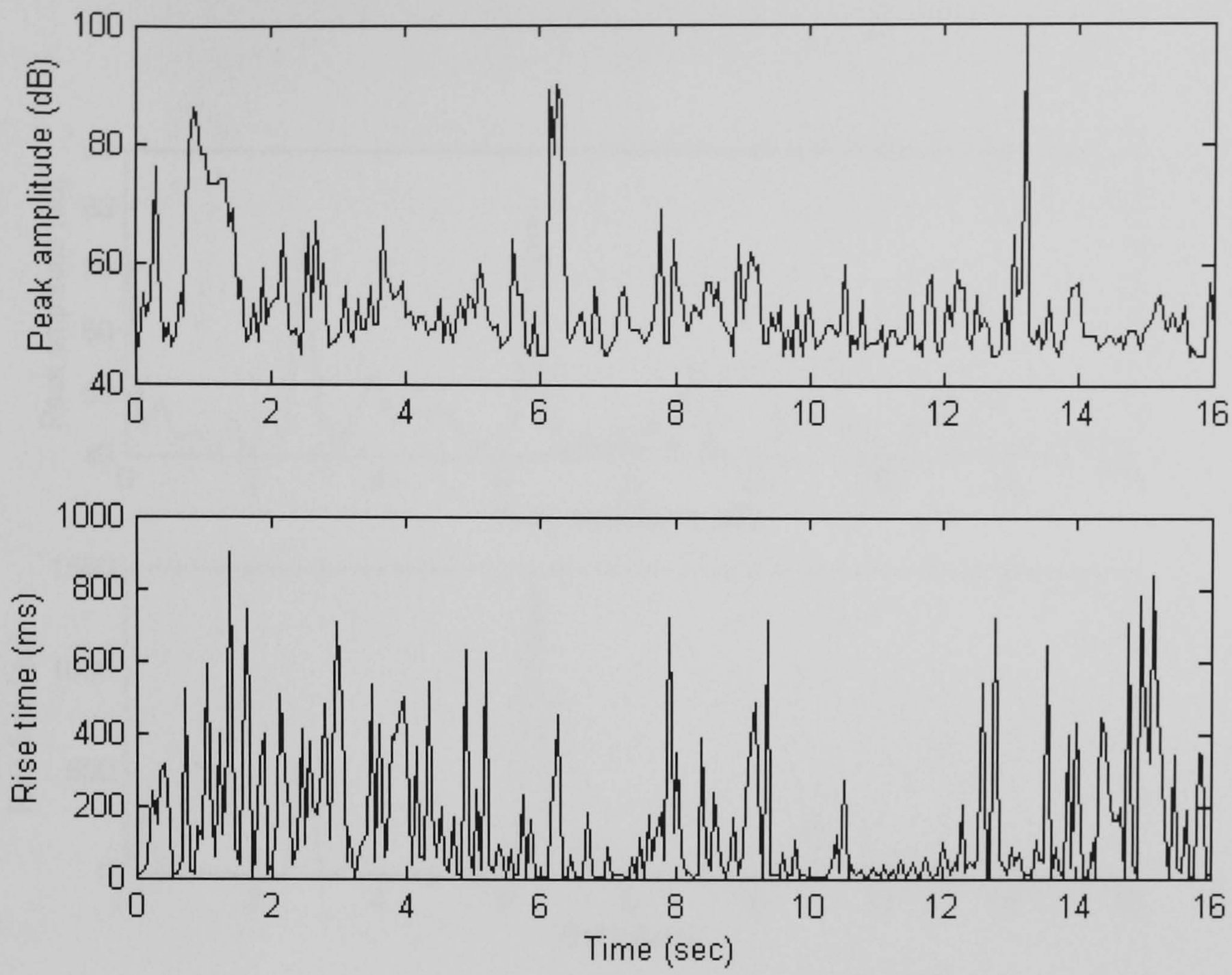

Figure B3 AE parameters versus time for Lactose compression

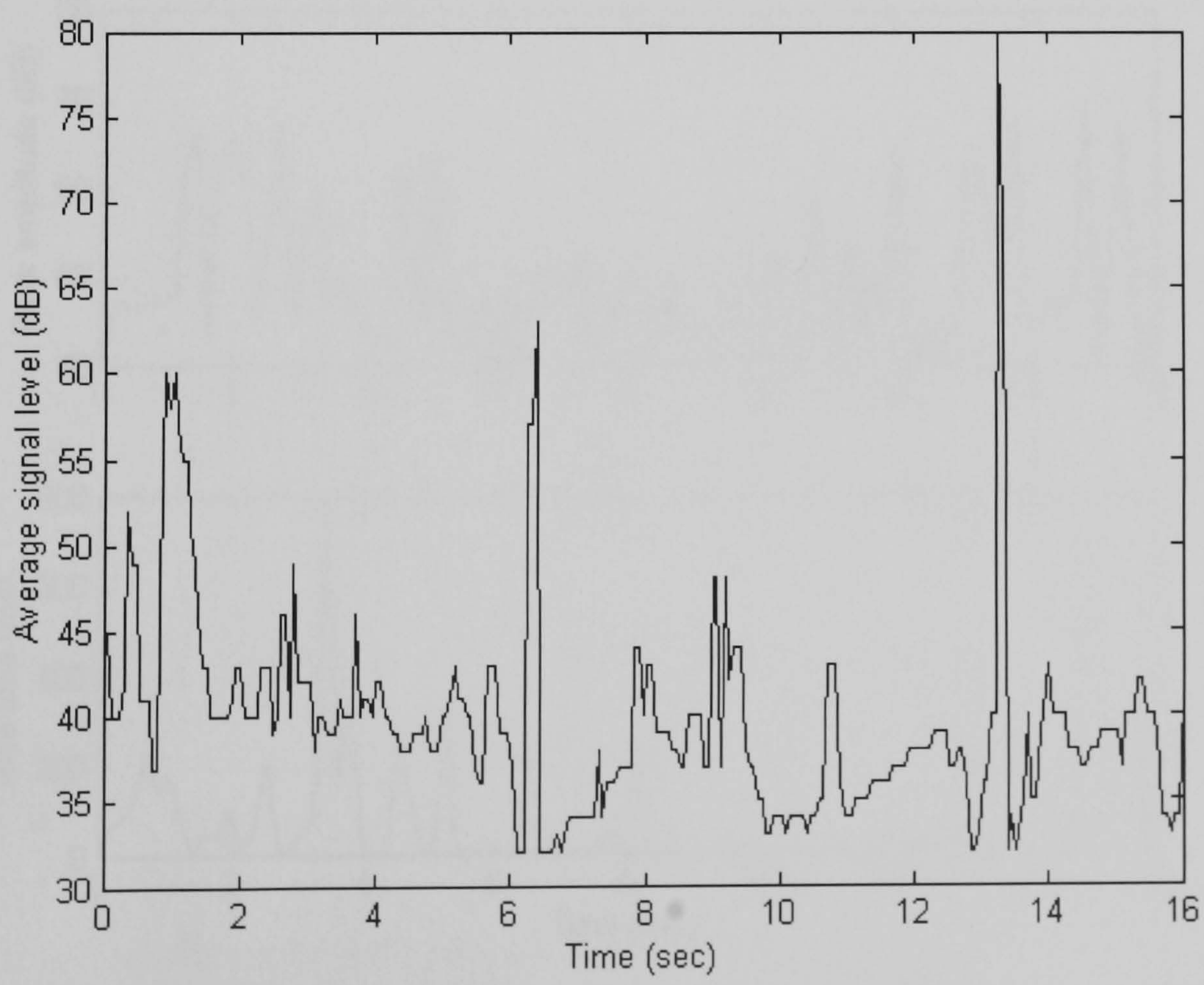

Figure B4 Average signal level for Lactose compression

B2 AE generated from pharmaceutical powders

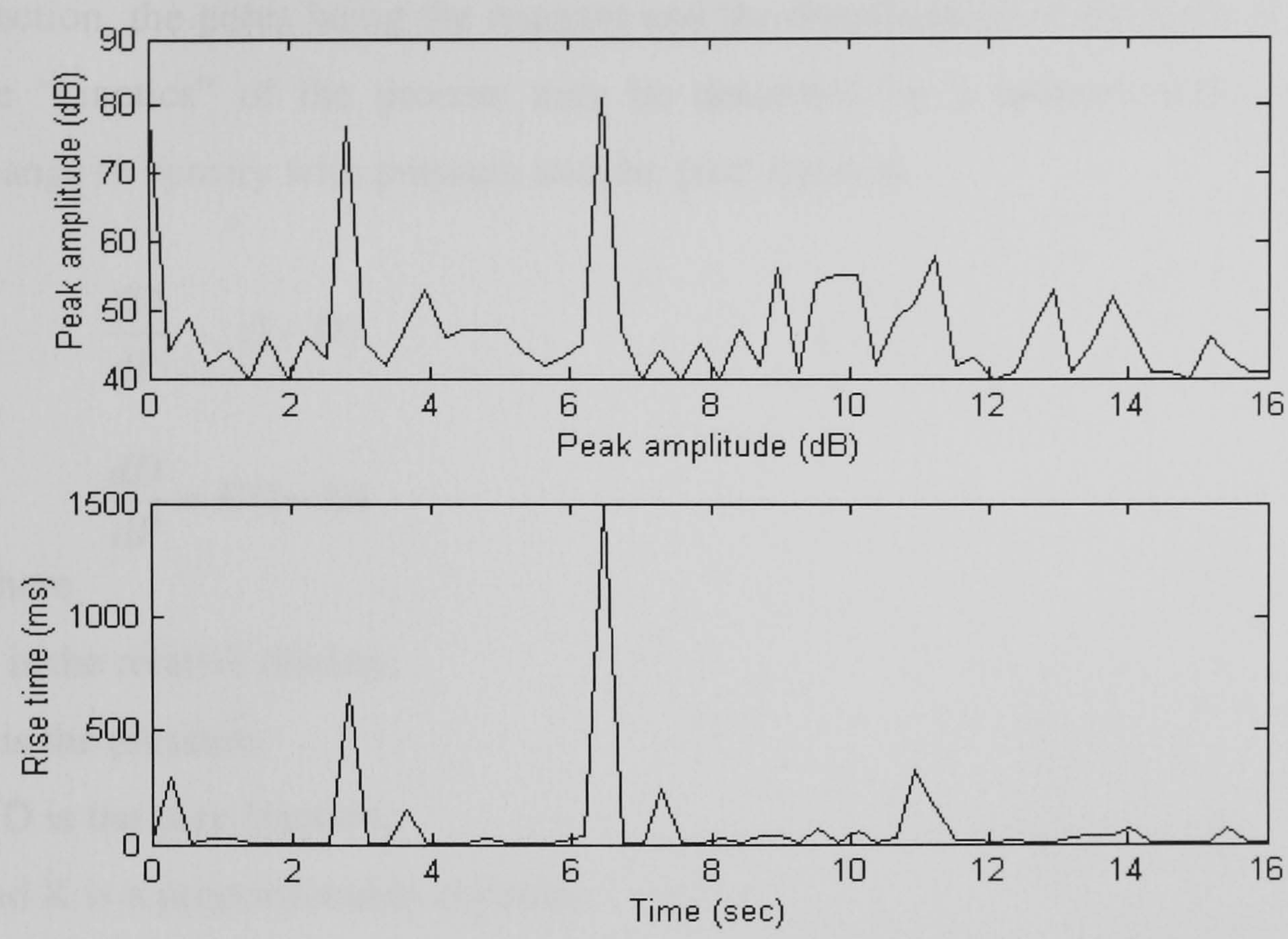

Figure B5 Peak amplitude and rise time for Aspartame compression

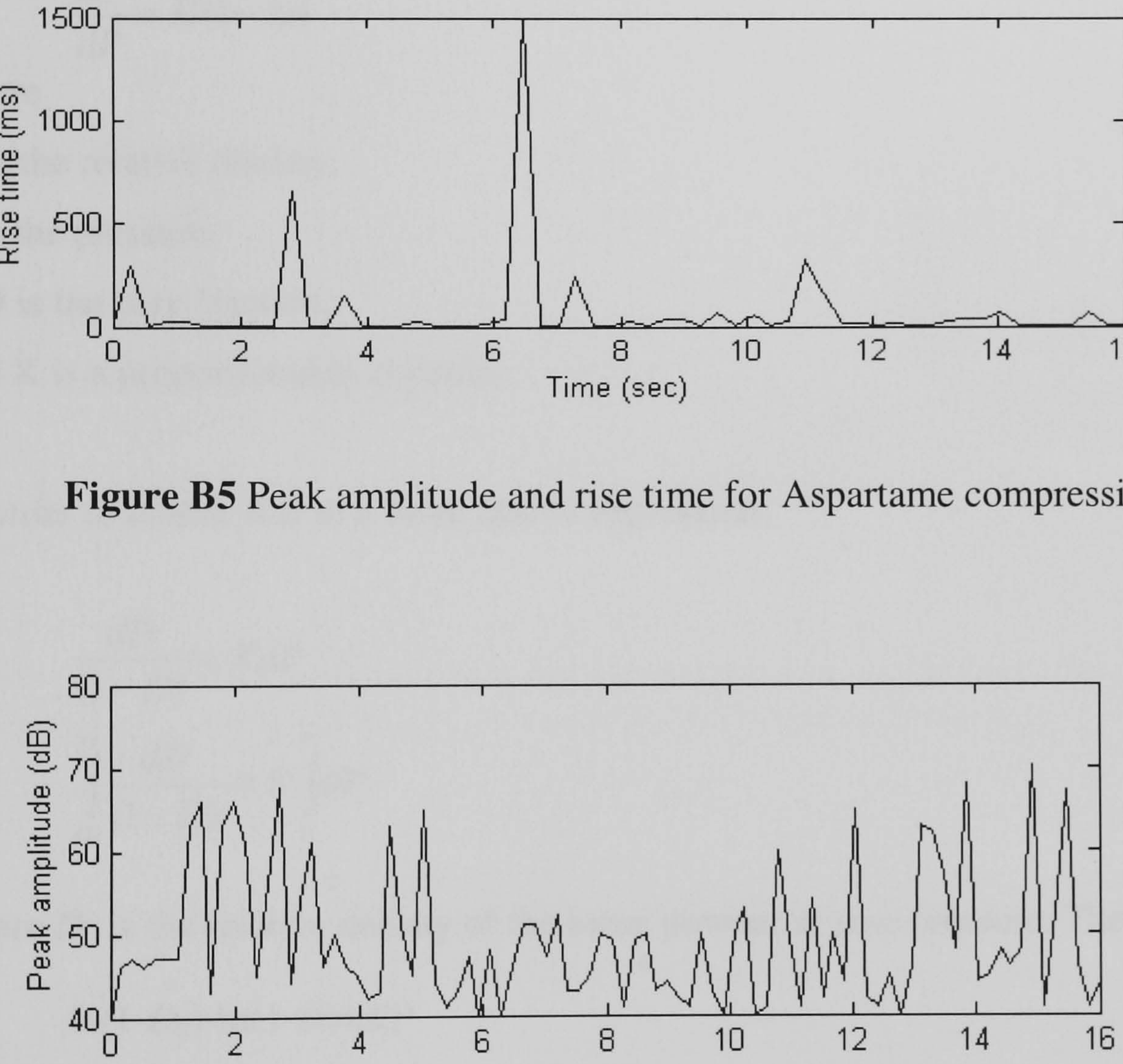

Figure B6 Peak amplitude and rise time for calcium carbonate compression

B3 Derivation of Heckel equation

If the compaction of powder is considered to be analogous to a first-order chemical reaction, the pores being the reactant and the densification of the bulk of the product, the "kinetics" of the process may be described by a proportionality between the change in density with pressure and the pore fraction.

$$\frac{dD}{dP} \qquad (1-D)$$

or

$$\frac{dD}{dP} = K(1-D)$$

where

D is the relative density,

P is the pressure

1-D is the pore fraction,

and K is a proportionality constant

In order to reduce this to a more usable expression:

$$\frac{dD}{(1-D)} = KdP$$

$$\int_{D_0}^{D} \frac{dD}{(1-D)} = K\int_{0}^{P} dP$$

where D_0 is the relative density of the loose powder at zero pressure. Therefore:

$$\ln(1\text{-}D_0)\text{-}\ln(1\text{-}D)=KP$$

or

$$\ln\left(\frac{1}{1-D}\right) = KP + \ln\left(\frac{1}{1-D_0}\right)$$

The validity of this analysis was checked by plotting ln(1/1-D) vs P for the powder used. Since the Heckel curve exhibit some curvature at low pressures, the above expression does not describe the process quantitatively. The replacement of the term $\ln(1/1\text{-}D_0)$ in the above equation with a constant, A, gives an expression shown below, which is quantitatively valid except at the lowest pressures.

$$\ln\left(\frac{1}{1-D}\right) = KP + A$$ which is known as Heckel equation.

B4 Particle size characterisation

Sieving

Sieving is a very simple procedure used to determine particle size distribution. Its simplicity brings about its wide range of use and popularity. Gyrating a sample of powder through a sieve with a squared or circular wire cloth bottom achieves the method of sieving. The squared wire cloth bottom is produced using wire mesh, while punching holes in a flat metal produces the circular holes.

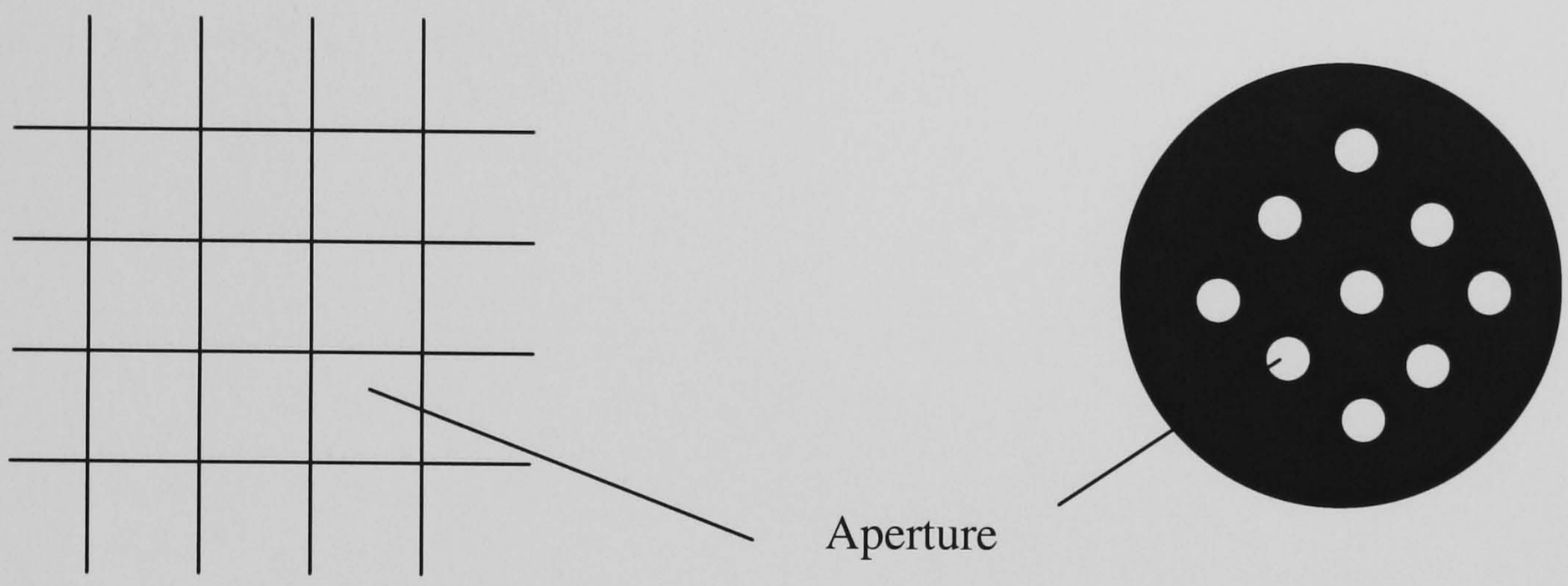

Figure B7 (A): Squared wire cloth bottom using a wire mesh. (B): Circular holes produced by punching holes in a flat metal. (wire meshes in sieving).

For analysis of particle size distribution, several levels of sieves can be stacked on top of each other. The difference between each level of sieves, is the aperture size. The sample is fed through the top of the stacked sieves, where the largest holes on the sieve are found, and the sieve is manually or mechanically gyrated. Gyrating the sieve, allows particles smaller than the size of the aperture in the top level, to fall to lower levels. This results in the separation of particle into a series of fraction on the individual sieve level. The bottom of the stacked sieves consists of a collector. The particles, which are smaller than the size of the lowest level sieve apertures, can be found in the collector.

The separated particles in the sieve are usually expressed in a cumulative frequency, in terms of the different aperture size ranges used to separate the sample.

The gyration of the sieve could be carried out manually, or mechanically, depending on the accuracy required for the separation. Mechanical systems employ the use of electronic devices to gyrate a sample through a sieve. The gyration force of such a device must be specific, measurable, and time framed. Manual systems require an operator to manually gyrate a sample though a sieve.

C1: MATLAB source code for Fuzzy C-mean clustering

```
clear all;
s = load('20l10.txt');
% data = rand(100, 2);
nb_clusters = 3;
feature_names = ['Tim';'RiT'; 'cou'; 'EvD';'Amp';'ASL';'RMS';'Eng'];
%
data = prestd(s) ; % s(:,[i,j]);
%data = [10 + randn(1000,8); 13 + randn(1000,8)*diag(rand(8,1))];
[center,U,obj_fcn] = fcm(data, nb_clusters,10);

maxU = max(U);
index1 = find(U(1,:) == maxU);
index2 = find(U(2, :) == maxU);
index3 = find(U(3, :) == maxU);
%index4 = find(U(4, :) == maxU);
%index5 = find(U(5, :) == maxU);

for i = 3:7
  for j = i+1:7
    figure
    plot(data(:,i), data(:,j),'o');
    hold on
    plot(data(index1,i),data(index1,j), 'LineStyle', '.',...
      'marker','*','color','g');
plot(data(index2,i),data(index2,j),'LineStyle', '.', ...
  'marker','*','color','r');
plot(data(index3,i),data(index3,j),'LineStyle', '.', ...
  'marker','*','color','m');
plot(center(1,i),center(1,j),'ko','markersize',12,'LineWidth',2);
plot(center(2,i),center(2,j),'kx','markersize',12,'LineWidth',2);
            plot(center(3,i),center(3,j),'k+','markersize',12,'LineWidth',2);

%plot(data(index4,i),data(index4,j),'LineStyle', '.', ...
  %'marker','*','color','k');
            %plot(data(index5,i),data(index5,j),'LineStyle', '.', ...
 %  'marker','*','color','y');

title([feature_names(i,:), '  versus  ', feature_names(j,:)]);
    xlabel(feature_names(i,:));
            ylabel(feature_names(j,:));

  end
end
```

Tablet Weights and Disintegration times for tablets compressed using F press

Crushing Strength								
	Tablet 1	Tablet 2	Tablet 3	Tablet 4	Tablet 5	Mean	SD	%RSD
Aspartame	154.7	231.8	208.3	176.8	212.9	196.9	30.8	15.7
Povidone 90	176.6	174.4	177.2	177.5	172.5	175.6	2.1	1.2
Povidone 30	114.7	114.6	115.6	113.3	115.3	114.7	0.89	0.78
Lactose (5Kg)	222.8	242.1	201.1	207.8	188.4	212.4	20.7	10
Lactose (10Kg)	207.5	196.4	206.4	183.6	189.3	196.6	10.5	5.3
Cellulose (5Kg)	155	154.9	144.4	156.6	156.5	153.5	5.1	3.3
Cellulose (10Kg)	156.7	156.6	156.1	156.7	156.4	156.5	0.25	0.16
2 Minute blend	5.7	6.3	6.34	5.94	6.44	236.2	2.6	1.1
6 Minute blend	279.7	244.3	240.1	245.8	247.1	251.4	16	6.4
10 Minute blend	226.2	223.3	270.1	226.9	272.3	243.8	25.1	10.3

Disintegration Time/ min					
	Tablet 1	Tablet 2	Tablet 3	Tablet 4	Tablet 5
Aspartame	19.32	26.12	18.29	7.25	15.27
Povidone 90	35.09	39.17	40.36	38.42	41.4
Povidone 30	13.55	13.38	14.17	13.34	14.03
Lactose (5Kg)	4.16	4.34	4.27	4.59	4.08
Lactose (10Kg)	2.21	2.26	2.17	2.27	2.12
Cellulose (5Kg)	~150.0				
Cellulose (10Kg)	>180				
2 Minute blend	4.45	4.53	4.59		
6 Minute blend	5.25	6.26	6.18	6.08	6.03
10 Minute blend	3.36	3.42	7.37*	3.32	7.48*

*Tablet weights slightly heavier than for tablets 1, 2 and 4.

Appendix D

D1: Normal probability plot

This type of graph is used to evaluate the normality of a variable, that is, whether and to what extent the distribution of variable follows the normal distribution. The selected variable will be plotted in a scatter plot against the values "expected from the normal distribution" the standard normal probability plot is constructed as follows. First, the deviations from the mean (residual) are rank ordered. From these ranks the program computes z values (i.e. standardised values of the normal distribution) based on the assumption that the data come from a normal distribution. These z values are plotted on the y-axis in the plot. If the observed residuals (plotted on the x-axis) are normally distributed, then all values should fall onto a straight line. If the residuals are not normally distributed, then they will be deviated from the line to form a clear pattern (e.g. an S shape) around the line.

D2: Matlab source code for constructing ROC curve

```
% Theoretical ROC
clear all;

mu1 = 225156250;
mu2 = 64130436;
sigma1 = 64422730;
sigma2 = 30882924;
d = mu1 - mu2;
% x = linspace(-4, 6, 200);
x = linspace(0, mu2+15.*sigma2, 5000);

y = zeros(length(x), 1);
z = zeros(length(x), 1) ;

for k = 1:length(x)
   %y(k) = exp(- 0.5.*(x(k)/sigma).^2);
   %z(k) = exp(- 0.5.* (x(k)- d).^2);
   y(k) = (1/sigma1.*sqrt(pi)).*exp(- 0.5.*((x(k)-mu1)/sigma1).^2);
   z(k) = (1/sigma2.*sqrt(pi)).*exp(- 0.5.* ((x(k)- mu2)/sigma2).^2);

end
figure(1)
plot(x, y, 'b');
%fill(x,y, 'r');
hold on
plot(x, z, 'r');
%fill(x,z, 'b');

%for d = [0,0.5, 1, 2]

  threshold = x; %0.001:0.1:100;
  pd = zeros(length(threshold),1);
  pf = zeros(length(threshold),1);
  k = 1;
  for i = threshold
     % pd(k) = 0.5.*erfc((log(i)./d) - 0.5.*d);
     % pf(k) = 0.5.*erfc((log(i)/d) + 0.5.*d);
     pd(k) = 0.5.*erfc((i-mu1)/(sqrt(2).*sigma1));
     pf(k) = 0.5.*erfc((i-mu2)/(sqrt(2).*sigma2));

     k = k+1;
end
figure (2)
plot(pf,pd);
figure(3);
plot(x, 1-pd, 'b.');
hold on
```

```
  plot(x, pf, 'r.');



  title('ROC');
  xlabel('false alarm probability');
  ylabel('detection probability');
  hold on
  roc_area = - trapz(pf,pd)

%1end;
```

D3: Area under the ROC curve calculation

RAPZ Trapezoidal numerical integration.

Z = TRAPZ(Y) computes an approximation of the integral of Y via the trapezoidal method (with unit spacing). To compute the integral for spacing different from one, multiply Z by the spacing increment.

Matlab source code:

```
perm = []; nshifts = 0;
if nargin == 3, % trapz(x,y,dim)
  perm = [dim:max(ndims(y),dim) 1:dim-1];
  y = permute(y,perm);
  m = size(y,1);
elseif nargin==2 & length(y)==1 % trapz(y,dim)
  dim = y; y = x;
  perm = [dim:max(ndims(y),dim) 1:dim-1];
  y = permute(y,perm);
  m = size(y,1);
  x = 1:m;
else
  if nargin < 2, y = x; end
  [y,nshifts] = shiftdim(y);
  m = size(y,1);
  if nargin < 2, x = 1:m; end
end
x = x(:);
if length(x) ~= m
   error('length(x) must equal length of first non-singleton dim of y.');
end

%  Trapezoid sum computed with vector-matrix multiply.
```

```
z = diff(x,1,1)' * (y(1:m-1,:) + y(2:m,:))/2;

siz = size(y); siz(1) = 1;
z = reshape(z,[ones(1,nshifts),siz]);
if ~isempty(perm), z = ipermute(z,perm);
end
```